NEW ROLES OF NEUTROPHILS AND GRANULOCYTIC MDSC IN AUTOIMMUNE DISEASES, INFLAMMATION, AND ANTI-MICROBIAL IMMUNITY

EDITED BY: Dragana Odobasic, Marko Radic and Clare Hawkins

PUBLISHED IN: Frontiers in Immunology

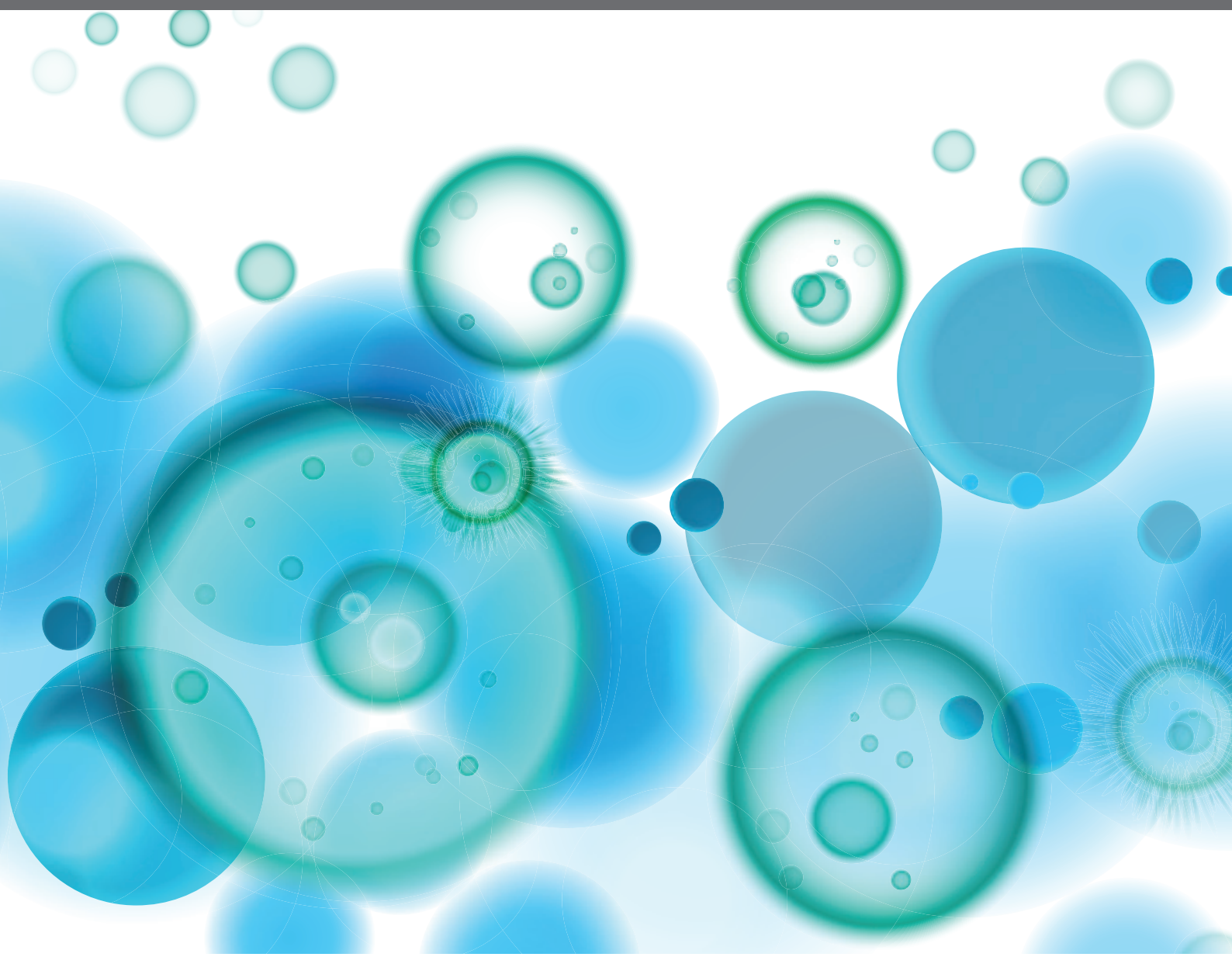

frontiers Research Topics

frontiers

ISSN 1664-8714
ISBN 978-2-88976-902-5
DOI 10.3389/978-2-88976-902-5

About Frontiers

Frontiers is more than just an open-access publisher of scholarly articles: it is a pioneering approach to the world of academia, radically improving the way scholarly research is managed. The grand vision of Frontiers is a world where all people have an equal opportunity to seek, share and generate knowledge. Frontiers provides immediate and permanent online open access to all its publications, but this alone is not enough to realize our grand goals.

Frontiers Journal Series

The Frontiers Journal Series is a multi-tier and interdisciplinary set of open-access, online journals, promising a paradigm shift from the current review, selection and dissemination processes in academic publishing. All Frontiers journals are driven by researchers for researchers; therefore, they constitute a service to the scholarly community. At the same time, the Frontiers Journal Series operates on a revolutionary invention, the tiered publishing system, initially addressing specific communities of scholars, and gradually climbing up to broader public understanding, thus serving the interests of the lay society, too.

Dedication to Quality

Each Frontiers article is a landmark of the highest quality, thanks to genuinely collaborative interactions between authors and review editors, who include some of the world's best academicians. Research must be certified by peers before entering a stream of knowledge that may eventually reach the public - and shape society; therefore, Frontiers only applies the most rigorous and unbiased reviews.
Frontiers revolutionizes research publishing by freely delivering the most outstanding research, evaluated with no bias from both the academic and social point of view. By applying the most advanced information technologies, Frontiers is catapulting scholarly publishing into a new generation.

What are Frontiers Research Topics?

Frontiers Research Topics are very popular trademarks of the Frontiers Journals Series: they are collections of at least ten articles, all centered on a particular subject. With their unique mix of varied contributions from Original Research to Review Articles, Frontiers Research Topics unify the most influential researchers, the latest key findings and historical advances in a hot research area! Find out more on how to host your own Frontiers Research Topic or contribute to one as an author by contacting the Frontiers Editorial Office: frontiersin.org/about/contact

NEW ROLES OF NEUTROPHILS AND GRANULOCYTIC MDSC IN AUTOIMMUNE DISEASES, INFLAMMATION, AND ANTI-MICROBIAL IMMUNITY

Topic Editors:
Dragana Odobasic, Monash University, Australia
Marko Radic, University of Tennessee College of Medicine, United States
Clare Hawkins, University of Copenhagen, Denmark

Citation: Odobasic, D., Radic, M., Hawkins, C., eds. (2022). New Roles of Neutrophils and Granulocytic MDSC in Autoimmune Diseases, Inflammation, and Anti-microbial Immunity. Lausanne: Frontiers Media SA.
doi: 10.3389/978-2-88976-902-5

Table of Contents

frontiers | Frontiers in Immunology

TYPE Editorial
PUBLISHED 29 July 2022
DOI 10.3389/fimmu.2022.974062

OPEN ACCESS

EDITED AND REVIEWED BY
Uday Kishore,
Brunel University London,
United Kingdom

*CORRESPONDENCE
Marko Radic
mradic@uthsc.edu

SPECIALTY SECTION
This article was submitted to Molecular Innate Immunity, a section of the journal Frontiers in Immunology

RECEIVED 20 June 2022
ACCEPTED 12 July 2022
PUBLISHED 29 July 2022

CITATION
Odobasic D, Hawkins CL and Radic M (2022) Editorial: New roles of neutrophils and granulocytic MDSC in autoimmune diseases, inflammation, and anti-microbial immunity. *Front. Immunol.* 13:974062. doi: 10.3389/fimmu.2022.974062

Editorial: New roles of neutrophils and granulocytic MDSC in autoimmune diseases, inflammation, and anti-microbial immunity

Dragana Odobasic[1], Clare Louise Hawkins[2] and Marko Radic[3]*

[1]Centre for Inflammatory Diseases, Department of Medicine, Monash Medical Centre, Monash University, Clayton, VIC, Australia, [2]Department of Biomedical Sciences, University of Copenhagen, Copenhagen, Denmark, [3]Department of Microbiology, Immunology and Biochemistry, University of Tennessee Health Science Center, Memphis, TN, United States

KEYWORDS

neutrophils (PMNs), MDSC (myeloid-derived suppressor cells), infection, inflammation, autoimmunity

Editorial on the Research Topic
New roles of neutrophils and granulocytic MDSC in autoimmune diseases, inflammation, and anti-microbial immunity

Neutrophils are known as the "first responders" that arrive at sites of infection and inflammation. There, they rapidly respond and attack microbes. However, recent discoveries reveal that neutrophils make a more multilayered contribution to the immune response (1). Neutrophils use an array of molecules to interact with other immune and non-immune cells. Consequently, neutrophils are important in shaping both innate and adaptive immune responses and are critical players in the protective immunity against pathogens as much as in the development and progression of various inflammatory and autoimmune diseases (2).

We now know that neutrophils can have both pro and anti-inflammatory functions, which are highly dependent on the timing, the context, and the type of signals they receive. They can promote inflammation through the release of microvesicles and various granule enzymes such as proteases and myeloperoxidase (MPO), as well as reactive oxidants, neutrophil extracellular traps (NETs), cytokines, and chemokines (3). The release of neutrophil enzymes and other bioactive macromolecules may introduce post-translational modifications into surrounding host tissues, in the process providing neo-antigens and contributing to tissue damage. Neutrophils also provide a rich source of autoantigens such as proteinase-3 and MPO, and autoimmunity to these causes severe inflammation of small blood vessels (4).

In contrast, neutrophils also have a critical role in the resolution of inflammation, often through their interactions with macrophages, and subsequent tissue repair.

Notably, neutrophils can either positively or negatively regulate the development of adaptive immunity in secondary lymphoid organs through their effects on dendritic cells, T cells, and B cells (5). In some instances, it has become evident that neutrophils can even themselves act as antigen-presenting cells to activate T cells. Additionally, research in the last decade has uncovered that neutrophils, acting as immunosuppressive granulocytic myeloid-derived suppressor cells (MDSC), can promote cancer growth, whereas, in autoimmune diseases, neutrophils may have a protective role (6).

This Research Topic presents original research and reviews the rich contribution of neutrophils to immunity. We focus on the diverse roles neutrophils and granulocytic MDSC play as regulators of the immune system. The contributions in this Special Topic examine the implications of neutrophils in various aspects of inflammation, immunity against pathogens, and in cancer.

In this collection of articles, Haist et al. describe experiments that examine the effect of Ly6-G-targeted knock-down of β2 integrins on the severity of invasive pulmonary aspergillosis. The deficiency of neutrophil adhesion receptors leads to more extensive disease, less NET release, reduced cytokine and reactive oxygen production, and an increase in apoptosis compared to control animals.

The laboratory of Mihaila et al. examine the functional dichotomy between N1 and N2 neutrophils and draw attention to the contribution of the S100A9 alarmin to elevated N1 proinflammatory activity, chemotaxis and oxidative burst. The authors suggest that S100A9 inhibition may reduce inflammation.

Deerhake et al. use single cell transcriptomics to dissect aspects of pathway selection in neutrophils that respond to Cryptococcus by enhanced oxidation versus an alternative subset that delays apoptosis and increases cytokine secretion which activates dendritic cells and alveolar macrophages.

Piatek et al. pursue the puzzle of the reduced activation potential of neutrophils in HIV-infected individuals and determine that the levels and chromatin distribution of tri-methylated lysine 4 in histone H3 are linked to reduced anti-microbial functions and greater abundance of this chromatin mark along genes regulated by NF-kB.

Valadez-Cosmes et al. examined low-density neutrophils from non-small cell lung cancer (NSCLC) patients by using an unbiased flow cytometry screen of over 300 potential cell surface markers, and pinpoint CD36, CD41 and CD61 as reliable indicators of this disease-associated neutrophil population.

Mollenhauer et al. observed the enhanced participation of granulocytes in ischemia reperfusion injury and the remodeling of heart muscle in six-transmembrane protein of prostate 2 (Stamp2) deficient mice, which exhibited increased reactive oxygen production and greater MPO release, leading to impaired heart function post-injury.

An underappreciated anti-bacterial mechanism, the production of chlorinated lipids by neutrophil MPO, was examined by Amunugama et al. and evaluated with regard to bacterial killing.

Finally, review articles highlighted potential reasons for the inadequacy of neutrophils that attack but not eliminate pathogenic mycobacteria (Parker et al.), and profiled the emerging role of MDSC in promoting severe COVID-19 by exacerbating the pro-inflammatory cytokine milieu and reducing the efficacy of T lymphocytes (Rowlands et al.). The rich diversity of topics discussed in this Research Topic are an indication of the many emerging roles of neutrophils in immunity.

Author contributions

The authors contributed equally and in mutual agreement to the reviews of the submitted manuscripts and the writing of the editorial.

Conflict of interest

The authors declare that the research was conducted in the absence of any commercial or financial relationships that could be construed as a potential conflict of interest.

Publisher's note

References

1. Rosales C. Neutrophil: A cell with many roles in inflammation or several cell types? *Front Physiol* (2018) 9:113. doi: 10.3389/fphys.2018.00113

2. Mortaz E, Alipoor SD, Adcock IM, Mumby S, Koenderman L. Update on neutrophil function in severe inflammation. *Front Immunol* (2018) 9:2171. doi: 10.3389/fimmu.2018.02171

3. Herrero-Cervera A, Soehnlein O, Kenne E. Neutrophils in chronic inflammatory diseases. *Cell Mol Immunol* (2022) 19:177–91. doi: 10.1038/s41423-021-00832-3

4. Xiao H, Hu P, Falk RJ, Jennette JC. Overview of the pathogenesis of ANCA-associated vasculitis. *Kidney Dis* (2015) 1:205–15. doi: 10.1159/000442323

5. Peiseler M, Kubes P. More friend than foe: the emerging role of neutrophils in tissue repair. *J Clin Invest* (2019) 129:2629–39. doi: 10.1172/JCI124616

6. Zhou J, Nefedova Y, Lei A, Gabrilovich D. Neutrophils and PMN-MDSC: Their biological role and interaction with stromal cells. *Sem Immunol* (2018) 35:19–28. doi: 10.1016/j.smim.2017.12.004

frontiers in Immunology

HYPOTHESIS AND THEORY
published: 29 April 2021
doi: 10.3389/fimmu.2021.670574

Single-Cell Transcriptional Heterogeneity of Neutrophils During Acute Pulmonary *Cryptococcus neoformans* Infection

M. Elizabeth Deerhake[1], *Estefany Y. Reyes*[1], *Shengjie Xu-Vanpala*[1] *and Mari L. Shinohara*[1,2*]

[1] Department of Immunology, Duke University School of Medicine, Durham, NC, United States, [2] Department of Molecular Genetics and Microbiology, Duke University School of Medicine, Durham, NC, United States

Neutrophils are critical as the first-line defense against fungal pathogens. Yet, previous studies indicate that neutrophil function is complex during *Cryptococcus neoformans (Cn)* infection. To better understand the role of neutrophils in acute pulmonary cryptococcosis, we analyzed neutrophil heterogeneity by single-cell transcriptional analysis of immune cells in the lung of *Cn*-infected mice from a published dataset. We identified neutrophils by reference-based annotation and identified two distinct neutrophil subsets generated during acute *Cn* infection: A subset with an oxidative stress signature (Ox-PMN) and another with enhanced cytokine gene expression (Cyt-PMN). Based on gene regulatory network and ligand-receptor analysis, we hypothesize that Ox-PMNs interact with the fungus and generate ROS, while Cyt-PMNs are longer-lived neutrophils that indirectly respond to *Cn*-derived ligands and cytokines to modulate cell-cell communication with dendritic cells and alveolar macrophages. Based on the data, we hypothesized that, during *in vivo* fungal infection, there is a division of labor in which each activated neutrophil becomes either Ox-PMN or Cyt-PMN.

Keywords: neutrophils, fungal infection, pulmonary, *Cryptococcus neoformans*, heterogeneity, single-cell RNA sequencing (scRNA-seq)

OPEN ACCESS

Edited by:
Marko Radic, University of Tennessee College of Medicine, United States

Reviewed by:
Karen L. Wozniak, Oklahoma State University, United States
Frank R. DeLeo, Rocky Mountain Laboratories (NIAID), United States

***Correspondence:**
Mari L. Shinohara
mari.shinohara@duke.edu

Specialty section:
This article was submitted to Molecular Innate Immunity, a section of the journal Frontiers in Immunology

Received: *22 February 2021*
Accepted: *14 April 2021*
Published: *29 April 2021*

Citation:
Deerhake ME, Reyes EY, Xu-Vanpala S and Shinohara ML (2021) Single-Cell Transcriptional Heterogeneity of Neutrophils During Acute Pulmonary Cryptococcus neoformans Infection. Front. Immunol. 12:670574. doi: 10.3389/fimmu.2021.670574

INTRODUCTION

Opportunistic fungal infections are a serious complication of immunosuppression in patients undergoing transplantation, patients with HIV-AIDS, and those with immunosuppression induced by leukemia or lymphoma (1). Among opportunistic fungal infections, *Cryptococcus neoformans* (*Cn*) is one of the pathogens with the highest disease burden and risk of complications. Inhaled from the environment, *Cn* begins as a primary pulmonary infectious agent and can disseminate through the vasculature to the central nervous system (CNS) resulting in meningoencephalitis (1).

Neutrophils are critical as the first-line of defense against fungal pathogens, effectively engulfing and killing *Cn*, arguably more efficacious than monocytes (2, 3). For instance, neutrophils produce the majority of reactive oxygen species (ROS) during cryptococcosis in attempts to control and clear the infection (4, 5). Treatment with granulocyte colony-stimulating factor (G-CSF) decreased fungal

burdens in mice with cryptococcosis (6) and reduced risk of infection in AIDS patients (7), suggesting that neutrophils contribute to host immune defenses during cryptococcal infection. Using *in vivo* antibody-mediated neutrophil depletion, studies have demonstrated that neutrophils are crucial for the clearance of intravascular *Cn* in the lung and brain (8, 9). Additionally, myeloperoxidase (MPO), the neutrophil azurophilic granule factor, is protective in murine *Cn* infection when administered *via* intravenous (*i.v.*) and intranasal (*i.n.*) routes (10).

However, the role of neutrophils in *Cn* infection is not straightforward. In contrast to intravascular infection, neutrophil depletion leads to a paradoxical increase in survival in the setting of intratracheal infection (11–13). One explanation is that acute neutrophil recruitment to the lung and the associated anti-fungal response following *Cn* infection could cause host-detrimental inflammation, leading to tissue damage. However, neutrophil depletion also leads to an increase – not a decrease – in inflammatory cytokine production in the lung (11, 14); and increased inflammatory cytokine levels may promote anti-fungal immunity and increase host survival. Thus, neutrophils may be detrimental both through off-target tissue damage or by reducing immune responses.

The *in vivo* functions of neutrophils in pulmonary *Cn* infection are not well understood and likely involve a complex balance of antifungal and regulatory activities. In addition, neutrophils have a short half-life, and *ex vivo* analyses are extremely challenging. To map neutrophil heterogeneity during acute pulmonary infection with *Cn*, we analyzed a single-cell RNA sequencing (scRNA-seq) dataset of lung extra-vascular and intra-vascular immune cells. Following reference-based annotation of neutrophils, we identified multiple neutrophil subsets with distinct transcriptional profiles, including two subsets which were found in *Cn*-infected mice, not in naïve mice. Using both gene regulatory network and ligand-receptor analyses, we discovered predicted pathways which may contribute to neutrophil subset identity and modulate interactions between neutrophils and other myeloid cells during acute pulmonary *Cn* infection. These preliminary data lead us to further hypothesize the distinct functions and longevity of neutrophil subsets. Further characterization of these distinct neutrophil subsets may provide potential therapeutic targets to enhance anti-*Cn* immunity.

METHODS

Dataset Availability

The single-cell RNA sequencing dataset analyzed in this study (NCBI GEO: GSE146233) was previously published (15) and focused on analysis of alveolar macrophages (AM) (15). This dataset has not previously been used to analyze neutrophils or other immune cell populations.

Sample Preparation and Single-Cell RNA Sequencing

Samples were prepared as previously described (15): Mice heterozygous for the *Cxcl2-Egfp* reporter were administered *Cn* by orotracheal instillation (10^4 yeasts cells/mouse, H99 strain) and cells from the lungs of infected and naïve control mice were harvested 9 hrs post-instillation. $CD45^+$ cells from lung homogenates were isolated using MACS beads. Cells from three mice per group were pooled for subsequent analysis. Intra-vascular cells were not depleted prior to cell isolation. Because of this, the dataset contains both extra- and intra-vascular lung immune cells. scRNA-seq was then performed on $CD45^+$ cell samples with the 10X Genomics Chromium platform. Detailed scRNA-seq library preparation methods were previously described (15).

Reference-Based Annotation of Immune Cell Subsets

Cell Ranger v3.0.1 (10X Genomics) was used to process raw sequencing files into fastq format as previously described (15). Briefly, reads were aligned with a modified mouse mm10 transcriptome containing the *Egfp* transgene along with all protein coding and long non-coding RNA genes. CellRanger was used to generate a matrix file with expression counts for each sample, with genes as rows and cell Unique Molecular Identifier (UMI) as columns. We obtained 5,635 median UMI counts per cell, 1771 median genes per cell, and 82,314 mead reads per cell.

Seurat v3.1.0 (16) was used to calculate the number of expressed genes, counts per cell, and the percentage of mitochondrial genes as previously described (15). The following criteria were used to filter cells: total number of genes between 200 and 20,000; number of counts between 500 and 75,000; mitochondrial gene frequency <10%. A total of 4,586 cells from naïve and 5,694 cells from infected samples were used for downstream analysis. The SCTransform method (17) was used to perform normalization and variance stabilization of expression counts using regularized binomial regression, with regression on percent mitochondrial genes per cell (15). For cell-type identification, integration between samples was performed using the anchor-based canonical correlation analysis (CCA) method. PCA was then performed, and the top 50 principal components were selected for Uniform Manifold Approximation and Projection (UMAP) for two-dimensional projection. Calculation of k-nearest neighbors and cluster identification were performed.

SingleR (18) was used to perform automated reference-based annotation using curated bulk RNA-seq data from ImmGen for major immune populations as previously described (15). We also examined expression of canonical cell-type specific marker genes as well as unbiased cluster-specific markers for each population to confirm our annotation of major immune cell populations. This allowed us to confidently identify neutrophils within our dataset by confirming neutrophil canonical markers (*S100a8*, *Ly6g*). Detailed results of reference-based annotation can be found in Xu-Vanpala et al. (15).

Cluster Analysis of Neutrophils

Cells annotated as neutrophils in the scRNA-seq dataset were selected for further analysis using Seurat v3.1.0 (16). Normalization and variance stabilization with SCTransform (17) and PCA were performed, and the top 40 principal

components were selected for UMAP visualization. Calculation of k-nearest neighbors and cluster identification was performed. Hierarchical clustering of the neutrophil subsets was used to annotate major branches (I, II, III) and subclusters (*i.e.* IIa, IIb). Numbering of the clusters was based on relative size of each subpopulation. Cluster-specific expression markers were identified, specifically focusing on upregulated genes.

Pathway Enrichment Analysis

Pathway enrichment analysis was performed on cluster-specific markers using *ReactomePA* (19). Among the resulting enriched pathways with adjusted p-value<0.05, top hits were selected and plotted in a heatmap as -log(adjusted p-value) to illustrate shared enriched pathways between clusters.

Gene Regulatory Network Analysis

SCENIC (single-cell regulatory network inference and clustering) (20) was used to identify transcription factors predicted to regulate neutrophil heterogeneity. Default parameters were used for the *SCENIC* workflow in R and the normalized single-cell gene expression matrix from Seurat was used as input. Co-expression analysis was performed with *GENIE3*. For visualization, we calculated the average regulon activity (AUC) scores for each neutrophil cluster and selected the top regulons to plot as a heatmap using *pheatmap*.

Ligand-Receptor Interaction Analysis

NicheNet (*nichnetr*) (21) was used to identify predicted ligand-receptor interactions between neutrophil subsets of interest (Ox-PMN, Cyt-PMN) and myeloid cell types of interest (AMs, DCs) using default parameters for the workflow in R. AMs and DCs were separately selected as the "receiver cell types" for independent analyses and the condition of interest selected was "post-*Cn* instillation" compared to "naïve". Neutrophils were selected as the "sender cell type" and the set of potential ligands was defined as the combined list of Ox-PMN (IIa) and Cyt-PMN (IIb) marker genes. Top predicted ligand-receptor interactions were visualized using the *circlize* R package (22) as a circos plot in which link transparency and width reflected the regulatory potential of a given ligand-target interaction.

RESULTS OF SINGLE CELL RNA-SEQ ANALYSIS

Acute *Cryptococcus neoformans* Pulmonary Infection Induces Neutrophil Subsets With Distinct Transcriptional Profiles

To characterize the immune response to acute *Cn* infection, we performed analysis of a previously published scRNA-seq dataset consisting of lung immune cells from naïve and *Cn*-infected mice. Specifically, $CD45^+$ immune cells were isolated from the lungs of mice 9-hr post infection (hpi) with *Cn* (10^4 yeasts cells/mouse, H99 strain, administered by orotracheal instillation) and compared to cells from naïve controls, including both extra- and intravascular lung immune cells (15). Because we sought to understand early host responses, we selected the 9-hpi timepoint, at which the level of a neutrophil chemoattractant CXCL2 has already increased in bronchoalveolar lavage fluid and neutrophils start to infiltrate in the lung (15). Reference-based annotation with *SingleR* (18) was used for initial classification of immune cell types in the dataset, including neutrophils. In the infected mice, we observed a dramatic increase in the relative frequency of neutrophils among $CD45^+$ immune cells in our dataset (GEO: GSE146233) (15). Among neutrophils, we identified three major neutrophil subsets, termed clusters I-III (**Figures 1A, B**). While clusters I and III were present in both naïve and infected conditions, cluster II only emerged following *Cn*-exposure (**Figures 1A, B**).

To identify potential functions of neutrophil subsets, we performed pathway enrichment analysis on cluster-specific markers (**Figures 1C, D**). Overall, total cluster I neutrophils did not exhibit very distinct marker expression, although subclusters Ic and Id showed enrichment of genes encoding antimicrobial peptide and NADPH oxidase pathways (*S100a8/9, Lyz2, Pglyrp1*). In contrast, cluster III neutrophils showed strong enrichment of Interferon signaling pathway genes (*Oasl1, Isg15, Irf9*), similar to recently described interferon stimulated genes (ISG) expressing blood neutrophil subset (23). While cluster I and III neutrophils were present in both naive and post-*Cn* instillation conditions, cluster II neutrophils were specific to the *Cn*-stimulated condition and thus are of greater interest in this study. Among cluster II neutrophils, we identified two distinct subsets. Both subclusters IIa and IIb were enriched in PRR signaling pathway genes, specifically Toll-like receptor (TLR) cascades and C-type lectin receptors (CLRs), particularly Dectin-1 signaling (**Figure 1D**). However, IIb cells showed the greatest enrichment in interleukin and cytokine signaling pathway genes (*Il1a, Csf1, Tnf*), while IIa cells showed enrichment in iron processing (*Hmox1, Hmox2*), ROS/RNS (*Atp6v1e1*), and glycolysis (*Pfkl, Gapdh*) pathway genes. Based on these markers, we named cluster IIa as oxidative-signature neutrophils (Ox-PMN) and cluster IIb as cytokine-signature neutrophils (Cyt-PMN). We hypothesize that Ox-PMN and Cyt-PMN may represent distinct neutrophil activation states triggered by acute *Cn* exposure.

To investigate whether specific neutrophil subsets reflect different stages of neutrophil maturation, we examined expression of neutrophil ageing-related markers (24), as well as granule and secretory vesicle components, which are typically expressed sequentially during neutrophil development (25). We observed enrichment of tertiary granule factors (*e.g.*, *Mmp8*) in subcluster Id neutrophils (**Figure 1E**) and markers of ageing (*e.g.*, *Icam1*) in subcluster IIb (**Figure 1F**). Subcluster Id expression of tertiary granule factors suggests these neutrophils are transitioning from the metamyelocyte stage to the band stage, and thus may be more immature neutrophils (25). In contrast, IIb (Cyt-PMN) showed elevation of genes associated with neutrophil ageing (*Cxcr4* and *Icam1*). In addition, Cyt-PMNs also showed enrichment in Bcl2 family genes (*Bcl2a1a, Bcl2a1d, Bcl2a1b*) encoding anti-apoptotic proteins and thus may facilitate or respond to neutrophil ageing.

In summary, based on single-cell transcriptional profiling, we hypothesize that acute *Cn* exposure induces two distinct neutrophil activation states: Ox-PMN (subcluster IIa) and Cyt-

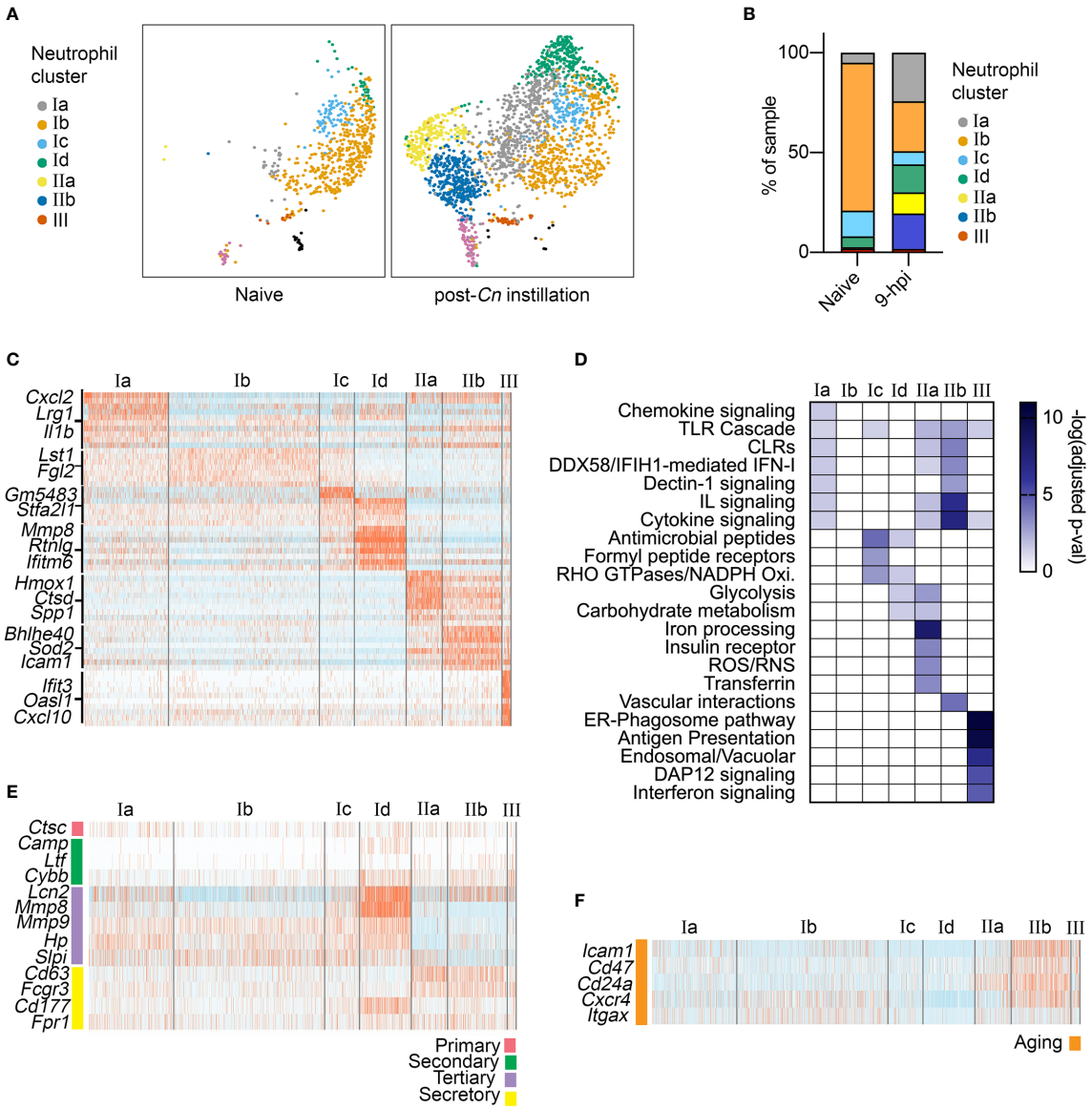

FIGURE 1 | Single-cell RNA-seq analysis of neutrophil heterogeneity following acute pulmonary *C neoformans* infection. **(A)** UMAP projection of neutrophils (611 neutrophils in naïve condition, 2,139 neutrophils at 9-hpi), colored by clusters and separated by condition. Samples were pooled from three mice per group for analysis from a single experiment. **(B)** Frequency of each neutrophil subset, comparing naïve and infected samples. **(C)** Heatmaps showing expression of subset-enriched markers. **(D)** Heatmap of -log (Adjusted p-value) for Reactome pathway enrichment in different neutrophil subsets. **(E, F)** Heatmaps showing expression of select neutrophil granule genes **(E)**, markers of aged neutrophils **(F)**.

PMN (subcluster IIb) with distinct gene expression profiles and functions. In addition, we found the Cyt-PMN are also enriched in markers of neutrophil ageing, suggesting that Cyt-PMN may be longer-lived than other neutrophil subsets profiled.

Distinct Transcription Factors Are Predicted to Regulate Ox-PMN and Cyt-PMN Subsets

To identify transcription factors (TFs) that may regulate neutrophil heterogeneity, we used single-cell regulatory network inference and clustering (SCENIC) (20). The method evaluates TFs and *cis*-regulatory sequences to predict biological states of cells. This approach involved three steps: (A) identifying groups of genes that are co-expressed with TFs ("modules"), (B) identifying predicted TF binding sites near co-expressed genes ("regulons") using motif analysis of the mouse reference genome, and (C) calculating predicted activity of candidate TF regulons across cell subsets ("regulon activity"). The majority of significant TF regulons, which were identified by SCENIC, showed increased activity particularly in cluster II neutrophils. However, IIa and IIb neutrophils (Ox-PMN and Cyt-PMN, respectively) exhibited distinct patterns in predicted activity (**Figure 2A**).

Cyt-PMN-active regulons included NFκB family TFs (encoded by *Nfkb1, Nfkb2, Rel, Relb, Rela*), which mediate neutrophil response to cytokines and PRR signaling. In contrast, Ox-PMN active regulons included small Maf (sMaf) transcription factors (encoded by *Mafk, Mafg*), as well as other TFs in the CNC and Bach families (encoded by *Bach1, Nrf1*), which form heterodimers with sMaf TFs (26). sMaf heterodimerizes with CNC or Bach and mediates cellular responses to oxidative stress (26, 27), although the function of the sMaf heterodimers remains largely uncharacterized in neutrophil biology. Based on this analysis, we hypothesize that Cyt-PMN (IIb) may be regulated by NFκB TFs, while Ox-PMN (IIa) appears to be under control of sMaf, CNC, and Bach TFs.

Ligand-Receptor Analysis Identifies Potential Neutrophil Interactions With DCs and AMs

To identify potential cell-cell communication between neutrophil subsets (Ox-PMN and Cyt-PMN) and other immune cells during *Cn* infection, we used "NicheNet" to predict ligand-receptor interactions (21). Specifically, this approach leverages prior knowledge of ligand-receptor interactions and intracellular signaling pathways to predict which ligand-receptor pairs may regulate gene expression in target cells. Our interest was in neutrophil interactions with alveolar macrophages (AMs) or dendritic cells (DCs), because these cell types are involved in modulating the immune response during the early stages of infection.

We found that Ox-PMN (IIa) express only a few unique ligands that are predicted to be detected by AMs and DCs (**Figure 2B**). Among these, the strongest potential interaction was between Alcam (Activated leukocyte adhesion molecule) on the Ox-PMN side and CD6 on the DC side. This predicted mechanism for neutrophil-DC communication has not been previously studied to our knowledge. In contrast, Cyt-PMN (IIb) expressed multiple genes encoding ligands with strong predicted interactions with both DCs and AMs. These suggested cell-cell communications *via* IL-1α and IL-1R1/IL1-

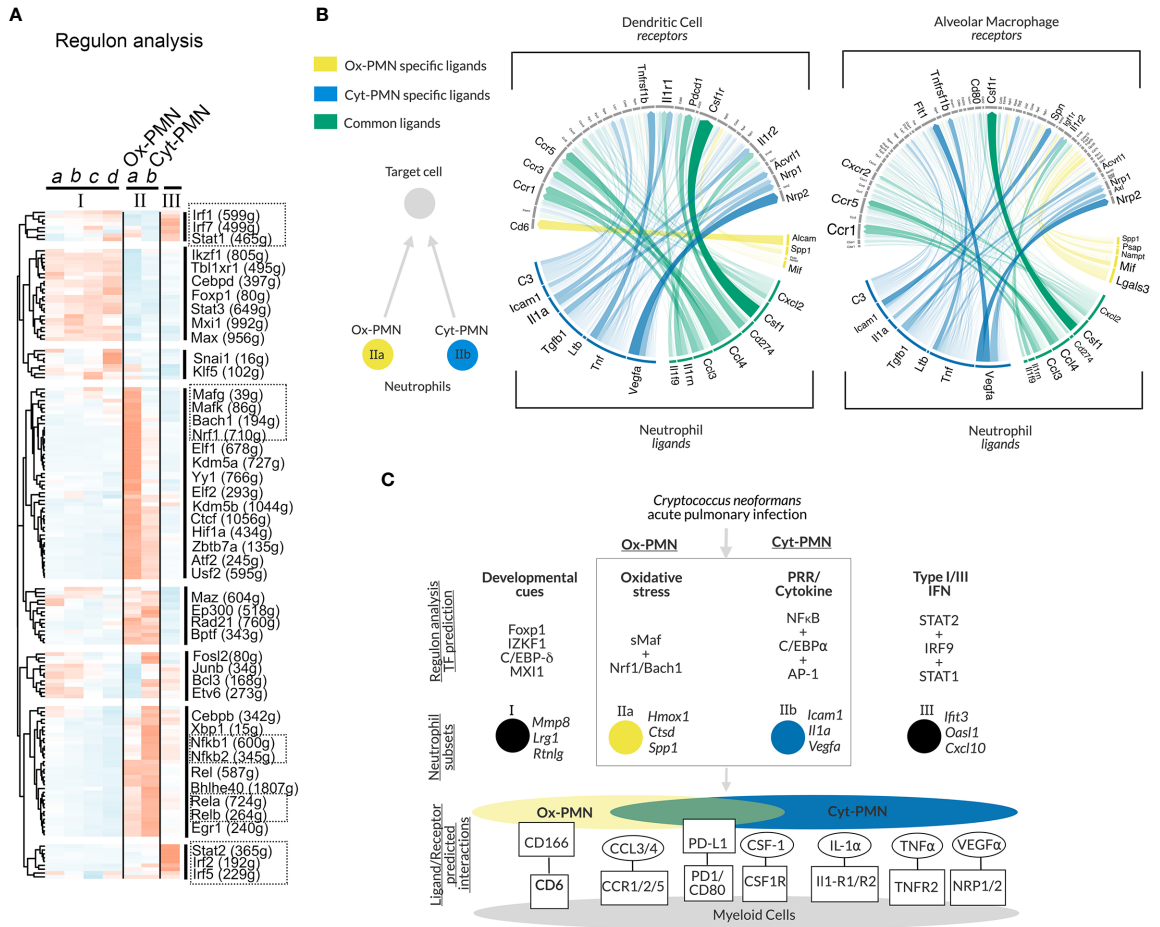

FIGURE 2 | Gene regulatory network analysis of neutrophil subsets and predicted cell-cell communication – **(A)** Heatmap of regulon activity across neutrophil subsets with hierarchical clustering of regulons displayed in dendrogram on left-hand side. Selected TFs of interest are highlighted by boxes with dotted lines. The number of predicted genes targeted by the TFs are indicated with parentheses. **(B)** Circos plot showing arrows between IIa-specific (yellow), IIb-specific (blue) or IIa/b (green) ligands and their target receptors on DCs (left panel) or AMs (right panel). Significance of potential interaction is indicated by the opacity and thickness of the connecting arrow. **(C)** Hypothesized model of neutrophil subset regulation during acute pulmonary *Cn* infection and predicted ligand/receptor interactions with other immune cells.

R2, TNFα and TNFR2, and VEGFα and NRP1/NRP2. While the role of VEGFα in *Cn* infection is less understood, both IL-1α and TNFα are important drivers of anti-fungal response to *Cn* (12). Among ligands expressed by both Cyt-PMN and Ox-PMN neutrophils, CCL3 and CCL4 are notable chemo-attractants for immune cells expressing CCR5, which is important for host immune response to *Cn* (28). Other ligand-receptor pairs identified include PD-L1 (*Cd274*) and PD-1 (*Pdcd1*), as well as CSF1 (*Csf1*) and CSF1R (*Csf1r*). The role of these ligand-receptor pairs between neutrophils and DCs (or AMs) merits further investigation.

In summary, our analysis suggests that both Cyt-PMN and Ox-PMN neutrophils express common ligands (CCL3, CCL4), which are detected by DCs and AMs through CCR5 and CCR1, respectively. However, inflammatory cytokine expression, including IL-1α and TNFα, may be specific to Cyt-PMN subset. Furthermore, Cyt-PMNs also appear to specifically express complement C3, critical for complement-mediated phagocytosis of *Cn* by DCs and other phagocytes. Thus, the Cyt-PMN subset may promote phagocytosis and anti-fungal immune responses *via* ligand-receptor interactions with other immune cells.

DISCUSSION AND HYPOTHESIS

In this study, we performed in-depth scRNA-seq analysis of a published dataset and identified multiple neutrophil subsets. Among the subsets, we focused on Ox-PMN (IIa) and Cyt-PMN (IIb), which appear after *Cn* infection and possess distinct gene expression profiles. As summarized in **Figure 2C**, our analysis suggests that Ox-PMN are regulated by sMaf, CNC, and Bach TFs, and these signaling pathways may mediate oxidative stress response and regulate oxidative burst in response to *Cn*. In contrast, the gene expression profile of Cyt-PMN is highly enriched with genes encoding NFκB signaling molecules and pro-inflammatory cytokines, IL-1α and TNFα. Based on ligand-receptor analysis, these cytokines are predicted to mediate cross-talk of Cyt-PMN with DCs and AMs. In contrast, fewer unique interactions were found between Ox-PMN-specific ligands and receptor on DCs and AMs. With our data, we hypothesize that, during acute pulmonary *Cn* infection, there is a division of labor, in which activated neutrophils become either ROS-producing Ox-PMN or cytokine-producing Cyt-PMN.

As reflected in distinct gene expression patterns, we also hypothesize that neutrophils subsets have distinct spatial localization in the lung. For example, cluster II neutrophils including Ox-PMN and Cyt-PMN are infection-specific subsets; thus, we expect that they are located in the lung parenchyma, where the subsets are exposed to *Cn* and exert subsequent immune responses. In contrast, the cluster Ib neutrophil subset showed a quiescent gene expression phenotype and were mainly identified in naïve mice. Thus, we expect the Ib subset to be mainly found in the lung vasculature. It is possible that cluster III neutrophils also localized in the lung vasculature because their IFN-signature gene expression profile is similar to a subset of steady-state neutrophils in circulation (23).

We predict that Cyt-PMN may consist of aged neutrophils based on their expression of markers of neutrophil ageing. It is also possible that Cyt-PMN further facilitate enhanced cytokine production over an extended period of time. In contrast, Ox-PMNs may reflect neutrophils which are in direct contact with or have phagocytosed *Cn* based on the pattern of highly expressed genes related to oxidative stress responses. Ox-PMNs may also be poised to undergo NETosis, triggered by ROS. To test these hypotheses, subset-specific markers and ROS indicators can be used to identify Cyt-PMN and Ox-PMN for analysis of location, maturity, interaction with *Cn*, and NETosis.

A previous study, using a *Staphylococcus aureus* infection model, identified two distinct neutrophil subsets, described as PMN-I and PMN-II with their dichotomous gene expression patterns characterized by highly expressed IL-12 and IL-10, respectively (29). However, we did not find a similar dichotomous pattern between Cyt-PMN and Ox-PMN. Instead, Ox-PMN gene expression reflects an activation state likely triggered by ROS production or exposure to ROS, while that of Cyt-PMN reflect PRR and cytokine receptor signaling to mediate NFκB-driven *Il1a* and *Tnf* production.

Although neutrophils are known to have anti-fungal functions, neutrophil depletion leads to a paradoxical increase in survival of animals in pulmonary cryptococcosis (11–13). These paradoxical results may reflect the delicate balance of heterogeneous subsets in neutrophils: Some subsets may be host-protective, and others may be host-detrimental. Thus, specific targeting of Ox-PMN and Cyt-PMN subsets may help clarify neutrophil functions during pulmonary *Cn* infection. This could be accomplished by either (A) targeting upstream transcription factors and signaling pathways predicted to regulate Ox-PMN and Cyt-PMN identity, (B) using subset-specific markers for targeted depletion studies, or (C) targeting predicted functions such as ROS-production or cytokine production in a neutrophil-specific manner. Furthermore, understanding and testing the role of cell-cell interactions between Cyt-PMNs and other myeloid cells could also clarify neutrophil function in pulmonary *Cn* infection. Beyond known pro-inflammatory cytokines such as IL-1α (*Il1a*) and TNFα (*Tnf*), we also found that both Ox-PMN and Cyt-PMN are predicted to interact with other myeloid cells through expression of PD-L1 (*Cd274*), VEGFα (*Vegfa*), and CSF1 (*Csf1*). These factors are relatively uncharacterized in neutrophils, and elucidating their roles is a novel area for investigation in neutrophil biology more broadly.

In this study, we developed a hypothesis that acute pulmonary *Cn* infection leads to distinct neutrophil activation states, which is exampled by a division of labor between ROS-producing Ox-PMN and cytokine-producing Cyt-PMN. In addition to proposing specific testable questions for investigation of neutrophils in *Cn* infection, it will also be important to understand whether this form of neutrophil heterogeneity is broadly relevant in fungal infections. In summary, our in-depth analysis of single-cell RNA sequencing of lung neutrophils provides both a detailed reference and theoretical model to guide new studies of neutrophil function in *Cn* infection.

LIMITATIONS OF STUDY

In this Hypothesis and Theory article, we analyzed single-cell transcriptional heterogeneity of neutrophils in acute *Cn* pulmonary infection and developed a theoretical framework for future investigation of neutrophil function during *Cn* infection. We acknowledge that we used three pooled mice per group for analysis without distinguishing intra-vascular from extra-vascular neutrophils in the lung. Our findings are limited to the 9-hpi timepoint. Future studies using multiple timepoints during infection, as well as validation of neutrophil phenotypes and functions, would be valuable to characterize the full dynamics of immune cell transcriptional heterogeneity in pulmonary *Cn* infection.

DATA AVAILABILITY STATEMENT

The datasets presented in this study can be found in online repositories. The names of the repository/repositories and accession number(s) can be found below: https://www.ncbi.nlm.nih.gov/, GSE146233.

ETHICS STATEMENT

The animal study was reviewed and approved by Duke University IACUC.

AUTHOR CONTRIBUTIONS

MED performed data analysis and created figures for the manuscript under the guidance of MLS. MED, EYR, SX-V, and MLS drafted, edited and revised the manuscript. All authors contributed to the article and approved the submitted version.

FUNDING

This work was supported in part by the NIH to MS (R01-AI088100), MD (F30-AI140497, T32-GM007171), and ER (T32-AI052077).

REFERENCES

1. Maziarz EK, Perfect JR. Cryptococcosis. *Infect Dis Clin North Am* (2016) 30:179–206. doi: 10.1016/j.idc.2015.10.006
2. Miller MF, Mitchell TG. Killing of Cryptococcus neoformans strains by human neutrophils and monocytes. *Infect Immun* (1991) 59:24–8. doi: 10.1128/IAI.59.1.24-28.1991
3. Zhang M, Sun D, Shi M. Dancing cheek to cheek: Cryptococcus neoformans and phagocytes. *SpringerPlus* (2015) 4:410. doi: 10.1186/s40064-015-1192-3
4. Chaturvedi V, Wong B, Newman SL. Oxidative killing of Cryptococcus neoformans by human neutrophils. Evidence that fungal mannitol protects by scavenging reactive oxygen intermediates. *J Immunol* (1996) 156:3836–40.
5. Diamond RD, Root RK, Bennet JE. Factors Influencing Killing of Cryptococcus neoformans by Human Leukocytes In Vitro. *J Infect Dis* (1972) 125:367–76. doi: 10.1093/infdis/125.4.367
6. Graybill JR, Bocanegra R, Lambros C, Luther MF. Granulocyte colony stimulating factor therapy of experimental cryptococcal meningitis. *Med Mycol* (1997) 35:243–7. doi: 10.1080/02681219780001221
7. Vecchiarelli A, Monari C, Baldelli F, Pietrella D, Retini C, Tascini C, et al. Beneficial Effect of Recombinant Human Granulocyte Colony-Stimulating Factor on Fundicidal Activity of Polymorphonuclear Leukocytes from Patients with AIDS. *J Infect Dis* (1995) 171:1448–54. doi: 10.1093/infdis/171.6.1448
8. Zhang M, Sun D, Liu G, Wu H, Zhou H, Shi M. Real-time in vivo imaging reveals the ability of neutrophils to remove Cryptococcus neoformans directly from the brain vasculature. *J Leukoc Biol* (2016) 99:467–73. doi: 10.1189/jlb.4AB0715-281R
9. Sun D, Zhang M, Liu G, Wu H, Li C, Zhou H, et al. Intravascular clearance of disseminating Cryptococcus neoformans in the brain can be improved by enhancing neutrophil recruitment in mice. *Eur J Immunol* (2016) 46:1704–14. doi: 10.1002/eji.201546239
10. Aratani Y, Kura F, Watanabe H, Akagawa H, Takano Y, Ishida-Okawara A, et al. Contribution of the myeloperoxidase-dependent oxidative system to host defence against Cryptococcus neoformans. *J Med Microbiol* (2006) 55:1291–9. doi: 10.1099/jmm.0.46620-0
11. Mednick AJ, Feldmesser M, Rivera J, Casadevall A. Neutropenia alters lung cytokine production in mice and reduces their susceptibility to pulmonary cryptococcosis. *Eur J Immunol* (2003) 33:1744–53. doi: 10.1002/eji.200323626
12. Shourian M, Ralph B, Angers I, Sheppard DC, Qureshi ST. Contribution of IL-1RI Signaling to Protection against Cryptococcus neoformans 52D in a Mouse Model of Infection. *Front Immunol* (2017) 8:1987. doi: 10.3389/fimmu.2017.01987
13. Hole CR, Lam WC, Upadhya R, Lodge JK. Cryptococcus neoformans Chitin Synthase 3 Plays a Critical Role in Dampening Host Inflammatory Responses. *mBio* (2020) 11:e03373-19. doi: 10.1128/mBio.03373-19
14. Wozniak KL, Kolls JK, Wormley FL Jr. Depletion of neutrophils in a protective model of pulmonary cryptococcosis results in increased IL-17A production by gammadelta T cells. *BMC Immunol* (2012) 13:65. doi: 10.1186/1471-2172-13-65
15. Xu-Vanpala S, Deerhake ME, Wheaton JD, Parker ME, Juvvadi PR, Maciver N, et al. Functional heterogeneity of alveolar macrophage population based on expression of CXCL2. *Sci Immunol* (2020) 5:eaba7350. doi: 10.1126/sciimmunol.aba7350
16. Stuart T, Butler A, Hoffman P, Hafemeister C, Papalexi E, Mauck WM,3, et al. Comprehensive Integration of Single-Cell Data. *Cell* (2019) 177:1888–902.e1821. doi: 10.1016/j.cell.2019.05.031
17. Hafemeister C, Satija R. Normalization and variance stabilization of single-cell RNA-seq data using regularized negative binomial regression. *Genome Biol* (2019) 20:296. doi: 10.1186/s13059-019-1874-1
18. Aran D, Looney AP, Liu L, Wu E, Fong V, Hsu A, et al. Reference-based analysis of lung single-cell sequencing reveals a transitional profibrotic macrophage. *Nat Immunol* (2019) 20:163–72. doi: 10.1038/s41590-018-0276-y
19. Yu G, He QY. ReactomePA: an R/Bioconductor package for reactome pathway analysis and visualization. *Mol Biosyst* (2016) 12:477–9. doi: 10.1039/c5mb00663e
20. Aibar S, Gonzalez-Blas CB, Moerman T, Huynh-Thu VA, Imrichova H, Hulselmans G, et al. SCENIC: single-cell regulatory network inference and clustering. *Nat Methods* (2017) 14:1083–6. doi: 10.1038/nmeth.4463
21. Browaeys R, Saelens W, Saeys Y. NicheNet: modeling intercellular communication by linking ligands to target genes. *Nat Methods* (2020) 17:159–62. doi: 10.1038/s41592-019-0667-5
22. Gu Z, Gu L, Eils R, Schlesner M, Brors B. circlize Implements and enhances circular visualization in R. *Bioinformatics* (2014) 30:2811–2. doi: 10.1093/bioinformatics/btu393
23. Xie X, Shi Q, Wu P, Zhang X, Kambara H, Su J, et al. Single-cell transcriptome profiling reveals neutrophil heterogeneity in homeostasis and infection. *Nat Immunol* (2020) 21:1119–33. doi: 10.1038/s41590-020-0736-z
24. Casanova-Acebes M, Pitaval C, Weiss LA, Nombela-Arrieta C, Chevre R, A-González N, et al. Rhythmic modulation of the hematopoietic niche through neutrophil clearance. *Cell* (2013) 153:1025–35. doi: 10.1016/j.cell.2013.04.040

25. Lawrence SM, Corriden R, Nizet V. The Ontogeny of a Neutrophil: Mechanisms of Granulopoiesis and Homeostasis. *Microbiol Mol Biol Rev* (2018) 82:e00057-17. doi: 10.1128/MMBR.00057-17
26. Zhou Y, Wu H, Zhao M, Chang C, Lu Q. The Bach Family of Transcription Factors: A Comprehensive Review. *Clin Rev Allergy Immunol* (2016) 50:345–56. doi: 10.1007/s12016-016-8538-7
27. Bugno M, Daniel M, Chepelev NL, Willmore WG. Changing gears in Nrf1 research, from mechanisms of regulation to its role in disease and prevention. *Biochim Biophys Acta* (2015) 1849:1260–76. doi: 10.1016/j.bbagrm.2015.08.001
28. Huffnagle GB, Mcneil LK, Mcdonald RA, Murphy JW, Toews GB, Maeda N, et al. Cutting edge: Role of C-C chemokine receptor 5 in organ-specific and innate immunity to Cryptococcus neoformans. *J Immunol* (1999) 163:4642–6.
29. Tsuda Y, Takahashi H, Kobayashi M, Hanafusa T, Herndon DN, Suzuki F. Three different neutrophil subsets exhibited in mice with different susceptibilities to infection by methicillin-resistant Staphylococcus aureus. *Immunity* (2004) 21:215–26. doi: 10.1016/j.immuni.2004.07.006

Conflict of Interest: The authors declare that the research was conducted in the absence of any commercial or financial relationships that could be construed as a potential conflict of interest.

frontiers in Immunology

MINI REVIEW
published: 18 June 2021
doi: 10.3389/fimmu.2021.697405

Myeloid-Derived Suppressor Cells as a Potential Biomarker and Therapeutic Target in COVID-19

Marianna Rowlands[1], *Florencia Segal*[1] *and Dominik Hartl*[2,3]*

[1] Novartis Institutes for BioMedical Research (NIBR) Translational Medicine, Cambridge, MA, United States, [2] Novartis Institutes for BioMedical Research (NIBR), Translational Medicine, Basel, Switzerland, [3] Department of Pediatrics I, University of Tübingen, Tübingen, Germany

Clinical presentations of COVID-19 are highly variable, yet the precise mechanisms that govern the pathophysiology of different disease courses remain poorly defined. Across the spectrum of disease severity, COVID-19 impairs both innate and adaptive host immune responses by activating innate immune cell recruitment, while resulting in low lymphocyte counts. Recently, several reports have shown that patients with severe COVID-19 exhibit a dysregulated myeloid cell compartment, with increased myeloid-derived suppressor cells (MDSCs) correlating with disease severity. MDSCs, in turn, promote virus survival by suppressing T-cell responses and driving a highly pro-inflammatory state through the secretion of various mediators of immune activation. Here, we summarize the evidence on MDSCs and myeloid cell dysregulation in COVID-19 infection and discuss the potential of MDSCs as biomarkers and therapeutic targets in COVID-19 pneumonia and associated disease.

Keywords: COVID-19, immunology, immunity, MDSC, biomarkers

OPEN ACCESS

Edited by:
Dragana Odobasic,
Monash University, Australia

Reviewed by:
Girdhari Lal,
National Centre for Cell Science, India
Ishak Ozel Tekin,
Bülent Ecevit University, Turkey

***Correspondence:**
Dominik Hartl
dominik.hartl@med.uni-tuebingen.de

Specialty section:
This article was submitted to Molecular Innate Immunity, a section of the journal Frontiers in Immunology

Received: *19 April 2021*
Accepted: *07 June 2021*
Published: *18 June 2021*

Citation:
Rowlands M, Segal F and Hartl D (2021) Myeloid-Derived Suppressor Cells as a Potential Biomarker and Therapeutic Target in COVID-19. Front. Immunol. 12:697405. doi: 10.3389/fimmu.2021.697405

INTRODUCTION

It has been more than a year since the initial reports of an outbreak of pneumonia in the Hubei province of China, and the subsequent identification of a novel *betacoronavirus* severe acute respiratory syndrome coronavirus 2 (SARS-CoV-2) infection as the cause for the coronavirus disease 2019 (COVID-19) (1). During this time, despite global efforts for containment and the declaration of a pandemic on March 2020, there have been more than 126 million confirmed cases of COVID-19 worldwide, and over 3.5 million deaths reported to the World Health Organization (2).

Patients with SARS-CoV-2 infection can experience a range of clinical manifestations, from no symptoms to severe pneumonia, respiratory and/or multiple organ failure (1, 3, 4). Increasing evidence suggests that the immune response to SARS-CoV2 plays a critical role in the pathogenesis of COVID-19 disease. On one end of the spectrum, SARS-CoV-2 can disrupt normal immune responses, resulting in uncontrolled inflammation in severe and critical patients with COVID-19 (5). Specifically, lung infiltration and activation of pro-inflammatory myeloid cells such as monocytes, macrophages and neutrophils, is thought to play a key role in the cytokine storm syndrome and the hyper-inflammatory response observed in severe cases (6–8). On the other hand,

adaptive immune responses elicited by emerging COVID-19 vaccines have shown to be highly protective against severe disease and mortality (9).

Understanding the immunopathology of SARS-CoV-2 can be harnessed for the identification of novel biomarkers for disease progression, as well as potential therapeutic targets for COVID-19. In this review, we summarize the characteristics of COVID-19 related dysregulation of the myeloid cell compartment, and discuss their potential use as biomarkers and future targets for therapeutic intervention.

MDSC DEFINITION AND FUNCTIONALITY

Myeloid-derived suppressor cells (MDSCs) are defined as innate bone-marrow-derived immune cells suppressing effector T cell responses (10). MDSCs are a heterogeneous population mainly composed of two distinct subtypes, neutrophilic/granulocytic MDSCs (PMN-/G-MDSCs) and monocytic MDSCs (M-MDSCs) (10, 11). Differences compared to terminally differentiated granulocytes and monocytes respectively have been previously described in detail (11) but also key differences are summarized in **Table 1**. While initial investigations focused on T cells as targets of MDSC-mediated suppression, subsequent studies expanded this concept by showing that MDSCs are able to regulate a broad variety of adaptive (T cells, B cells) and innate (natural killer cells, macrophages, dendritic cells) immune cells (12, 13). Beyond dampening immune cell functionalities, MDSCs were further found to promote the development of regulatory T cells (14) and regulatory B cells (15). The effector mechanisms employed by MDSCs to control immune cell subsets depend on the MDSC subtype with PMN-MDSCs mainly use reactive oxygen species (ROS) and arginase I, whereas M-MDSCs use inducible nitric oxide synthase (iNOS) and arginase I to dampen bystander cells. In addition to these major suppressive mechanisms, other immuno-modulatory MDSC functions have been reported, including secretion of anti-inflammatory mediators such as interleukin-10 (IL-10), transforming growth factor beta (TGF-β) or Prostaglandin E2 (PGE2) or the tryptophan/kynurenine pathway through Indoleamine 2,3 dioxygenase (IDO) (12, 13, 16).

TABLE 1 | Differences between MDSCs and other myeloid cells*.

Proposed differences between monocytes and M-MDSC	• Suppressive function • Reduced HLA-DR expression • Increased iNOS expression • Increased ARG1 expression • Increased pSTAT3 expression • Reduced IRF8 expression • Increased cEBP/b expression • Increased S100A8/9 expression • Increased IL-4R (CD124) expression
Proposed differences between neutrophils/ granulocytes and PMN-MDSC	• Suppressive function • Density (Ficoll gradients) • Increased ROS expression • Increased ARG1 expression • Increased CD33 & CD66b expression

*non-exhaustive list.

While MDSCs were discovered in malignant diseases and the majority of studies assessed MDSCs in cancer conditions, emerging evidence shows that MDSCs are more diverse and are involved in inflammation, autoimmunity and infection (17). The factors inducing MDSC accumulation and suppressive function in these disease contexts remain only partially defined, but probably include a variety of microenvironmental factors including hypoxia, Granulocyte- and Granulocyte-Macrophage Colony Stimulating Factor (G-/GM-CSF), IL-6, Tumor necrosis factor alpha (TNF-α), Vascular Endothelial Growth Factor (VEGF), IL-1β and other cytokines, chemokines, damage-associated molecular patterns (DAMPs) and alarmins, such as High mobility group box protein 1 (HMGB1) or S100A8/9 (Calprotectin), checkpoint regulators, such as PD-1/PD-L1 and pathogen-associated molecular patterns (PAMPs), such as flagellin (12, 13, 16, 18, 19). At the transcriptional level, signaling through the transcription factors signal transducer and activator of transcription 3 (STAT3) and STAT5 are key for MDSC expansion (18) (**Figure 1**) whereas transcriptional regulators such as the Inhibitor of Differentiation 1 (Id1) have also been implicated in MDSC expansion (20).

MDSCs were studied in bacterial, viral, parasitic and fungal infections (21). Most so far studied infectious disease settings provided evidence for the accumulation of MDSCs in the peripheral blood and/or the affected tissue, yet the functional role of MDSCs has been reported as both detrimental by downregulating host defense or beneficial by dampening excessive infection-associated inflammation (or other less-defined mechanisms). In some infection models, the protective *vs.* harmful role of MDSCs is rather complex and depends on the animal species/model system used, the stage of disease, and the ratio/balance between pathogens, T cells and MDSC (21–23). Another layer of complexity in host-pathogen interactions is added by the fact that MDSCs as phagocytes can directly act anti-microbial or can be exploited by intracellular pathogens as survival niche. With regards to viral infections, most evidence for MDSC involvement exists for hepatitis B/C (HBV/HCV), human immunodeficiency virus-1 (HIV-1), herpes simplex virus (HSV) or influenza with indications that chronic, rather than acute viral infections induce MDSC expansion (24–26). Intriguingly, MDSC expansion in chronic HCV infection was shown to favor viral persistence (27), whereas in HBV infection MDSC were linked to a protective role by ameliorating hepatic tissue damage (28). In HIV infections, high numbers of MDSC were reported that correlated positively with viral loads, negatively with $CD4^+$ T cell numbers and dropped upon antiviral therapy (29).

IMMUNOLOGICAL ASPECTS OF COVID-19

Despite a rapidly increasing number of publications on COVID immunopathogenesis, the precise mechanisms that govern the pathophysiology of the different disease courses of COVID-19 remain poorly defined owing to the complex multi-organ, co-

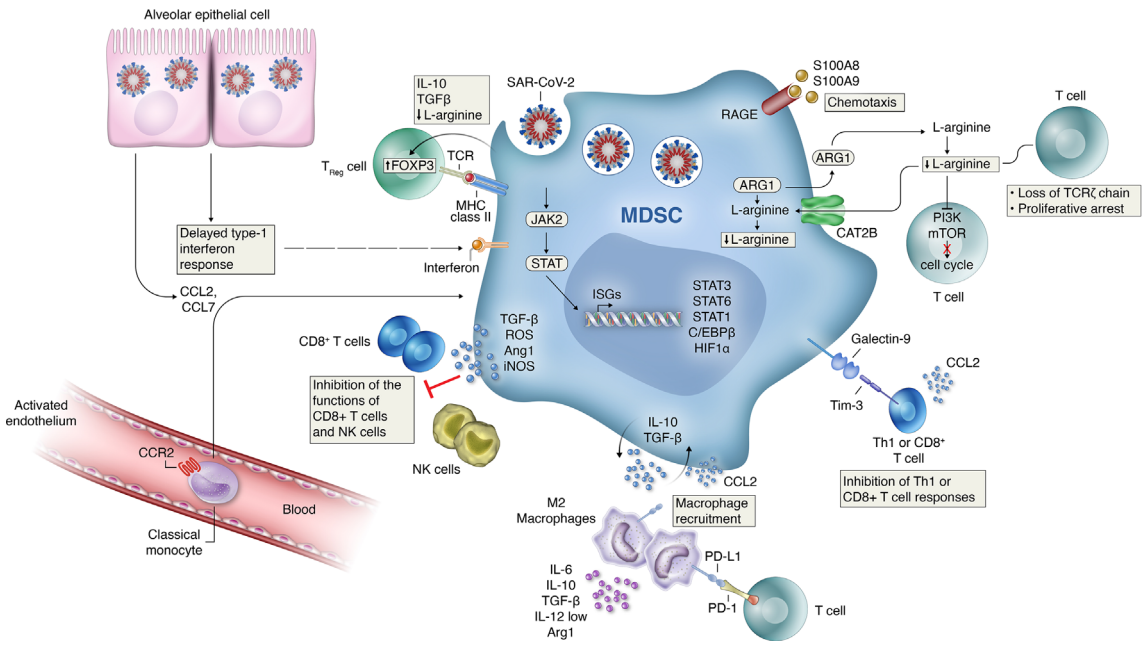

FIGURE 1 | Mechanisms of MDSC-induced immune suppression and development of hyper-inflammation activation in COVID-19. Several mechanisms likely contribute to the MDSC-induced immune suppression and development of hyper-inflammation activation seen in patients with COVID-19. Delayed production of type I interferon leading to enhanced release of monocyte chemoattractants by alveolar epithelial cells leading to sustained recruitment of MDSCs into the lungs. TGFβ and IL-10 release by MDSCs can induce further inflammatory programs in resident (M2) macrophages while recruiting inflammatory monocytes, as well as granulocytes and lymphocytes from circulation. Signaling through activation of Janus kinase (JAK)–signal transducer and activator of transcription (STAT) pathways is necessary for MDSC expansion. Increased HIF1α expression can induce the transcription of inflammation related genes. The effector mechanisms employed by MDSCs to control immune cell subsets depend on the MDSC subtype with PMN-MDSCs mainly use reactive oxygen species (ROS) and arginase I, whereas M-MDSCs use inducible nitric oxide synthase (iNOS) and arginase I to dampen bystander cells. Increased PDL1 expression on recruited macrophages and MDSCs can directly decrease antigen-specific T-cell activation through interactions with the PD-1 receptor on T-cells. Increased signaling through the Galectin-9 and Tim-3 pathway can lead to the inhibition of Th1 or CD8+ T cell responses. Increased production of TGFb, ROS and L-arginine production by MDSC can inhibit the function of NK and CD8+ T cells during disease progression. Activated MDSCs contribute to the COVID-19 cytokine storm by releasing high amounts of pro- inflammatory cytokines.

morbidity-, age- and gender-dependent host and evolving viral nature of this condition. Peripheral blood immune signatures across COVID-19 patients revealed changes in both the innate and adaptive arm of immune responses, particularly in B and myelomonocytic cell composition, profoundly altered T cell phenotypes and selective cytokine/chemokine upregulation and SARS-CoV-2-specific antibodies (30). While most studies focused their attention on T cells, more comprehensive immune profiling approaches found that in severe cases the number of T and B lymphocytes, dendritic cells, natural killer (NK) cells, and HLA-DR^{high} expressing cells were found to be substantially decreased in COVID-19 disease (31). High-dimensional flow cytometry-analysis focusing on mononuclear phagocyte (MNP) lineages in SARS-CoV-2-infected patients with moderate and severe COVID-19 identified a redistribution of monocyte subsets toward intermediate monocytes and a general decrease in circulating DCs, which coincided with the appearance of MDSCs and a higher frequency of pre-DC2. Furthermore, the presence of a MNP profile was associated with a cluster of COVID-19 non-survivors (32).

Innate immune sensing serves as the first line of antiviral defense and is essential for immunity to viruses. Coronaviruses (CoVs) have evolved several mechanisms to inhibit IFN-I induction and signaling, e.g. suppression of MAV signaling (33, 34). Patients with severe COVID-19 demonstrate remarkably impaired IFN-I signatures as compared to mild or moderate cases and fail to elicit an early IFN-I response (35–37). Perhaps timing is key, as IFN is protective early in disease but later becomes pathogenic. Furthermore, while pathogenic CoVs block IFN signaling, they may actively promote other inflammatory pathways contributing to disease pathology. Among innate immune cells, particularly neutrophil counts were found to be significantly elevated in patients with COVID-19 and correlated with disease severity (38–40). An elevated neutrophil-to-lymphocyte ratio has been further suggested as clinical marker for predicting fatal complications related to Acute Respiratory Distress Syndrome (ARDS) in patients with COVID-19 (38). Increased production of pro-inflammatory cytokines and MDSCs inversely correlated with perforin-expressing NK and CD3+ T cells during disease

progression (38, 39, 41). An early elevation in cytokine levels was associated with a maladapted immune response profile and worse disease outcomes (42). Elevated levels of cytokines, such as IP-10/CXCL10, interleukin-10 and interleukin-6, were shown to predict subsequent clinical progression (30).

There is increasing evidence to suggest that distinct innate immune responses, specifically, underlie the different clinical trajectories of COVID-19 patients and that the hyperinflammatory syndrome in severe COVID-19 results from a dysregulated host innate immune response (43). Transcriptomic, epigenomic, and proteomic analyses revealed widespread dysfunction of peripheral innate immunity in severe and fatal COVID-19, with the most profound disturbances including a prominent neutrophil hyper-activation signature and monocytes with anti-inflammatory features (7, 44, 45). Several studies have identified emergency myelopoiesis as a hallmark of severe or fatal COVID-19 (7, 45–47). Collectively, COVID-19 dysregulates both the innate and the adaptive immune system with a decrease of adaptive T cells and an increase of innate immune cell populations. However, the inter-connectedness of innate and adaptive immune changes remained largely elusive. Very recent studies provide evidence that MDSCs could represent that missing link as discussed below in detail.

MDSCs IN COVID-19

As outlined above, MDSCs are innate immune cells regulating (mostly downregulating) adaptive immune responses. MDSC activity can be enhanced by malignant or infectious triggers as described for a variety of viral, bacterial and fungal infections. Several recent reports have shown that patients with severe COVID-19 exhibit a dysregulated myeloid cell compartment, with increased MDSC levels and activity correlating with disease severity. In mild COVID-19 disease course, studies have reported an increase in HLA-$DR^{hi}CD11c^{hi}$ inflammatory monocytes with an interferon-stimulated gene signature, indicative of terminally differentiated monocytes, whereas severe COVID-19 was characterized by a lack of type I IFNs, high levels of HLA-DR^{low} classical monocytes and $CD10^{low}CD101^{-}CXCR4^{+/-}$ neutrophils with an immunosuppressive profile in blood and lungs of severe cases, suggestive of emergency myelopoiesis (7, 47–50).

In severe COVID-19 patients with ARDS an increased ratio of MDSC to CD8 effector memory T cell was observed compared to patients hospitalized for COVID-19 moderate pneumonia, with COVID-19-related MDSC expansion directly correlating with lymphopenia and enhanced arginase activity (51). Marked expansion of MDSCs was observed, up to 90% of total circulating mononuclear cells in patients with severe disease, and up to 25% in the patients with mild disease with frequency decreasing with recovery (52). Granulocytic (neutrophil, eosinophil, and basophil) markers were enriched during COVID-19 and discriminated between patients with mild and severe disease, suggestive of PMN-MDSC activity (53). Increased counts of $CD15^{+}CD16^{+}$ neutrophils, decreased granulocytic expression of integrin CD11b, and Th2-related CRTH2 downregulation in eosinophils and basophils established a COVID-19 signature. Severity was also associated with emergence of PD-L1 checkpoint expression in basophils and eosinophils (53).

In summary, COVID-19 patients show a shift towards an immature myeloid cell profile in peripheral blood together with mature monocytes and segmented neutrophils, likely the result of emergency myelopoiesis in response to the significantly elevated levels of cytokines and other pro-inflammatory mediators in these patients. As myeloid cells are the main immune cell subsets associated with severe COVID-19, identification of their inflammatory and chemotactic gene signatures could be of potential prognostic as well as therapeutic relevance (54).

MDSCs AS POTENTIAL BIOMARKER IN COVID-19

There is compelling evidence that primarily PMN-MDSC (55) but also M-MDSC subtypes accumulate in COVID-19 patients and are associated with distinct gene and protein signatures. Given the increase of circulating MDSCs in COVID-19 and a correlation with disease outcome, an obvious clinical implication is to consider their utilization as biomarkers of immune dysregulation in COVID-19.

PMN-MDSC expanded during COVID-19 in patients who required intensive care treatments, and correlated with IL-1beta, IL-6, IL-8, and TNF-alpha plasma levels (55, 56). The expression of lectin-type oxidized LDL receptor 1 (LOX-1) on PMN-MDSC, in particular, has been proposed to identify a subset of MDSCs with the most potent immunosuppressive properties, the elevation of which, was found to be more pronounced in patients with ARDS (57). Furthermore, a marked increase in Hexokinase II+ PMN-MDSC was found exclusively in the acute COVID-19 patients with moderate or severe disease (58). PMN-MDSC inhibited T-cell IFN-gamma production upon SARS-CoV-2 peptides stimulation, through TGF-beta- and iNOS-mediated mechanisms, possibly counter-acting virus elimination (55). An observed MDSC decline at convalescent phase was associated to a reduction in TGF-beta and to an increase of inflammatory cytokines in plasma samples (52). Finally, a multivariate regression analysis found a strong association between PMN-MDSC percentages and fatal disease outcome and PMN-MDSC frequencies were higher in non-survivors than survivors (55).

M-MDSCs were also found to expand in blood of COVID-19 patients, suppress T cells and strongly associate with disease severity. More specifically, a population of M-MDSC expressing high carnitine palmitoyltransferase I (CPT1a) and VDAC, were present in the PBMC of the acute COVID-19 patients and correlated with severity of disease (58). Furthermore, M-MDSC frequencies were elevated in blood but not in nasopharyngeal or endotracheal aspirates of COVID-19 patients compared to controls (59). M-MDSCs isolated from COVID-19 patients suppressed T cell proliferation and IFN-gamma production

partly *via* an arginase-1 (Arg-1) dependent mechanism. Furthermore, these patients showed increased Arg-1 and IL-6 plasma levels. COVID-19 patients had fewer T cells, and displayed downregulated expression of the CD3zeta chain (59). In related studies, T cell proliferative capacity *in vitro* was significantly reduced among COVID-19 patients and could be restored through arginine supplementation (51).

Single-cell RNA sequencing (scRNAseq) data from bronchoalveolar lavage (BAL) also revealed the presence of neutrophils and macrophages as a hallmark of severe COVID-19 (54). Among the identified gene signatures, IFITM2, IFITM1, H3F3B, SAT1, and S100A8 gene signatures were highly associated with neutrophils, while CCL8, CCL3, CCL2, KLF6, and SPP1 were associated with macrophages in severe-COVID-19 patients. These findings are in agreement with high levels of calprotectin (S100A8/S100A9) found in plasma of severe cases (47). Genes associated with the inflammatory response and chemotaxis of myeloid cells, phagocytes, and granulocytes were among the top activated functional categories in BAL from severe COVID-19-affected patients (54). A lack of type I IFNs, reduced HLA-DR in myeloid cells and transient expression of IFN-stimulated genes characterized the transcriptome of patients with severe COVID-19 (50). Similarly, in a meta-analysis of transcriptomic data, the upregulation of the monocytic compartment in severe COVID-19, was dependent on the cytokines IL-6 and IL-10, and was characterized by broadly immunosuppressive properties and decreased responsiveness to stimulation (46). Myeloid cells of severe patients showed higher expression of pro-inflammatory cytokines and chemokines such as CXCL8 (60).

ScRNAseq profiling was further used to characterize the PBMC compartment of uninfected controls and COVID-19 patients and cells in paired broncho-alveolar lavage fluid (BALF) (61). A close association of decreased DCs and increased monocytes resembling MDSCs, correlated with lymphopenia and inflammation in the blood of severe COVID-19 patients. Those MDSC-like monocytes were characterized as 'immune-paralyzed'. In contrast, monocyte-macrophages in BALFs of COVID-19 patients produced massive amounts of cytokines and chemokines, but secreted little interferons (61). In similar meta-analyses, an overall upregulation of immuno-inhibitory receptors mRNA during SARS-CoV-2 infection, expressed on both lymphoid and myeloid cells were upregulated in nasopharyngeal swabs and autopsies (e.g. BTLA, LAG3, FCGR2B, PDCD1, CEACAM1, CTLA4, CD72, and SIGLEC7), also directly correlated with viral levels (62). Integration of plasma proteomics with nine published scRNAseq datasets also revealed that disease severity in lung tissue is driven by myeloid cell phenotypes and cell-cell interactions with lung epithelial cells and T cells. Epithelial damage more specifically was associated with neutrophil infiltration (63).

Immature myeloid subsets and bronchoalveolar cells of critically-ill COVID-19 patients have been found to express HIF1alpha, a critical regulator of the differentiation and function of MDSCs, and transcriptional targets related to inflammation (CXCL8, CXCR1, CXCR2, and CXCR4); virus sensing, (TLRs); and metabolism (SLC2A3, PFKFB3, PGK1, GAPDH and SOD2) (64). The up-regulation and participation of HIF1alpha in events such as inflammation and immunometabolism make it a potential biomarker of COVID-19 severity. HIF1alpha and its transcriptionally regulated genes are also expressed in lung cells from severe COVID-19 patients, which may partially explain the hypoxia related events (64).

Calprotectin (S100A8/9) plasma level and a routine flow cytometry assay detecting decreased frequencies of non-classical monocytes have been shown to discriminate patients who develop a severe form of COVID-19, suggesting a prognostic value that deserves prospective evaluation (47). Elevated S100A-family alarmins in myeloid cells and marked enrichment of serum proteins that map to myeloid cells and pathways including cytokines, complement/coagulation, and fluid shear stress were also identified in pediatric MIS-C patients even in the absence of active infection (65). Soluble triggering receptor also expressed on myeloid cells had the best prognostic accuracy for 30-day intubation/mortality (66).

In summary, various observational retrospective investigations suggest that MDSCs, their subsets or MDSC-related markers and signatures (**Figure 1**) could serve as biomarkers for severe COVID-19 (Summarized in **Table 2**), yet prospective and multi-center biomarker-focused studies are required to (i) standardize MDSC assays used and (ii) define the prognostic and/or, if linked to therapeutic treatments, the predictive biomarker potential of MDSCs in COVID-19.

MDSCs AS POTENTIAL THERAPEUTIC TARGET IN COVID-19

Given the emerging role of MDSCs in COVID-19, another consequent question is how to therapeutically exploit and target this cell population. Based on insights from other, more established disease areas, such as oncology, therapeutic targeting of MDSCs can be achieved through different routes (16, 67): (i) drugs forcing MDSC differentiation into mature cells (e.g. vitamin D3 or retinoic acid), (ii) drugs inhibiting MDSC maturation from cellular precursors (e.g. bevacizumab, tyrosine kinase inhibitors, STAT3 inhibitors, MMP9 inhibitors), (iii) drugs reducing MDSC accumulation in peripheral organs (e.g. CXCR2/CXCR4 antagonists, 5-Flurouracil, Gemcitabine) or (iv) drugs affecting MDSC inhibitory functions (ROS scavengers, cyclooxygenase 2 (COX2) or phosphodiesterase type 5 (PDE5) inhibitors). Prostaglandin D2 (PGD2) has been proposed a key meditator of lymphopenia in COVID-19 and is known to upregulate M-MDSCs *via* the DP2 receptor signaling in group 2 innate lymphoid cells (ILC2). Targeting PGD2/DP2 signaling using a receptor antagonist such as ramatroban could be used in immunotherapy for immune dysfunction and lymphopenia in COVID-19 disease (68).

Alarmin S100A8 was robustly induced in SARS-CoV-2-infected animal models as well as in COVID-19 patients.

TABLE 2 | Candidate myeloid biomarkers associated with COVID-19 disease severity.

Proposed Biomarker	Description of COVID-19 related findings	References
Neutrophil-to-lymphocyte ratio	Increased with severity Predicting ARDS complications	(38–40)
MDSC to T-cell and NK-cell ratios	Increased with severity	(38, 39, 41, 51)
IP-10/CXCL10, interleukin-10 and interleukin-6	Increased with severity Prognostic markers	(30)
HLA-DR^{high} expressing cells	Decreased with disease severity	(31)
IFN-I signature	Downregulated with severity	(35–37)
HLA-DR^{low} classical monocytes	Increased with severity	(7, 47–50)
CD10^{low}CD101^{-}CXCR4$^{+/-}$ neutrophils	Increased with severity	(7, 47–50)
LOX-1 on PMN-MDSC	Increased with ARDS	(57)
Hexokinase II+ PMN-MDSC	Increased with severity	(58)
CD15^{+}CD16^{+} CD11b^{low} neutrophils	Increased with severity	(53)
TGF-beta plasma levels	Increased with severity	(52) (55)
Arg-1 and IL-6 plasma levels	Increased with severity	(59)
M-MDSC expressing high CPT1a and VDAC	Increased with severity	(58)
HIF1-alpha expression	Upregulation with severity	(64)
Calprotectin (S100A8/9) plasma level	Prognostic marker for severe disease	(47)
Soluble triggering receptor	Prognostic marker for intubation/mortality	(66)

Paquinimod, a specific inhibitor of S100A8/A9, could rescue the pneumonia with substantial reduction of viral loads in SARS-CoV-2-infected mice (69). A group of neutrophils that contributes to the uncontrolled pathological damage and onset of COVID-19 was induced by coronavirus infection. Paquinimod treatment could reduce these neutrophils and regain anti-viral responses, unveiling key roles of S100A8/A9 and aberrant neutrophils in the pathogenesis of COVID-19 and highlighting new opportunities for therapeutic intervention (69).

Therapeutic strategies targeting the migration/recruitment of myeloid cells from bone marrow as mentioned above could be considered for the treatment of COVID-19 induced hyper-inflammation and immune dysregulation (39). Inhibitors of CXCR2 or CCR2 and CCR5 may be able to reduce mobilization and migration of MDSC from the bone marrow to the circulation (70, 71). Following compassionate care treatment with the CCR5 blocking antibody leronlimab, a rapid reduction of plasma IL-6, restoration of the CD4/CD8 ratio, and a significant decrease in SARS-CoV-2 plasma viremia was observed. Consistent with reduction of plasma IL-6, single-cell RNA-sequencing also revealed declines in transcriptomic myeloid cell clusters expressing IL-6 and interferon-related genes (72).

Given the expression of inhibitory receptor upregulation observed in a variety of cell subsets during the progression of COVID-19 (62), targeting immuno-inhibitory receptors could also represent an effective therapeutic approach for the treatment of COVID-19 early and reversal of late immune dysregulation and suppression (73). Finally, reprogramming MDSCs by targeting immunometabolism and epigenetics may also holds promise in resolving lung inflammation associated with COVID-19 (74). As patients with severe COVID-19 have an increased inflammatory response that depletes arginine, and subsequently impairs T cell function, inhibition of arginase-1 and/or replenishment of arginine may be a potential future therapeutic approach in preventing/treating severe COVID-19 (75). Furthermore, the fatty acid transport protein 2 (FATP2), responsible for the uptake of arachidonic acid and for the subsequent synthesis of PGE2 was identified as a regulator of the suppressive functions of PMN-MDSCs (76). IDO dependent tryptophan metabolism is another pathway used by MDSCs to inhibit immune responses (77). Targeting metabolic mediators as FATP2 or enzymes such as IDO may be able to reverse MDSC induced suppression of virus-specific T-cell responses seen in severe COVID-19 cases.

Regarding potential targeting of MDSCs in COVID-19, it is essential to define the disease stage and disease severity level where such a therapeutic approach might have the greatest potential and would be beneficial rather than harmful to disease outcome. This consideration is key, as, in analogy to other viral infections (24–26). MDSCs may play a pathogenic or protective role depending on the time-course, pathogen load and severity of the individual disease condition. Given the COVID-19-associated lymphopenia, MDSCs were proposed as causal culprits to decrease T cells and thereby impair T cell-mediated host defense (**Figure 1**). On the other hand, MDSCs are capable of dampen overshooting tissue inflammation and might be beneficial at certain stages of disease. Therapeutic targeting would make sense at stages where MDSCs cause more harm than good and it is key to first identify those stages precisely.

CONCLUSIONS

COVID-19 activates the innate immune system and suppresses adaptive T cell responses. MDSCs are key cellular players connecting innate and adaptive immunity. Both M-MDSCs and PMN-MDSCs accumulate in patients with COVID-19 and reflect disease outcome, but what does this mean for the future of COVID-19 diagnosis, monitoring and treatment? Currently,

inflammation, cell-death- and coagulation-associated serum proteins such as CrP, LDH and IL-6 as well as D-Dimers are used to characterize COVID-19 severity and disease progression clinically; it remains to be assessed how MDSC frequencies in peripheral blood and/or airway fluids relate to these clinical serum markers and whether combined/composite biomarker scores composed of both serum proteins and cells (PMN-MDSCs and/or M-MDSCs) could be superior than clinical serum markers alone to monitor and predict the outcome and treatment response in COVID-19. Targeting MDSCs as future therapeutic approach in COVID-19 is farer away, yet could add substantial value, particularly in combination with other immunomodulatory drugs, such as cytokine blockers.

AUTHOR CONTRIBUTIONS

MR contributed to manuscript research and writing. FS contributed to manuscript research and writing. DH contributed to manuscript research and writing. All authors contributed to the article and approved the submitted version.

ACKNOWLEDGMENTS

We wish to thank Alan Abrams, Novartis Institutes for BioMedical Research (Cambridge, USA) for contributing the scientific artwork for **Figure 1**.

REFERENCES

1. Zhou F, Yu T, Du R, Fan G, Liu Y, Liu Z, et al. Clinical Course and Risk Factors for Mortality of Adult Inpatients With COVID-19 in Wuhan, China: A Retrospective Cohort Study. *Lancet* (2020) 395(10229):1054–62. doi: 10.1016/S0140-6736(20)30566-3
2. W. H. O. *Covid-19: World Health Organization*. (2021). Available at: https://www.who.int/.
3. Manson JJ, Crooks C, Naja M, Ledlie A, Goulden B, Liddle T, et al. Covid-19-associated Hyperinflammation and Escalation of Patient Care: A Retrospective Longitudinal Cohort Study. *Lancet Rheumatol* (2020) 2(10): e594–602. doi: 10.1016/S2665-9913(20)30275-7
4. Wiersinga WJ, Rhodes A, Cheng AC, Peacock SJ, Prescott HC. Pathophysiology, Transmission, Diagnosis, and Treatment of Coronavirus Disease 2019 (Covid-19): A Review. *JAMA* (2020) 324(8):782–93. doi: 10.1001/jama.2020.12839
5. Berlin DA, Gulick RM, Martinez FJ. Severe Covid-19. *N Engl J Med* (2020) 383(25):2451–60. doi: 10.1056/NEJMcp2009575
6. Gomez-Rial J, Rivero-Calle I, Salas A, Martinon-Torres F. Role of Monocytes/Macrophages in Covid-19 Pathogenesis: Implications for Therapy. *Infect Drug Resist* (2020) 13:2485–93. doi: 10.2147/IDR.S258639
7. Schulte-Schrepping J, Reusch N, Paclik D, Bassler K, Schlickeiser S, Zhang B, et al. Severe COVID-19 Is Marked by a Dysregulated Myeloid Cell Compartment. *Cell* (2020) 182(6):1419–40.e23. doi: 10.1016/j.cell.2020.08.001
8. Merad M, Martin JC. Pathological Inflammation in Patients With COVID-19: A Key Role for Monocytes and Macrophages. *Nat Rev Immunol* (2020) 20 (6):355–62. doi: 10.1038/s41577-020-0331-4
9. Forni G, Mantovani AR. Covid-19 Commission of Accademia Nazionale dei Lincei. Covid-19 Vaccines: Where We Stand and Challenges Ahead. *Cell Death Differ* (2021) 28(2):626–39. doi: 10.1038/s41418-020-00720-9
10. Gabrilovich DI, Nagaraj S. Myeloid-Derived Suppressor Cells as Regulators of the Immune System. *Nat Rev Immunol* (2009) 9(3):162–74. doi: 10.1038/nri2506
11. Bronte V, Brandau S, Chen SH, Colombo MP, Frey AB, Greten TF, et al. Recommendations for Myeloid-Derived Suppressor Cell Nomenclature and Characterization Standards. *Nat Commun* (2016) 7:12150. doi: 10.1038/ncomms12150
12. Ostrand-Rosenberg S, Fenselau C. Myeloid-Derived Suppressor Cells: Immune-Suppressive Cells That Impair Antitumor Immunity and Are Sculpted by Their Environment. *J Immunol* (2018) 200(2):422–31. doi: 10.4049/jimmunol.1701019
13. Veglia F, Perego M, Gabrilovich D. Myeloid-Derived Suppressor Cells Coming of Age. *Nat Immunol* (2018) 19(2):108–19. doi: 10.1038/s41590-017-0022-x
14. Serafini P, Mgebroff S, Noonan K, Borrello I. Myeloid-Derived Suppressor Cells Promote Cross-Tolerance in B-Cell Lymphoma by Expanding Regulatory T Cells. *Cancer Res* (2008) 68(13):5439–49. doi: 10.1158/0008-5472.CAN-07-6621
15. Sarvaria A, Madrigal JA, Saudemont A. B Cell Regulation in Cancer and Anti-Tumor Immunity. *Cell Mol Immunol* (2017) 14(8):662–74. doi: 10.1038/cmi.2017.35
16. Veglia F, Sanseviero E, Gabrilovich DI. Myeloid-Derived Suppressor Cells in the Era of Increasing Myeloid Cell Diversity. *Nat Rev Immunol* (2021) 2:1–14. doi: 10.1038/s41577-020-00490-y
17. Pawelec G, Verschoor CP, Ostrand-Rosenberg S. Myeloid-Derived Suppressor Cells: Not Only in Tumor Immunity. *Front Immunol* (2019) 10:1099. doi: 10.3389/fimmu.2019.01099
18. Condamine T, Gabrilovich DI. Molecular Mechanisms Regulating Myeloid-Derived Suppressor Cell Differentiation and Function. *Trends Immunol* (2011) 32(1):19–25. doi: 10.1016/j.it.2010.10.002
19. Rieber N, Brand A, Hector A, Graepler-Mainka U, Ost M, Schafer I, et al. Flagellin Induces Myeloid-Derived Suppressor Cells: Implications for Pseudomonas Aeruginosa Infection in Cystic Fibrosis Lung Disease. *J Immunol* (2013) 190(3):1276–84. doi: 10.4049/jimmunol.1202144
20. Papaspyridonos M, Matei I, Huang Y, do Rosario Andre M, Brazier-Mitouart H, Waite JC, et al. Id1 Suppresses Anti-Tumour Immune Responses and Promotes Tumour Progression by Impairing Myeloid Cell Maturation. *Nat Commun* (2015) 6:6840. doi: 10.1038/ncomms7840
21. Medina E, Hartl D. Myeloid-Derived Suppressor Cells in Infection: A General Overview. *J Innate Immun* (2018) 10(5-6):407–13. doi: 10.1159/000489830
22. Dorhoi A, Du Plessis N. Monocytic Myeloid-Derived Suppressor Cells in Chronic Infections. *Front Immunol* (2017) 8:1895. doi: 10.3389/fimmu.2017.01895
23. Ost M, Singh A, Peschel A, Mehling R, Rieber N, Hartl D. Myeloid-Derived Suppressor Cells in Bacterial Infections. *Front Cell Infect Microbiol* (2016) 6:37. doi: 10.3389/fcimb.2016.00037
24. Goh C, Narayanan S, Hahn YS. Myeloid-Derived Suppressor Cells: The Dark Knight or the Joker in Viral Infections? *Immunol Rev* (2013) 255(1):210–21. doi: 10.1111/imr.12084
25. Norris BA, Uebelhoer LS, Nakaya HI, Price AA, Grakoui A, Pulendran B. Chronic But Not Acute Virus Infection Induces Sustained Expansion of Myeloid Suppressor Cell Numbers That Inhibit Viral-Specific T Cell Immunity. *Immunity* (2013) 38(2):309–21. doi: 10.1016/j.immuni.2012.10.022
26. O'Connor MA, Rastad JL, Green WR. The Role of Myeloid-Derived Suppressor Cells in Viral Infection. *Viral Immunol* (2017) 30(2):82–97. doi: 10.1089/vim.2016.0125
27. Tacke RS, Lee HC, Goh C, Courtney J, Polyak SJ, Rosen HR, et al. Myeloid Suppressor Cells Induced by Hepatitis C Virus Suppress T-Cell Responses Through the Production of Reactive Oxygen Species. *Hepatology* (2012) 55 (2):343–53. doi: 10.1002/hep.24700
28. Pallett LJ, Gill US, Quaglia A, Sinclair LV, Jover-Cobos M, Schurich A, et al. Metabolic Regulation of Hepatitis B Immunopathology by Myeloid-Derived Suppressor Cells. *Nat Med* (2015) 21(6):591–600. doi: 10.1038/nm.3856
29. Vollbrecht T, Stirner R, Tufman A, Roider J, Huber RM, Bogner JR, et al. Chronic Progressive HIV-1 Infection Is Associated With Elevated Levels of Myeloid-Derived Suppressor Cells. *AIDS* (2012) 26(12):F31–7. doi: 10.1097/QAD.0b013e328354b43f
30. Laing AG, Lorenc A, Del Molino Del Barrio I, Das A, Fish M, Monin L, et al. A Dynamic COVID-19 Immune Signature Includes Associations With Poor Prognosis. *Nat Med* (2020) 26(10):1623–35. doi: 10.1038/s41591-020-1038-6

31. Matic S, Popovic S, Djurdjevic P, Todorovic D, Djordjevic N, Mijailovic Z, et al. Sars-CoV-2 Infection Induces Mixed M1/M2 Phenotype in Circulating Monocytes and Alterations in Both Dendritic Cell and Monocyte Subsets. *PloS One* (2020) 15(12):e0241097. doi: 10.1371/journal.pone.0241097
32. Kvedaraite E, Hertwig L, Sinha I, Ponzetta A, Hed Myrberg I, Lourda M, et al. Major Alterations in the Mononuclear Phagocyte Landscape Associated With COVID-19 Severity. *Proc Natl Acad Sci USA* (2021) 118(6):1–12. doi: 10.1073/pnas.2018587118
33. Shi CS, Qi HY, Boularan C, Huang NN, Abu-Asab M, Shelhamer JH, et al. SARS-Coronavirus Open Reading Frame-9b Suppresses Innate Immunity by Targeting Mitochondria and the MAVS/TRAF3/TRAF6 Signalosome. *J Immunol* (2014) 193(6):3080–9. doi: 10.4049/jimmunol.1303196
34. Gordon DE, Jang GM, Bouhaddou M, Xu J, Obernier K, O'Meara MJ, et al. A SARS-CoV-2-Human Protein-Protein Interaction Map Reveals Drug Targets and Potential Drug-Repurposing. *bioRxiv* (2020). doi: 10.1101/2020.03.22.002386
35. Bastard P, Rosen LB, Zhang Q, Michailidis E, Hoffmann HH, Zhang Y, et al. Autoantibodies Against Type I IFNs in Patients With Life-Threatening COVID-19. *Science* (2020) 370(6515):1–13. doi: 10.1126/science.abd4585
36. Hadjadj J, Yatim N, Barnabei L, Corneau A, Boussier J, Smith N, et al. Impaired Type I Interferon Activity and Inflammatory Responses in Severe COVID-19 Patients. *Science* (2020) 369(6504):718–24. doi: 10.1126/science.abc6027
37. Channappanavar R, Fehr AR, Vijay R, Mack M, Zhao J, Meyerholz DK, et al. Dysregulated Type I Interferon and Inflammatory Monocyte-Macrophage Responses Cause Lethal Pneumonia in SARS-CoV-Infected Mice. *Cell Host Microbe* (2016) 19(2):181–93. doi: 10.1016/j.chom.2016.01.007
38. Chiang CC, Korinek M, Cheng WJ, Hwang TL. Targeting Neutrophils to Treat Acute Respiratory Distress Syndrome in Coronavirus Disease. *Front Pharmacol* (2020) 11:572009. doi: 10.3389/fphar.2020.572009
39. Mann ER, Menon M, Knight SB, Konkel JE, Jagger C, Shaw TN, et al. Longitudinal Immune Profiling Reveals Key Myeloid Signatures Associated With COVID-19. *Sci Immunol* (2020) 5(51):1–11. doi: 10.1126/sciimmunol.abd6197
40. Godkin A, Humphreys IR. Elevated interleukin-6, interleukin-10 and Neutrophil : Lymphocyte Ratio as Identifiers of Severe Coronavirus Disease 2019. *Immunology* (2020) 160(3):221–2. doi: 10.1111/imm.13225
41. Tomic S, Dokic J, Stevanovic D, Ilic N, Gruden-Movsesijan A, Dinic M, et al. Reduced Expression of Autophagy Markers and Expansion of Myeloid-Derived Suppressor Cells Correlate With Poor T Cell Response in Severe Covid-19 Patients. *Front Immunol* (2021) 12:614599. doi: 10.3389/fimmu.2021.614599
42. Lucas C, Wong P, Klein J, Castro TBR, Silva J, Sundaram M, et al. Longitudinal Analyses Reveal Immunological Misfiring in Severe COVID-19. *Nature* (2020) 584(7821):463–9. doi: 10.1038/s41586-020-2588-y
43. Gustine JN, Jones D. Immunopathology of Hyperinflammation in COVID-19. *Am J Pathol* (2021) 191(1):4–17. doi: 10.1016/j.ajpath.2020.08.009
44. Cicco S, Cicco G, Racanelli V, Vacca A. Neutrophil Extracellular Traps (Nets) and Damage-Associated Molecular Patterns (Damps): Two Potential Targets for COVID-19 Treatment. *Mediators Inflamm* (2020) 2020:7527953. doi: 10.1155/2020/7527953
45. Wilk AJ, Lee MJ, Wei B, Parks B, Pi R, Martínez-Colón GJ, et al. Multi-Omic Profiling Reveals Widespread Dysregulation of Innate Immunity and Hematopoiesis in COVID-19. *bioRxiv* (2020) 2020:12.18.423363. doi: 10.1101/2020.12.18.423363
46. Reyes M, Filbin MR, Bhattacharyya RP, Sonny A, Mehta A, Billman K, et al. Induction of a Regulatory Myeloid Program in Bacterial Sepsis and Severe COVID-19. *bioRxiv* (2020). doi: 10.1101/2020.09.02.280180
47. Silvin A, Chapuis N, Dunsmore G, Goubet AG, Dubuisson A, Derosa L, et al. Elevated Calprotectin and Abnormal Myeloid Cell Subsets Discriminate Severe From Mild Covid-19. *Cell* (2020) 182(6):1401–18.e18. doi: 10.1016/j.cell.2020.08.002
48. Peruzzi B, Bencini S, Capone M, Mazzoni A, Maggi L, Salvati L, et al. Quantitative and Qualitative Alterations of Circulating Myeloid Cells and Plasmacytoid DC in SARS-CoV-2 Infection. *Immunology* (2020) 161(4):345–53. doi: 10.1111/imm.13254
49. Benlyamani I, Venet F, Coudereau R, Gossez M, Monneret G. Monocyte HLA-DR Measurement by Flow Cytometry in COVID-19 Patients: An Interim Review. *Cytometry A* (2020) 97(12):1217–21. doi: 10.1002/cyto.a.24249
50. Arunachalam PS, Wimmers F, Mok CKP, Perera R, Scott M, Hagan T, et al. Systems Biological Assessment of Immunity to Mild Versus Severe COVID-19 Infection in Humans. *Science* (2020) 369(6508):1210–20. doi: 10.1126/science.abc6261
51. Reizine F, Lesouhaitier M, Gregoire M, Pinceaux K, Gacouin A, Maamar A, et al. SARS-Cov-2-Induced ARDS Associates With MDSC Expansion, Lymphocyte Dysfunction, and Arginine Shortage. *J Clin Immunol* (2021) 41:515–25. doi: 10.1007/s10875-020-00920-5
52. Agrati C, Sacchi A, Bordoni V, Cimini E, Notari S, Grassi G, et al. Expansion of Myeloid-Derived Suppressor Cells in Patients With Severe Coronavirus Disease (COVID-19). *Cell Death Differ* (2020) 27(11):3196–207. doi: 10.1038/s41418-020-0572-6
53. Vitte J, Diallo AB, Boumaza A, Lopez A, Michel M, Allardet-Servent J, et al. A Granulocytic Signature Identifies Covid-19 and Its Severity. *J Infect Dis* (2020) 222(12):1985–96. doi: 10.1093/infdis/jiaa591
54. Shaath H, Vishnubalaji R, Elkord E, Alajez NM. Single-Cell Transcriptome Analysis Highlights a Role for Neutrophils and Inflammatory Macrophages in the Pathogenesis of Severe Covid-19. *Cells* (2020) 9(11):1–19. doi: 10.3390/cells9112374
55. Sacchi A, Grassi G, Bordoni V, Lorenzini P, Cimini E, Casetti R, et al. Early Expansion of Myeloid-Derived Suppressor Cells Inhibits SARS-CoV-2 Specific T-cell Response and may Predict Fatal COVID-19 Outcome. *Cell Death Dis* (2020) 11(10):921. doi: 10.1038/s41419-020-03125-1
56. Takano T, Matsumura T, Adachi Y, Terahara K, Moriyama S, Onodera T, et al. Myeloid Cell Dynamics Correlating With Clinical Outcomes of Severe COVID-19 in Japan. *Int Immunol* (2021) 33(4):241–7. doi: 10.1093/intimm/dxab005
57. Coudereau R, Waeckel L, Cour M, Rimmele T, Pescarmona R, Fabri A, et al. Emergence of Immunosuppressive LOX-1+ Pmn-MDSC in Septic Shock and Severe COVID-19 Patients With Acute Respiratory Distress Syndrome. *J Leukoc Biol* (2021) 28:1–8. doi: 10.1002/JLB.4COVBCR0321-129R
58. Thompson E, Cascino K, Ordonez A, Zhou W, Vaghasia A, Hamacher-Brady A, et al. Mitochondrial Induced T Cell Apoptosis and Aberrant Myeloid Metabolic Programs Define Distinct Immune Cell Subsets During Acute and Recovered SARS-CoV-2 Infection. *medRxiv* (2020). doi: 10.1101/2020.09.10.20186064
59. Falck-Jones S, Vangeti S, Yu M, Falck-Jones R, Cagigi A, Badolati I, et al. Functional Monocytic Myeloid-Derived Suppressor Cells Increase in Blood But Not Airways and Predict COVID-19 Severity. *J Clin Invest* (2021) 131:1–15. doi: 10.1172/JCI144734
60. Park JH, Lee HK. Re-Analysis of Single Cell Transcriptome Reveals That the NR3C1-CXCL8-Neutrophil Axis Determines the Severity of COVID-19. *Front Immunol* (2020) 11:2145. doi: 10.3389/fimmu.2020.02145
61. Xu G, Qi F, Li H, Yang Q, Wang H, Wang X, et al. The Differential Immune Responses to COVID-19 in Peripheral and Lung Revealed by Single-Cell RNA Sequencing. *Cell Discovery* (2020) 6:73. doi: 10.1038/s41421-020-00225-2
62. Sharif-Askari NS, Sharif-Askari FS, Mdkhana B, Al Heialy S, Alsafar HS, Hamoudi R, et al. Enhanced Expression of Immune Checkpoint Receptors During SARS-CoV-2 Viral Infection. *Mol Ther Methods Clin Dev* (2020) 20:109–21. doi: 10.1016/j.omtm.2020.11.002
63. Filbin MR, Mehta A, Schneider AM, Kays KR, Guess JR, Gentili M, et al. Plasma Proteomics Reveals Tissue-Specific Cell Death and Mediators of Cell-Cell Interactions in Severe COVID-19 Patients. *bioRxiv* (2020). doi: 10.1101/2020.11.02.365536
64. Taniguchi-Ponciano K, Vadillo E, Mayani H, Gonzalez-Bonilla CR, Torres J, Majluf A, et al. Increased Expression of Hypoxia-Induced Factor 1alpha mRNA and its Related Genes in Myeloid Blood Cells From Critically Ill COVID-19 Patients. *Ann Med* (2021) 53(1):197–207. doi: 10.1080/07853890.2020.1858234
65. Ramaswamy A, Brodsky NN, Sumida TS, Comi M, Asashima H, Hoehn KB, et al. Post-Infectious Inflammatory Disease in MIS-C Features Elevated Cytotoxicity Signatures and Autoreactivity That Correlates With Severity. *medRxiv* (2020). doi: 10.1101/2020.12.01.20241364
66. Van Singer M, Brahier T, Ngai M, Wright J, Weckman AM, Erice C, et al. Covid-19 Risk Stratification Algorithms Based on sTREM-1 and IL-6 in

Emergency Department. *J Allergy Clin Immunol* (2020). doi: 10.1016/j.jaci.2020.10.001
67. Ugel S, Delpozzo F, Desantis G, Papalini F, Simonato F, Sonda N, et al. Therapeutic Targeting of Myeloid-Derived Suppressor Cells. *Curr Opin Pharmacol* (2009) 9(4):470–81. doi: 10.1016/j.coph.2009.06.014
68. Gupta A, Chander Chiang K. Prostaglandin D2 as a Mediator of Lymphopenia and a Therapeutic Target in COVID-19 Disease. *Med Hypotheses* (2020) 143:110122. doi: 10.1016/j.mehy.2020.110122
69. Guo Q, Zhao Y, Li J, Liu J, Yang X, Guo X, et al. Induction of Alarmin S100A8/A9 Mediates Activation of Aberrant Neutrophils in the Pathogenesis of COVID-19. *Cell Host Microbe* (2020) 29(2):222–35.E4. doi: 10.1016/j.chom.2020.12.016
70. Stadtmann A, Zarbock A. Cxcr2: From Bench to Bedside. *Front Immunol* (2012) 3:263. doi: 10.3389/fimmu.2012.00263
71. Lu Z, Zou J, Li S, Topper MJ, Tao Y, Zhang H, et al. Epigenetic Therapy Inhibits Metastases by Disrupting Premetastatic Niches. *Nature* (2020) 579 (7798):284–90. doi: 10.1038/s41586-020-2054-x
72. Patterson BK, Seethamraju H, Dhody K, Corley MJ, Kazempour K, Lalezari JP, et al. Disruption of the CCL5/RANTES-CCR5 Pathway Restores Immune Homeostasis and Reduces Plasma Viral Load in Critical Covid-19. *medRxiv* (2020). doi: 10.1101/2020.05.02.20084673
73. Gruber CN, Patel RS, Trachtman R, Lepow L, Amanat F, Krammer F, et al. Mapping Systemic Inflammation and Antibody Responses in Multisystem Inflammatory Syndrome in Children (Mis-C). *Cell* (2020) 183(4):982–95.e14. doi: 10.1016/j.cell.2020.09.034
74. D'Alessio FR, Heller NM. Covid-19 and Myeloid Cells: Complex Interplay Correlates With Lung Severity. *J Clin Invest* (2020) 130(12):6214–7. doi: 10.1172/JCI143361
75. Dean MJ, Ochoa JB, Sanchez-Pino M, Zabaleta J, Garai J, Del Valle L, et al. Transcriptome and Functions of Granulocytic Myeloid-Derived Suppressor Cells Determine Their Association With Disease Severity of COVID-19. *medRxiv* (2021). doi: 10.1101/2021.03.26.21254441
76. Veglia F, Tyurin VA, Blasi M, De Leo A, Kossenkov AV, Donthireddy L, et al. Fatty Acid Transport Protein 2 Reprograms Neutrophils in Cancer. *Nature* (2019) 569(7754):73–8. doi: 10.1038/s41586-019-1118-2
77. Platten M, Nollen EAA, Rohrig UF, Fallarino F, Opitz CA. Tryptophan Metabolism as a Common Therapeutic Target in Cancer, Neurodegeneration and Beyond. *Nat Rev Drug Discovery* (2019) 18(5):379–401. doi: 10.1038/s41573-019-0016-5

Conflict of Interest: Authors MR, FS and DH were employed by the company Novartis.

frontiers in Immunology

ORIGINAL RESEARCH
published: 15 July 2021
doi: 10.3389/fimmu.2021.682094

H3K4me3 Histone ChIP-Seq Analysis Reveals Molecular Mechanisms Responsible for Neutrophil Dysfunction in HIV-Infected Individuals

Paweł Piatek[1†], Maciej Tarkowski[2†], Magdalena Namiecinska[1], Agostino Riva[2], Marek Wieczorek[3], Sylwia Michlewska[4], Justyna Dulska[5], Małgorzata Domowicz[1], Małgorzata Kulińska-Michalska[6], Natalia Lewkowicz[6] and Przemysław Lewkowicz[1]*

[1] Department of Neurology, Laboratory of Neuroimmunology, Medical University of Lodz, Lodz, Poland, [2] Department of Biomedical and Clinical Sciences, 'Luigi Sacco', University of Milan, Milan, Italy, [3] Department of Neurobiology, Faculty of Biology and Environmental Protection, University of Lodz, Lodz, Poland, [4] Laboratory of Microscopic Imaging and Specialized Biological Techniques, Faculty of Biology and Environmental Protection, University of Lodz, Lodz, Poland, [5] Genomed SA, Warsaw, Poland, [6] Department of Periodontology and Oral Mucosal Diseases, Medical University of Lodz, Lodz, Poland

OPEN ACCESS

Edited by:
Dragana Odobasic, Monash University, Australia

Reviewed by:
Olivier Binda, Université Claude Bernard Lyon 1, France
Mihaela Gadjeva, Harvard Medical School, United States

***Correspondence:**
Przemysław Lewkowicz
przemyslaw.lewkowicz@umed.lodz.pl

[†]These authors have contributed equally to this work

Specialty section:
This article was submitted to Molecular Innate Immunity, a section of the journal Frontiers in Immunology

Received: *17 March 2021*
Accepted: *25 May 2021*
Published: *15 July 2021*

Citation:
Piatek P, Tarkowski M, Namiecinska M, Riva A, Wieczorek M, Michlewska S, Dulska J, Domowicz M, Kulińska-Michalska M, Lewkowicz N and Lewkowicz P (2021) H3K4me3 Histone ChIP-Seq Analysis Reveals Molecular Mechanisms Responsible for Neutrophil Dysfunction in HIV-Infected Individuals. Front. Immunol. 12:682094. doi: 10.3389/fimmu.2021.682094

Peripheral neutrophils in HIV-infected individuals are characterized by impairment of chemotaxis, phagocytosis, bactericidal activity, and oxidative burst ability regardless of whether patients are receiving antiretroviral therapy or not. Neutrophil dysfunction leads not only to increased susceptibility to opportunistic infections but also to tissue damage through the release of reactive oxygen species (ROS), proteases, and other potentially harmful effector molecules contributing to AIDS progression. In this study, we demonstrated high levels of histone H3 lysine K4 trimethylated (H3K4me3) and dysregulation of DNA transcription in circulating neutrophils of HIV-infected subjects. This dysregulation was accompanied by a deficient response of neutrophils to LPS, impaired cytokine/chemokine/growth factor synthesis, and increased apoptosis. Chromatin immunoprecipitation sequencing (ChIPseq) H3K4me3 histone analysis revealed that the most spectacular abnormalities were observed in the exons, introns, and promoter-TSS regions. Bioinformatic analysis of Gene Ontology, including biological processes, molecular function, and cellular components, demonstrated that the main changes were related to the genes responsible for cell activation, cytokine production, adhesive molecule expression, histone remodeling *via* upregulation of methyltransferase process, and downregulation of NF-κB transcription factor in canonical pathways. Abnormalities within H3K4me3 implicated LPS-mediated NF-κB canonical activation pathway that was a result of low amounts of κB DNA sites within histone H3K4me3, low NF-κB (p65 RelA) and TLR4 mRNA expression, and reduced free NF-κB (p65 RelA) accumulation in the nucleus. Genome-wide survey of H3K4me3 provided evidence that

chromatin modifications lead to an impairment within the canonical NF-κB cell activation pathway causing the neutrophil dysfunction observed in HIV-infected individuals.

Keywords: neutrophils, human immunodeficiency virus, H3K4me3, ChIPSeq, innate immunity

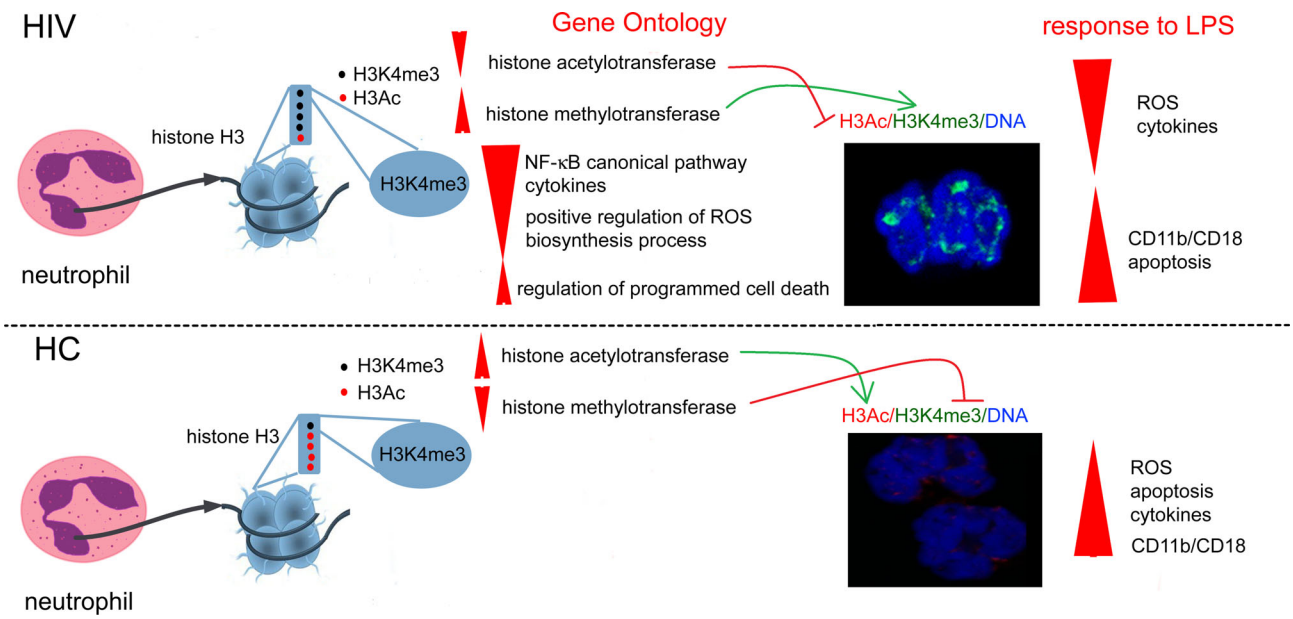

GRAPHICAL ABSTRACT | Overexpression of histone H3K4me3-marked in HIV individuals leads to impaired regulation of main cellular processes critical for obtaining high antimicrobial activity by neutrophils. Due to the fact that the posttranscriptional modifications of H3K4me3 histone are also activated via histone H3K4me3-marked itself, this process is enhanced in a positive feedback loop manner and is probably irreversible.

INTRODUCTION

Neutrophils, the most abundant peripheral blood cells of the immune system, are the first responders to most infections (1). In response to pathogens, neutrophils migrate from the blood to the site of microbial invasion, where their activation drives microbicidal mechanisms such as the release of proteolytic enzymes, antimicrobial peptides, and rapid production of reactive oxygen species (ROS). Although neutrophils are not the direct target of HIV, they can contribute to HIV infection pathomechanism in diverse ways. Before the infection, the presence of neutrophil-associated proteins and cytokines in genital tissues was found to associate with HIV acquisition (2). During HIV infection, these cells may, in an uncontrolled way, release proinflammatory mediators in response to the gut bacteria (3), a phenomenon frequently encountered in HIV patients. In such conditions, neutrophil prompt reactions can contribute to the permanent inflammation observed even in patients with undetectable viral load during antiretroviral therapy (ART) or without it (4), a phenomenon known as microbial translocation. On the contrary, some studies demonstrated that neutrophil involvement in HIV infection pathogenesis was mainly associated with their low frequencies and proapoptotic state (5), reduced antimicrobial activity (6), and contribution to the immunosuppression by enhanced release of amino acid depleting enzymes (7) and PD-L1 mediated suppression of T cells (8). Enhanced immunosuppressive activity of neutrophils in already immune deficient conditions together with reduced antimicrobial function was related to higher risk of the secondary infections in HIV positive patients (9). The basis of the dual function of the neutrophils during HIV infection have not been studied and, besides potential differences between peripheral blood and tissue neutrophils (9, 10), it can be a result of the specific molecular pattern of two main groups of determinants: the transcription factors with the central role of NF-κB in induction of a wide spectrum of proinflammatory genes and the presence of cell type-specific patterns of genes associated with chromatin organization (11).

The DNA is folded into nucleosomes comprising approximately 147 bp of DNA and wrapped around a histone octamer. Specific chromatin configuration enables diversified access and activity of regulatory elements, which determines unique cellular phenotypes and guarantees the plasticity of immune cells to adequately respond to external factors (12–14). Neutrophil nucleus is characterized by loosely arranged chromatins, which not only allows for faster formation of

neutrophil extracellular trap (NET) cross-links at the site of inflammation, but also easier access of transcription factors to DNA. Although the high plasticity of the nucleus allows neutrophils to react rapidly to invading pathogens, during chronic inflammation, this property may be undesirable, resulting in nonspecific activation. Therefore, analysis of the reorganization of a 'chromatin landscape', especially transcriptional start sites (TSSs) of inflammatory genes associated with the activation of neutrophils, may provide a critical advance in understanding HIV-related malfunction of neutrophils. In humans, a strong positive correlation between H3K4me3 and H3K27ac modification of chromatin in relation to activation of immune cells in response to different stimuli was revealed (15, 16). Enhancers, which are classically defined as cis-acting DNA sequences that can increase gene transcription, are typically located far from TSSs and are characterized by the presence of specific post-translational modifications of H3K27ac histones. Contrary to enhancers, TSSs are located mainly in H3K4me3 domains (17). Rapidly activated genes are connected with constitutively high histone H3 acetylation, while genes with slower recruitment of NF-κB and slower kinetics are characterized by low to undetectable baseline level of H3 acetylation. This phenomenon may be responsible for physiologic pre-activation of leukocytes determining stronger and more rapid reaction to pathogens during inflammation. Pre-activation, which is well-described in macrophages, is also observed in circulating neutrophils during inflammation. Macrophages preactivated with IFN-γ before LPS stimulation were found to increase acetylation of 'slow genes' and switch them into fast NF-κB recruitment (18). In chronic inflammation, inadequate activation of immune cells can lead to the persistent activation of H3K4me3 domains resulting in disease progression (19, 20).

In this study, we used chromatin immunoprecipitation sequencing (ChIP-Seq) analysis of H3K4me3-marked histone to identify various TSSs associated with NF-κB-mediated response in peripheral blood neutrophils in HIV-infected individuals. We provide comprehensive epigenome analysis of histone H3K4me3 modification in HIV individuals and healthy controls. Observed differences allowed us to identify DNA regions corresponding to pathological activation of neutrophils in HIV-infected individuals. Specific differences within H3K4me3-marked histone corresponded with NF-κB-dependent gene expression as well as biological processes corresponded with their target genes, leading together to the decreased antimicrobial properties of neutrophils and proinflammatory cytokine synthesis driving inflammation.

MATERIALS AND METHODS

Patients and Samples

Fourteen HIV-infected individuals (two females and 12 males; median age 39.9) were diagnosed and recruited at the 'Luigi Sacco' hospital, University of Milan. All HIV-infected individuals were naïve to highly active antiretroviral therapy (HAART). Median Log values of viral load in these patients was 4.11 copies/uL, ranging 2.4-6.3 copies/uL, $CD4^+$T cells absolute counts ranged from 219 to 1115/μL, with median 514 cells/uL, and CD4/CD8 median value was 0.48 with a range from 0.11 to 1.35. Twelve age- and gender-matched healthy controls (HC) were recruited.

The appropriate Institutional Ethics Committee approved all protocols and informed written consent was obtained from all participants: HIV-infected individuals (approval number 433/08/25/AP, Comitato Etico Locale ET/nb, Ospedale Luigi Sacco, University of Milan) and healthy volunteers (approval number RNN/25/15/KE, Medical University of Lodz).

Neutrophil Isolation

20 mL of the whole blood on lithium heparin anticoagulant was collected from HIV-infected individuals and HC. Neutrophils were purified by negative selection by microbeads, which allowed the removal of DCs, B cells, monocytes, macrophages, activated T cells, and activated NK cells (MACSxpress Whole Blood Neutrophil Isolation Kit; cat. 130-104-434). Residual erythrocytes were lysed with the use of 2mL ammonium chloride Lysing Reagent (BD cat. 555899) for 5 minutes. The final purity of PMN population was assessed by flow cytometry using CD14-PE (clone M5E2), CD15-FITC (MMA), and CD16-PECy7 (3G8, all from BD Pharmingen) mAbs. Flow cytometric analysis of isolated populations of cells showed that the percentage of $CD15^{high}CD16^+CD14^-$ neutrophils was >98%. The level of contaminating $CD14^+CD15^+$ monocytes was about 0.4% and $CD15^+CD16^-$ eosinophils was <0.1% after isolation (**Figure S1A** in **Supplementary Material**). $2x10^6$ neutrophils were incubated without stimulation, in the presence of 100ng/mL ultrapure LPS from *E. coli* (serotype R515, Alexis Biochemicals) in RPMI 1640 for 6 h (5%CO_2, 37°C, humid atmosphere). For DNA isolation, samples of isolated neutrophils were frozen and kept at -150°C.

Reactive Oxygen Species (ROS) Production

To avoid isolation-dependent activation of neutrophils, ROS production was assessed by means of the whole blood luminol-enhanced chemiluminescence (CL) using MLX Microtiter Plate Luminometr (DYNEX, USA). The experiments were performed in the non- and LPS-stimulated (10 ng/mL for 10 min in RT before analysis) neutrophils (21).

The results were expressed as Relative Light Units (RLU) corrected by the whole blood neutrophil amounts and haemoglobin concentration according to the formula:

$$CL\ calculated = CL\ measured\ [RLU\ \max] \times \frac{Hb[\%]}{WBC[10^3/100\mu L] \times \mathrm{PMN}[\%]}$$

WBC – white blood cell
CL – chemiluminescence
Hb – haemoglobin
PMN – polymorphonuclear leukocytes

CD11b/CD18 Expression

200 µL isolated neutrophils ($2x10^6$ cells/mL in PBS) were incubated at RT with conjugated monoclonal antibodies: anti-CD11b-PE (ICRF44, BD) and CD18-FITC (L130, BD). After 30 minutes of incubation and rinsing, the samples were fixed with 1% paraformaldehyde and analyzed (LSRII, BD).

Immunocytochemical Analysis (ICC)

For ICC analysis, neutrophils were transferred to gelatin-coated microscope slides by cytospin (300xg, 10 min) and fixed with 4% formaldehyde solution for 20 min at RT. Fixed cells were washed with PBS and blocked with 10% rabbit blocking serum (Santa Cruz Biotechnology, Dallas, TX, USA) supplemented with 3% TritonTM X-100 (Sigma-Aldrich, St. Louis, MO, USA) for 45 min at RT. Next, they were washed and double stained for NF-κB/IκB, H3K4me3/NF-κB, AnnexinV/Caspase3, or H3K4me3/H3Ac. Anti-H3K4me3 (2 µg/mL, clone CMA304, mouse, cat 05-1339 Millipore, Temecula, USA), Anti-H3Ac (Lys4, rabbit, cat 08-539 Millipore, Temecula, CA, USA), anti-NFκB p65 (RelA) (1:100, C-20, rabbit, cat. sc-372, Santa Cruz Biotechnology, Dallas, TX, USA), anti-NFκB p65 (RelA) (1:100, F6, mouse, cat. sc-8008, Santa Cruz Biotechnology, Dallas, TX, USA), anti-IκB (1:100, H4, mouse, cat. sc-1643, Santa Cruz Biotechnology, Dallas, TX, USA), Annexin V (1:100, H-3, mouse, cat. sc-74438, Santa Cruz Biotechnology, Dallas, TX, USA), anti-Caspase 3 (2 µg/mL, 9H19L2, rabbit, cat. 700182, Invitrogen, USA), and rat IgG2b kappa (eB149/10H5 eBioscience) as negative isotype control, were used. All antibodies were suspended in PBS supplemented with 1.5% blocking rabbit serum and 0.3% Triton X-100, 0.01% sodium azide, and incubated overnight at 4°C. Cells were washed and secondary fluorescent Abs were added for 1h at RT: goat pAb to mouse TR (5 µg/mL, cat. T862, Invitrogen, USA) with goat pAbs to rabbit FITC (2 µg/mL, cat. F2765, Invitrogen, USA) or goat pAb to mouse FITC (1:100, cat. ab97239, Abcam) with goat pAbs to rabbit TR (4 µg/mL, cat. T-2767, Invitrogen, USA). For nuclei DNA staining, DAPI (1.5 µg/mL UltraCruz Mounting Medium, Santa Cruz Biotechnology, Dallas, TX, USA) was used. The confocal laser scanning microscopy platform TCS SP8 (Leica Microsystems, Germany) with the objective 63×/1.40 (HC PL APO CS2, Leica Microsystems, Germany) was used for microscopic imaging. Leica Application Suite X (LAS X, Leica Microsystems, Germany) was used for cell imaging. Fluorescence intensity was determined as the arbitrary units (a.u.) of the sum of the fluorescence from all segments divided by the number of segments. The average fluorescence was calculated using at least 100 single cells for each sample. The level of baseline fluorescence was established individually for each experiment. Nonspecific fluorescence (signal noise) was electronically diminished to the level where nonspecific signal was undetectable (22). ICC data were additionally presented as the values of overlap coefficient that indicates the overlap of the fluorescence signals between the channels FITC, TR, and DAPI (nucleus). It was calculated as the mean value from every single Region of Interest (ROI) using Leica Microsystem (LAS - X, ver. 3.7.020979 software, Leica, Germany). The overlap coefficient ranges from 0 (no co-localization) to 1 (complete co-localization).

Chromatin Immunoprecipitation (ChIP)

Cells were cultured in T75 Nunc flasks in RPMI medium for 8h. ChIP was carried out in neutrophils according to the manual for Magna ChIP™ A/G Chromatin Immunoprecipitation Kit (Merck Millipore, cat.17-1010). Cells were fixed with 1% formaldehyde in RPMI solution for 10 min. at RT, which was quenched with 10x glycine in 5-minute incubation at RT to stop the fixation. After washing with cold PBS, cells were treated sequentially with 1x Protease Inhibitor Cocktail II, Lysis Buffer with Protease Inhibitor Cocktail II, and Protease Inhibitor Cocktail II with Nuclear Lysis Buffer. Next, supernatant was carefully removed and the cell pellet was resuspended in Nuclear Lysis Buffer. Sonication (10 cycles; 30sec. "ON" 30sec. "OFF") was done using Bioruptor® Pico Sonicator (Diagenode, Belgium). The obtained chromatin was spun at a minimum of 10,000 x g at 4°C for 10 minutes to remove insoluble material. Each immunoprecipitation required the addition of Dilution Buffer and Protease Inhibitor Cocktail II. 25 µL of the diluted chromatin as 'Input' was saved at 4°C for further proceeding. Chromatin immunoprecipitation was performed with the use of a set of antibodies: Normal mouse IgG (negative control), anti-RNA Polymerase II (clone CTD4H8) as positive control, and anti-trimethyl-Histone H3 (Lys4) (MC315, Merck Millipore, cat. 04-745) mAbs. Both antibodies were recommended for the use in ChIP-Seq technique (23). Immunoprecipitation reactions were incubated overnight at 4°C with rotation. DNA was eluted with the use of ChIP Elution Buffer/RNase A mixture and purified using spin columns. The DNA concentrations of obtained samples were measured by Qubit 4 Fluorometer (ThermoFisher Scientific).

Library Preparation and NGS Sequencing

Double-stranded DNA was generated from a single-stranded fraction of ChIPed DNA using NEBNext® Ultra™ II Non-Directional RNA Second Strand Synthesis Module (E6111S, New England Biolabs). Reaction was carried out in the presence of random primers from NEBNext® RNA First Strand Synthesis Module (E7525, New England Biolabs). Libraries for sequencing were prepared using NEBNext® Ultra™ II DNA Library Prep Kit for Illumina® (E7645L, New England Biolabs). Single-end sequencing with read length of 75 bases (SE75) was performed with NextSeq550 (Illumina) in order to obtain at least 20 million reads per sample that could be mapped to the human genome (24). ChIPseq library quality control analysis is presented in Supplementary Materials (**Figure S1B**).

Bioinformatic Methodology of the ChIPseq Analysis

In the first stage, the quality of the raw sequence reads was checked using the FASTQC software (version: 0.11.8). Next, all reads were subjected to the adapter and quality filtering (minimum quality (-q 25), minimum length (-m 15)) using the Cutadapt tool (version: 1.18) in NextSeq reads mode. Trimmed reads were aligned to the reference genome (GRCh38) using the Bowtie2 (version: 2.2.9) in the single-end mode. Duplicated reads were located and tagged using the Picard MarkDuplicates

tool (version: 2.18.4). Reads with low mapping quality score (MAPQ <10) were removed from downstream analysis with the Samtools software (version: 1.6). Protein binding sites identification in the previously prepared BAM files was performed with the MACS2 (Model-based Analysis of ChIP-seq) software (version: 2.1.0) in narrow peak mode (25). Subsequently, identified peaks were annotated using annotatePeaks.pl from Homer software (version: 4.11.1, hg38 annotation library). Additionally, a functional enrichment analysis for various categories (e.g. gene function, biological pathways, domain structure, etc.) was executed (26). To find enriched motifs in ChIPseq peaks the findMotifsGenome.pl program from Homer software (version: 4.11.1) was used. The quantitative assessment of ChIPseq quality was checked applying the ChIPQC package (version: 1.21.0) from R Bioconductor (version: 3.6.0) (**Figure S1C** in **Supplementary Material**). Differentially enriched sites between two experimental conditions were identified using the DiffBind package (version: 2.12.0) from R Bioconductor (version: 3.6.0).

Human Chemokine Multiple Profiling Assays

Chemokine and cytokine concentrations in neutrophil culture supernatants were measured using Bio-Plex Pro™ Human Chemokine Assays (Bio-Rad Laboratories). Standards and samples were diluted (1:4) in sample diluent and transferred to the plate containing magnetic beads for 1h at RT. The plate was washed (3x) and detection antibody was added for 30 min on a shaker (850 rpm) at RT. After that, the plate was washed (3x) and streptavidin-PE solution was added for 10 min. Subsequently, the plate was washed (3x) and samples were re-suspended in 125 μL of assay buffer and analyzed within 15 min. All samples were analyzed at the same time in duplicates. All reagents and technology were provided by Bio-Rad Laboratories (Bio-Plex 200).

Multiple Gene Profiling Microarray

168 genes' expression was analyzed using Human NF-κB Signaling Pathway RT2 Profiler PCR Array and NFκB Signaling Targets RT2 Profiler PCR Array (cat. PAHS-025 and PAHS-225, both Qiagen, UK). cDNA was amplified in the presence of specific primers (RefSeq accession numbers provided in **Supplementary Table 5**) and coated in 96-well microtiter plates on a 7500 Real Time PCR System (Applied Biosystems) according to the following program: 95°C, 10 min (activation of HotStart DNA polymerase); 50 cycles of (95°C, 15s; 60°C, 60s). We used RT2 Real-Time™ SYBR Green/PCR Master Mix (Qiagen, UK) that contains all of the reagents and buffers required for qRT-PCR. The mean expression levels of the following housekeeping genes were used for the normalization of the cDNA samples: hypoxanthine phosphoribosyltransferase 1, β-actin, and glyceraldehyde-3-phosphate dehydrogenase. Data from real-time PCR were calculated using the ΔΔCt method and the PCR Array Data Analysis Template v3.0 (Qiagen, UK).

Statistics

Arithmetic means and standard deviations were calculated for all parameters. Statistical verification was made using the Kolmogorov-Smirnov normality test and the Fisher's test. Statistical significance of differences among the groups was determined by the t-Student test and Cochran test (parametric distributions) or the Wald-Wolfowitz runs test and the Wilcoxon's rank sum test (non-parametric distributions).

RESULTS

Peripheral Blood Neutrophils Isolated From HIV-Infected Individuals Are Characterized by Impaired Antimicrobial Functions

In the initial phase of the study, we analyzed neutrophil effector functions in HIV-infected individuals. The expression of adhesion molecules CD11b and CD18, the ability of neutrophils to generate reactive oxygen species (ROS) and synthetize cytokines/chemokines/growth factors, and the rates of neutrophil apoptosis were analyzed in 8-hour incubations with/without LPS in the HIV individuals and healthy controls (HCs). We showed that the expression of CD11b and CD18 on freshly isolated neutrophils of HIV-infected people was significantly higher than in HCs (**Figure 1A**). Moreover, the expression of these adhesion molecules in HIV-infected individuals but not HCs seemed to be saturated since stimulation of neutrophils with LPS has not caused a further increase in their expression. The analysis of ROS production using the chemiluminescence method revealed that HIV neutrophils were characterized by increased 'resting' (non-stimulated) ROS production, while after stimulation with LPS, ROS production ability appeared to be dramatically reduced compared to HC neutrophils (**Figure 1B**). The profile comparison of 27 cytokines/chemokines/growth factors released by unstimulated (**Figure 1C** left panel) and LPS-stimulated neutrophils (**Figure 1C** right panel) revealed significant differences in contrast to HC neutrophils. Unstimulated neutrophils isolated from HIV-infected individuals released significantly higher amounts of IL-8, G-CSF, and IFN-γ and significantly lower amounts of IL-1ra in comparison to HCs. The capacity of LPS-stimulated neutrophils to synthetize cytokines/chemokines/growth factors, with an exception of IFN-γ was dramatically diminished in comparison to HC neutrophils. We detected significantly lower supernatant concentrations of IL-1ra, IL-2, IL-4, IL-5, IL-7, IL-8, IL-9, IL-10, IL-15, IL-17, Eotoxin, FGFbasic, G-CSF, GM-CSF, IP-10, MCP-1, MIP-1α, MIP-1β PDGF-bb, RANTES, TNF, and VEGA (**Table S1** in **Supplementary Material**).

Neutrophils rapidly respond to pathogens but are short-lived cells. One of the effects of their stimulation results in inhibition of apoptosis, an essential process through which neutrophils gain 'additional time' necessary for more efficient elimination of pathogens. Using ICC labelling of Annexin V, Caspase 3, and DNA, we demonstrated higher rates of apoptosis in the freshly isolated neutrophils from HIV individuals compared to HCs. Moreover, in contrast to the neutrophils of HCs, LPS stimulation of HIV neutrophils did not inhibit their apoptosis (**Figure 1D**).

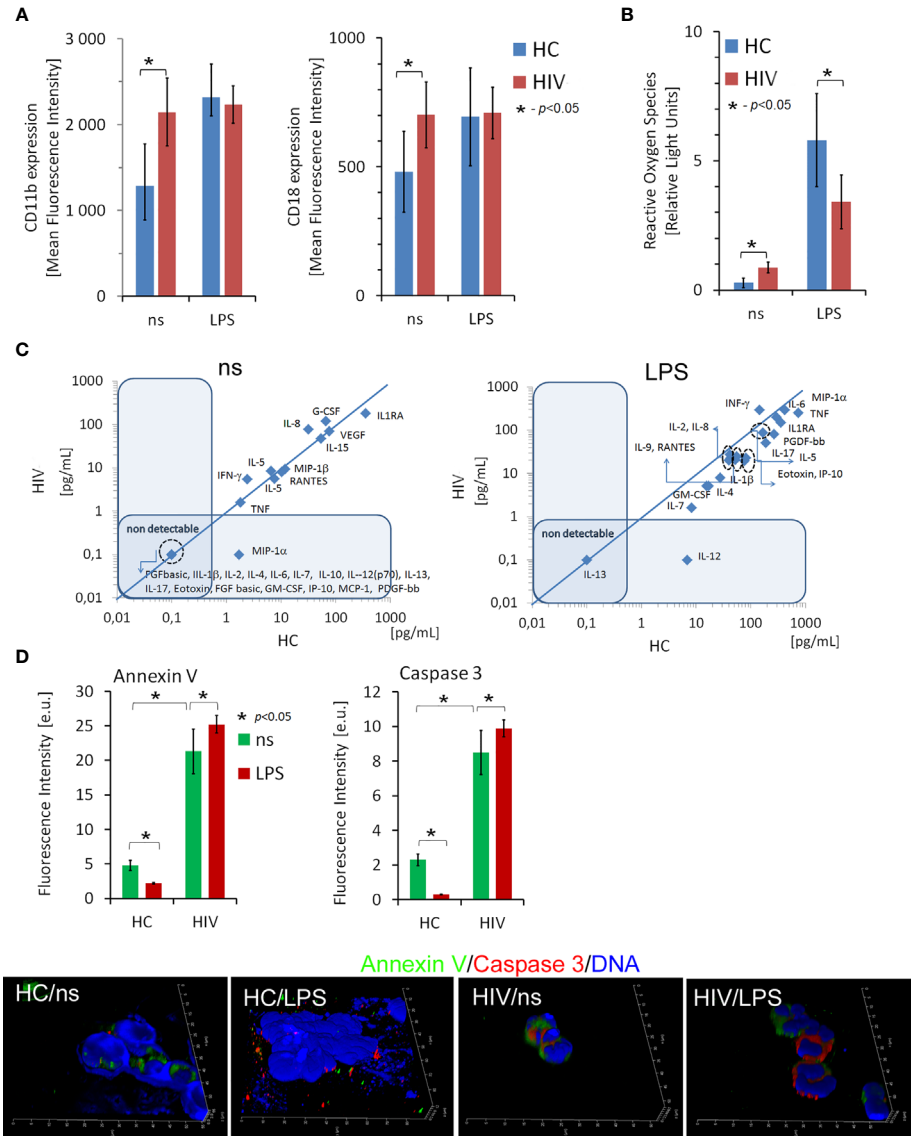

FIGURE 1 | Dysfunction of non-stimulated and LPS-stimulated HIV neutrophils. **(A)** Expression of CD11b and CD18 adhesion molecules on the surface of neutrophils in HIV *vs.* HCs. The bars represent the mean of fluorescence intensity ± SD **(B)** Reactive oxygen species production by non- and LPS-stimulated neutrophils. The bars represent the mean of ROS production in Relative Fold Units ± SD. **(C)** The comparison of the profile of cytokine/chemokine/growth factors released by non-stimulated (left panel) and LPS-stimulated (right panel) neutrophils. The blue line determines the border between up- and down-regulated factors. **(D)** ICC double labeling for caspase-3 (red pseudocolor) and annexin-V (green) revealed that circulating HIV neutrophils are apoptotic. Additional LPS stimulation does not inhibit neutrophil apoptosis as it takes place in HC neutrophils. Nonspecific fluorescence (signal noise) was electronically diminished to the level when nonspecific signal was undetectable (background). The bars represent average fluorescence intensity ± SD calculated from four patients, using at least 100 single cells for each test.

To summarise, these experiments demonstrated impaired ability of HIV neutrophils to develop the appropriate reaction following LPS stimulation. Diminished neutrophil function can be an important aspect in increasing the susceptibility of HIV-positive individuals to opportunistic infections. We selected the three samples most accurately representing each group in terms of functional test values (closest to the mean values in HIV+ and HC groups) for further ChIPseq analysis.

HIV Neutrophil H3K4me3-Marked Histones Are Characterized by Large Fluctuations Within DNA Annotation

A deficient functional response of HIV neutrophils to LPS stimulation suggests some changes in functional genome organization at the stage of posttranscriptional histone modification. The nucleosome H2A, H2B, H3, and H4 histones, extended with other variants, their positioning to

each other and chemically modifications defined as 'nucleosome code' orchestrate inactive or active transcription (27). Among the over 20 sites of methylation that have been identified on the core histone, the posttranscriptional modification of histone H3 lysine K4 trimethylation is associated with the 5' open reading frame and directly corresponds to mRNA expression profiling of inflammatory genes. In the next step of our investigation, we focused on the changes within H3K4me3-marked histone in non-stimulated neutrophils using ChipSeq technique. DNA annotation, which describes the function of detected DNA in H3K4me3-marked regions, revealed only slight differences between the HIV and HC groups. Active transcriptional sites (TSSs) were only 2% more prevalent in HIV individuals (**Figure 2A**). Binding sites overlap analysis of allocating genes revealed 1832 peaks within H3K4me3 specific for HIV, 2728 for HC and 11,338 shared by both groups (**Figure 2B**). The accurate description of all identified peaks, with the division of particular Pie chart compartments, was attached in **Supplementary Table 2**. Further DNA annotation analysis of the genes specific for HIV-1 and HC showed that the major differences were observed in exons (49%), introns (16%), and TSS (15%) genomic location (**Figure 2C**). In the next step, we performed a comparison of peak densities which belongs to both groups. Based on the computational algorithm described as Model-based Analysis of ChIP-seq (MACS), we selected 254 peaks with highest density and 42 peaks with lowest density for HIV+ compared to HC group. All selected peaks were characterized by high statistical significance and a very low empirical false discovery rate (FDR) value. **Figure 2D's** upper panel shows Volcano plot (-log10 *p*-value *vs.* log2 fold expression) of the merged HIV+ and HC peaks. The low panel of **Figure 2D** presents the first ten peaks with the highest *p*-value and the lowest FDR. Based on MACS algorithm, all selected peaks have been assigned to appropriate annotation, closest to the promoter ID, distance to TSSs, as well as gene descriptions (**Table S3** in **Supplementary Material**).

The Changes Within the Histone H3K4me3 Affect the Main Processes Responsible for Antimicrobial Functions of Neutrophils in HIV-Infected Individuals

Numerous changes in the TSS regions affect the metabolic processes of the cell. Consequently, in the next step of our investigation, we performed Gene Ontology (GO) analysis on the biological process, molecular function, cellular components, and pathway interactions (26). GO components displayed many significant differences in the HIV group in comparison to HC. In particular 'Metabolic process', 'DNA binding', 'Activity transcription regulator', 'RNA binding', and 'Nucleoplasm' terms were in the top twenty processes with the highest statistically significant differences. The pathway interaction analysis also revealed considerable variation in HIV+ group. The most spectacular, which appeared in ten main processes, were: 'Signaling events mediated by HDAC Class I', 'RAC1 signaling pathway', and 'Hedgehog signaling events mediated by Gli proteins' (**Table S4** in **Supplementary Material**).

Next, we searched for the processes directly related to neutrophil activation and histone modification as the primary source of their inflammatory dysfunction. We evidenced that HIV neutrophils were characterized by a reduced amount of target genes within the histone H3K4me3 in terms: 'Cytokines', 'Positive regulation of ROS production', 'Oxidoreductase activity acting on NAD(P)H' and 'Histone acetyltransferase complex'; and upregulation of target genes in terms: 'Immune response-regulating cell surface receptor signaling pathway involved in phagocytosis', 'Neutrophil activation', 'Histone modification', 'Histone methyltransferase activity', and 'DNA-binding transcription factor activity'. However, no statistically significant differences were demonstrated in 'NADPH oxidase complex' (**Figure 3A**). As the major statistical differences were detected in 'Neutrophil activation' and 'Cytokines', we focused on the particular target genes, and classified them into three groups based on the comparison of peak density. We found 14 specific target genes for HIV neutrophils, 81 for HC, and 281 genes without differences in the process of 'Neutrophil activation'. In the process of 'Cytokines' we noted only one specific target gene (TTC19) in HIV neutrophils, 24 DNA peaks with high density in HC (**Figure 3B**), and 31 without differences. As peripheral neutrophils are characterized by impaired ROS production after LPS stimulation and as we have shown above it is associated with gene disorders within H3K4me3, we focused on the 'Positive regulation of ROS production' process. We revealed the deficiency of 11 target genes within H3K4me3-marked in HIV samples including genes coding TLR4 and TLR6 that recognize bacteria and fungi pathogen-associated molecular patterns.

Chromatin organization and regulation of the gene expression allow neutrophils to achieve high plasticity during inflammation. Molecular analyses have demonstrated that this plasticity results from histone posttranslational modifications (HPTMs), mediated predominantly by enzymes catalyzing processes of acetylation and methylation (28). Gene ontology analysis revealed statistically significant histone modification with the predominance of histone H3 methylation over acetylation (**Figure 3A** middle panel). Binding site overlap analysis in the term 'Histone methyltransferase complex' revealed 13 DNA peak regions which were particularly characteristic for HIV-infected individuals, 58 DNA peaks as common for both groups, and four DNA peaks present only in HCs (**Table S6** in **Supplementary Material**). In turn, binding site overlap analysis in the term 'Histone acetyltransferase complex' revealed one DNA peak region characteristic for HIV-infected individuals, 58 peaks common for both groups, and 18 present only in HCs (**Table S6** in **Supplementary Material**). To validate histone modification, we performed IHC double-staining of non-stimulated neutrophils for H3K4me3 *vs.* H3Ac. We used polyclonal H3Ac antibody that covers the known spectrum of histone H3 acetylation (K4, 9, 14, 18, 23, 27, 36, and 56). This set of experiments revealed high H3K4me3 and low H3Ac fluorescent signals in HIV compared to HC neutrophils, confirming the predominance of H3K4 methylation processes in histone posttranslational modifications (**Figure 3C**).

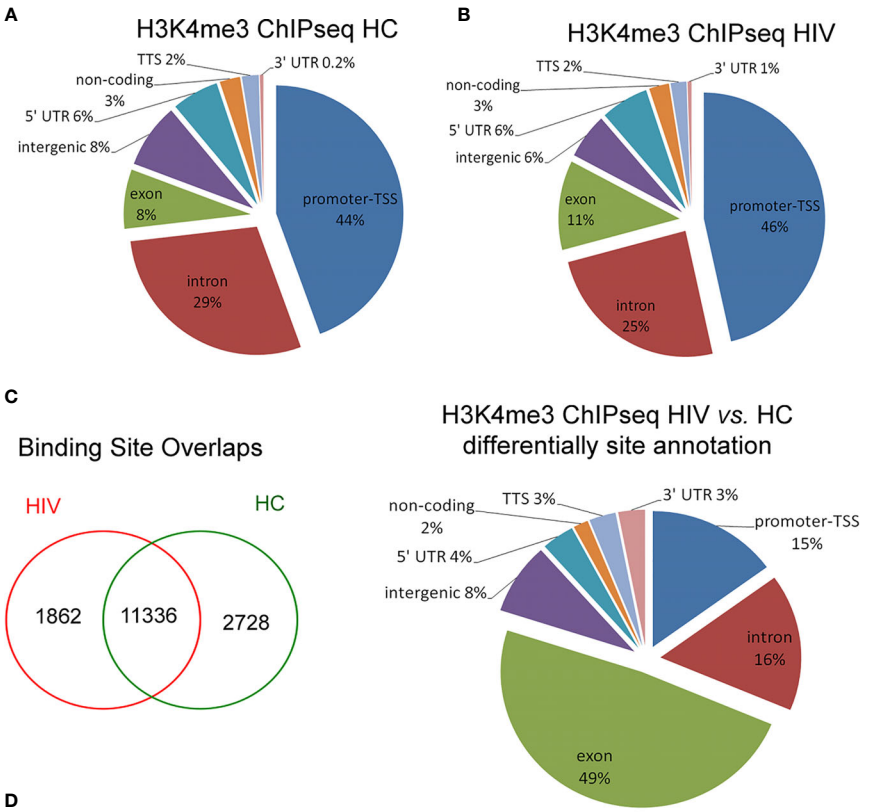

Chr	Annotation	Fold	*p* - value	FDR	Nearest PromoterID	Gene Description
chr16	Intergenic	11.05	5.37e-26	6.78e-22	NR_026556	ankyrin repeat domain 26 pseudogene 1
chr8	exon (NM_001354870, exon 2 of 3)	5.95	9.41e-23	5.94e-19	NM_002467	MYC proto-oncogene, bHLH transcription factor
chr2	intron (NM_020184, intron 5 of 6)	8.27	4.01e-15	1.69e-11	NR_036074	microRNA 3127
chr6	3' UTR (NM_001159673, exon 11 of 11)	8.0	4.68e-14	1.48e-10	NM_001297614	sorting nexin 14
chr3	Intergenic	2.66	4.95e-13	1.05e-09	NM_001314077	protein S
chr1	intron (NM_001098721, intron 1 of 3)	7.82	5.01e-13	1.05e-09	NM_001098722	G protein subunit gamma 4
chr18	Intergenic	7.76	5.94e-13	1.07e-09	NM_001358689	tubulin beta 8 pseudogene 12
chr11	3' UTR (NM_001418, exon 22 of 22)	5.49	1.89e-11	2.97e-08	NR_004403	small nucleolar RNA, C/D box 97
chr5	exon (NM_002700, exon 2 of 2)	6.99	5.16e-10	7.11e-07	NM_002700	POU class 4 homeobox 3
chr2	exon (NM_018014, exon 4 of 5)	7.02	5.63e-10	7.11e-07	NR_132992	MIR4432 host gene

FIGURE 2 | HIV neutrophil H3K4me3-marked histones are characterized by large fluctuations within DNA annotation. **(A)** Pie chart analysis of separate samples within H3K4me3 in HIV and HCs showed only minor differences in DNA annotation of genomic regions. **(B)** Binding sites overlap analysis revealed 1,862 DNA sequences associated with H3K4me3 that specific characterize HIV patients. **(C)** Compression of HIV *vs.* HCs demonstrated the most important changes in exon, intron and promoter TSS genomic features. **(D)** Analysis of statistic differences in protein binding to the H3K4me3 region revealed that most of the binding sites in HIV neutrophils are upregulated. Left and bottom panel show statically significant differences in binding sites as enlarged region. Low panel displays ten peaks with highest statistically significant differences and lowest FDR. More details and all peaks with statistically significant differences are presented in the **Supplementary Table S2**.

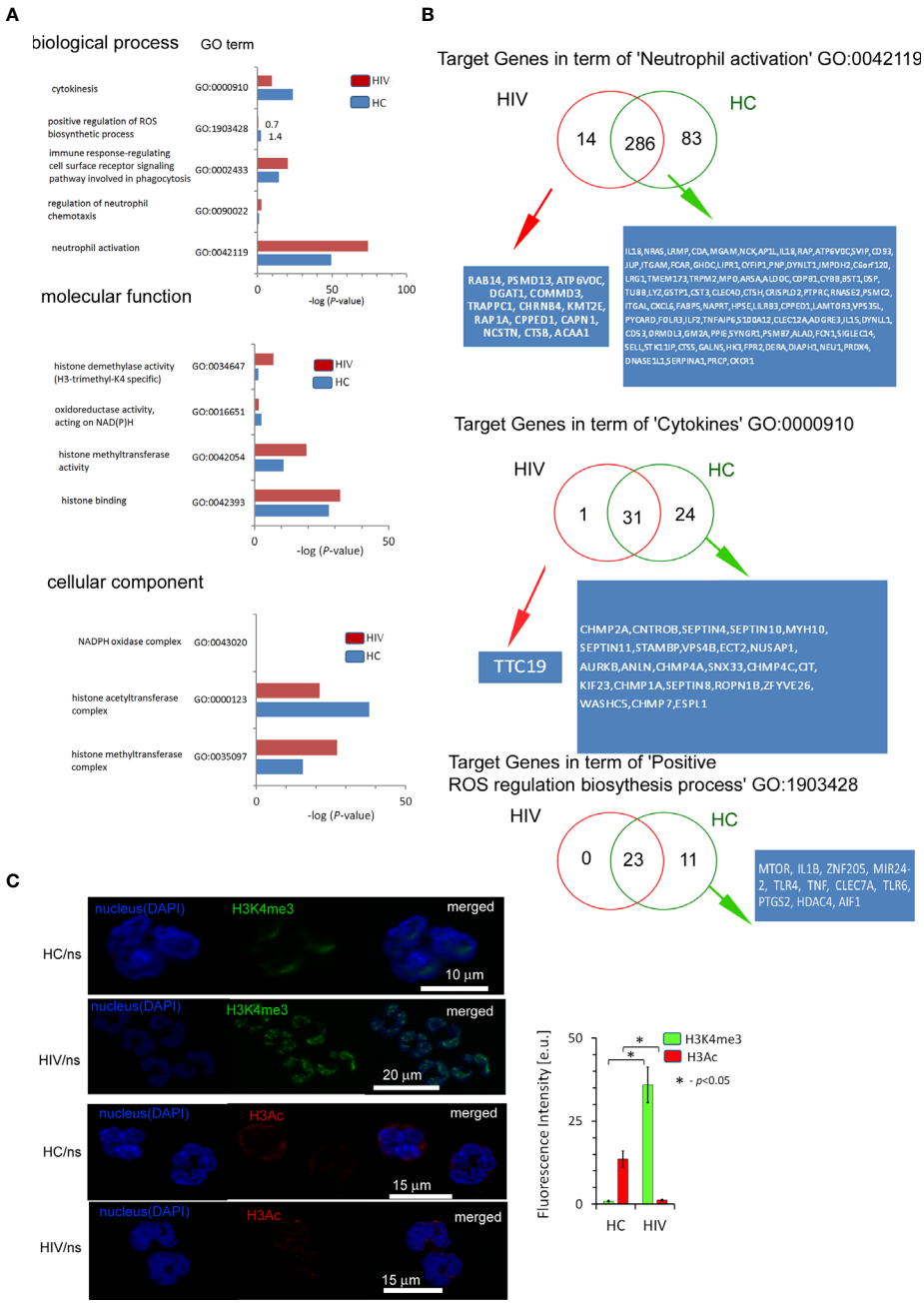

FIGURE 3 | The changes within the histone H3K4me3 affect principle processes responsible for antimicrobial functions of neutrophils in HIV-infected individuals. **(A)** A list of selected biological processes, molecular functions, and cellular components responsible for the ability to neutralize pathogens by neutrophils and in further posttranscriptional histone modifications. The bars represent mean values for HCs (n=3) and HIV-infected individuals (n=3). The analysis of all Gene Ontology (GO) processes with statistic and FDR analysis are provided in the **Supplementary Table S4**. **(B)** The analysis of target genes in the GO term 'Neutrophil activation' revealed 14 specific genes in HIV individuals and 83 in HC. The analysis of target genes in the GO term 'Cytokines' revealed only specific gene *TTC19* for HIV. **(C)** The ICC analysis with double labeling for H3K4me3 (green pseudocolor) and H3Ac (red) confirmed GO findings suggesting the increased methylation and decreased acetylation process within histone H3 in HIV-infected individuals. Nonspecific fluorescence (signal noise) was electronically diminished to the level when nonspecific signal was undetectable (background). The bars represent average fluorescence intensity ± SD calculated from four patients, using at least 100 single cells for each test.

Neutrophils of HIV-Infected Individuals Are Characterized by NF-κB Canonical Pathway Disturbances as Well as Decreased Number of NF-κB Binding Sites Within Histone H3K4me3

High production of ROS by unstimulated neutrophils in HIV individuals and impaired respiratory burst in response to LPS suggests the existence of significant changes of molecular pathways which control these processes. The transcription factor NF-κB plays a critical role in acute inflammation mediated by neutrophils and should be activated only transiently (29). The non-covalent association of IκB (inhibitor of NF-κB) with NF-κB shifts the steady-state subcellular localization of NF-κB dimers to the cytoplasm. Biological inactive NF-κB–IκB complex is interrupted during cell activation by IKK kinase leading to liberation of NF-κB, its translocation to the nucleus, and binding to the site-specific transcription sequences (κB DNA sites). Using IHC double-staining method to detect NF-κB subunit RelA(p65) and IκB, we observed lower expression of NF-κB RelA(p65) in non-stimulated neutrophils of HIV in comparison to HCs. In contrast to neutrophils of HCs, LPS-stimulation of HIV neutrophils did not cause an increase in NF-κB RelA(p65) expression. In both groups, there was no change in IκB expression regardless of whether the cells were stimulated or not (**Figure 4A**). The co-localization analysis of NF-κB RelA (p65) *vs.* IκB and NF-κB RelA(p65) *vs.* DNA after LPS exposure revealed deficiency in the dislocation of NF-κB RelA(p65) to the nucleus as well as a lack of NF-κB RelA(p65) detachment from its IκB inhibitor (**Figure 4B**). Subsequently, we noted statistically significant low amounts of κB DNA sites within histone H3K4me3-marked in HIV-infected individuals compared to HCs (**Figure 4C**). In the last set of experiments, we considered how these changes affect gene expression related to NF-κB activation of cells and those regulating NF-κB activity. We noted 50 genes up- and seven down-regulated as well as 78 without statistical significance in non-stimulated neutrophils isolated from HIV-infected individuals (**Figure 4D** and **Table S5** in **Supplementary Material**). Among others, we observed low mRNA expression for: NF-κB RelA(p65), IL-8, IL-10, and TNF-α (**Figure 4D**; red arrows point NF-κB RelA(p65) and TLR4). mRNA of IκBα IκBβ and IκBε were without changes in non-stimulated neutrophils compared to HCs (**Table S5** in **Supplementary Material**).

In the next step, we verified whether the NF-κB RelA(p65) down-regulation is a result of H3K4me3-marked histone dysregulation. Gene Ontology analysis revealed statistically significant down-regulation of target genes associated with 'Canonical NF-κB pathways' term (**Figure 5A**). The canonical NF-κB pathway is stimulated by ligands of diverse immune receptors and involves three processes: IκB kinase (IKK) activation; IκBα phosphorylation; and its ubiquitination and nuclear translocation of NF-κB units such as p50, RelA(p65), and cREL. Detailed analysis of individual target genes associated with this term indicated an undetectable DNA peak in TNF-α, IκBKG, and ERC1 regions in histone H3K4me3-marked (**Figure 5B**). Overlap peak density comparison revealed additional changes within peaks assigned to RelA(p65), TRAF6, and IkBKB genes (**Figure 5C**). In our studies, we also took into consideration other alternative NF-κB pathways. 'Non-canonical (alternative) NF-κB pathway' is associated with pre-activation of immune cells in response to signals from a subset of tumor necrosis factor receptor (TNFR) superfamily members and involves slow and persistent activation of NF-κB-inducing kinase (NIK). NIK-mediated p100 phosphorylation results in nuclear translocation of p52 and RelB (30). In turn, 'atypical NF-κB signaling pathway' is initiated by genotoxic stress, which in the first step leads to a translocation of NEMO (NF-κB Essential Modulator, IKKγ) to the nucleus where it is sumoylated and subsequently ubiquitinated. This process is mediated by the ataxia telangiectasia mutated kinase, which, in cooperation with NEMO, causes an activation of IKKβ and subsequently NF-κB (31). We did not observe any changes within GO term 'Atypical NF-κB pathway' or 'Alternative NF-κB pathway' (**Figures 5A, B**). This set of experiments directed on 'Canonical NF-κB pathway' as a central point of neutrophil dysfunction in response to LPS suggests that this phenomenon is caused by the changes within H3K4me3-marked histone.

One of the most important processes in binding transcription factors with a chromatin template is destabilization of nucleosomes by SWI/SNF Complex throughout ATP-driven translocation of the protein along nucleosomal DNA (32, 33). In our experiment, we noted statistically important changes within H3K4me3-marked in term 'SWI/SNF superfamily-type complex (GO:0070603)' in HIV non-stimulated neutrophils (–20.4 log10 *p*-value in HIV and -17.2 in HCs, respectively, **Table S4** in **Supplementary Material**).

Changes Within H3K4me3-Marked Histone in HIV Neutrophils Involve Deregulation of Histone 1 Which Is Responsible for DNA Fragmentation Pathway but Not Bcl-2 Pathway

In our preliminary experiments, we found that neutrophils of HIV-infected individuals succumb easily to apoptosis. Thus, in the last step of our investigation, we analyzed the Gene Ontology associated with apoptosis. For these analyses were considered neutrophils isolated from HIV-infected individuals with significantly down-regulated expression of genes found within Gene Ontology terms 'Regulation of programmed cell death' and 'Apoptotic process' (**Figure 6A**). Binding sites overlap in term of 'Apoptotic process' analysis revealed 55 DNA peak regions which are particularly characteristic for HIV-infected individuals, 672 as common for both groups, and 256 present only in HC (**Figure 6B**, **Table S6** in **Supplementary Material**). Compression of read density overlap of peak regions highlighted high concentration regions within histone H1 protein's (H1F0, HIST1H1A, HIST1H1B, HIST1H1C, HIST1H1D, and HIST1H1E) mainly presented on chromosome 6 in the HIV group (**Figure 6C**). We performed a similar comparison for target genes responsible for caspase 8/10- dependent apoptosis and Bcl-2 pathway. We found no differences within investigated regions (**Figure 6D**). These data hypothesized that H3K4me3-

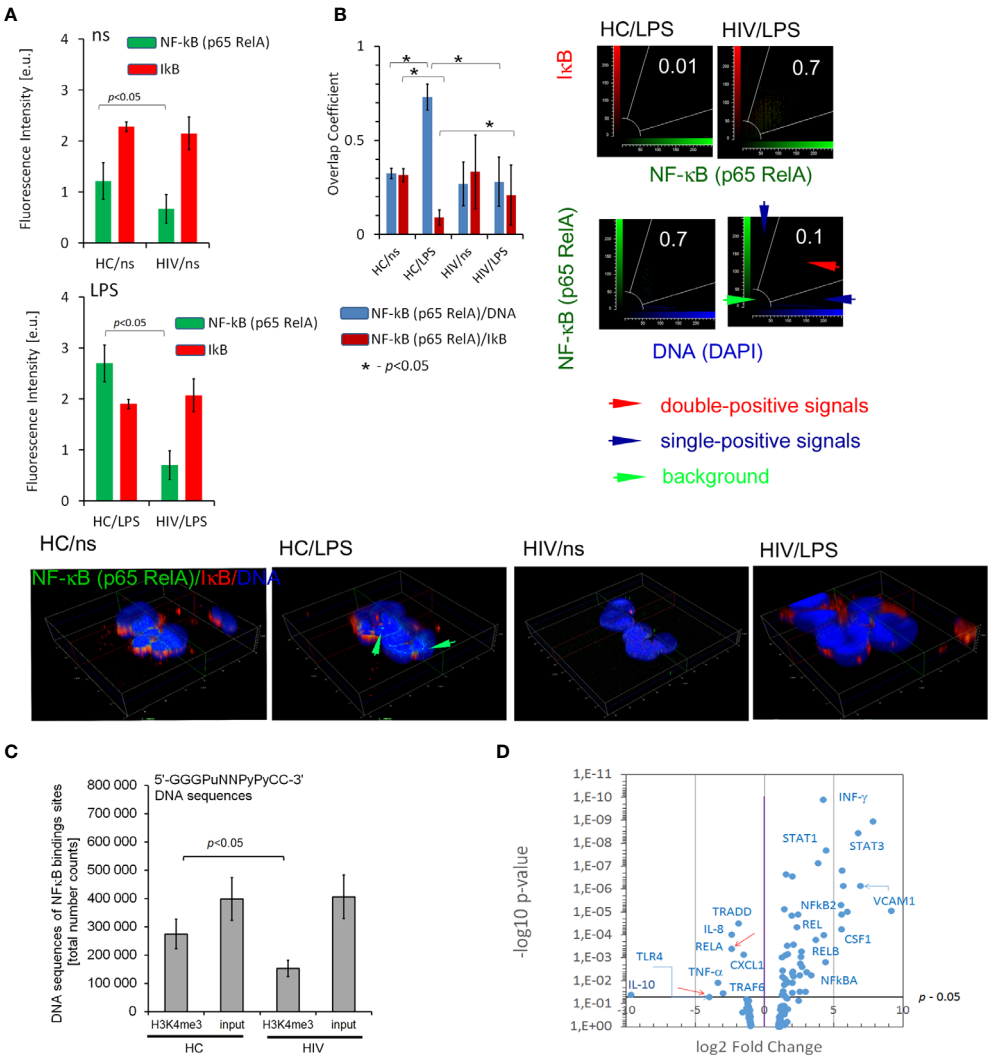

FIGURE 4 | HIV neutrophils are characterized by impaired NF-κB activation dependent on the p65-RelA subunit. **(A)** ICC florescent intensity analysis with double labeling for p65-RelA (green pseudocolor) and IκB (red) in non- and LPS-stimulated neutrophils. The bars represent average fluorescence intensity ± SD calculated from four patients, using at least 100 single cells for each test. (**B** right panel) Overlap coefficient of p65-RelA *vs.* IκB and p65-RelA *vs.* DNA analysis suggests p65-RelA colocalization with its inhibitor IκB which results in disturbance of p65-RelA relocation to the cell nucleus. (**B** Low panel) ICC 3D projection of nucleus visualizes the lack of NF-κB (p65-RelA) colocalization with DNA after LPS-stimulation in HIV individuals. Green arrows show an overlap of signal from NF-κB (p65-RelA) and DNA in HCs. **(C)** Total amount of NF-κB binding sites within histone H3K4me3-marked in non-stimulated neutrophils. The bars represent mean ± SD for HCs (n=3) and HIV-infected individuals (n=3). **(D)** Disturbances in translocation of NF-κB to the nucleus are reflected in the profile of mRNA expression of proinflammatory genes. The mRNA expression of all targets and genes associated with NF-κB are provided in the **Supplementary Table S5**.

marked histone also implies a participation in apoptosis by triggering of H1histone genes'.

DISCUSSION

Regulation of gene expression depends on histone posttranslational modifications (HPTMs), DNA methylation, histone variants, remodeling enzymes, and effector proteins that influence the structure and function of chromatin. All these processes are interrelated and dependent on each other, creating a specific 'histone code' (34) allowing immune cells to achieve high plasticity during inflammation. One of the well-known mechanisms of chromatin remodeling in response to the pathogen relates to the polarization of naive T lymphocytes to CD4 or CD8 subpopulation described by Harrison group (35). Human activated lymphocytes are characterized by coordinated changes at different levels of chromatin architecture. These changes affect all levels of chromatin organization, starting from the primary level of organization of nucleosome-mediated by HPTMs, then, intermediated level where the genome is organized into protein-mediated loops that facilitates

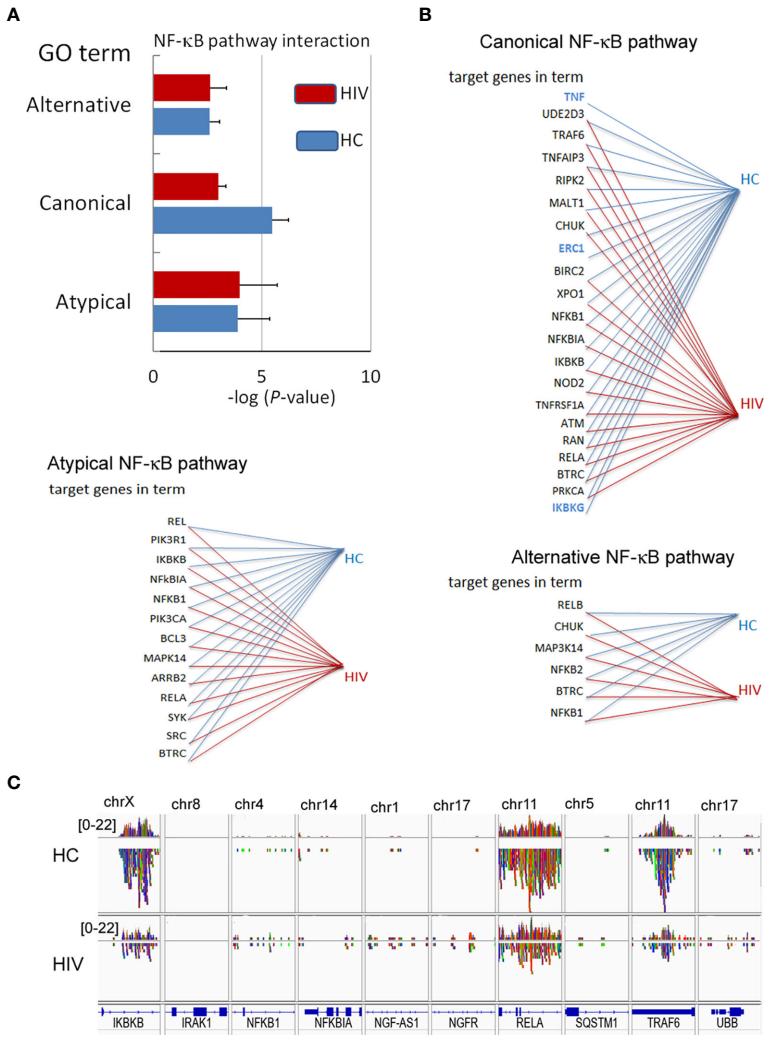

FIGURE 5 | Changes in the DNA within H3K4me3-marked histone affect canonical NF-κB pathways. **(A)** The analyses of GO terms: alternative, canonical, and atypical NF-κB pathways. The bars represent mean values for HCs (n=3) and HIV-infected individuals (n=3) **(B)** The analysis of target genes in the GO term 'Canonical NF-κB pathway' indicated the lack of signals for *TNF*, *ERC1*, and *IKBKG* within H3K4me3 in HIV neutrophils (blue color). **(C)** The comparison of selected genes related to NF-κB shows a statistically significant smaller number of NGS readings (low density) within *RelA*, *IKBKB*, and *TRAF6* coding genes related to the GO term 'Canonical NF-κB pathway'.

interaction between the pairs of promotors and enhancers, and finally, at a high level with the genome organized into self-interacting chromatin (35). Euchromatin of immune cells is characterized by high levels of acetylation and H3K4me1/2/3 (28). It seems highly probable that the mutual proportions of HPTMs as well as the time of particular modifications determine the functional state of different types of leukocytes according to the role played at a specific phase of inflammation. In this study, we have demonstrated in two independent sets of experiments (Gene Ontology of histone H3K4me3-marked annotation analysis and H3K4me3/H3Ac protein expressions) that HIV neutrophils are characterized by increased expression of histone modification process associated with methylation and a simultaneous inhibition of the acetylation. Gene Ontology of H3K4me3-marked histone has revealed overexpression in 'Histone methyltransferase activity' term, suggesting that actively transcribed genes are responsible for H3K4me3 modification themselves. As this observation was also confirmed by the high expression of H3K4me3 in ICC method, it seems highly probable that H3K4me3 modification and its intensity are orchestrated by positive feedback reaction. In addition, Gene Ontology of histone H3K4me3 has revealed the downregulation in 'Histone actetyltransferase activity' term, which corresponds with low expression of H3Ac protein. As both processes are interrelated and controlled by H3K4me3 in a positive feedback manner, the changes associated with H3K4me3 modification may be definitive and irreversible, determining neutrophil fate during its short lifespan.

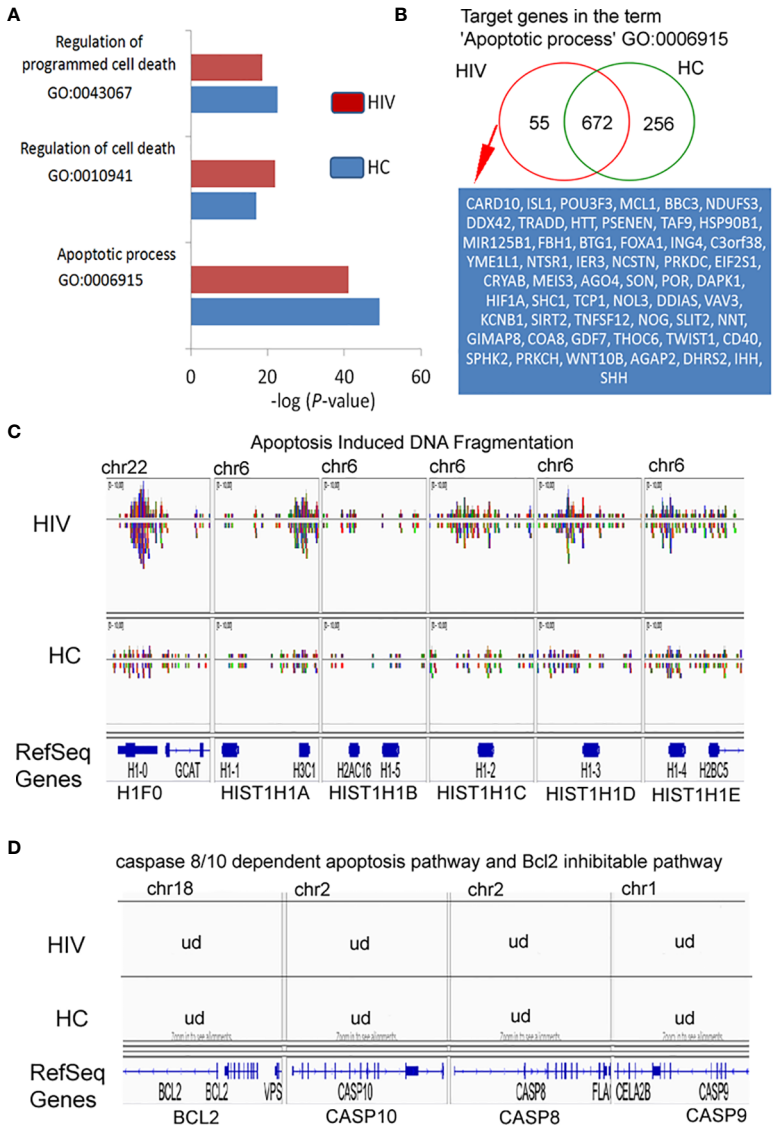

FIGURE 6 | H3K4me3-associated genes affect apoptosis by deregulation of DNA fragmentation but not BCL2- or caspase-regulated execute phase of apoptosis. **(A)** Gene Ontology analysis of apoptosis and cell death. The bars represent mean values for HCs (n=3) and HIV-infected individuals (n=3). **(B)** Binding site overlap in the GO term 'Apoptotic process'. A detailed list of all target genes is attached in the **Supplementary Table 6**. **(C)** The comparison of peak density in the genes responsible for histone-1-induced DNA fragmentation revealed high density DNA within histone H1 in HIV neutrophils. **(D)** The comparison of peak in the representative genes responsible for execution phase of apoptosis as well as Bcl2 pathway revealed undetectable DNA within H3K4me3. ud- undetectable level of DNA.

Posttranscriptional modification of H3 histone leads to getting access to DNA regions rich in enhancers and promoters. Modification of H3K4me3 is observed at the 5' open reading frame of actively transcribed genes, while H3 acetylation is localized rather far from specific gene regions other than just at TSSs (20). This is related to physiological mechanisms involved in pathogen eliminations. Rapidly triggered genes have showed constitutively high histone acetylation, while genes recruiting NF-κB with slower kinetics were characterized by low or undetectable basal levels of H3 acetylation. Immune competitive cell pretreatment with low concentrations of pro-inflammatory cytokines (eg. INF-γ and TNF), before LPS stimulation, was found to increase acetylation of slow genes switching them into fast NF-κB pathway (36). We can suspect that a similar phenomenon, described as priming or pre-activation, takes place in neutrophil functioning. The first pro-inflammatory signal of TNF, C5a, or IL-8, applied at a very low concentration for a short period of time, leads to a much more intensive neutrophil 'burst of ROS' and phagocytosis in response to pathogens compared with neutrophils without any 'pre-activation' (37). Therefore, the low expression of H3Ac-marked histone probably results from dysregulation in neutrophil pre-activation in HIV-infected

individuals, causing a deficiency of effective antimicrobial response and low pro-inflammatory cytokine/chemokine/growth factor synthesis after LPS stimulation.

In turn, the increased expression of H3K4me3 causes low-grade permanent gene transcription resulting in enhanced ROS synthesis as well as high expression of CD11b/CD18 adhesive molecules in HIV non-stimulated neutrophils. This observation is also in accordance with Gene Ontology analysis, where significantly increased biological processes 'Neutrophil activation', 'Regulation of neutrophil chemotaxis', and 'Immune response-regulating cell surface receptor signaling pathway involved in phagocytosis' were detected. In addition, an easier access to TSSs is connected with requirement of Swi/Snf chromatin remodeling complex which cooperates with DNA-histone exposing DNA on the nucleosome surface (38, 39). In our study, we have noted high statistical differences within H3K4me3-marked histone in term of 'SWI/SNF superfamily-type complex (GO:0070603)' in HIV non-stimulated neutrophils. Under physiological conditions, this process is associated with histone acetylation leading to wide access to TSS regions, while genes with a constitutive nucleosome-accessible configuration in the TSS regions are activated in the absence of SWI/SNF activity (40). Therefore, the high activity of this process observed *in vitro* without H3 acetylation in unstimulated neutrophils of HIV-infected individuals may be the cause of their low-grade permanent activation.

NF-κB affects most aspects of neutrophil cellular physiology associated with an antimicrobial immune response that involves inhibition of neutrophil apoptosis, ROS and proteolytic enzyme production, and neutrophil extracellular trap (NETs) formation responsible for pathogen elimination, and chemokine/cytokine production for recruitment of other immune cells. Five genes encode the entire family of NF-κB transcription factors: NFKB1, NFKB2, RELA, RELB, and REL (41). Their polypeptide products give rise to the mature NF-κB subunits p50, p52, RelA(p65), RelB, and cRel, which combined in pairs produce 15 distinctly functioning NF-κB dimers (42). In this study, we have shown that mRNA and polypeptide RelA (p65) expression are decreased in HIV neutrophils. Other NF-κB mRNA factors were upregulated. This pattern of NF-κB subunits mRNA expression results from the regulation based on a positive feedback manner, as transcription of the genes encoding the NF-kB polypeptides is upregulated during NF-κB activation, with the exception of RelA (43). Next, we addressed the activity of an inhibitor of NF-κB (IκB) that controls NF-κB dimers throughout NFκB-IκB complex. IκBα, IκBβ and IκBε–mediated canonical IκB activities orchestrate NF-kB dimers that contain at least RelA or c-Rel subunits binding in the nucleus. We have shown that IkBα IκBβ and IκBε mRNA expression and polypeptide specific for all subunits of IkB (IkBα IκBβ, IκBε) were without any changes in HIV neutrophils in comparison to HC. To summarise, these data indicate dysregulation in NF-κB activity in HIV neutrophils related to deficiency in RelA subunit but not in IκB expression.

Next, we found that decreased expression of mRNA for RalA in HIV neutrophils corresponded with RelA gene low peak density within histone H3K4me3-marked. The downstream GO analysis of NF-κB function and putative target genes in GO annotation revealed inhibition in the transcription of canonical NF-κB pathway. Detailed analysis of individual target genes has demonstrated the absence of TNF-α, IκBKG, TLR4, TLR6, and ERC1 peaks within H3K4me3-marked histone in HIV *vs.* HC neutrophils. Absence of TLR4 peak within H3K4me3-marked histone in HIV-infected individuals may be the reason for low TLR4 mRNA expression and reduced functional response of HIV neutrophils to LPS.

Further analysis has revealed differences in peak density in HIV neutrophils within RelA, TRAF6 (TNF Receptor Associated Factor), and IκBKB (Inhibitor of nuclear factor kappa B Kinase subunit Beta). These changes within H3K4me3 histone were responsible for both dysfunction of NF-κB–IκB complex and impairment of NF-κB translocation to nucleus. Another aspect that affects activation of genes dependent on the NF-κB activity is the small number of NF-κB binding sites within H3K4me3-marked histone. Dysregulation of NF-κB activity and reduced availability for NF-κB binding sites appear to be two independent phenomena. In our opinion, the reduced number of NF-κB binding sites may arise from the reduction of H3 acetylation processes that control the primary access of NF-κB to promotor/TSS regions (11, 44). Moreover, it was previously demonstrated that the enhancer chromatin signature consists of acetylated histones associated with high levels of H3K4me1 histone modification (45, 46).

Based on this observation, we have concluded that a dichotomy between non- and LPS-stimulated HIV neutrophils is the result of posttranscriptional histone modifications with predominate methylation of H3K4me3 and simultaneous inhibition of acetylation. This may explain why circulating non-activated neutrophils in HIV-infected individuals exhibit some characteristics of activated cells with elevated basic ROS production and high expression of adhesive molecules but, at the same time, are unresponsive to additional stimulation with LPS. Similar observations were made by others showing that isolated neutrophils from untreated HIV patients exhibited increased CD11b and decreased L-selectin (CD62L) expression, increased actin polymerization and ROS production, but a reduced capacity to respond to stimulation (47).

The last aspect of our study was devoted to explanation of abnormal apoptosis observed in circulating HIV neutrophils characterized by the high rate of apoptotic cells and inability of LPS to induce apoptosis inhibition. In the execution phase of apoptosis, effector caspases cleave vital cellular proteins leading to the morphological changes including destruction of the nucleus and other organelles, DNA fragmentation, chromatin condensation, cell shrinkage, cell detachment, and membrane blebbing (48). Our study has demonstrated that neutrophils isolated from HIV patients were apoptotic with high expression of Annexin V as well as caspase-3 in the cytosol and in the nucleus. Surprisingly, this process, in opposition to HC neutrophils, was not only irreversible but even intensified following LPS exposure. As apoptotic neutrophils are characterized by reorganized multidivided nuclei, this process should be associated with a change in chromatin condensation mediated by posttranslational modification of histone H1.

Histone H1 protein binds to linker DNA between nucleosomes forming the chromatin fiber which is necessary for the condensation of nucleosome chains (49). In addition, histone H1.2 can translocate to the cytosol and induce apoptosis through a Bak-mediated mitochondrial release of cytochrome C, allowing for caspase activation (50, 51). Gene Ontology analysis of putative genes attendant with executive phase of apoptosis has revealed DNA regions with high peak concentration of histone H1 proteins including H1.2 within H3K4me3 in HIV-infected individuals. Since in H3K4me3-marked histone, no differences in DNA peak concentration of the principal intrinsic pathway components of apoptosis Bcl-2, caspase-8, and -10 have been observed, engagement of H3K4me3 by impelling the histone H1 may point to histone modification of H3K4me3 as a primary process in apoptosis induction. This finding can also explain why neutrophils in HIV-infected individuals were unresponsive to apoptosis inhibition after LPS stimulation. Acceleration of spontaneous neutrophil apoptosis at early stages of untreated HIV patients was also noted by others, displaying the engagement of caspase-3 independently of caspase-8 and suggesting the existence of the intrinsic pathway (52–56).

The limitation of our study is connected with the relatively small group size. We limited our investigation to three selected representatives of the entire group of patients, whose functional neutrophil tests (ROS production, adhesive molecule expression, cytokine production, and apoptosis) were closest to the mean values of all cases taken for our preliminary study. Another limitation of our research is the examination of only one histone in posttranscriptional modification. There are many other possibilities of HPTMs, such as acetylation, methylation, phosphorylation, ubiquitination, SUMOylation, ADP-ribosylation, deamination, and the non-covalent proline isomerization (28), that can also affect the chromatin condensation to organize the genome into transcriptionally active or inactive regions. In HIV neutrophils, histone H3K4me3-marked modified H1 histone regions which may affect chromatin condensation and nucleosome density. Neutrophil nucleus density, in comparison to lymphocytes or NK cells, is characterized by loosely arranged chromatin that facilitate an access of transcription factors to DNA and its remodeling during NETosis. Therefore, neutrophil nucleus density may dynamically change during infection, and ideally, H3K4me3 ChIP-Seq data should be normalized to total H3.

An important aspect which needs to be solved is finding the direct trigger leading to the histone H3 modification. It seems probable that these modifications take place during myelopoiesis. This view is supported by several independent observations. Firstly, there is the large scale of dysregulation in all neutrophil fundamental functions in the relatively short time of their existence in periphery. Secondly, there is the functional homogeneity of neutrophils (relatively low value of standard deviation within average value) within the HIV group. Thirdly, there is the morphological homogeneity observed in FSC *vs.* SSC dot plot of flow cytometry during CD11b/CD18 analysis as well as in ICC performed in freshly isolated neutrophils. Finally, the range of posttranscriptional histone H3 modification observed in HIV neutrophils seems to be too wide to occur just in a few hours of neutrophil existence in the periphery. Potential mechanisms affecting histone H3 modifications during myelopoesis include an altered bone marrow cytokine environment, direct suppression of hematopoiesis by viral proteins, and possible HIV infection of hematopoietic stem cells (57). In this context, activation of interferon-related antiviral immune mechanisms seems to be of particular interest (58, 59). In the animal models of lymphocytic choriomeningitis virus (LCMV) and of poly(I:C) infections, induction of IFN-α/β, but not IFN-γ resulted in reduction of cellularity of hematopoietic progenitors in bone marrow (60). In our study, we found that IFN-α/β synthesis was not elevated in HIV neutrophils, while IFN-γ synthesis was increased not only by LPS- but also non-stimulated cells, suggesting that IFN-γ synthesis may occur at myelopoiesis. Experiments performed by Buro et al. demonstrated that H3K4me3 is increased in parallel with STAT1 (signal transducer and activator of transcription 1) activity after 30' IFN-γ (5ng/mL) exposition. They also confirm inhibition of global H3K4me3 after IFN-γ stimulation of 2fTGH cells by methyltransferase inhibitor: 5'-deoxy-5'-methyl-thioadenosine (MTA) (61). The effects of IFN on the cell can be also observed through triggered IRF (interferon regulatory factor) molecules (62). We noted high mRNA expression of IRF1, STAT1, as well as INF-γ in non-stimulated neutrophils which indicate possible IFN-γ involvement in the disturbance of HIV neutrophils at the maturating stage of these cells. This hypothesis requires verification.

Another aspect that has not been explored is the participation of histone-modifying enzymes which not only modify the histone proteins, but also play a role in the modification of p65 subunit of NF-κB (63). The six methylated K sites, K37, 218, 221, 310, 314, and 315, of NF-κB (p65, RelA) are modified by different histone-modifying enzymes (63). Verification of these possibilities by analysis of bone marrow cells, an environment affecting myelopoesis as well as histone-modifying enzyme activity during maturation of these cells, could bring us closer to the primary factors responsible for neutrophil dysfunction in HIV-1 individuals.

To summarize, our study has demonstrated that neutrophil dysfunction in HIV-infected individuals is associated with overexpression of H3K4me3 with simultaneous H3Ac downregulation. Overexpression of H3K4me3-marked histone leads to impaired regulation of basic cellular processes critical for obtaining high antimicrobial activity of neutrophils. Due to the fact that the posttranscriptional modifications of H3K4me3 histone are also activated *via* histone H3K4me3-marked itself, this process is enhanced in a positive feedback loop manner and is probably irreversible. Our study allowed us to identify possible target genes within H3K4me3 responsible for the neutrophil dysfunction in HIV-infected individuals, however, the data should be validated on a larger cohort of patients with additional use of standard ChIP-qPCR.

DATA AVAILABILITY STATEMENT

The ChIPseq data has been deposited to the GEO, accession number GSE169310.

ETHICS STATEMENT

The studies involving human participants were reviewed and approved by (1) HIV-infected individuals (approval number 433/08/25/AP, Comitato Etico Locale ET/nb, Ospedale Luigi Sacco, University of Milan) and (2) healthy volunteers (approval number RNN/25/15/KE, Medical University of Lodz). The patients/participants provided their written informed consent to participate in this study.

AUTHOR CONTRIBUTIONS

MT designed, performed, and analyzed experiments (AIDS neutrophil isolation and ROS and adhesive molecules analysis), and carried out manuscript review. PP designed, performed, and analyzed experiments (HC neutrophil isolation, Chromatin Immunoprecipitation, cytokine/chemokine/growth factors profiling assays in both groups, and mRNA concentration analysis). MN performed HC neutrophil isolation, Chromatin Immunoprecipitation, and mRNA concentration analysis (Multiple Gene Profiling Microarray) and contributed to manuscript editing. MD participated in QC DNA shearing analysis by DNA electrophoresis. SM and MW performed ICC analysis. AR enrolled HIV-infected individuals and assisted in manuscript review. MK-M enrolled healthy volunteers. JD performed NGS and bioinformatics analysis. NL prepared the manuscript (review and editing). PL supervised and designed the study and experiments, interpreted the data, and wrote the manuscript (original draft). All authors revised the manuscript. All authors contributed to the article and approved the submitted version.

FUNDING

This work was supported by the grants from the National Science Centre 2015/17/B/NZ6/04251.

SUPPLEMENTARY MATERIAL

The Supplementary Material for this article can be found online at: https://www.frontiersin.org/articles/10.3389/fimmu.2021.682094/full#supplementary-material

Supplementary Figure 1 | (A). Phenotypic analysis of purified neutrophils used for ChIPseq experiments. Flow cytometry analysis of CD14, CD15 and CD16 in the population of isolated neutrophils. Cells double-positive for CD16 and CD15 were identified as neutrophils, $CD14^{high}CD15^{+}$ cells as monocytes and with $CD16^{-}$ $CD15^{+}$ cells as eosinophils. **(B)**. ChIPseq library quality control analysis. ChIPseq library was generated from 1 ng ChIP DNA with 18 cycles of PCR. The size of the library distribution is approximately 200-300 bp. **(C)**. ChIPseq quality control report as principal component analysis (PCA). Replicate samples of high quality can be expected to be spatially grouped within the PCA plot. Evaluation of the PCA plot has shown that all samples are suitable and representative for bioinformatic analysis. The analysis was performed by ChIPQC:1.21.0 software (author: Tom Carroll, Wei Liu, Ines de Santiago, Rory Stark).

Supplementary Table 1 | The profile of cytokines/chemokines/growth factors released by non- and LPS-stimulated neutrophils in healthy controls and HIV-infected individuals. Data are presented in pg/mL as means ± SD.

Supplementary Table 2 | The list of all identified peaks within HIV and HCs divided into HIV specific, HC specific, and common for both groups.

Supplementary Table 3 | The list of all statistically significant differences in the peak density between HIV and HCs. The comparison was performed using MACS algorithm. All selected peaks were sorted from the highest statistically significant value to the lowest one. All selected peaks have been assigned to appropriate annotation, closest to the promoter ID, distance to TSSs, as well as gene descriptions.

Supplementary Table 4 | The list of all Gene Ontology (GO) processes, which characterize HIV and HC group. GO was performed by analyses of biological processes, molecular function, cellular components as well as pathway interactions. Data was arranged from the highest statistically significant value to the lowest one.

Supplementary Table 5 | The list of all tested mRNA for genes associated with activation of neutrophil *via* NF-κB. Data are presented as the relative fold differences between HIV and HC group.

Supplementary Table 6 | The list of all target genes in the GO term 'Apoptotic process' GO:0006915, 'Histone methyltransferase complex GO:0035097 and 'Histone acetyltransferase complex' GO:0000123 divided into HIV specific, HC specific and common for both groups.

REFERENCES

1. Nathan C. Neutrophils and Immunity: Challenges and Opportunities. *Nat Rev Immunol* (2006) 6:173–82. doi: 10.1038/nri1785
2. Prodger JL, Gray RH, Shannon B, Shahabi K, Kong X, Grabowski K, et al. Chemokine Levels in the Penile Coronal Sulcus Correlate With HIV-1 Acquisition and Are Reduced by Male Circumcision in Rakai, Uganda. *PloS Pathog* (2016) 12(11):e1006025. doi: 10.1371/journal.ppat.1006025
3. Hensley-McBain T, Wu MC, Manuzak JA, Cheu RK, Gustin A, Driscoll CB, et al. Increased Mucosal Neutrophil Survival Is Associated With Altered Microbiota in HIV Infection. *PloS Pathog* (2019) 15(4):e1007672. doi: 10.1371/journal.ppat.1007672
4. Hunt PW. HIV and Inflammation: Mechanisms and Consequences. *Curr HIV/AIDS Rep* (2012) 9:139–47. doi: 10.1007/s11904-012-0118-8
5. Salmen S, Terán G, Borges L, Goncalves L, Albarrán B, Urdaneta H, et al. Increased Fas-Mediated Apoptosis in Polymorphonuclear Cells From HIV-Infected Patients. *Clin Exp Immunol* (2004) 137(1):166–72. doi: 10.1111/j.1365-2249.2004.02503
6. Flø RW, Naess A, Nilsen A, Harthug S, Solberg CO. A Longitudinal Study of Phagocyte Function in HIV-Infected Patients. *AIDS* (1994) 8(6):771–7. doi: 10.1097/00002030-199406000-00008
7. Cloke TE, Garvey L, Choi BS, Abebe T, Hailu A, Hancock M, et al. Increased Level of Arginase Activity Correlates With Disease Severity in HIV-Seropositive Patients. *J Infect Dis* (2010) 202(3):374–85. doi: 10.1086/653736
8. Bowers NL, Helton ES, Huijbregts RP, Goepfert PA, Heath SL, Hel Z. Immune Suppression by Neutrophils in HIV-1 Infection: Role of PD-L1/PD-1 Pathway. *PloS Pathog* (2014) 10(3):e1003993. doi: 10.1371/journal.ppat.1003993
9. Hensley-McBain T, Klatt NR. The Dual Role of Neutrophils in HIV Infection. *Curr HIV/AIDS Rep* (2018) 15(1):1–10. doi: 10.1007/s11904-018-0370-7
10. Campillo-Gimenez L, Casulli S, Dudoit Y, Seang S, Carcelain G, Lambert-Niclot S, et al. Neutrophils in Antiretroviral Therapy-Controlled HIV Demonstrate Hyperactivation Associated With a Specific IL-17/IL-22 Environment. *J Allergy Clin Immunol* (2014) 134(5):1142–52.e5. doi: 10.1016/j.jaci.2014.05.040
11. Natoli G, Ghisletti S, Barozzi I. The Genomic Landscapes of Inflammation. *Genes Dev* (2011) 25(2):101–6. doi: 10.1101/gad.2018811

12. Beyaz S, Kim JH, Pinello L, Xifaras ME, Hu Y, Huang J, et al. The Histone Demethylase UTX Regulates the Lineage-Specific Epigenetic Program of Invariant Natural Killer T Cells. *Nat Immunol* (2017) 18:184–95. doi: 10.1038/ni.3644
13. Bunting KL, Soong TD, Singh R, Jiang Y, Beguelin W, Poloway DW, et al. Multi-Tiered Reorganization of the Genome During B Cell Affinity Maturation Anchored by a Germinal Center-Specific Locus Control Region. *Immunity* (2016) 45:497–512. doi: 10.1016/j.immuni.2016.08.012
14. Johnson JL, Georgakilas G, Petrovic J, Kurachi M, Cai S, Harly C, et al. Lineage-Determining Transcription Factor TCF-1 Initiates the Epigenetic Identity of T Cells. *Immunity* (2018) 48:243–57. doi: 10.1016/j.immuni.2018.01.012
15. Northrup DL, Zhao K. Application of ChIP-Seq and Related Techniques to the Study of Immune Function. *Immunity* (2011) 34(6):830–42. doi: 10.1016/j.immuni.2011.06.002. 28 ed. 2003. 32: 475-481.
16. Cildir G, Toubia J, Yip KF, Zhou M, Pant H, Hissaria P, et al. Genome-Wide Analyses of Chromatin State in Human Mast Cells Reveal Molecular Drivers and Mediators of Allergic and Inflammatory Diseases. *Immunity* (2019) 51 (5):949–965.e6. doi: 10.1016/j.immuni.2019.09.021
17. Pennacchio LA, Bickmore W, Dean A, Nobrega MA, Bejerano G. Enhancers: Five Essential Questions. *Nat Rev Genet* (2013) 14(4):288–95. doi: 10.1038/nrg3458
18. Glass C, Natoli G. Molecular Control of Activation and Priming in Macrophages. *Nat Immunol* (2015) 17(1):26–33. doi: 10.1038/ni.3306
19. Chen K, Chen Z, Wu D, Zhang L, Lin X, Su J, et al. Broad H3K4me3 is Associated With Increased Transcription Elongation and Enhancer Activity at Tumor-Suppressor Genes. *Nat Genet* (2015) 47:1149–57. doi: 10.1038/ng.3385
20. Park S, Go Woon K, So Hee K, Jung-Shin L. Broad Domains of Histone H3 Lysine 4 Trimethylation in Transcriptional Regulation and Disease. *FEBS J* (2020) 287:2891–902. doi: 10.1111/febs.15219
21. Lewkowicz N, Lewkowicz P, Kurnatowska A, Banasik M, Głowacka E, Cedzyński M, et al. Innate Immune System Is Implicated in Recurrent Aphthous Ulcer Pathogenesis. *J Oral Pathol Med* (2003) 32(8):475–81. doi: 10.1034/j.1600-0714.2003.00181.x
22. Piątek P, Namiecinska M, Domowicz M, Wieczorek M, Michlewska S, Matysiak M, et al. Multiple Sclerosis CD49d+CD154+ As Myelin-Specific Lymphocytes Induced During Remyelination. *Cells* (2020) 9(1):15. doi: 10.3390/cells9010015
23. Egelhofer TA, Minoda A, Klugman S, Lee K, Kolasinska-Zwierz P, Alekseyenko AA, et al. An Assessment of Histone-Modification Antibody Quality. *Nat Struct Mol Biol* (2011) 18(1):91–3. doi: 10.1038/nsmb.1972
24. Landt SG, Marinov GK, Kundaje A, Kheradpour P, Pauli F, Batzoglou S, et al. ChIP-Seq Guidelines and Practices of the ENCODE and modENCODE Consortia. *Genome Res* (2012) 22(9):1813–31. doi: 10.1101/gr.136184.111
25. Feng JX, Qin B, Zhang Y, Liu XS. Identifying ChIP-Seq Enrichment Using MACS. *Nat Protoc* (2012) 7:17. doi: 10.1038/nprot.2012.101
26. Schaefer CF, Anthony K, Krupa S, Buchoff J, Day M, Hannay T, et al. PID: The Pathway Interaction Database. *Nucleic Acids Res* (2009) 37(Database issue): D674–9. doi: 10.1093/nar/gkn653
27. Zhou VW, Goren A, Bernstein BE. Charting Histone Modifications and the Functional Organization of Mammalian Genomes. *Nat Rev Genet* (2011) 12 (1):7–18. doi: 10.1038/nrg2905
28. Kouzarides T. Chromatin Modifications and Their Function. *Cell* (2007) 128 (4):693–705. doi: 10.1016/j.cell.2007.02.005
29. Lu T, Stark GR. NF-κB Regulation by Methylation. *Cancer Res* (2015) 75 (18):3692–5. doi: 10.1158/0008-5472.CAN-15-1022
30. Sun SC. The Non-Canonical NF-κB Pathway in Immunity and Inflammation. *Nat Rev Immunol* (2017) 17:545–58. doi: 10.1038/nri.2017.52
31. Hoesel B, Schmid JA. The Complexity of NF-κb Signaling in Inflammation and Cancer. *Mol Cancer.* (2013) 12:86. doi: 10.1186/1476-4598-12-86
32. Pazin MJ, Kadonaga JT. SWI2/SNF2 and Related Proteins: ATP-Driven Motors That Disrupt-Protein–DNA Interactions? *Cell* (1997) 88(6):737–40. doi: 10.1016/S0092-8674(00)81918-2
33. Clapier CR, Iwasa J, Cairns BR, Peterson CL. Mechanisms of Action and Regulation of ATP-Dependent Chromatin-Remodelling Complexes. *Nat Rev Mol Cell Biol* (2017) 18(7):407–22. doi: 10.1038/nrm.2017.26
34. Rothbart SB, Strahl BD. Interpreting Thelanguage of Histone and DNA Modifications. *Biochim Biophys Acta* (2014) 1839(8):627–43. doi: 10.1016/j.bbagrm.2014.03.001
35. Bediaga NG, Coughlan HD, Johanson TM, Garnham AL, Naselli G, Schröder J, et al. Multi-Level Remodelling of Chromatin Underlying Activation of Human T Cells. *Sci Rep* (2021) 11(1):528. doi: 10.1038/s41598-020-80165-9
36. Hoffmann A, Levchenko A, Scott ML, Baltimore D. The Iκb-NF-κb Signaling Module: Temporal Control and Selective Gene Activation. *Science* (2002) 298 (5596):1241–5. doi: 10.1126/science.1071914
37. Piatek P, Domowicz M, Lewkowicz N, Przygodzka P, Matysiak M, Dzitko K, et al. C5a-Preactivated Neutrophils Are Critical for Autoimmune-Induced Astrocyte Dysregulation in Neuromyelitis Optica Spectrum Disorder. *Front Immunol* (2018) 9:169. doi: 10.3389/fimmu.2018.0169
38. Tang L, Nogales E, Ciferrie C. Structure and Function of SWI/SNF Chromatin Remodeling Complexes and Mechanistic Implications for Transcription. *Prog Biophys Mol Biol* (2010) 102(2–3):122–8. doi: 10.1016/j.pbiomolbio.2010.05.001
39. Ramirez-Carrozzi VR, Nazarian AA, Li CC, Gore SL, Sridharan R, Imbalzano AN, et al. Selective and Antagonistic Functions of SWI/SNF and Mi-2beta Nucleosome Remodeling Complexes During an Inflammatory Response. *Genes Dev* (2006) 20(3):282–96. doi: 10.1101/gad.1383206
40. Liu N, Balliano A, Hayes JJ. Mechanism(s) of SWI/SNF-Induced Nucleosome Mobilization. *Chembiochem* (2011) 12(2):196–204. doi: 10.1002/cbic.201000455
41. Ghosh S. New Regulators of NF-kappaB in Inflammation. *Nat Rev Immunol* (2008) 8(11):837–48. doi: 10.1038/nri2423
42. Gilmore TD, Wolenski FS. NF-κb: Where did it Come From and Why? *Immunol Rev* (2012) 246(1):14–35. doi: 10.1111/j.1600-065X.2012.01096.x
43. Huxford T, Hoffmann A, Ghosh G. Understanding the Logic of Iκb:NF-κb Regulation in Structural Terms. *Curr Topics Microbiol Immunol* (2011) 349:1–24. doi: 10.1007/82_2010_99
44. Smale ST, Natoli G. Transcriptional Control of Inflammatory Responses. *Cold Spring Harb Perspect Biol* (2014) 6(11):a016261. doi: 10.1101/cshperspect.a016261
45. Heintzman N, Stuart R, Hon G, Fu Y, Ching C, Hawkins R, et al. Distinct and Predictive Chromatin Signatures of Transcriptional Promoters and Enhancers in the Human Genome. *Nat Genet* (2007) 39:311–8. doi: 10.1038/ng1966
46. Rada-Iglesias A, Bajpai R, Swigut T, Brugmann SA, Flynn RA, Wysocka J. A Unique Chromatin Signature Uncovers Early Developmental Enhancers in Humans. *Nature* (2011) 470:279–83. doi: 10.1038/nature09692
47. Elbim C, Prevot M, Bouscarat F, Franzini E, Chollet-Martin S, Hakim J, et al. Polymorphonuclear Neutrophils From Human Immunodeficiency Virus-Infected Patients Show Enhanced Activation, Diminished fMLP-Induced L -Selectin Shedding, and an Impaired Oxidative Burst After Cytokine Priming. *Blood* (1994) 84:2759–66. doi: 10.1182/blood.V84.8.2759.bloodjournal8482759
48. Bröker LE, Kruyt FAE, Giaccone G. Cell Death Independent of Caspases: Review. *Clin Cancer Res* (2005) 11(9):3155–62. doi: 10.1158/1078-0432.CCR-04-2223
49. Hergeth SP, Schneider R. The H1 Linker Histones: Multifunctional Proteins Beyond the Nucleosomal Core Particle. *EMBO Rep* (2015) 16(11):1439–53. doi: 10.15252/embr.201540749
50. Konishi A, Shimizu S, Hirota J, Takao T, Fan Y, Matsuoka Y, et al. Involvement of Histone H1.2 in Apoptosis Induced by DNA Double-Strand Breaks. *Cell* (2003) 114(6):673–88. doi: 10.1016/s0092-8674(03)00719-0
51. Giné E, Crespo M, Muntañola A, Calpe E, Baptista MJ, Villamor N, et al. Induction of Histone H1.2 Cytosolic Release in Chronic Lymphocytic Leukemia Cells After Genotoxic and Non-Genotoxic Treatment. *Haematologica* (2008) 93(1):75–82. doi: 10.3324/haematol.11546
52. Baldelli F, Preziosi R, Francisci D, Tascini C, Bistoni F, Nicoletti I. Programmed Granulocyte Neutrophil Death in Patients at Different Stages of HIV Infection. *AIDS* (2000) 14:1067–9. doi: 10.1097/00002030-200005260-00024
53. Pitrak DL, Tsai HC, Mullane KM, Sutton SH, Stevens P. Accelerated Neutrophil Apoptosis in the Acquired Immunodeficiency Syndrome. *J Clin Invest* (1996) 98(12):2714–9. doi: 10.1172/JCI119096
54. Mastroianni CM, Mengoni F, Lichtner M, D'Agostino C, d'Ettorre G, Forcina G, et al. Ex Vivo and *In Vitro* Effect of Human Immunodeficiency Virus Protease Inhibitors on Neutrophil Apoptosis. *J Infect Dis* (2000) 182:1536–9. doi: 10.1086/315858

55. Elbim C, Katsikis PD, Estaquier J. Neutrophil Apoptosis During Viral Infections. *Open Virol J* (2009) 3:52–9. doi: 10.2174/18743579 00903010052
56. Salmen S, Montes H, Soyano A, Hernández D, Berrueta L. Mechanisms of Neutrophil Death in Human Immunodeficiency Virus-Infected Patients: Role of Reactive Oxygen Species, Caspases and Map Kinase Pathways. *Clin Exp Immunol* (2007) 150:539–45. doi: 10.1111/j.1365-2249.2007.03524.x
57. Casulli S, Elbim C. Interactions Between Human Immunodeficiency Virus Type 1 and Polymorphonuclear Neutrophils. *J Innate Immun* (2014) 6(1):13–20. doi: 10.1159/000353588
58. Billiau A, Matthys P. Interferon-Gamma: A Historical Perspective. *Cytokine Growth Factor Rev* (2009) 20(2):97–113. doi: 10.1016/j.cytogfr. 2009.02.004
59. Chiba Y, Mizoguchi I, Hasegawa H, Ohashi M, Orii N, Nagai T, et al. Regulation of Myelopoiesis by Proinflammatory Cytokines in Infectious Diseases. *Cell Mol Life Sci* (2018) 75(8):1363–76. doi: 10.1007/s00018-017-2724-5
60. Binder D, Fehr J, Hengartner H, Zinkernagel RM. Virus-Induced Transient Bone Marrow Aplasia: Major Role of Interferon-Alpha/Beta During Acute Infection With the Noncytopathic Lymphocytic Choriomeningitis Virus. *J Exp Med* (1997) 185(3):517–30. doi: 10.1084/jem.185.3.517
61. Buro LJ, Chipumuro E, Henriksen MA. Menin and RNF20 Recruitment Is Associated With Dynamic Histone Modifications That Regulate Signal Transducer and Activator of Transcription 1 (STAT1)-Activated Transcription of the Interferon Regulatory Factor 1 Gene (IRF1). *Epigenet Chromatin* (2010) 3(1):16. doi: 10.1186/1756-8935-3-16
62. Essers MA, Offner S, Blanco-Bose WE, Waibler Z, Kalinke U, Duchosal MA, et al. IFNalpha Activates Dormant Haematopoietic Stem Cells *In Vivo*. *Nature* (2009) 458(7240):904–8. doi: 10.1038/nature07815
63. Lu T, Yang M, Huang DB, Wei H, Ozer GH, Ghosh G, et al. Role of Lysine Methylation of NF-κb in Differential Gene Regulation. *Proc Natl Acad Sci USA* (2013) 110(33):13510–5. doi: 10.1073/pnas.1311770110

Conflict of Interest: The authors declare that the research was conducted in the absence of any commercial or financial relationships that could be construed as a potential conflict of interest.

frontiers in Immunology

ORIGINAL RESEARCH
published: 10 August 2021
doi: 10.3389/fimmu.2021.708770

Transcriptional Profiling and Functional Analysis of N1/N2 Neutrophils Reveal an Immunomodulatory Effect of S100A9-Blockade on the Pro-Inflammatory N1 Subpopulation

Andreea C. Mihaila[1†], Letitia Ciortan[1†], Razvan D. Macarie[1], Mihaela Vadana[1], Sergiu Cecoltan[1], Mihai Bogdan Preda[1], Ariana Hudita[1], Ana-Maria Gan[1], Gabriel Jakobsson[2], Monica M. Tucureanu[1], Elena Barbu[3], Serban Balanescu[3], Maya Simionescu[1‡], Alexandru Schiopu[2,4‡] and Elena Butoi[1‡]*

[1] Biopathology and Therapy of Inflammation, Institute of Cellular Biology and Pathology "Nicolae Simionescu", Bucharest, Romania, [2] Department of Clinical Sciences Malmö, Lund University, Malmö, Sweden, [3] Departament of Cardiology, Elias Emergency Hospital, Carol Davila University of Medicine and Pharmacy, Bucharest, Romania, [4] Department of Pathophysiology, University of Medicine, Pharmacy, Sciences and Technology of Targu-Mures, Targu-Mures, Romania

Neutrophils have been classically viewed as a homogenous population. Recently, neutrophils were phenotypically classified into pro-inflammatory N1 and anti-inflammatory N2 sub-populations, but the functional differences between the two subtypes are not completely understood. We aimed to investigate the phenotypic and functional differences between N1 and N2 neutrophils, and to identify the potential contribution of the S100A9 alarmin in neutrophil polarization. We describe distinct transcriptomic profiles and functional differences between N1 and N2 neutrophils. Compared to N2, the N1 neutrophils exhibited: i) higher levels of ROS and oxidative burst, ii) increased activity of MPO and MMP-9, and iii) enhanced chemotactic response. N1 neutrophils were also characterized by elevated expression of NADPH oxidase subunits, as well as activation of the signaling molecules ERK and the p65 subunit of NF-kB. Moreover, we found that the S100A9 alarmin promotes the chemotactic and enzymatic activity of N1 neutrophils. S100A9 inhibition with a specific small-molecule blocker, reduced CCL2, CCL3 and CCL5 chemokine expression and decreased MPO and MMP-9 activity, by interfering with the NF-kB signaling pathway. Together, these findings reveal that N1 neutrophils are pro-inflammatory effectors of the innate immune response. Pharmacological blockade of S100A9 dampens the function of the pro-inflammatory N1 phenotype, promoting the alarmin as a novel target for therapeutic intervention in inflammatory diseases.

Keywords: neutrophil polarization, N1 neutrophils, N2 neutrophils, S100A8/A9, ABR-238901, RNA-Seq, neutrophil chemotaxis

OPEN ACCESS

Edited by:
Marko Radic, University of Tennessee College of Medicine, United States

Reviewed by:
Nishant Dwivedi, EMD Millipore, United States
Scott John Denstaedt, University of Michigan, United States

****Correspondence:***
Elena Butoi
elena.dragomir@icbp.ro

[†]These authors have contributed equally to this work and share first authorship

[‡]These authors have contributed equally to this work and share last authorship

Specialty section:
This article was submitted to Molecular Innate Immunity, a section of the journal Frontiers in Immunology

Received: *12 May 2021*
Accepted: *23 July 2021*
Published: *10 August 2021*

Citation:
Mihaila AC, Ciortan L, Macarie RD, Vadana M, Cecoltan S, Preda MB, Hudita A, Gan A-M, Jakobsson G, Tucureanu MM, Barbu E, Balanescu S, Simionescu M, Schiopu A and Butoi E (2021) Transcriptional Profiling and Functional Analysis of N1/N2 Neutrophils Reveal an Immunomodulatory Effect of S100A9-Blockade on the Pro-Inflammatory N1 Subpopulation. Front. Immunol. 12:708770. doi: 10.3389/fimmu.2021.708770

INTRODUCTION

Neutrophils are the first responders in host defense, with an important role in promoting the innate immune response. They originate from the bone marrow and are released in the circulation when they mature and are stimulated by invasive pathogens and inflammatory signals that facilitate their migration to sites of infection or tissue injury. At the site of infection, neutrophils eliminate the invading pathogens utilizing a combination of NADPH oxidase-derived reactive oxygen species (ROS), cytotoxic granule components, and neutrophil extracellular traps (NETs) (1).

Although regarded for a long time as a homogenous population with conserved phenotype and function, recent evidence has suggested the existence of neutrophil heterogeneity with different functional phenotypes, both in healthy individuals and in pathological conditions including cancer, infections, and autoimmune and inflammatory disorders (2, 3). The heterogeneity of neutrophil populations is characterized by differences in life span, cytokine release, surface proteins, antibacterial responses, as well as pro-inflammatory, proangiogenic, or immunosuppressive functions (2–5). It has been reported that a unique neutrophil population emerging during acute inflammation suppresses T cell function, a process dependent of neutrophil Mac-1 and ROS (6). Infection with *Staphylococcus aureus* leads to two subsets of murine polymorphonuclear neutrophils with important differences in their expression of surface markers, cytokine production and macrophage activation potential (7). In systemic lupus erythematosus and other autoimmune diseases, a subpopulation of low-density neutrophils (LDN) with an unclear physiological role has been detected (8). The LDN population with immunosuppressive properties has also been found to accumulate in tumor-bearing mice and cancer patients. In contrast, the high-density neutrophils (HDN) have been shown to have anti-tumorigenic functions (9). Moreover, circulating neutrophil subsets in advanced lung cancer patients have unique immune signatures and are associated with the disease prognosis (10).

Recently, the consecutive myocardial infiltration of two neutrophil subpopulations has been described in a mouse model of myocardial infarction (MI). Cardiac N1 neutrophils isolated on day one post-MI, during the inflammatory phase, showed high levels of pro-inflammatory markers (CCL3, IL-1β, IL-12a, and TNF-α). In contrast, cardiac N2 neutrophils isolated at days 5 and 7, during the reparatory phase, exhibited increased expression of anti-inflammatory markers CD206 and IL-10. Moreover, neutrophils polarized *in vitro* with a combination of lipopolysaccharide (LPS) and interferon-γ (IFN-γ) for N1 or interleukin-4 (IL-4) for N2, exhibited similar markers as the subpopulations found *in vivo* (11). Uncovering the potentially important role of the different neutrophil subtypes in driving inflammation or the resolution of inflammation could have significant therapeutic relevance, as targeting a specific subpopulation may modulate the course of the disease.

S100A8/A9 is an immune mediator abundantly secreted by neutrophils that plays a complex role in various pathologies with an immune and inflammatory component. S100A9 and its dimerization partner S100A8 are rapidly released as the S100A8/A9 heterodimer upon cell activation (12) and functions as a damage-associated molecular pattern (DAMPs) that binds to toll-like receptor 4 (TLR4) (13), and to the receptor for advanced glycation end products (RAGE) (14). Activation of TLR4 by S100A8/A9 has been shown to have an important pro-inflammatory role in the pathogenesis of endotoxin-induced shock (15), autoimmune disease and cancer (16).

After MI, S100A8/A9 is abundantly secreted by activated neutrophils and promotes cardiac inflammation by stimulating myeloid cell production and trafficking to the ischemic myocardium (17). We have recently found that short-term S100A9 blockade with the specific blocker ABR-238901 during the inflammatory phase of MI reduces myocardial and systemic inflammation, and improves cardiac function (17). The precise mechanisms behind these beneficial therapeutic effects remain to be investigated. Interestingly, binding of S100A8/A9 to TLR4 on neutrophils has subsequently been shown to drive IL-1β production, leading to increased myelopoesis in MI (18). As IL-1β secretion is characteristic for the N1 neutrophil phenotype, we hypothesize that S100A8/A9 might play an important role in the development of this particular subpopulation.

In this work, our main aims were: i) to perform a comparative study of N1 and N2 neutrophil genotype, phenotype and function, and ii) to investigate the effects of S100A9 blockade with ABR-238901 on the functions of the two neutrophil subpopulations. Elucidating the immunomodulatory properties of S100A9 inhibition is highly relevant for further development of the compound toward a potential anti-inflammatory treatment in MI and other immune and inflammatory diseases.

MATERIALS AND METHODS

Mice

Male and female C57BL/6J mice, between 12-16 weeks old, were bred and housed in pathogen-free conditions at the Institute of Cellular Biology and Pathology (ICBP) "Nicolae Simionescu". The mice were euthanized through cervical dislocation, and the femurs and tibias were collected in a Petri dish containing ice-cold RPMI 1640 supplemented with 10% FBS and 1% Penicillin/streptomycin, for further isolation of bone marrow.

All animal experiments were performed in strict accordance with the European Guidelines for animal welfare (Directive 2010/63/EU) and approved by The National Sanitary Veterinary and Food Safety Authority (nr. 425/22.10.2018). All procedures were approved by the Institutional Ethics Committee of ICBP "N. Simionescu" (Bucharest, Romania).

Isolation and Polarization of Neutrophils

Isolation of Neutrophils

Cells were isolated from mouse bone marrow by Percoll gradient centrifugation, using a simplified and improved version of a previous protocol (19). Briefly, the bones were placed in HBSS-Prep to prevent drying, the ends were cut and the bone marrow (BM) was flushed into a 50 ml conical tube with HBSS-Prep and

centrifuged at 400 × g for 5 min. For erythrocyte lysis, the pellet was resuspended in 10 ml NaCl 0.2% for 30-40 s and the osmolarity was then restored with 10 ml 1.6% NaCl. The resulting suspension was centrifuged in 62.5% Percoll in HBSS-Prep for 30 min at 1000 × g, without brake. At the end of centrifugation, the neutrophils-containing pellet was transferred to another 15 ml tube, washed twice with HBSS and cells were resuspended in RPMI. The purity of isolated neutrophils was confirmed by flow cytometry using the neutrophil marker Ly-6G and by fluorescence microscopy using Hoechst/PI staining (**Figure S1**).

Polarization of Neutrophils

Freshly isolated neutrophils were pooled from 6–10 mice and cultured for 2h/18h in RPMI medium, in the presence of 100 ng/ml lipopolysaccharide (LPS) and 20 ng/ml interferon gamma (IFNγ) or 20 ng/ml interleukin 4 (IL-4) - in order to obtain polarized N1 (inflammatory) and N2 (anti-inflammatory) neutrophil subsets respectively. This polarization protocol has previously been shown by Ma et al. to generate neutrophil sub-populations with a similar phenotype as the N1/N2 neutrophils isolated from infarcted hearts *in vivo* (11). Unstimulated neutrophils were used as controls (N). In the experiments when S100Ab was blocked, N1 and N2 neutrophils were polarized in the presence of the S100A9 inhibitor ABR-238901 (100μM, Active Biotech AB, Sweden).

mRNA-Sequencing

To profile the gene expression of N1 and N2 neutrophils after 2h polarization, we used 3 samples per condition and $20x10^6$ neutrophils per sample, pooled from several mice. Total RNA was isolated using TRIzol reagent and Phasemaker Tubes (Thermo Fischer, Waltham, Massachusetts, US) and was sent to Novogene (Cambridge, UK) for mRNA-seq analysis. RNA degradation and contamination were monitored on 1% agarose gels. RNA purity was checked using the NanoPhotometer® spectrophotometer (IMPLEN, CA, USA). RNA integrity and quantitation were assessed using the RNA Nano 6000 Assay Kit with the Bioanalyzer 2100 system (Agilent Technologies, CA, USA). A sample from the LPS+IFNγ polarization did not pass the quality control test and was excluded from the downstream analysis.

A total amount of 1 μg RNA per sample was used as input material for RNA analysis. Sequencing libraries were generated using the NEBNext UltraTM RNA Library Prep Kit for Illumina (NEB, USA) following the manufacturer's recommendations and index codes were added to attribute sequences to each sample. Library quality was assessed on the Agilent Bioanalyzer 2100 system (Agilent Technologies, CA, USA). The clustering of index-coded samples was performed on a cBot Cluster Generation System using the PE Cluster Kit cBot-HS (Illumina). After cluster generation, the library preparations were sequenced using Illumina NovaSeq 6000 (Illumina) and paired-end reads were generated.

Raw data (raw reads) of FASTQ format were first processed through fastp (20). Clean data were obtained by removing reads containing adapter and poly-N sequences and reads with low quality from raw data. Simultaneously, Q20, Q30 and GC content of the clean data were calculated (**Supplementary Table 1**). Paired-end clean reads were aligned to the Ensembl mouse reference genome (GRCm38.p6) (21) using the Spliced Transcripts Alignment to a Reference (STAR) software (22). A summary of the mapping result is presented in (**Supplementary Table 2**). Gene expression values FPKM (expected number of Fragments Per Kilobase of transcript sequence per Millions base pairs sequenced) were calculated and used for the PCA and Pearson correlation coefficient matrix, using R software (23).

Differential Expression Analysis

Differential expression analysis was performed using the DESeq2R package (2_1.6.3) (24). The resulting P values were adjusted using Benjamini and Hochberg's approach for controlling the false discovery rate (FDR). Genes with an adjusted P-value <0.05 found by DESeq2 were assigned as differentially expressed (DEGs). Using a built-in R package, pheatmap, a hierarchical clustering heatmap was generated presenting the log2(FPKM+1) of DEG union within all comparison groups. Volcano plots were realized using EnhancedVolcano R package (25).

Functional Analysis of DEGs

Functional enrichment analysis of the up-regulated N1 gene cluster was performed using g:GOSt function in gProfiler version e102_eg49_p15_7a9b4d6, database updated on 15/12/2020 (26). The selected organism was *Mus musculus*, the significance threshold was g:SCS, with a user threshold of 0.01. Gene Ontology, pathways from KEGG, Reactome and regulatory motif matches from TRANSFAC databases were inquired.

GO enrichment and KEGG database enrichment analysis was performed using the clusterProfiler R package (27) on all the DEGs, either down or up-regulated and the terms with a corrected P value less than 0.05 were considered significantly enriched.

Quantitative RT-PCR

Validation of key molecules found to be highly increased by RNA-seq was performed by qPCR using RNA obtained from pooled neutrophils isolated from subsequent experiments. Total cellular RNA was extracted from N, N1 and N2 neutrophils using TRIzol or Qiagen PureLink RNA Kit (Ambion™, Carlsbad, CA). First-strand cDNA synthesis was performed employing 1 μg of total RNA and MMLV reverse transcriptase, according to the manufacturer's protocol (Invitrogen). Assessment of mRNA expression was done by amplification of cDNA using a LightCycler 480 Real-Time PCR System (Roche) and SYBR Green I. The primer sequences for the mRNAs of interest are shown in **Supplementary Table 3**. The relative quantification was done by the comparative CT method and expressed as arbitrary units. Beta-actin was used as reporter gene.

Cytokine Array

The presence of soluble pro-inflammatory cytokines and chemokines in the neutrophil condition media was analyzed using the Proteome Profiler Mouse Cytokine Array Kit (ARY006, R&D Systems) in conditioned media from the N, N1 and N2 subpopulations. Detection of the chemiluminescent signal was

performed using the Luminescent image analyzer LAS 4000 (Fujifilm). The mean pixel density of each point was calculated using ImageJ (Bethesda, MD).

Enzyme Linked Immunosorbent Assay (ELISA)

The supernatant was harvested from control (N) or polarized N1 and N2 neutrophils cultured in the presence or absence of ABR-238901 (100 μM). We measured the amount of the proteins of interest released in the condition media by using specific kits (R&D Systems & Mabtech), following the manufacturer's instructions.

Measurement of Reactive Oxygen Species

Control (N) or activated neutrophils (N1 and N2) were assayed for intracellular ROS using 2′,7′-dichlorofluorescein diacetate (DCFH-DA) as previously described (28). Briefly, the cells were incubated with 5 μM DCFH-DA (30 min at 37°C) and the DCF fluorescence emission was detected at 535 nm with an excitation wavelength of 485 nm in a 96-well microplate reader (GENios, Tecan). Immediately after DCF measurements, cells were further incubated for 20 min with Hoechst 33342 (0.2 μg/ml) and the fluorescence was measured at 460 nm (with an excitation wavelength of 345 nm). ROS was expressed as DCF/Hoechst fluorescence units.

The Cellular Energetics of N1 and N2 Neutrophils

An XFp Extracellular Flux Analyzer (Seahorse, Agilent Technologies) was used to measure the oxygen consumption rate (OCR) and the proton efflux rate (PER) as a measure of extracellular acidification in control (N) or polarized neutrophils (N1 and N2). Immediately following isolation, neutrophils were added at 5 x 10^5 cells/well onto a poly-L-lysine coated XFp plate and stimulated for 2 h to obtain polarized N1 and N2 neutrophil subsets. The OCR and PER were measured in XF media (non-buffered DMEM containing 10 mM glucose, 4 mM L-glutamine, and 2 mM sodium pyruvate) under basal conditions and in response to phorbol 12-myristate 13-acetate (PMA) activation. After 3 h, 500 nM Rotenone was injected to measure the amount of OCR due to mitochondrial activity. After the measurements, data were normalized to the cell number by staining the cells for 10 min with Hoechst 33342 (5 μg/ml) followed by measurement on a microplate reader (GENios, Tecan). The assay was performed twice in duplicates for each condition.

Determination of Cell Migration by Chemotaxis Assay

Real-time migration was monitored using CIM-plate-16 and the xCELLigence System RTCA DP Instrument (Roche). We used a 16-well modified Boyden chamber composed of an upper chamber (UC) and a lower chamber (LC) that snapped together to form a tight seal. The bottom of the UC consists of a microporous polyethylene terephthalate membrane that permits the translocation of cells from the upper to the bottom side. Cell migration was monitored by interdigitated gold microelectrode sensors that generate an impedance signal by contact with the migrated cells. IL-8 (300ng/ml) was added as a chemoattractant in the LC. We seeded 4x10^5 neutrophils in the UC of the CIM-plate-16 in RPMI medium without FCS. Cell migration was monitored for up to 20 h.

Gelatin Zymography

The gelatinolytic activity of the MMP-9 released by N, N1 and N2 neutrophils in the culture medium was evaluated by gelatin zymography, as previously described (29). Briefly, the cell culture medium was collected and the nonreducing Laemmli's buffer was added to the cell-free neutrophil supernatants and subjected to electrophoresis under non-reducing conditions on 10% polyacrylamide gels containing 1 mg/mL gelatin as substrate. After electrophoresis, the gels were re-natured in 2.5% Triton X-100 (2 × 30 minutes) and incubated with 50 mmol/L Tris-HCl pH 7.4, containing 10 mmol/L $CaCl_2$ and 0.2 mmol/L PMSF (18 hours, 37° C). The gels were subsequently stained with 0.2% Coomassie brilliant blue R-250 and de-stained with 10% acetic acid and 25% methanol. The white bands against the blue background were indicative of the gelatinolytic activity of MMP-2/-9. Image acquisition was done with a transillumination imaging system LAS 4000 (Fujifilm). Data are presented as fold increase over the unstimulated control.

Western Blot

Following polarization, neutrophils were rapidly chilled by the addition of ice-cold HBSS. Neutrophils were pelleted, supernatants were collected and the cell pellets were lysed using RIPA lysis buffer supplemented with a protease inhibitor cocktail. After centrifugation (12000 × g), the proteins were quantified by bicinchoninic acid (BCA) Protein Assay Kit. Samples (30 μg protein) were separated on 10% SDS-PAGE (sodium dodecyl sulfate-polyacrylamide) gel electrophoresis and transferred to nitrocellulose membranes, which were subsequently probed with specific antibodies. The signals were visualized using SuperSignal West Pico chemiluminescent substrate (Pierce) and quantified by densitometry employing the gel analyzer system Luminescent image analyzer LAS 4000 (Fujifilm) and the Image reader LAS 4000 software.

Detection of Myeloperoxidase (MPO) and Nitric Oxide (NO)

Quantification of MPO activity was performed in the cell lysate, and of NO levels in the conditioned media, using specific kits from Elabscience (K074 and K035, respectively). Following polarization, conditioned media from N, N1, N2 neutrophils were harvested and used for NO detection, while neutrophils were rapidly chilled with ice-cold PBS, centrifugated and the resulted cell lysate used for MPO quantification according to the manufacturer's instructions.

Statistical Analyses

GraphPad Prism 7.0 with data points expressed as mean ± standard deviation (SD) was used for all statistical analyses. We used a two-tailed Student's t-test when comparing two experimental groups and a one-way ANOVA and Tukey's multiple comparison test when comparing more than two groups. A p-value of $p<0.05$ was considered statistically significant.

Data Access

All sequencing data have been deposited in the ArrayExpress database, https://www.ebi.ac.uk/arrayexpress/E-MTAB-10508. All other data are available from the authors on request.

RESULTS

N1 and N2 Neutrophils Exhibit a Distinct Transcriptomic Profile

RNA obtained from freshly isolated neutrophils polarized for 2h with LPS+IFNγ (N1) or IL-4 (N2), was analyzed by RNA-seq. The sample replicates showed a high degree of correlation, as determined by Pearson correlation matrix (**Figure S1**).

The hierarchical clustering analysis showed a distinct transcriptomic profile of the N1 and N2 neutrophil populations compared with control neutrophils (N) (**Figure 1A**). Additionally, we performed a differential expression analysis to generate modules of genes that are significantly modulated in each neutrophil population. With a cutoff criterion of absolute fold change ≥ 1.0 and adjP < 0.05, 966 genes were found to be differentially expressed in N1 neutrophils compared to control (771 genes were increased and 195 genes were decreased), and 532 genes were found to be differentially expressed in N2 neutrophils (408 genes were increased and 124 genes were decreased) (**Figures 1B, C**). In N1 neutrophils, a substantial number of up-regulated genes code for inflammatory cytokines and chemokines such as TNF-α, IL-10, IL-12, IL-1β, IL-1α, CCL3, CCL4, CCL5, CCL7, CCL9, CXCL1, CXCL2, CXCL3, CXCL10, CXCL16 (**Figure 1D**). These molecules were either unmodified in N2 neutrophils or were down-regulated compared to controls (TNF-α, IL-1β, CXCL16, CXCL2, CXCL10) (**Figure 1D**).

The gene ontology (GO) enrichment analysis highlighted biological processes and functions that are significantly associated with the modified genes in N1 and N2 neutrophils. The differentially modulated genes in N1 neutrophils are associated with cytokine production, cell response to LPS, cell chemotaxis and cytokine mediated-signaling pathways (**Figure S2A**). In contrast, genes found to be modified in N2 cells are related to T cell activation and differentiation, cell-cell adhesion and immune response (**Figure S2B**).

Interestingly, a central cluster of 391 highly up-regulated genes is well represented in N1 neutrophils compared with N2 and control cells (**Figures 1A** and **S3**). Functional enrichment analysis for the genes in this cluster revealed as significantly enriched the following terms: i) biological process - "defense response"; ii) molecular function - "cytokine activity" and "cytokine receptor binding"; iii) KEGG pathway analysis - "TNF signaling pathway", "NF-kappa B signaling pathway"; iv) TRANSFAC - Factor: RelA-p65 as the most enriched transcription factor (**Figure 1E**). The results emphasize that the highly up-regulated genes in the N1 subset are associated with an inflammatory response. A list of the 10 most enriched terms for each database searched is presented in **Figure S4**.

Following the RNA-seq analysis, we validated a selection of differentially expressed inflammatory/anti-inflammatory genes by qPCR in neutrophils polarized for 2h or 18h. Compared to control neutrophils, the N1 neutrophils exhibited higher gene expression of the pro-inflammatory mediators TNF-α, IL-12, IL-1β, CCL2 (MCP-1), CCL3 (MIP-1α), and CCL5 (RANTES) both at 2h and 18h (**Figures 2A–G**). The gene expression of inflammatory cytokines was time-dependent, reaching higher levels at 18h compared with 2h of activation. IL-6 was highly induced in N1 neutrophils only after 18h of activation (**Figure 2D**). The anti-inflammatory markers CD206, Ym1 and Arg1 were increased in N2 neutrophils, but not in N1 cells (**Figures 2I–K**). However, the IL-10 gene expression was unchanged in N2 neutrophils and was overexpressed in N1 cells (**Figure 2H**). The data are in agreement with the results of RNA-seq expression where the gene encoding for IL-10 was found to be ~10-fold upregulated in N1 neutrophils.

Expression of inflammatory genes in N2 neutrophils was similar to unstimulated controls, except for the IL-1β that was decreased (**Figure 2C**). These results are in agreement with the results obtained by RNA-seq, where IL-1β and TNF-α were significantly decreased in N2 neutrophils compared with controls.

To validate these findings in an inflammatory state in humans, we analyzed the gene expression of CCL3, IL-6, IL-1β, and CD206 in human blood neutrophils isolated from MI patients during the first 24h after infarction. We found that the gene expression of CCL3 and IL-6 was significantly increased in neutrophils from these patients compared with healthy controls (**Figure S6**). These data demonstrate the involvement in human pathology of N1-like inflammatory neutrophils with a gene expression profile similar to the N1 neutrophils isolated from the infarcted myocardium (11) and to the N1 neutrophils derived *in vitro*. The gene expression of the N2 marker CD206 was not significantly affected in this early stage of the disease.

Additionally, we investigated the expression of N1/N2 surface markers by flow cytometry in a mouse model of endotoxemia (LPS-induced acute systemic inflammation). Circulating neutrophils were analyzed at 24h after the LPS treatment. Neutrophils from these mice were characterized by a significantly higher surface expression of CD11b (Mac-1) and ICAM-1 (**Figures S7D, E**), molecules involved in neutrophil adhesion, rolling and recruitment into the tissue. These results offer *in vivo* support for our *in vitro* data: RNA-seq data where ICAM-1 expression was 11 times increased in N1 compared with control neutrophils (log2FC:3,56; **Figure 1D**), cytokine array showing the increased shedding of sICAM-1 in N1 neutrophils (**Figures 4A, B**), and with the increased chemotactic activity of N1 neutrophils (**Figure 5G**). Similar to MI patients, LPS treatment did not modulate the surface CD206 expression of mice circulating neutrophils (**Figures S7D, E**), suggesting that N2-like neutrophils are not present in blood during the inflammatory stage.

S100A9 Blockade Decreases Gene Expression of the Myeloid Chemotactic Chemokines CCL2, CCL3 and CCL5 in N1 Neutrophils

To assess the importance of S100A8/A9 for the immunostimulatory function of N1 neutrophils, we polarized bone marrow-derived neutrophils with LPS and IFNγ in the presence of the specific

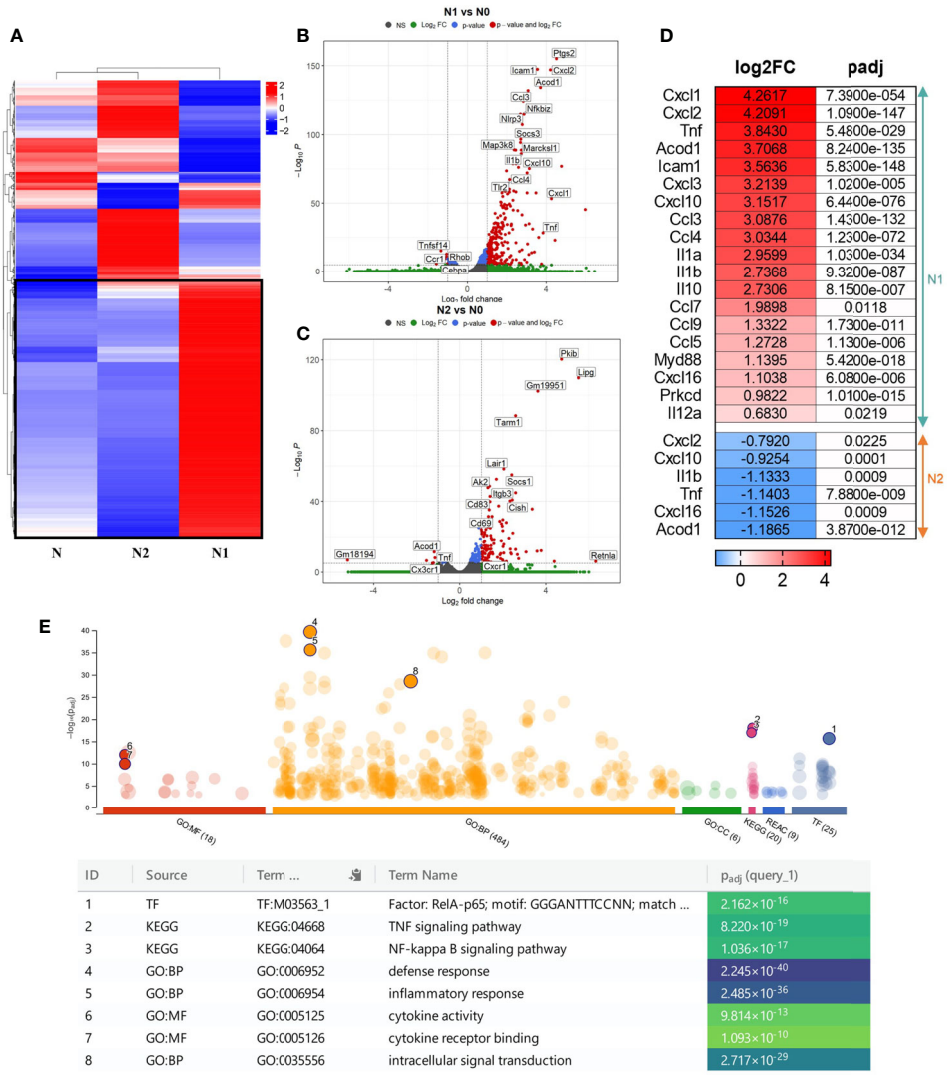

ID	Source	Term ...	Term Name	p_{adj} (query_1)
1	TF	TF:M03563_1	Factor: RelA-p65; motif: GGGANTTTCCNN; match ...	2.162×10^{-16}
2	KEGG	KEGG:04668	TNF signaling pathway	8.220×10^{-19}
3	KEGG	KEGG:04064	NF-kappa B signaling pathway	1.036×10^{-17}
4	GO:BP	GO:0006952	defense response	2.245×10^{-40}
5	GO:BP	GO:0006954	inflammatory response	2.485×10^{-36}
6	GO:MF	GO:0005125	cytokine activity	9.814×10^{-13}
7	GO:MF	GO:0005126	cytokine receptor binding	1.093×10^{-10}
8	GO:BP	GO:0035556	intracellular signal transduction	2.717×10^{-29}

FIGURE 1 | Gene expression profiling of the different neutrophil subsets. **(A)** Hierarchical Clustering Heatmap analysis of N, N1, and N2 neutrophils. Hierarchical clustering analysis was conducted of log2(FPKM+1) of differential expression genes union within all comparison groups. The color coding indicates different levels of expression: red indicates genes with high expression, and blue indicates genes with low expression levels. A major cluster of DEGs up-regulated in N1 is highlighted in a black square. **(B, C)** Volcano plot of differential gene expression between N1/N2 and N cells. The red dots represent significantly up-regulated and down-regulated genes with – adjP < 0.05 and Log2FC > 1: 771 genes were up-regulated and 195 genes were down-regulated in N1 *vs* N neutrophils; 532 genes were up-regulated and 124 genes were down-regulated in N2 *vs* N cells. **(D)** Heatmap showing log2 Fold change and adjusted p-value for selected inflammatory cytokines and chemokines differentially expressed either in N1 (upper panel) or N2 neutrophils (lower panel). Red color indicates the up-regulated, and blue the down-regulated genes. **(E)** Manhattan plot illustrating the results of the enrichment analysis of the gene cluster of highly up-regulated genes in N1 compared with N and N2 neutrophils. The functional terms are grouped and color-coded by data sources, i.e., molecular function (MF) in red, biological processes (BP) in orange, cellular components (CC) in green, KEGG in pink and TRANSFAC in dark blue. Numbered terms are detailed below the plot with their respective adjP values.

S100A9 blocker ABR-238901 (ABR). ABR-238901 inhibits the binding of S100A9 to its cognate receptors, as previously described (17).

Gene expression of the inflammatory cytokines TNFα, IL-12, and IL-1β, and of the chemokines CCL2 (MCP-1), CCL3 (MIP-1α), and CCL5 (RANTES) was measured after 2h and 18h of stimulation. We found that S100A9 blockade significantly reduces the expression of CCL2, CCL3, and CCL5 (**Figures 3D–F**), but has no effect on the gene expression for inflammatory cytokines (**Figures 3A–C**).

Soluble Immune Mediators Released by N1 and N2 Neutrophils

To confirm the mRNA results on protein expression level, we evaluated the levels of cytokines and chemokines present in the condition media of N1/N2 neutrophils after 18h polarization

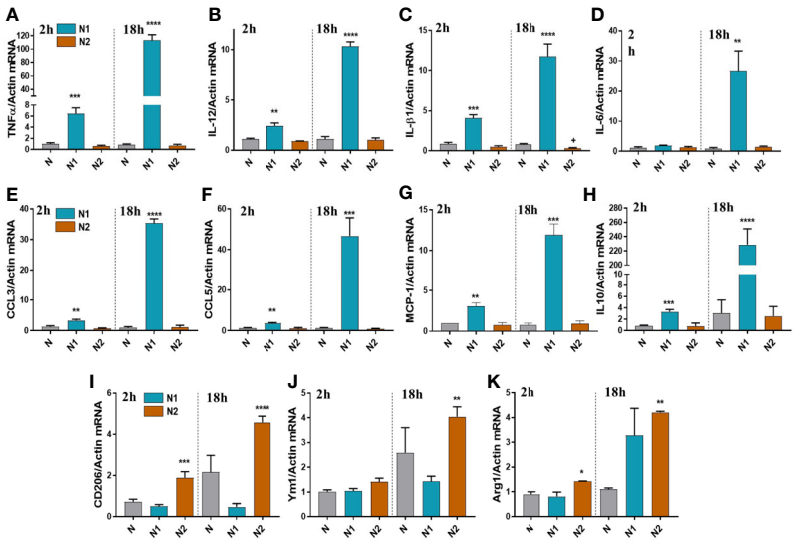

FIGURE 2 | Gene expression of inflammatory and anti-inflammatory markers in neutrophils polarized for 2 or 18h with LPS+IFNγ (N1) or IL-4 (N2). **(A–G)** qPCR for inflammatory markers: TNFα, IL-12, IL-1β, IL-6, CCL3, CCL5, MCP-1, in N1 and N2 compared to control neutrophils (N). **(H–K)** qPCR for anti-inflammatory markers: IL-10, CD206, Ym1 and Arg1, in N1, N2 and N. n = 5, *p < 0.05, **p < 0.01, ***p < 0.001, ****p < 0.0001 (N1 or N2 *vs*. N).

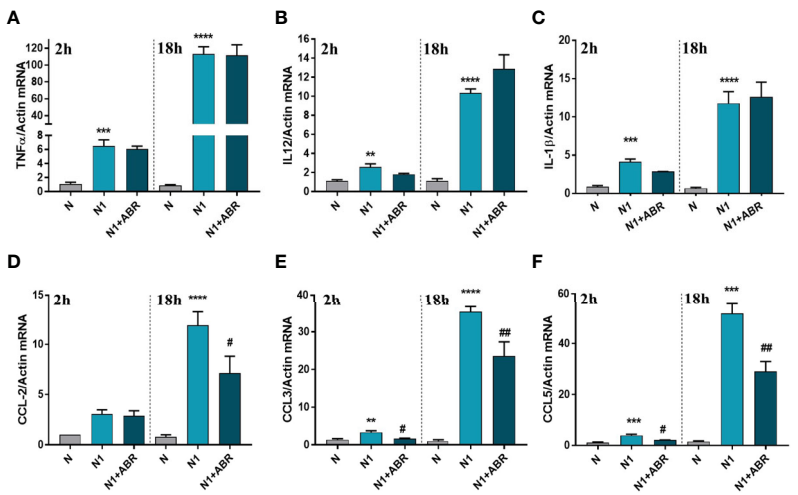

FIGURE 3 | The effect of S100A9 blockade on gene expression of immune mediators **(A–F)** in neutrophils exposed to LPS+IFNγ (N1) or IL-4 (N2) in the presence of ABR-238901 (ABR). The treatment decreases significantly the gene expression of CCL2, CCL3 and CCL5 in N1 neutrophils at both 2h and 18h. n = 3; **p < 0.01, ***p < 0.001, ****p < 0.0001 (N1 *vs* N); #p < 0.05, ##p < 0.01 (N1+ABR *vs* N1).

with LPS and IFNγ, with or without ABR-238901. The levels of inflammatory molecules were measured by a Proteome Profiler Mouse Cytokine array kit or by ELISA.

The cytokine protein profiler was assessed in the neutrophil condition media pooled from 3 independent experiments. We found that control neutrophils secrete only 6 of the 40 cytokines determined by the kit, namely, IL-1ra, sICAM-1, IL-16, CXCL10, SDF1 and TREM. Compared with controls, N1 neutrophils secreted higher levels of 18 inflammatory cytokines/chemokines including CCL2, CCL3, CCL5, TNF-α (>30-fold change), as well as IL-6 and IL-1β (>2-fold change) (**Figures 4A, B**). S100A9 blockade significantly decreased the secretion of IL-1ra, IL-10, CCL2, CCL3, CCL5 and increased the production of IL-16. The inhibitory effects of the treatment on chemokine secretion agree well with the gene expression data (**Figure 3**).

To further verify the gene and protein array data, we have used ELISA to quantify the levels of a mediator that was modulated by ABR (CCL3) and one that was not (IL-12). The

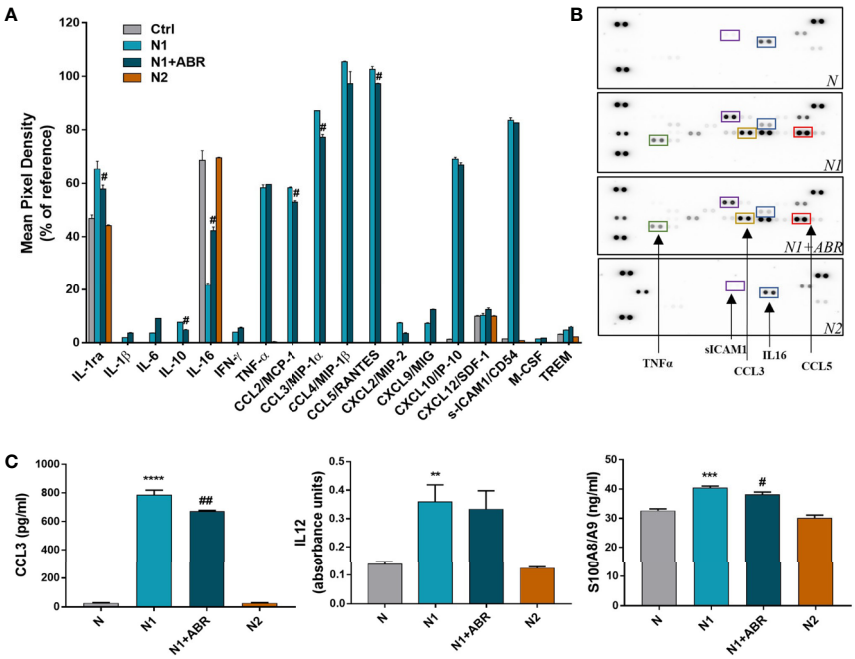

FIGURE 4 | Effects of S100A9 blockade on neutrophil mediators released in the conditioned media after 18h of culture. **(A)** Quantification of mediators present in the culture medium from N1, N1 treated with ABR-23901, and N2 neutrophils compared to control neutrophils (N), as detected by the Proteome Profiler mouse cytokine array. The culture medium was pooled from three experiments. Protein levels were normalized to references on each membrane. $^{\#}p < 0.05$ (N1+ABR versus N1 neutrophils). **(B)** Representative membranes incubated with the condition media from N, N1, N1+ABR and N2 neutrophils. **(C)** Measurement of CCL3, IL-12 and S100A8/A9 in the neutrophil s condition media by ELISA. The data represent mean ± SD from three experiments; $^{**}p < 0.01$, $^{***}p < 0.001$, $^{****}p < 0.0001$ (N1 *vs* N); $^{\#}p < 0.05$; $^{\#\#}p < 0.01$ (N1+ABR *versus* N1).

levels of both molecules were significantly higher in the N1 culture medium compared with control neutrophils, but S100A9 inhibition only reduced the secretion of CCL3 (**Figure 4C**). Additionally, we found a significantly higher S100A8/A9 secretion by N1 neutrophils compared to unstimulated controls and N2 neutrophils (**Figure 4C**), which was reduced by the ABR-238901 treatment. Taken together, the results suggest that S100A8/A9 promotes the secretion of chemotactic factors by N1 neutrophils, and that ABR-238901 has a dual inhibitory effect on S100A8/A9 secretion and function.

Functional Assessment of the N1 and N2 Neutrophil Subtypes

Production of ROS and NO

It has previously been shown that stimulated neutrophils activate NADPH oxidase (NOX2) to generate large amounts of superoxide, which acts as a precursor of hydrogen peroxide and other ROS (30). Intriguingly, factors that stimulate the oxidative burst might also simultaneously trigger iNOS activation in neutrophils or vice versa (31). We set up experiments to compare the capacity of N1 and N2 neutrophils to produce ROS and NO, and to determine whether S100A9 blockade influences these processes. We found that, in contrast with the N2 subtype, N1 neutrophils have significantly higher levels of ROS and NO compared to controls (**Figures 5A, D**). The S100A9 inhibition significantly reduced NO production in N1 neutrophils but did not affect ROS levels in either population.

The Energetic Profile of N1 and N2 Neutrophils

Cellular metabolism plays a decisive role in the function and plasticity of immune cells (1). Since the effector functions of neutrophils during inflammation are tightly linked to their metabolic state, we have investigated the energetic changes occurring in the N1 and N2 populations. The oxidative burst of neutrophils in basal conditions (control) or the presence of LPS + IFNγ (N1) or IL-4 (N2) was quantified by measuring the oxygen consumption rate (OCR) in response to phorbol 12-myristate 13-acetate (PMA). We found an increased OCR by N1 neutrophils compared to controls or N2. The increase in OCR or oxidative burst after activation with PMA was associated with a simultaneous increase in the Proton Efflux Rate (PER), indicating that neutrophils depend on glycolysis for activation (**Figures 5B, C**). Exposure to LPS+IFNγ increased the glycolytic function of neutrophils, which were transformed into metabolically less efficient cells. Inhibition of mitochondrial respiration with rotenone revealed that mitochondria only have a modest contribution to neutrophil oxidative burst after PMA activation (**Figures 5B, C**).

MPO and MMP-9 Activity in Polarized Neutrophils

MPO and MMP-9, along with elastase, are the main tissue destructive enzymes produced by neutrophils and are involved in matrix and protein degradation. We measured the activity of

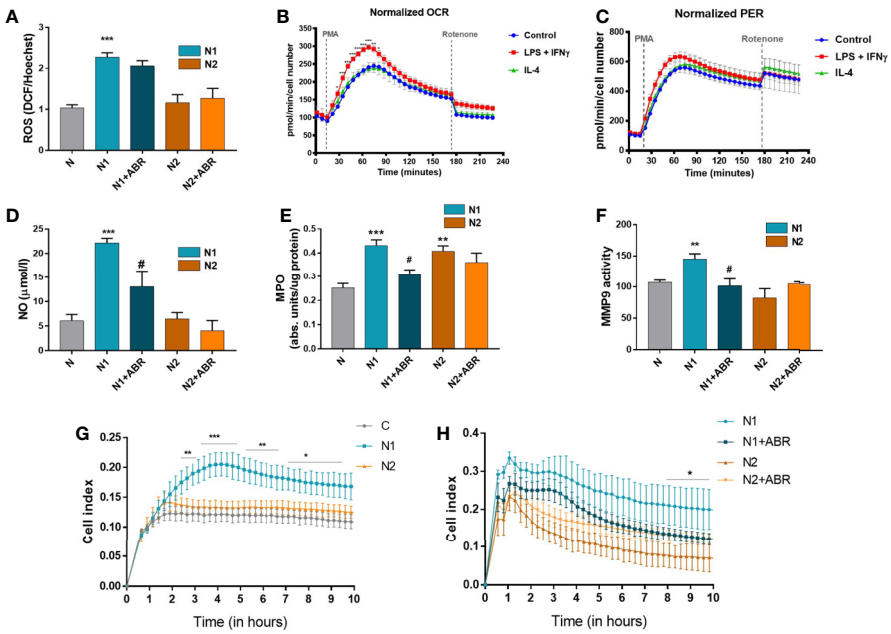

FIGURE 5 | Functional analysis of neutrophil populations. The cells were treated for 18h with LPS + IFNγ(N1) or IL-4 (N2) in the presence or absence of ABR-238901 (ABR). **(A)** Quantification of intracellular ROS using the DCFDA assay. **(B, C)** Measurement of the neutrophil oxidative burst evaluated in response to phorbol 12-myristate 13-acetate (PMA): **(B)**the oxygen consumption rate (OCR) and **(C)** the glycolytic proton efflux rate (PER), calculated using extracellular acidification rate (ECAR) measurements. **(D)** Quantification of NO released in the conditioned medium of neutrophil subtypes. **(E)** evaluation of MPO enzymatic activity in the cell lysate of neutrophil populations. **(F)** Quantification of MMP-9 gelatinase activity assessed by SDS-PAGE zymography in the condition media of neutrophils. **(G, H)** The chemotactic activity of neutrophil populations toward IL-8 evaluated using a CIM-plate 16 and the xCELLigence RTCA DP system. The cell index (CI), proportional to the number of transmigrated neutrophils, was measured as the cell electrical impedance every 15 min over 10h. Data are from four independent experiments; every experiment used pooled neutrophils from at least 5 mice. Data are shown as mean fold change to control ± SE (n = 4). Statistical significance is shown as $^{*}p < 0.05$, $^{**}p < 0.01$, $^{***}p < 0.001$, $^{\#}p \leq 0.05$.

MPO in the cell lysate and of MMP-9 released in the condition media collected from N1 and N2 neutrophils. As shown in **Figure 5E**, MPO activity was significantly increased in both neutrophil phenotypes compared to control. In contrast, MMP-9 activity was only augmented in N1 neutrophils (**Figure 5F**). S100A9 inhibition with ABR-238901 restored both MPO and MMP-9 activity in N1 neutrophils to levels similar to the unstimulated control (**Figures 5E, F**).

Transmigration of Polarized N1 and N2 Neutrophils

The transmigration capacity of polarized neutrophils was monitored using the chemokine IL-8 as a chemoattractant. Despite the lack of a gene coding for IL-8, mice express a receptor homologous to human CXCR2 that mediates neutrophil chemotaxis in response to human IL-8 (32). Neutrophils were placed in the upper chamber of a CIM-plate, and RPMI culture medium containing IL-8 was added to the lower chamber. The chemotactic activity was monitored over 20h using the xCELLigence software. As shown in **Figure 5G**, N1 neutrophils exhibited significantly increased migration capacity compared with N2 or control neutrophils. Only a few neutrophils transmigrated in the lower chamber when RPMI without IL-8 was used as a negative control (not shown). The addition of ABR-238901 in the upper chamber inhibited the migratory capacity of N1 neutrophils (**Figure 5H**).

Molecular Players Involved in the Function of Polarized Neutrophils

NADPH Oxidase Subunits Regulate ROS Production in Neutrophils

Upon activation, neutrophils produce large amounts of ROS *via* the NADPH oxidase complex (33). To investigate the mechanisms responsible for the differences in ROS production between the N1 and N2 neutrophils, we assessed the expression of the main subunits of NADPH oxidase complex in both neutrophil subtypes by real-time PCR and Western blot. Gene expression of Nox2, p47phox and p22phox was significantly increased in N1 neutrophils compared to control (**Figure 6A–C**). Inhibition of S100A9 significantly reduced gene expression of the p22phox subunit. Protein expression of Nox2 and p47phox was also increased in N1 cells. Interestingly, the treatment of polarized neutrophils with ABR-238901 significantly reduced p47phox and Nox2 protein level in N1 neutrophils (**Figure 6D–F**), although no effect was observed at gene expression level (**Figure 6A, B**). Expression of the NADPH subunits in N2 neutrophils was similar to controls on both gene and protein levels and was not influenced by the S100A9 blockade.

Signaling Pathways Activated in N1 and N2 Polarized Neutrophils

RNA-seq analysis identified over 20 signaling pathways that were significantly enriched in N1 and N2 neutrophils [-log10(p adj)>5]

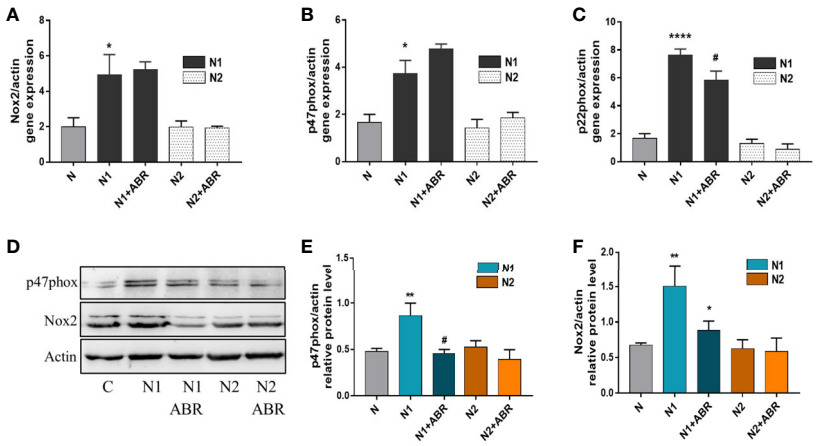

FIGURE 6 | Gene and protein expression of NADPH oxidase subunits in the different neutrophil populations in the presence or absence of ABR-238901 (ABR). **(A-C)** Quantification of gene expression for NADPH oxidase subunits Nox2, p47phox and p22phox by qPCR. **(D-F)** Protein expression of NADPH oxidase subunits p47phox and Nox2 determined by Western blot. n = 3, *p < 0.05, **p < 0.01 ****p < 0.0001 (N1 *versus* control); $^{\#}$p<0.05 (N1 *versus* N1 + ABR).

(**Figures 7A, B**), with NF-kB signaling pathway comprising over 30 DEGs (**Figure 7A**). Among the transcription factors, RelA-p65 was the most up-regulated in N1 neutrophils compared to control (adjP: 2.162×10^{-16}) (**Figure 1E**). To validate these results, we compared the activation status of the NF-kB signaling pathway in N1 *versus* N2 neutrophils. Phosphorylated p65 was significantly increased in N1 neutrophils and unchanged in N2 cells compared with unstimulated control, as assessed by Western Blot (**Figure 7C**). We also evaluated the activation of two other signaling molecules associated with inflammation and oxidative burst, ERK1/2 and PKC. We found a significant increase in pERK1/2 protein expression, but no differences in pPKC levels (**Figures 7D, E**). Blockade of S100A9 with ABR-238901 significantly inhibited both pERK and pp65, supporting its anti-inflammatory properties. pPKC was not modified by ABR-238901 in any of the neutrophil subtypes (**Figure 7E**).

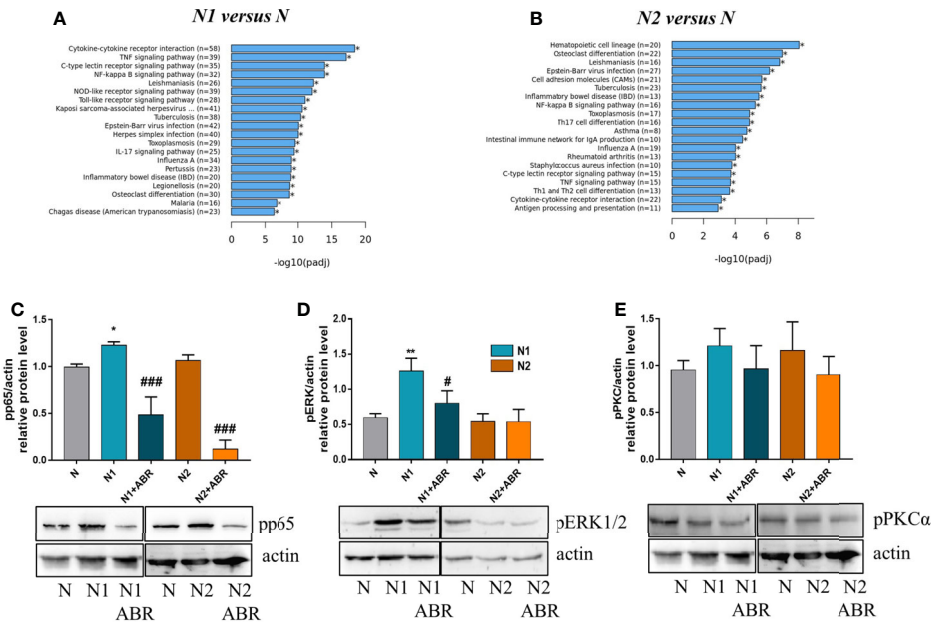

FIGURE 7 | Signaling pathways activated in neutrophils subtypes. **(A, B)** The top 20 signaling pathways revealed by the KEGG signaling pathway enrichment analysis in N1 and N2 compared with control neutrophils (N). **(C-E)** Analysis of the phosphorylation form of p65, ERK and PKC in neutrophil subsets. Cell lysate from control (N), or polarized neutrophils (N1 and N2) cultured for 18h in the presence or absence of ABR-238901 (ABR) was analyzed by Western blot; n = 3, *p < 0.05, **p < 0.01 (N1 *vs* N), $^{\#}$p < 0.05, $^{\#\#\#}$p < 0.001 (N1 *vs* N1 + ABR).

DISCUSSION

Neutrophils, the most abundant leukocytes in human blood, are the first innate immune effectors in infections and sterile inflammation. Aberrant neutrophil responses are associated with various diseases such as sepsis, asthma, MI, and rheumatoid arthritis (34, 35). Recent data have shed new light on the neutrophil responses in various pathologies and the classical view that neutrophils are a homogeneous population has been revised following the identification of novel functions and phenotypic diversity (33, 34). Pro-inflammatory (N1) and anti-inflammatory (N2) neutrophils have been identified under various pathological conditions *in vivo* (2, 11, 36). Recently, Ma et al. have described the sequential infiltration of N1 and N2 neutrophils in infarcted mouse hearts and demonstrated that these cells share phenotypic features with N1 neutrophils derived *in vitro* from naïve neutrophils in the presence of LPS/IFNγ and with IL-4 derived N2 neutrophils (11).

The purpose of our study was to examine the functional differences between the N1 and N2 subpopulations, and to assess the importance of the abundant neutrophil mediator S100A8/A9 in promoting these phenotypes. We have therefore used the same *in vitro* protocol employed by Ma et al. (11). We found that N1 and N2 neutrophil populations have distinct transcriptomic profiles and functions. N1 neutrophils exhibit increased production of inflammatory cytokines/chemokines, elevated levels of ROS and NO, augmented oxidative burst, increased activity of protein and matrix-degrading enzymes, as well as enhanced chemotactic response. Conversely, N2 neutrophils display increased expression of CD206, Ym1 and Arg1, and have similar ROS and NO levels, oxidative burst and chemotactic response as the unstimulated controls. Further, we found that the phosphorylated forms of ERK1/2 and p65, signaling molecules associated with an inflammatory phenotype, are increased in N1 but not in N2 neutrophils. Finally, S100A8/A9 blockade lowered the phosphorylation of ERK1/2 and p65 in N1 neutrophils, leading to reduced production of the chemokines CCL2, CCL3, CCL5, reduced NO, MPO and MMP-9 activity, and slower N1 migration. These data are all the more important as *in vivo* we found that similar N1 inflammatory neutrophils are present in a human inflammation state (post-MI patients), as well as in a mouse model of endotoxemia.

Our RNA-seq analysis of the transcriptomic profile of the two neutrophil populations polarized *in vitro* revealed that N1 neutrophils overexpress genes associated with cytokine production, chemotaxis and cytokine mediated-signaling pathways involved in pro-inflammatory responses. In contrast, the N2 gene profile includes genes involved in T cell activation and differentiation, cell-cell adhesion and other immune responses. Our data confirm the previously described expression of CCL3, CCL5, IL-12a, and TNF-α in N1 neutrophils (11), and identify additional inflammatory chemokines and cytokines up-regulated in this population, such as IL-1α, CCL4, CCL7, CCL9, CXCL1, CXCL2, CXCL3, CXCL10, and CXCL16. Importantly, we found that IL-16 was down-regulated in N1 neutrophils, and TNF-α and IL-1β were down-regulated in N2 neutrophils compared with controls. IL-16 has previously been found to be stored in the neutrophil cytosol and released under conditions of insufficient clearance of apoptotic neutrophils that typically occur at sites of infection and inflammation (37). However, the biological significance of the lower IL-16 release from N1 neutrophils found in our study remains unclear.

Our study is the first to identify that the alarmin S100A8/9, abundantly secreted by activated neutrophils, is an important promoter of the aggressive pro-inflammatory N1 phenotype through an autocrine mechanism. We show that N1 neutrophils secrete higher amounts of S100A8/A9 compared to N2 cells, and that inhibition of S100A9 with the specific blocker ABR-238901 reduces the secretion of S100A8/A9 and of the myeloid chemoattractants CCL2, CCL3 and CCL5. These results extend previous data showing that S100A8/A9 modulates the production of pro-inflammatory mediators including cytokines, chemokines, ROS, and NO in various cell types (38). The reduced production of myeloid chemoattractants induced by S100A9 inhibition provide important mechanistic support to our previous findings in a mouse model of MI *in vivo*, showing that treatment with ABR-238901 prevents neutrophil and monocyte migration from the bone marrow and spleen into the circulation, and recruitment into the heart (17, 39). Consequently, the treatment reduced myocardial inflammation and significantly improved cardiac function compared to controls (17). A close examination of the myocardial environment showed reduced S100A8/A9 staining and CCL5 gene expression at the end of the 3-day treatment (17), which is in agreement with the *in vitro* data presented here. Our findings support the important role of S100A8/A9 as a pro-inflammatory neutrophil mediator, adding to previous data showing that S100A8/A9 induces neutrophil release from the bone marrow and directs their migration in response to LPS (40), primes the NLRP3 inflammasome in neutrophils and stimulates IL-1β production post-MI (41), and is indispensable for MI-induced granulopoiesis (18). Interestingly, in the presence of extracellular calcium the S100A8/A9 heterodimers form inactive $(S100A8/A9)_2$ tetramers that prevent excessive systemic pro-inflammatory effects (42). S100A9 blockade did not have any consequences on N2 neutrophil phenotype and function evaluated in this study. However, we have previously shown that S100A8/A9 activates the transcription factor Nur77 in monocytes and promotes the generation of $MerTK^{hi}$ reparatory macrophages (39). These data add further evidence for the complex activity of these proteins, depending on their biological form, cell type and disease stage.

At the site of infections, activation of NOX2 in neutrophils generates large amounts of ROS, which are essential for antimicrobial host defense (30). However, excessive ROS production also induces tissue injury and exacerbation of the inflammatory reaction in different pathologies. In MI, excessive ROS production by neutrophils may damage the healthy myocardium and promote ventricular remodeling (43). We found that the level of ROS was significantly higher in N1 neutrophils, which have also been shown to dominate the pro-inflammatory phase of the immune response in MI (11). Inhibition of S100A9 significantly decreased the protein levels of the NADPH oxidase subunits Nox2 and p47 in N1 neutrophils, but the gene expression was unaffected. Previous

studies have found that S100A8/A9 heterodimer interacts directly with the cytosolic phox proteins p67 and p47phox (44) and with Nox2 (45) and induces ROS production by activating NADPH oxidases (45, 46). This interaction might explain the observed effects of S100A9 inhibition in our study, but the exact mechanisms remain to be elucidated.

We also found that N1 neutrophils migrate in higher numbers toward IL-8 compared with N2 or control neutrophils, and S100A9 inhibition with ABR-238901 significantly reduced N1 neutrophil transmigration. These data are in good agreement and extend previous results reporting that S100A8, S100A9, and S100A8/A9 are involved in neutrophil migration to inflammatory sites (47), and that leukocyte migration is deficient in S100A9-knockout mice (48). Limiting neutrophil chemotaxis by S100A9 blockade could be a therapeutic strategy for pathologies where excess neutrophil infiltration and activation cause inflammation, impair tissue repair and lead to loss of organ function. Neutrophils mediate tissue damage through the release of proteases from their cytoplasmic granules. As expected, we found that inflammatory N1 neutrophils release an increased level of active MMP-9 and MPO. Exposure of N1 neutrophils to ABR-238901 reduces the activity of both enzymes to levels similar to control cells, adding support to the possible importance of S100A9 blockade in limiting tissue damage.

Understanding the signaling mechanisms involved in the production and release of cytokines/chemokines, proteases, and ROS from neutrophils could provide novel targets for anti-inflammatory therapies. Both LPS and S100A8/A9 activate the TLR4/MD2 receptor complex, leading to recruitment of the adaptor protein MyD88 and sequential activation of IRAK1, ERK, p38 MAPK, and NF-κB (38). S100A8/A9 binding to RAGE also leads to NF-κB activation (14, 38). Here, we show that the MyD88 gene is significantly upregulated and the phosphorylated forms of ERK1/2 and the p65 subunit of NF-kB are more abundant in N1 neutrophils compared to controls. These pathways mediate the neutrophil response to aggressors, including ROS production, cytokine and chemokine synthesis, and induction of anti-apoptotic signals (49). S100A9 blockade reduced the phosphorylation of both p65 and ERK1/2, demonstrating an important contribution of the protein in triggering these pathways. Since both externally-supplied LPS and neutrophil-secreted S100A8/A9 are present in our *in vitro* system, it is difficult to distinguish the relative contribution of the two mediators in triggering TLR4 activation, as they compete for the receptor. The magnitude of the observed effects of S100A9-blockade on N1 neutrophils varied depending on the outcome. The treatment led to important inhibition of N1 migratory ability, NO, MPO and MMP-9 secretion, but only modest reduction in cytokine and chemokine secretion. These results suggest that only certain pathways are affected by the S100A9 inhibition in our system. One possibility could be that ABR-238901 only interferes with the activation of RAGE, while S100A8/A9 binding to TLR4/MD2 is prevented by the presence of LPS. However, this hypothesis is highly speculative and requires confirmation in future experiments employing different combinations of TLR4 and RAGE blockers or LPS-free experimental systems.

Recently, it has been demonstrated that the absence of TLR4 in a mouse model of stroke polarizes the cells toward an N2 phenotype associated with neuroprotection (50). The data suggest a different modulation of neutrophils in absence of TLR4. In N2 neutrophils we found an increased expression of anti-inflammatory markers and reduced production of the inflammatory cytokines TNF-α and IL-1β. Functionally, these cells were similar to control neutrophils in our experimental setting. However, the N2-like phenotype obtained by IL-4 stimulation *in vitro* may differ from the anti-inflammatory neutrophils found *in vivo*. While the N1 inflammatory phenotype appears to dominate the acute response to infection or inflammation *in vivo*, a complex microenvironment is likely to lead to higher neutrophil diversity after the acute phase has ended. This assumption is supported by a recent report investigating cardiac neutrophil diversity in murine MI. The study demonstrated the existence of temporal diversity of neutrophil states in the infarcted heart, identifying 6 transcriptionally distinct cell clusters with a time-dependent appearance (51). In a study focused on tumor-associated neutrophils, the authors also used LPS and IFNγ/IFNβ to derive N1 neutrophils and a much more complex mediator cocktail to derive N2 cells. The cocktail included L-lactate, adenosine, TGF-β, IL-10, prostaglandin E2, and G-CSF, in an attempt to mimic the tumor environment (52). The resulting N2 neutrophils are likely to differ from the IL-4-derived neutrophils used in the present study.

Study Limitations

Our study has several important limitations that have to be considered when interpreting the findings. Firstly, it is important to acknowledge that our simplified experimental system is unlikely to fully reproduce the complex environment present *in vivo*. We chose to employ the same *in vitro* conditions proposed by Ma et al., as these have been shown to generate N1/N2 neutrophils similar to the cells found by these authors in the infarcted mouse hearts *in vivo*. However, as mentioned above, a more detailed study of neutrophil genetic profile post-MI has identified 6 distinct cell clusters that sequentially infiltrated the post-ischemic myocardium (51). It remains unclear whether and how these cells will be able to be generated *in vitro* with enough fidelity in future studies. Secondly, as discussed above, LPS and S100A8/A9 are competing for the TLR4 receptor, which makes it difficult to discern to what extent the two mediators contribute to the observed effects. Lastly, ABR-238901 has specifically been developed to bind to S100A9 and inhibit activation of TLR4 and RAGE. Quinoline-3-carboxamides, first-generation S100A9 blockers, have been shown to block the binding of both the S100A9 homodimer and of the S100A8/A9 heterodimer to mouse and human TLR4 and RAGE (53). However, it has not been tested whether the next-generation blocker ABR-238901 is also able to inhibit the binding of both forms of the protein to the receptors. Therefore, we cannot determine with certainty whether the observed effects are solely due to S100A9 blockade or to the blockade of both forms of the protein.

In conclusion, our study contributes to the understanding of the transcriptomic, phenotypic and functional characteristics N1 and N2 neutrophils and is the first to identify an important

autocrine role of the neutrophil mediator S100A8/A9 in promoting the pro-inflammatory N1 phenotype. These data support previous results suggesting a pathogenic role of S100A8/A9 in clinical trials and *in vivo* models, and promote pharmacological blockade of S100A9 as a potentially important therapeutic strategy in inflammatory disorders with a neutrophil component.

DATA AVAILABILITY STATEMENT

The datasets presented in this study can be found in online repositories. The names of the repository/repositories and accession number(s) can be found below: https://www.ebi.ac.uk/arrayexpress/E-MTAB-10508.

ETHICS STATEMENT

The studies involving human participants were reviewed and approved by Ethics Committee of Elias University Emergency Hospital Bucharest. The patients/participants provided their written informed consent to participate in this study. The animal study was reviewed and approved by The National Sanitary Veterinary and Food Safety Authority (nr. 425/22.10.2018), the Institutional Ethics Committee of ICBP "N. Simionescu", and by the Regional Ethics Committee for Animal Research in Lund, Sweden.

AUTHOR CONTRIBUTIONS

EBu contributed to conception and design of the study, wrote the first draft of the manuscript and performed revision. AS and MS contributed to conception of the study and to manuscript revision. RDM performed RNA-seq analysis and organized the database. ACM, LC, SC, MV, AMG, AH, MMT isolated neutrophils from bone marrow and performed all the experiments. BP designed the RNA-seq experiment and Seahorse assay. ACM and EBu performed the statistical analysis. LC wrote sections of the manuscript. GJ performed experiments with in vivo mouse model of inflammation. EBa and SB recruted the MI patients, isolated blood and managed the ethical approval for research involving human participants. All authors contributed to the article, read and approved the submitted version.

FUNDING

This work was supported by a grant of Ministry of Research and Innovation, CNCS - UEFISCDI, project number PN-III-P4-ID-PCCF-2016-0172, within PNCDI III" and by the Romanian Academy. AS and GJ are also supported by grants from the Swedish Heart and Lung Foundation and from the Swedish Research Council (Vetenskapsrådet).

ACKNOWLEDGMENTS

We are thankful to Gabriela Mesca for skillful assistance.

SUPPLEMENTARY MATERIAL

The Supplementary Material for this article can be found online at: https://www.frontiersin.org/articles/10.3389/fimmu.2021.708770/full#supplementary-material

REFERENCES

1. Kumar S, Dikshit M. Metabolic Insight of Neutrophils in Health and Disease. *Front Immunol* (2019) 10:2099. doi: 10.3389/fimmu.2019.02099
2. Hong CW. Current Understanding in Neutrophil Differentiation and Heterogeneity. *Immune Netw* (2017) 17(5):298–306. doi: 10.4110/in.2017.17.5.298
3. Silvestre-Roig C, Fridlender ZG, Glogauer M, Scapini P. Neutrophil Diversity in Health and Disease. *Trends Immunol* (2019) 40(7):565–83. doi: 10.1016/j.it.2019.04.012
4. Fridlender ZG, Sun J, Kim S, Kapoor V, Cheng G, Ling L, et al. Polarization of Tumor-Associated Neutrophil Phenotype by TGF-β: "N1" Versus "N2" TAN. *Cancer Cell* (2009) 16(3):183–94. doi: 10.1016/j.ccr.2009.06.017
5. Denny MF, Yalavarthi S, Zhao W, Thacker SG, Anderson M, Sandy AR, et al. A Distinct Subset of Proinflammatory Neutrophils Isolated From Patients With Systemic Lupus Erythematosus Induces Vascular Damage and Synthesizes Type I IFNs. *J Immunol* (2010) 184(6):3284–97. doi: 10.4049/jimmunol.0902199
6. Pillay J, Kamp VM, van Hoffen E, Visser T, Tak T, Lammers JW, et al. A Subset of Neutrophils in Human Systemic Inflammation Inhibits T Cell Responses Through Mac-1. *J Clin Invest* (2012) 122(1):327–36. doi: 10.1172/jci57990
7. Tsuda Y, Takahashi H, Kobayashi M, Hanafusa T, Herndon DN, Suzuki F. Three Different Neutrophil Subsets Exhibited in Mice With Different Susceptibilities to Infection by Methicillin-Resistant Staphylococcus Aureus. *Immunity* (2004) 21(2):215–26. doi: 10.1016/j.immuni.2004.07.006
8. Hacbarth E, Kajdacsy-Balla A. Low Density Neutrophils in Patients With Systemic Lupus Erythematosus, Rheumatoid Arthritis, and Acute Rheumatic Fever. *Arthritis Rheumatism* (1986) 29(11):1334–42. doi: 10.1002/art.1780291105
9. Sagiv Jitka Y, Michaeli J, Assi S, Mishalian I, Kisos H, Levy L, et al. Phenotypic Diversity and Plasticity in Circulating Neutrophil Subpopulations in Cancer. *Cell Rep* (2015) 10(4):562–73. doi: 10.1016/j.celrep.2014.12.039
10. Shaul ME, Eyal O, Guglietta S, Aloni P, Zlotnik A, Forkosh E, et al. Circulating Neutrophil Subsets in Advanced Lung Cancer Patients Exhibit Unique Immune Signature and Relate to Prognosis. *FASEB J* (2020) 34(3):4204–18. doi: 10.1096/fj.201902467R
11. Ma Y, Yabluchanskiy A, Iyer RP, Cannon PL, Flynn ER, Jung M, et al. Temporal Neutrophil Polarization Following Myocardial Infarction. *Cardiovasc Res* (2016) 110(1):51–61. doi: 10.1093/cvr/cvw024
12. Edgeworth J, Gorman M, Bennett R, Freemont P, Hogg N. Identification of P8,14 as a Highly Abundant Heterodimeric Calcium Binding Protein Complex of Myeloid Cells. *J Biol Chem* (1991) 266(12):7706–13. doi: 10.1016/S0021-9258(20)89506-4
13. Riva M, Källberg E, Björk P, Hancz D, Vogl T, Roth J, et al. Induction of Nuclear Factor-κb Responses by the S100A9 Protein is Toll-Like Receptor-4-Dependent. *Immunology* (2012) 137(2):172–82. doi: 10.1111/j.1365-2567.2012.03619.x

14. Boyd JH, Kan B, Roberts H, Wang Y, Walley KR. S100A8 and S100A9 Mediate Endotoxin-Induced Cardiomyocyte Dysfunction *via* the Receptor for Advanced Glycation End Products. *Circ Res* (2008) 102(10):1239–46. doi: 10.1161/circresaha.107.167544
15. Vogl T, Tenbrock K, Ludwig S, Leukert N, Ehrhardt C, van Zoelen MA, et al. Mrp8 and Mrp14 are Endogenous Activators of Toll-Like Receptor 4, Promoting Lethal, Endotoxin-Induced Shock. *Nat Med* (2007) 13(9):1042–9. doi: 10.1038/nm1638
16. Ehrchen JM, Sunderkötter C, Foell D, Vogl T, Roth J. The Endogenous Toll-Like Receptor 4 Agonist S100A8/S100A9 (Calprotectin) as Innate Amplifier of Infection, Autoimmunity, and Cancer. *J Leukoc Biol* (2009) 86(3):557–66. doi: 10.1189/jlb.1008647
17. Marinković G, Grauen Larsen H, Yndigegn T, Szabo IA, Mares RG, de Camp L, et al. Inhibition of Pro-Inflammatory Myeloid Cell Responses by Short-Term S100A9 Blockade Improves Cardiac Function After Myocardial Infarction. *Eur Heart J* (2019) 40(32):2713–23. doi: 10.1093/eurheartj/ehz461
18. Sreejit G, Abdel-Latif A, Athmanathan B, Annabathula R, Dhyani A, Noothi SK, et al. Neutrophil-Derived S100A8/A9 Amplify Granulopoiesis After Myocardial Infarction. *Circulation* (2020) 141(13):1080–94. doi: 10.1161/CIRCULATIONAHA.119.043833
19. Mócsai A, Zhang H, Jakus Z, Kitaura J, Kawakami T. Lowell CA. G-Protein-Coupled Receptor Signaling in Syk-Deficient Neutrophils and Mast Cells. *Blood* (2003) 101(10):4155–63. doi: 10.1182/blood-2002-07-2346
20. Cock PJ, Fields CJ, Goto N, Heuer ML, Rice PM. The Sanger FASTQ File Format for Sequences With Quality Scores, and the Solexa/Illumina FASTQ Variants. *Nucleic Acids Res* (2010) 38(6):1767–71. doi: 10.1093/nar/gkp1137
21. Hunt SE, McLaren W, Gil L, Thormann A, Schuilenburg H, Sheppard D, et al. Ensembl Variation Resources. *Database* (2018) 2018:1–12. doi: 10.1093/database/bay119
22. Dobin A, Davis CA, Schlesinger F, Drenkow J, Zaleski C, Jha S, et al. STAR: Ultrafast Universal RNA-Seq Aligner. *Bioinformatics* (2013) 29(1):15–21. doi: 10.1093/bioinformatics/bts635
23. R Development Core Team. *R: A Language and Environment for Statistical Computing*. Vienna, Austria: R Foundation for Statistical Computing (2010).
24. Love MI, Huber W, Anders S. Moderated Estimation of Fold Change and Dispersion for RNA-Seq Data With Deseq2. *Genome Biol* (2014) 15(12):550. doi: 10.1186/s13059-014-0550-8
25. Blighe K RS, Lewis M. *EnhancedVolcano: Publication-Ready Volcano Plots With Enhanced Colouring and Labeling* (2021). Available at: https://github.com/kevinblighe/EnhancedVolcano.
26. Raudvere U, Kolberg L, Kuzmin I, Arak T, Adler P, Peterson H, et al. G: Profiler: A Web Server for Functional Enrichment Analysis and Conversions of Gene Lists (2019 Update). *Nucleic Acids Res* (2019) 47(W1):W191–8. doi: 10.1093/nar/gkz369
27. Yu G, Wang LG, Han Y, He QY. Clusterprofiler: An R Package for Comparing Biological Themes Among Gene Clusters. *OMICS* (2012) 16(5):284–7. doi: 10.1089/omi.2011.0118
28. Dragomir E, Tircol M, Manduteanu I, Voinea M, Simionescu M. Aspirin and PPAR-Alpha Activators Inhibit Monocyte Chemoattractant Protein-1 Expression Induced by High Glucose Concentration in Human Endothelial Cells. *Vascul Pharmacol* (2006) 44(6):440–9. doi: 10.1016/j.vph.2006.02.006
29. Macarie RD, Vadana M, Ciortan L, Tucureanu MM, Ciobanu A, Vinereanu D, et al. The Expression of MMP-1 and MMP-9 is Up-Regulated by Smooth Muscle Cells After Their Cross-Talk With Macrophages in High Glucose Conditions. *J Cell Mol Med* (2018) 22(9):4366–76. doi: 10.1111/jcmm.13728
30. Belambri SA, Rolas L, Raad H, Hurtado-Nedelec M, Dang PM, El-Benna J. NADPH Oxidase Activation in Neutrophils: Role of the Phosphorylation of its Subunits. *Eur J Clin Invest* (2018) 48 Suppl 2:e12951. doi: 10.1111/eci.12951
31. Jyoti A, Singh AK, Dubey M, Kumar S, Saluja R, Keshari RS, et al. Interaction of Inducible Nitric Oxide Synthase With Rac2 Regulates Reactive Oxygen and Nitrogen Species Generation in the Human Neutrophil Phagosomes: Implication in Microbial Killing. *Antioxid Redox Signal* (2014) 20(3):417–31. doi: 10.1089/ars.2012.4970
32. Singer M, Sansonetti PJ. IL-8 is a Key Chemokine Regulating Neutrophil Recruitment in a New Mouse Model of Shigella-Induced Colitis. *J Immunol* (2004) 173(6):4197–206. doi: 10.4049/jimmunol.173.6.4197
33. Mócsai A. Diverse Novel Functions of Neutrophils in Immunity, Inflammation, and Beyond. *J Exp Med* (2013) 210(7):1283–99. doi: 10.1084/jem.20122220
34. Amulic B, Cazalet C, Hayes GL, Metzler KD, Zychlinsky A. Neutrophil Function: From Mechanisms to Disease. *Annu Rev Immunol* (2012) 30:459–89. doi: 10.1146/annurev-immunol-020711-074942
35. Nathan C. Neutrophils and Immunity: Challenges and Opportunities. *Nat Rev Immunol* (2006) 6(3):173–82. doi: 10.1038/nri1785
36. Silvestre-Roig C, Hidalgo A, Soehnlein O. Neutrophil Heterogeneity: Implications for Homeostasis and Pathogenesis. *Blood* (2016) 127 (18):2173–81. doi: 10.1182/blood-2016-01-688887
37. Roth S, Agthe M, Eickhoff S, Möller S, Karsten CM, Borregaard N, et al. Secondary Necrotic Neutrophils Release Interleukin-16C and Macrophage Migration Inhibitory Factor From Stores in the Cytosol. *Cell Death Discov* (2015) 1(1):15056. doi: 10.1038/cddiscovery.2015.56
38. Wang S, Song R, Wang Z, Jing Z, Wang S, Ma J. S100A8/A9 in Inflammation. *Front Immunol* (2018) 9:1298. doi: 10.3389/fimmu.2018.01298
39. Marinkovic G, Koenis DS, de Camp L, Jablonowski R, Graber N, de Waard V, et al. S100A9 Links Inflammation and Repair in Myocardial Infarction. *Circ Res* (2020) 127(5):664–76. doi: 10.1161/CIRCRESAHA.120.315865
40. Vandal K, Rouleau P, Boivin A, Ryckman C, Talbot M, Tessier PA. Blockade of S100A8 and S100A9 Suppresses Neutrophil Migration in Response to Lipopolysaccharide. *J Immunol* (2003) 171(5):2602–9. doi: 10.4049/jimmunol.171.5.2602
41. Sager HB, Heidt T, Hulsmans M, Dutta P, Courties G, Sebas M, et al. Targeting Interleukin-1β Reduces Leukocyte Production After Acute Myocardial Infarction. *Circulation* (2015) 132(20):1880–90. doi: 10.1161/CIRCULATIONAHA.115.016160
42. Vogl T, Stratis A, Wixler V, Völler T, Thurainayagam S, Jorch SK, et al. Autoinhibitory Regulation of S100A8/S100A9 Alarmin Activity Locally Restricts Sterile Inflammation. *J Clin Invest* (2018) 128(5):1852–66. doi: 10.1172/jci89867
43. Hori M, Nishida K. Oxidative Stress and Left Ventricular Remodelling After Myocardial Infarction. *Cardiovasc Res* (2009) 81(3):457–64. doi: 10.1093/cvr/cvn335
44. Doussiere J, Bouzidi F, Vignais PV. The S100A8/A9 Protein as a Partner for the Cytosolic Factors of NADPH Oxidase Activation in Neutrophils. *Eur J Biochem* (2002) 269(13):3246–55. doi: 10.1046/j.1432-1033.2002.03002.x
45. Sylvie B, Athan B, Marie-Helene P, Philippe G, Francoise M. How Important are S100A8/S100A9 Calcium Binding Proteins for the Activation of Phagocyte NADPH Oxidase, Nox2. *Anti-Inflammatory Anti-Allergy Agents Med Chem* (2009) 8(4):282–9. doi: 10.2174/187152309789839000
46. Simard J-C, Simon M-M, Tessier PA, Girard D. Damage-Associated Molecular Pattern S100A9 Increases Bactericidal Activity of Human Neutrophils by Enhancing Phagocytosis. *J Immunol* (2011) 186(6):3622–31. doi: 10.4049/jimmunol.1002956
47. Ryckman C, Vandal K, Rouleau P, Talbot M, Tessier PA. Proinflammatory Activities of S100: Proteins S100A8, S100A9, and S100A8/A9 Induce Neutrophil Chemotaxis and Adhesion. *J Immunol* (2003) 170(6):3233–42. doi: 10.4049/jimmunol.170.6.3233
48. Vogl T, Ludwig S, Goebeler M, Strey A, Thorey IS, Reichelt R, et al. MRP8 and MRP14 Control Microtubule Reorganization During Transendothelial Migration of Phagocytes. *Blood* (2004) 104(13):4260–8. doi: 10.1182/blood-2004-02-0446
49. Schiopu A, Cotoi OS. S100A8 and S100A9: DAMPs at the Crossroads Between Innate Immunity, Traditional Risk Factors, and Cardiovascular Disease. *Mediators Inflammation* (2013) 2013:828354. doi: 10.1155/2013/828354
50. Garcia-Culebras A, Duran-Laforet V, Pena-Martinez C, Moraga A, Ballesteros I, Cuartero MI, et al. Role of TLR4 (Toll-Like Receptor 4) in N1/N2 Neutrophil Programming After Stroke. *Stroke* (2019) 50(10):2922–32. doi: 10.1161/STROKEAHA.119.025085
51. Vafadarnejad E, Rizzo G, Krampert L, Arampatzi P, Arias-Loza A-P, Nazzal Y, et al. Dynamics of Cardiac Neutrophil Diversity in Murine Myocardial Infarction. *Circ Res* (2020) 127(9):e232–e49. doi: 10.1161/CIRCRESAHA.120.317200
52. Ohms M, Möller S, Laskay T. An Attempt to Polarize Human Neutrophils Toward N1 and N2 Phenotypes *In Vitro*. *Front Immunol* (2020) 11:532(532). doi: 10.3389/fimmu.2020.00532
53. Björk P, Björk A, Vogl T, Stenström M, Liberg D, Olsson A, et al. Identification of Human S100A9 as a Novel Target for Treatment of

Autoimmune Disease *via* Binding to Quinoline-3-Carboxamides. *PloS Biol* (2009) 7(4):e97. doi: 10.1371/journal.pbio.1000097

Conflict of Interest: The authors declare that the research was conducted in the absence of any commercial or financial relationships that could be construed as a potential conflict of interest.

Publisher's Note: All claims expressed in this article are solely those of the authors and do not necessarily represent those of their affiliated organizations, or those of the publisher, the editors and the reviewers. Any product that may be evaluated in this article, or claim that may be made by its manufacturer, is not guaranteed or endorsed by the publisher.

frontiers in Immunology

ORIGINAL RESEARCH
published: 13 August 2021
doi: 10.3389/fimmu.2021.701227

Neutrophil Myeloperoxidase Derived Chlorolipid Production During Bacteria Exposure

Kaushalya Amunugama[1,2], *Grant R. Kolar*[3,4] *and David A. Ford*[1,2*]

[1] Edward A. Doisy Department of Biochemistry and Molecular Biology, Saint Louis University School of Medicine, St. Louis, MO, United States, [2] Center for Cardiovascular Research, Saint Louis University School of Medicine, St. Louis, MO, United States, [3] Department of Pathology, Saint Louis University School of Medicine, St. Louis, MO, United States, [4] Research Microscopy and Histology Core, Saint Louis University School of Medicine, St. Louis, MO, United States

Neutrophils are the most abundant white blood cells recruited to the sites of infection and inflammation. During neutrophil activation, myeloperoxidase (MPO) is released and converts hydrogen peroxide to hypochlorous acid (HOCl). HOCl reacts with plasmalogen phospholipids to liberate 2-chlorofatty aldehyde (2-ClFALD), which is metabolized to 2-chlorofatty acid (2-ClFA). 2-ClFA and 2-ClFALD are linked with inflammatory diseases and induce endothelial dysfunction, neutrophil extracellular trap formation (NETosis) and neutrophil chemotaxis. Here we examine the neutrophil-derived chlorolipid production in the presence of pathogenic *E. coli* strain CFT073 and non-pathogenic *E. coli* strain JM109. Neutrophils cocultured with CFT073 *E. coli* strain and JM109 *E. coli* strain resulted in 2-ClFALD production. 2-ClFA was elevated only in CFT073 coculture. NETosis is more prevalent in CFT073 cocultures with neutrophils compared to JM109 cocultures. 2-ClFA and 2-ClFALD were both shown to have significant bactericidal activity, which is more severe in JM109 *E. coli*. 2-ClFALD metabolic capacity was 1000-fold greater in neutrophils compared to either strain of *E. coli*. MPO inhibition reduced chlorolipid production as well as bacterial killing capacity. These findings indicate the chlorolipid profile is different in response to these two different strains of *E. coli* bacteria.

Keywords: neutrophils, 2-chlorofatty acid, 2-chlorofatty aldehyde, plasmalogen, inflammation, *E. coli*, myeloperoxidase

OPEN ACCESS

Edited by:
Clare Hawkins,
University of Copenhagen, Denmark

Reviewed by:
Lars Ingo Ole Leichert,
Ruhr University Bochum, Germany
Christine Winterbourn,
University of Otago, New Zealand

****Correspondence:***
David A. Ford
david.ford@health.slu.edu

Specialty section:
This article was submitted to Molecular Innate Immunity, a section of the journal Frontiers in Immunology

Received: *27 April 2021*
Accepted: *26 July 2021*
Published: *13 August 2021*

Citation:
Amunugama K, Kolar GR and Ford DA (2021) Neutrophil Myeloperoxidase Derived Chlorolipid Production During Bacteria Exposure. Front. Immunol. 12:701227. doi: 10.3389/fimmu.2021.701227

INTRODUCTION

Neutrophils play vital roles in host defense mechanisms against infections and acute inflammation. They are the initial white blood cells to arrive at sites of infection. Neutrophils kill microorganisms through phagocytosis and the release of antibacterial enzymes. Additionally, neutrophils release neutrophil extracellular traps, (NETs) (1), which may provide an additional mechanism for microbe

Abbreviations: 2-ClFA, 2-chlorofatty acid; 2-ClFALD, 2-chlorofatty aldehyde; ATZ, 3-amino-1,2,4-triazole; ARDS, acute respiratory distress syndrome; CFU, colony forming units; cyD, cytochalasin D; ESI-MS, electrospray ionization mass spectrometry; EPEC, enteropathogenic *E. coli*; EtOH, ethanol; ecDNA, extracellular DNA; HBSS, Hank's buffered salt solution; HOCl, hypochlorous acid; LB, Luria Bertani; max RFU, maximum relative fluorescence units; MPO, myeloperoxidase; NETs, neutrophil extracellular traps; PFB, pentafluorobenzyl; PMA, phorbol 12-myristate 13-acetate; PBS, phosphate buffered saline; and SD, standard deviation.

killing. During neutrophil activation, the primary granules release myeloperoxidase (MPO). MPO uses hydrogen peroxide and chloride to produce hypochlorous acid (HOCl). HOCl has a significant role as an antimicrobial agent and has deleterious effects on host cells. HOCl oxidizes proteins, lipids, and DNA (2–5). Previous studies have shown HOCl targets the vinyl ether bond at the *sn*-1 position of plasmalogen phospholipids liberating 2-chlorofatty aldehyde (2-ClFALD) (6, 7). Plasmalogens are enriched in plasma membranes of neutrophils, endothelial cells, monocytes, smooth muscle cells and cardiac muscles (8–11). 2-ClFALD is relatively short-lived due to its electrophilic nature as well as its metabolism. 2-ClFALD can be oxidized to 2-chlorofatty acid (2-ClFA), can be reduced to 2-chlorofatty alcohol, can form Schiff based adducts with amines and can undergo nucleophilic substitution with glutathione to produce the fatty aldehyde-glutathione adduct (12–15).

Increases in 2-ClFALD and 2-ClFA levels have been demonstrated in both sterile and septic inflammation. 2-ClFALD is elevated in human atherosclerotic lesions as well as infarcted myocardium (16, 17). Endotoxemia leads to elevated plasma levels of 2-ClFA and urinary 2-chloroadipic acid, which is the clearance product of 2-ClFA (18). In human sepsis, increased plasma levels of 2-ClFA associate with acute respiratory distress syndrome (ARDS) and 30-day mortality (19). Similarly, plasma levels of 2-ClFA levels are elevated in experimental septic rats that do not survive (20). Furthermore, in experimental sepsis studies 2-ClFA is elevated in many tissues (20). Other studies have shown blockade of chlorolipid production with MPO inhibitors reduces mesenteric microcirculatory dysfunction (21). In cell studies, 2-ClFALD and 2-ClFA have been shown to elicit endothelial dysfunction, endoplasmic reticulum stress, and apoptosis (22–24). Chlorolipids also are neutrophil chemoattractants and elicit NETosis (7, 25).

Although chlorolipids are produced during sepsis, and neutrophil activation by phorbol esters produces chlorolipids, the production of chlorolipids in response to bacteria has yet to be demonstrated. Additionally, the relative production of chlorolipids by neutrophils in response to different bacteria species or strains could be important mechanistically in the chlorolipid production during sepsis. *E. coli* is one of the common microorganisms causing extraintestinal infections, neonatal sepsis, neonatal meningitis, and bacteremia (26). Unlike most commensal *E. coli* strains enteropathogenic *E. coli* (EPEC) possess virulence factors that allow them to become more invasive. These virulence factors include adhesins, siderophores, toxins, protectins, and invasin that help them to colonize on host mucosal surfaces, injure and invade host cells and escape from host defense mechanisms (27, 28). The CFT073 *E. coli* strain is classified under EPEC strains causing urinary tract infections and sepsis. CFT073 suppresses innate immunity by disrupting the inflammasome that is crucial for pathogen recognition, survival within macrophages, and resistance to phagocyte mediated oxidative stress (29–31).

In this study, we compared chlorolipid production in the presence of *E. coli* CFT073 strain and the *E. coli* JM109 strain. The CFT073 strain generated significant amounts of neutrophil-derived 2-ClFA compared to the JM109 strain. Exogenously added 2-ClFALD was bactericidal to both strains but only the JM109 strain was susceptible to killing by 2-ClFA. 3-Aminotriazole (ATZ) blocked both 2-ClFALD and 2-ClFA production in incubations of neutrophils with either CFT073 or JM109 *E. coli* strains. These are the first studies examining chlorolipid production by human neutrophils elicited by different bacteria and reveal important differences in the production of specific chlorolipids dependent on *E. coli* strain.

MATERIALS AND METHODS

Lipids

2-Chlorohexadecanal and 2-chloropalmitic acid were synthesized and purified as previously described (7, 14). 2-Chlorohexadecanal and 2-chloropalmitic acid were used as representative molecular species of 2-ClFALD and 2-ClFA, respectively, in studies designed to examine the biological roles of these two chlorolipid classes. Hexadecanal and palmitic acid were used to delineate specifics effects of chlorolipids.

Human Neutrophils

Human neutrophils were isolated from healthy human donors as previously described under Saint Louis University IRB protocol 9952 (7). In brief, healthy human blood was layered on a density gradient in 1:1 volume with blood and centrifuged at 500g for 30 min. The polymorphonuclear cell band was isolated and washed in Hanks's balanced salt solution (HBSS). Following red cell lysis, the neutrophils were washed twice with HBSS. The isolated neutrophils were suspended in HBSS to prepare the final concentration of $2x10^6$ cell/ml.

Bacterial Strains and Growth Conditions

CFT073 urosepsis *E. coli* strain and JM109 *E. coli* strain were used in these studies. Bacteria were precultured overnight and subcultured in Luria Bertani (LB) agar broth under shaking condition (250RPM) at 37°C. Once cultures reached the exponential growth phase bacteria number was calculated using a pre-drawn growth curve based on O.D. 600nm spectrophotometric readings. Bacteria were washed and suspended in HBSS to prepare indicated concentrations.

Neutrophil and Bacteria Cocultures

Neutrophils were cocultured with bacteria in HBSS at 1:10 ratio for indicated time intervals at 37°C. Plasma was not included in these cocultures to minimize the contribution of plasma lipids in analyses. For MPO inhibition studies, neutrophils were preincubated with 10 mM of ATZ for 5 min before the addition of bacteria. Incubations were terminated by the addition of methanol. To quantify chlorolipids that were released into the media *versus* that which was associated with cells, cocultures were centrifuged at 200g for 10 min to prevent neutrophil rupture. Next, the supernatant was further centrifuged at 4700g for 10 min to sediment bacteria and

remaining cell debris. The cell pellets following centrifugation were combined to detect cell-associated chlorolipids. Lipids were extracted by the modified Bligh Dyer extraction method as described previously (7, 14, 32). 2-Chloro-[d_4]-hexadecanal and 2-chloro-[d_4]-palmitic acid were used as internal standards as previously described (7, 12, 33, 34).

Analyses of Chlorinated Lipids

Molecular species of 2-ClFALD were detected following derivatization to their pentafluorobenzyl (PFB) oximes using PFB hydroxylamine. The derivative products were analyzed using GC/MS using selected ion monitoring as previously described (33, 34). Free 2-ClFA was analyzed directly from the lipid extract while total 2-ClFA was measured following base hydrolysis and a modified Dole extraction as previously described (33, 34). 2-Chlorofatty acid molecular species were quantitated following liquid chromatography by selected reaction monitoring using electrospray ionization mass spectrometry (ESI-MS) on a triple quadrupole instrument (Thermo, Altis).

E. coli Killing by Neutrophils

After coculture of neutrophils with *E. coli*, the survival of *E. coli* was assessed by first adding 100U/ml of DNase to eliminate NETs and aggregated cells. For some experiments $2x10^6$/ml neutrophils were pretreated with 10μg/ml of cytochalasin D (cyD) and 10mM ATZ for 15 min and 5 min respectively prior to the addition of *E. coli* and further incubated for 30 min at 37°C. Next, 50μl of the sample was diluted in pH11 water and then incubated at room temperature for 5 min to lyse neutrophils as previously described (35). Sample were subsequently serially diluted in HBSS and plated on LB agar plates. Colony forming units (CFU)/ml were calculated following overnight incubation. The percentage of bacterial survival was calculated by dividing the bacteria number in the coculture by the control bacteria number without neutrophils (the baseline of 100% survival).

Extracellular DNA Assay

Extracellular DNA (ecDNA) release from neutrophils was assayed as previously described (25). $2x10^6$/ml neutrophils and $20x10^6$/ml *E. coli* were cocultured with 10μM Sytox Green (Invitrogen) and transferred to 96 well black clear bottom plate for incubation at 37°C. ecDNA was detected by fluorescence emission at 523nm by SpectraMax i3 Multi-Mode spectrophotometer. Fluorescence measurements were an average of 21 different regions in a single well to normalize the uneven distribution of ecDNA in the well. ecDNA was expressed as a % of 20 mM saponin-treated neutrophils, which is considered 100% ecDNA.

NET Isolation and Killing Assay

NET isolation from neutrophils was performed using modifications of a previously described method (36). Briefly, $2x10^6$/ml neutrophils in HBSS were plated on 6 well plates and stimulated with 200nM of phorbol 12-myristate 13-acetate (PMA) in 0.1% ethanol for 4 h at 37°C in the presence of 5% CO_2. The media was gently aspirated and discarded. The adherent NETs and neutrophils were collected by washing with cold phosphate buffered saline (PBS) and centrifuged at 400g for 10 min at 4°C to remove whole cells and debris. The NET rich supernatant was further centrifuged at 16300g for 10 min at 4°C. DNA in the isolated NET samples were quantified by QuantiFluor dsDNA system (Promega) according to manufacturer's instructions.

Bacteria killing by NETs was determined by treating $1x10^6$/ml of either CFT073 or JM109 with 50ng/ml of isolated NETs for 30 min at 37°C. Following incubation, 100U/ml of DNase was added for 10 min to break NETs to release the bacteria trapped within NETs. Some experiments were performed with NETs pretreated with 100U/ml DNase. Samples were serially diluted and plated on LB agar plates to determine CFU/ml. Percent bacterial survival was calculated relative to control bacteria without any treatment.

Phagocytosis Assay

CFT073 and JM109 were labeled with pH sensitive pHrodo deep red as specified by the manufacturer (Invitrogen catalogue no. P35357). Briefly, *E. coli* were harvested from the exponential growth phase and washed twice with the manufacturer-provided washing buffer. The cells were then incubated with pHrodo deep red labeling reagent for 2h at room temperature in the dark. Following labeling, cold LB media was added to scavenge unreacted dye and the cells were washed with HBSS. Labeling was confirmed by exposing the labeled bacteria to acidic pH range and measuring fluorescence intensity and the bacteria viability was also checked by plating on LB agar plates (data not shown).

The phagocytosis assay was performed with slight modifications of a previously described method (37). $5x10^5$/ml of neutrophils and $50x10^5$/ml of pHrodo deep red labeled CFT073 and JM109 were mixed together at Neu: *E. coli* ratio of 1:10 in 96-well black clear bottom plates for the incubation at 37°C. The fluorescence emission was measured at 655nm by SpectraMax i3 Multi-Mode spectrophotometer at given time intervals. Some experiments were performed with neutrophils pretreated with 10 μg/ml of cyD for 15 min before incubation with pHrodo deep red labeled *E. coli*. Net phagocytosis was calculated by subtracting the fluorescence intensity of the *E. coli* only wells (negative control without neutrophils) from the cocultured wells and expressed as a percentage of maximum relative fluorescence units (max RFU).

Immunofluorescence of NETs

Neutrophils ($2x10^6$/ml) in HBSS on coverslips were incubated at 37°C in the presence of either $20x10^6$/ml CFT073 or JM109 bacteria for either 30 min or 2h. At the end of the incubation, cells were fixed with 4% paraformaldehyde for 15 min. Following PBS washing, cells were blocked and permeabilized with 0.5% bovine serum albumin and 1% donkey serum in the presence of 0.05% Triton X-100 for 1 h. Next, cells were incubated with primary antibodies against MPO (1:500) (rabbit monoclonal anti-MPO; Abcam catalog no. ab208670) and *E. coli* (1:200) (goat polyclonal anti-*E. coli*; Abcam catalog no. ab13627) in blocking buffer for 1h at room temperature. Cells were then

incubated with secondary antibodies of donkey anti-rabbit Alexa Fluor 594 (1:300) (Jackson ImmunoResearch; catalog no.711-585-152) and donkey anti-goat Alexa Fluor 488 (1:300) (Jackson ImmunoResearch; catalog no.705-545-003) and DAPI (1:2500) (Sigma-Aldrich) for 1 h at room temperature. Slides were mounted with prolong gold antifade reagent. Fifteen contiguous image tiles were captured at 100x (1.40 NA) on a Leica SP8 TCS STED 3X instrument equipped with HyD detectors at full axial depth (0.15 µm increments) of DAPI signal before stitching with Huygens Professional software (SVI, Netherlands). Images were deconvolved in all three channels using Huygens Professional using built in optical parameters and suggested settings. For visualization, 3D reconstructions of image stacks were displayed using built in ray tracing algorithms in Huygens Professional. In all cases, capture settings and visualization thresholds were maintained across groups.

Lipid Treatment of *E. coli*

Bacteria 50x10^6 cells/ml in HBSS were treated with indicated lipid concentrations in 0.1% ethanol (EtOH) for an hour at 37°C. Then serial dilutions of bacteria in each condition were subjected to LB agar plating. Bacterial % survival was calculated by dividing bacteria number following the treatment by vehicle-treated (control) bacteria. To quantify bactericidal activity immediately following 2-ClFALD treatment, Live/Dead BacLight Bacterial Viability kit (Invitrogen) was used according to manufacturer's instructions.

Neutrophil, *E. coli* and Endothelial Cell Metabolism of 2-ClFALD

Neutrophils (1x10^6/ml) and bacteria (50x10^6/ml) were treated with indicated 2-ClFALD concentrations in 0.1% EtOH in HBSS for 1h at 37°C. EA.hy296 cells (passage 4) were grown to 100% confluency and treated with indicated 2-ClFALD concentrations in 0.1% EtOH in Dulbecco's Modified Eagle Medium with 2% FBS for 1h. Media and cells were collected for 2-ClFA analyses by liquid chromatography-ESI-MS. For some experiments supernatants of neutrophil-bacteria cocultures were added back to fresh neutrophils or bacteria with or without 2-ClFALD.

Statistics

Student's t-test was used to compare two groups while one-way ANOVA with Tukey's *post hoc* analysis and Dunnett's *post hoc* test were used to compare three or more multiple comparisons. All data were represented as mean with standard deviation (SD) with averages of 3 biological replicates unless otherwise indicated.

RESULTS

Neutrophil Chlorolipid Production in the Presence of CFT073 and JM109 Strains of *E. coli*

Levels of the 2-ClFALD molecular species, 2-chlorohexadecanal and 2-chlorooctadecanal, were significantly elevated in neutrophils exposed to both CFT073 and JM109 *E. coli* strains compared to control neutrophils (**Figure 1A**). The precursor of 2-ClFALD is plasmalogen (6). Plasmalogen is a major lipid in neutrophils, but not *E. coli* (38, 39). In contrast to 2-ClFALD levels, free and esterified 2-ClFA including chloropalmitic acid and 2-chlorostearic acid were increased only in CFT073 co-cultures **(Figure 1B).** These results were consistent among different neutrophil donors (2-males and 1-female) **(Figures 1A, B).** Although the trends were consistent for increases in chlorolipids in the presence of *E. coli* strains for each neutrophil biological replicate, we did observe a bimodal distribution of data among the biological replicates. One of the two male biological neutrophil replicates in this study consistently had higher levels of chlorinated lipids compared to the other male replicate and the sole female replicate. Additional

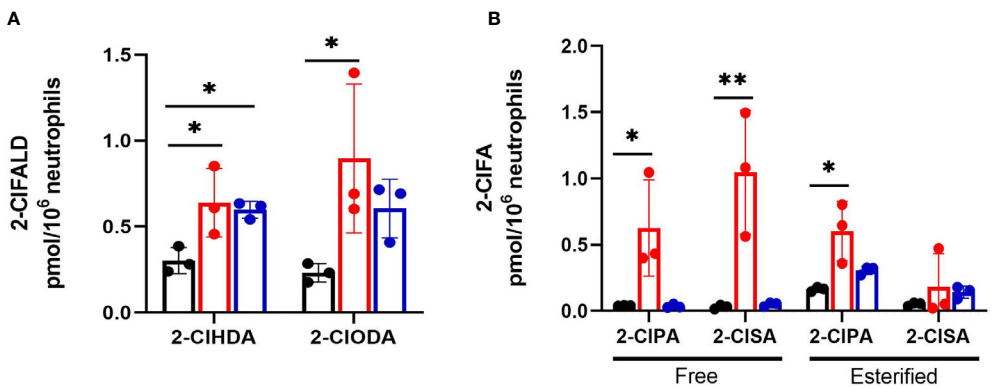

FIGURE 1 | 2-ClFALD and 2-ClFA production in cocultures of neutrophils with CFT073 and JM109 *E. coli* strains. 2x10^6/ml neutrophils were incubated with either no bacteria (control, black), or, CFT073 (red) or JM109 (blue) strains of *E. coli* at a neutrophil: *E. coli* ratio of 1:10 for 30 min at 37°C. 2-ClFALD **(A)** as well as free and esterified 2-ClFA **(B)** were quantified as described in "Materials and Methods". Data are from three neutrophil donors (biological replicates, 1 female, 2 males). 2-ClHDA, 2-ClODA, 2-ClPA, and 2-ClSA are 2-chlorohexadecanal, 2-chlorooctadecanal, 2-chloropalmitic acid and 2-chlorostearic acid, respectively. Multiple comparisons were performed using one-way ANOVA with Dunnett's multiple comparison test. Error bars represent ± SD, p-value: ** < 0.01; * < 0.05.

studies have shown the majority of chlorolipids (2-ClFALD and 2-ClFA) produced in cocultures of neutrophils with either CFT073 or JM109 *E. coli* strains are cell-associated in comparison to release from cells (**Figures 2A–F**).

Neutrophil Responses to JM 109 and CFT073 *E. coli* Strain

Since 2-ClFALD metabolism to 2-ClFA was reduced in neutrophil coculture with JM109 strain compared to CFT073

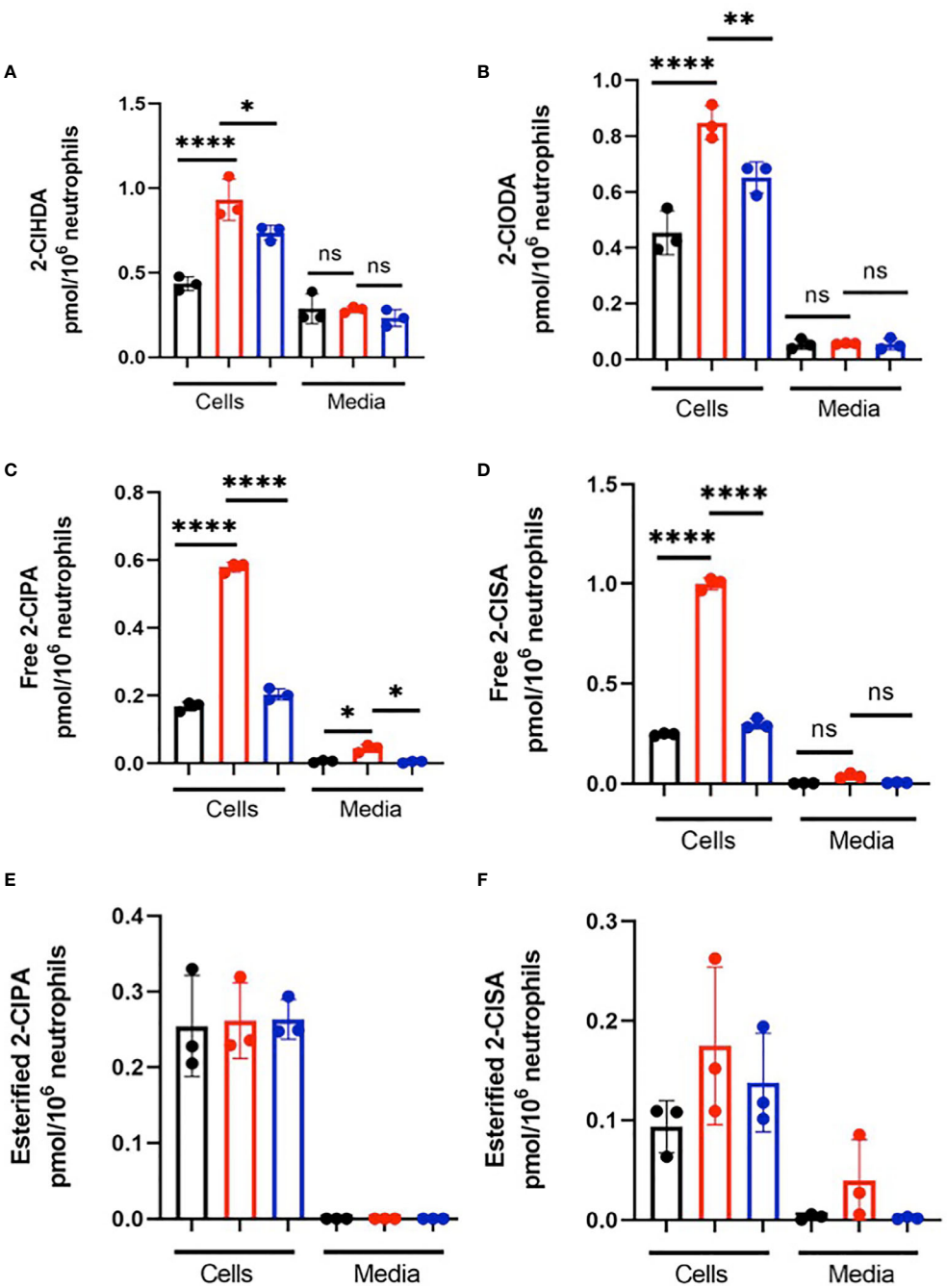

FIGURE 2 | Chlorolipids are cell-associated in neutrophils cocultured with *E. coli.* 2x10^6/ml neutrophils were incubated with either no bacteria (control, black), or, CFT073 (red) or JM109 (blue) strains of *E. coli* at a neutrophil: *E. coli* ratio of 1:10 for 30 min at 37°C. Cells were pelleted, and 2-ClFALD molecular species **(A**, **B)** and 2-ClFA molecular species **(C–F)** were quantified as described in "Material and Methods". 2-ClHDA, 2-ClODA, 2-ClPA, and 2-ClSA are 2-chlorohexadecanal, 2-chlorooctadecanal, 2-chloropalmitic acid and 2-chlorostearic acid, respectively. Multiple comparisons were performed using one-way ANOVA with Tukey's multiple comparison test. Data represent n=3, error bars for ± SD, p-value: ****< 0.0001; **< 0.01; * < 0.05. ns indicates not significant.

strain, we next examined other differences in neutrophil responses to these two strains. First, we examined CFT073 and JM109 survival from neutrophil killing. Similar to studies of others (40), data shown in **Figure 3A** demonstrate the JM109 strain is modestly more vulnerable to neutrophil killing mechanisms compared to CFT073 strain. Inhibiting reactive oxygen species production with ATZ as well as phagocytosis with cyD prevented significant neutrophil killing of both *E. coli* strains (**Figure 3A**). Although others have shown significant non-oxidative killing of *E. coli* (41, 42), it should be noted that conditions employed in the present studies did not include plasma for opsonization. Plasma was omitted to reduce the impact of plasma lipids on lipid analyses during coculture. Phagocytosis of the JM109 strain was marginally greater over

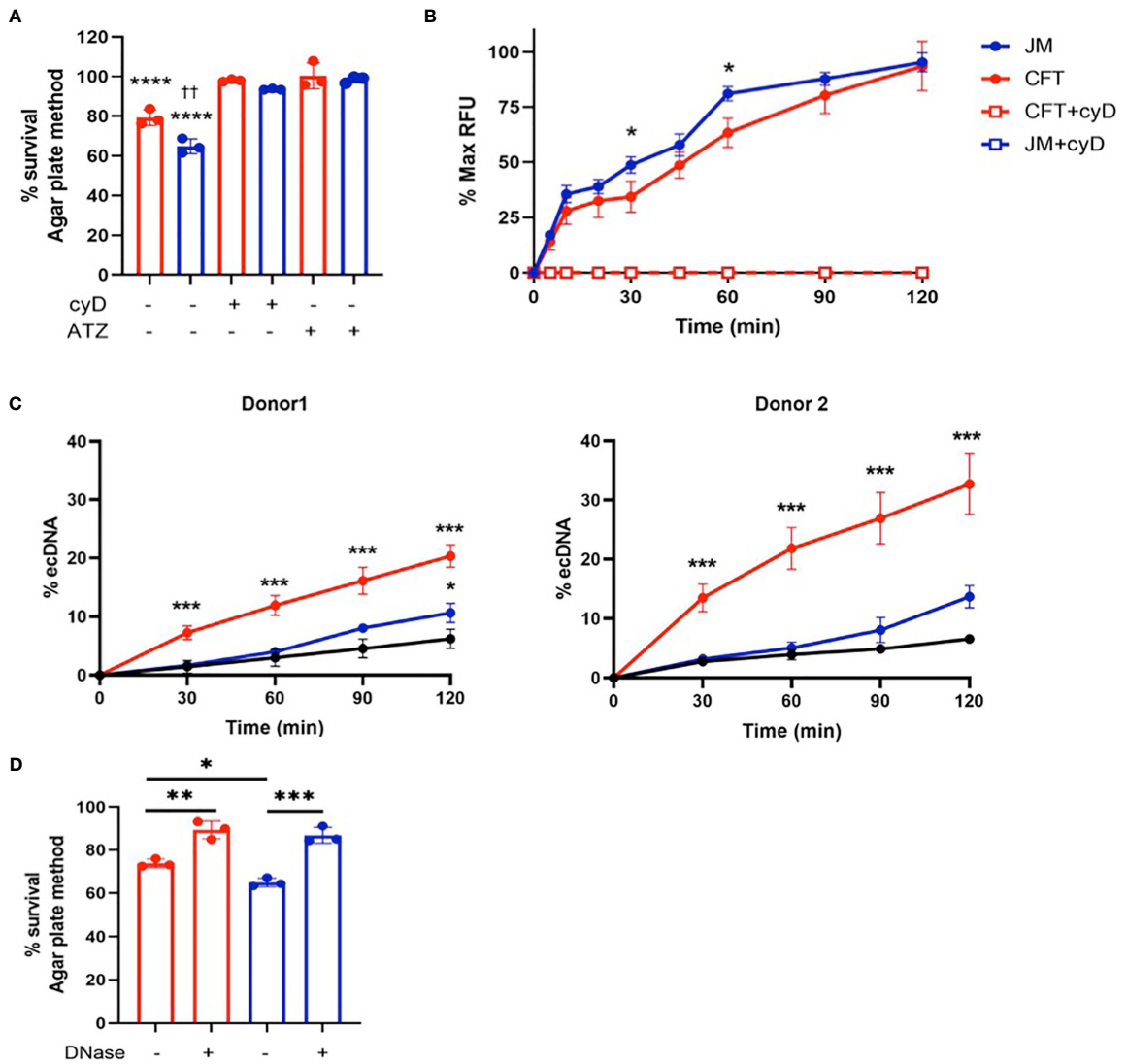

FIGURE 3 | Neutrophil killing mechanisms of *E. coli*. **(A)** 2x10^6/ml of neutrophils were cocultured with either CFT073 (red) or JM109 (blue) at a ratio of neutrophil: *E.coli* 1:10 for 30min at 37°C. Some coculture experiments were performed with neutrophils pretreated with 10mM ATZ for 5min or 10μg/ml cyD for 15 min. Bacteria survival % was calculated compared to control bacteria. p-value: ****< 0.0001, comparison between each treatment *versus* 100% survival control. p-value: ††<0.01, comparison between neutrophil coculture JM109 and coculture CFT073 cells. **(B)** Neutrophils were cocultured with pH sensitive pHrodo deep red labeled CFT073 or JM109 at neutrophil: *E. coli* ratio of 1:10 as well as in the presence of cyD. Phagocytic response is graphed as % max RFU as described in "Material and methods". cyD treated CFT073 (red open squares) and JM (blue open squares) data overlap in the graph. **(C)** ecDNA % was measured in the co-cultures and control neutrophils (black) in experiments with two different neutrophil donors by the Sytox green assay as described in "Materials and Methods" (mean ± SD, n=3). **(D)** 1x10^6 cells of either CFT073 or JM109 strains were incubated for 30 min with isolated 50ng/ml of NETs or NETs pretreated with 100U/ml DNase as indicated. Treatment condition with NETs was further incubated with 100U/ml DNase for 10 min prior to plating on LB plates. Bacterial survival (%) was calculated from CFU/ml relative to control bacteria not exposed to NETs. Values represent the mean ± SD for n=3. Statistics were performed using one-way ANOVA with Tukey's multiple comparison test **(A, C, D)** and unpaired t-test for neutrophil coculture CFT073 *versus* JM109 in **(B)** p-value; ****< 0.0001; ***< 0.001; **< 0.01; * < 0.05.

time in comparison to phagocytosis of the CFT073 strain (**Figure 3B**). Since 2-ClFA levels are increased in CFT073 cocultures with neutrophils and since we previously observed that 2-ClFA can stimulate NETosis (25), we next investigated NETosis in cocultures by measuring ecDNA. ecDNA formation was significantly increased in CFT073 cocultures with neutrophils at 30 min and increased further over time. In contrast, JM109 cocultures with neutrophils resulted in significant ecDNA only following 2h of coculture (**Figure 3C**). Confocal images shown in **Figure 4A** demonstrate the extensive network of NETs formed in cocultures with CFT073 and JM109 *E. coli* strains following 2h of coculture with modest NET formation at 30 min in CFT073 cocultures. Bacteria were trapped in the NETs and MPO was colocalized with NETs (**Figures 4B, C**). Although data shown in **Figures 3A, B** demonstrated phagocytosis is likely the major mediator of JM109 death, we also evaluated the ability of NETs to reduce survival of CFT073 and JM109 *E. coli* strains. NETs were isolated following PMA stimulation, and bacteria were exposed to these NETs for 30 min resulting in reduced viability of CFT073 by 25% and JM109 by 35% (**Figure 3D**). The effect of NETs on *E. coli* survival was reversed by DNase pretreatment.

Bactericidal Activity of Chlorolipids

To further understand the role of chlorolipids in bacteria-neutrophil interactions, we tested whether either 2-ClFALD (2-chlorohexadecanal molecular species) or 2-ClFA (2-chloropalmitic acid molecular species) are bactericidal lipids. JM109 and CFT073 viability was measured with either exogenously-added 2-ClFALD or 2-ClFA. In comparison to JM109, CFT073 is more resistant to chlorolipid-elicited killing by both chlorolipids at all concentrations tested (**Figures 5A, B**). JM109 viability to both 2-ClFALD or 2-ClFA decreases in a concentration dependent manner. Moreover, JM109 is more susceptible to 2-ClFA (~50% survival at 10μM) compared to 2-ClFALD (~70% survival at 10μM) (**Figures 5A, B**). In comparison to 2-chloropalmitic acid, palmitic acid did not kill either *E. coli* strains at any given concentration. However, hexadecanal treatment showed killing ability on JM109 at 1 and 10μM levels.

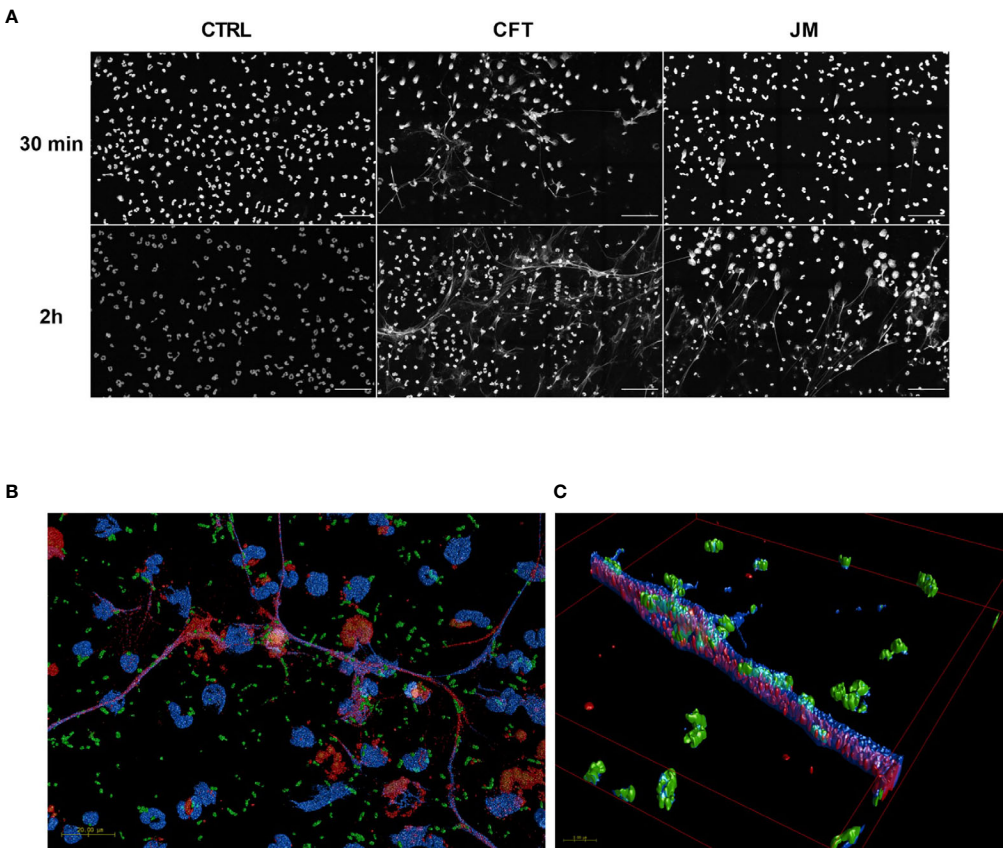

FIGURE 4 | Coculture conditions induce NETosis. 2x10^6/ml of neutrophils were seeded on coverslips and co-incubated with 20x10^6/ml CFT073 or JM109 or without bacteria for the indicated time durations at 37°C. Following incubation cells were fixed, permeabilized and stained with immunofluorescence for DNA with DAPI (blue), MPO (red) and *E. coli* (green) as mentioned in materials and methods. **(A)** Large field representation with 15 panels in gray scale using blue channel to show the extent of the NET formation. Scale bar is 50μm. **(B)** 3D representations of confocal data of fifteen 100x tiles of CFT073 cocultures at 30 min. Scale bar 20 μm. **(C)** A zoomed in area on a net **(B)**. The overlap between DAPI (which is made slightly transparent to visualize internal co-localization) and bacteria are seen as a teal color. Overlap between MPO and DAPI appears purple.

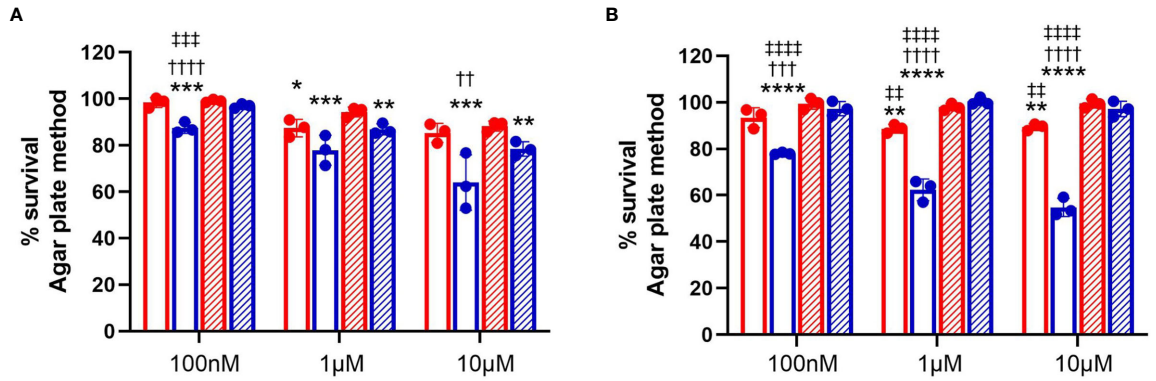

FIGURE 5 | Bactericidal activity of chlorolipids. 50x10^6/ml of CFT073 (red) and JM109 (blue) cells were incubated with indicated concentrations of either 2-chlorohexadecanal (clear bars, **A**), hexadecanal (hatched bars, **A**), 2-chloropalmitic acid (clear bars, **B**), or palmitic acid (hatched bars, **B**) for 1hr at 37°C. Bacterial survival (%) was determined by calculating CFU/ml over vehicle control bacteria. Values represent the mean ± SD for n=3. Statistics were performed ANOVA within each concentration tested. p-value: ****< 0.0001; ***< 0.001; **< 0.01; *< 0.05 for comparisons for each lipid compared to control (no lipid addition). ††††< 0.0001; †††< 0.001; ††< 0.01 for comparisons at each concentration for each lipid between treatments of JM109 and CFT073 cells. ‡‡‡‡< 0.0001; ‡‡‡< 0.001; ‡‡< 0.01 for comparisons at each concentration between chlorolipid and non-chlorolipid treatments.

2-ClFALD Metabolism in Cocultures and Individual Cells

2-ClFALD metabolism to 2-ClFA was examined in CFT073 and JM109 strains as well as in neutrophils. In contrast to disparate metabolism of 2-ClFALD to 2-ClFA in JM109 and CFT073 bacteria strains using endogenously produced 2-ClFALD (**Figure 1**), JM109 and CFT073 metabolized exogenous 2-ClFALD (2-chlorohexadecanal molecular species) nearly equally (**Figure 6A**). Since data in **Figures 5A, B** indicated 2-ClFALD at concentrations as low as 100 nM reduced JM109 survival (as determined by plate assays) we also examined viability (as opposed to ability to proliferate) by an alternate assay using the Live/Dead Baclight viability assay, which indicated both CFT073 and JM109 cells are viable during treatments with 100 nM and 1 μM 2-ClFALD, but both show significant viability loss with 10 μM treatments (**Figure 6B**). Neutrophils metabolized 2-ClFALD to 2-ClFA at a level approximately 1000-fold greater than that observed by either JM109 or CFT073 (**Figure 6C**). Since *in vivo* metabolism of 2-ClFALD during sepsis likely occurs at sites of neutrophil infiltration in the microvasculature, we also examined 2-ClFALD metabolism by EA.hy296 endothelial cells, which was ~two-fold greater than that by neutrophils (**Figure 6D**). To understand whether the coculture environment provides additional factors that modulate 2-ClFALD metabolism to 2-ClFA, we exogenously added 2-ClFALD in the coculture conditions and measured subsequent 2-ClFA production. JM109 coculture condition resulted in significantly lower 2-ClFA production in incubations with either 1 or 10 μM 2-ClFALD compared to CFT073 coculture conditions as well as control neutrophils in the absence of bacteria (**Figure 6E**). In subsequent studies we investigated the possibility that JM109 cocultures with neutrophils release factors that reduce endogenous (by neutrophils) or exogenous 2-ClFALD conversion to 2-ClFA. Data shown in **Figure 7A** show both CFT073 and neutrophil coculture supernatants and JM109 and neutrophil coculture supernatants nearly equally stimulate 2-chlorostearic acid production when applied to neutrophils. There was a modest decrease in 2-chloropalmitic acid production in treatments with JM109 coculture supernatants. Surprisingly, supernatants from both CFT073 and JM109 cocultures with neutrophils resulted in ~2-5-fold accelerated exogenous 2-ClFALD conversion to 2-ClFA when applied to either CFT073 or JM109 strains (**Figures 7B, C**) compared to the metabolism of exogenous 2-ClFALD in the absence of coculture supernatant addition (compare to **Figure 6A**). Further studies have shown the increase in 2-ClFALD metabolism to 2-ClFA in the presence of coculture supernatant additions are due to direct metabolic activity present in the supernatant rather than an effect on cellular metabolic activity (**Figures 7D, E**).

ATZ Inhibition of Chlorolipid Production and *E. coli* Rescue From Neutrophil Killing

We have previously shown that MPO inhibition can diminish 2-ClFALD levels in PMA-activated neutrophils (7). Accordingly, we examined the extent of ATZ inhibition of chlorolipid production in cocultures of neutrophils with JM109 and CFT073 *E. coli* strains. Significant reduction of 2-chlorohexadecanal was observed in both bacteria cocultures in the presence of ATZ (**Figure 8A**). Free 2-chloropalmitic acid was also decreased 7-fold with ATZ treatment (**Figure 8B**). Additionally, both JM109 and CFT073 survival in cocultures with neutrophils was improved in the presence of ATZ (**Figure 3A**).

DISCUSSION

In response to an infection, neutrophils deploy several microbicidal mechanisms against pathogens. Canonical bacterial neutrophil killing includes bacterial phagocytosis,

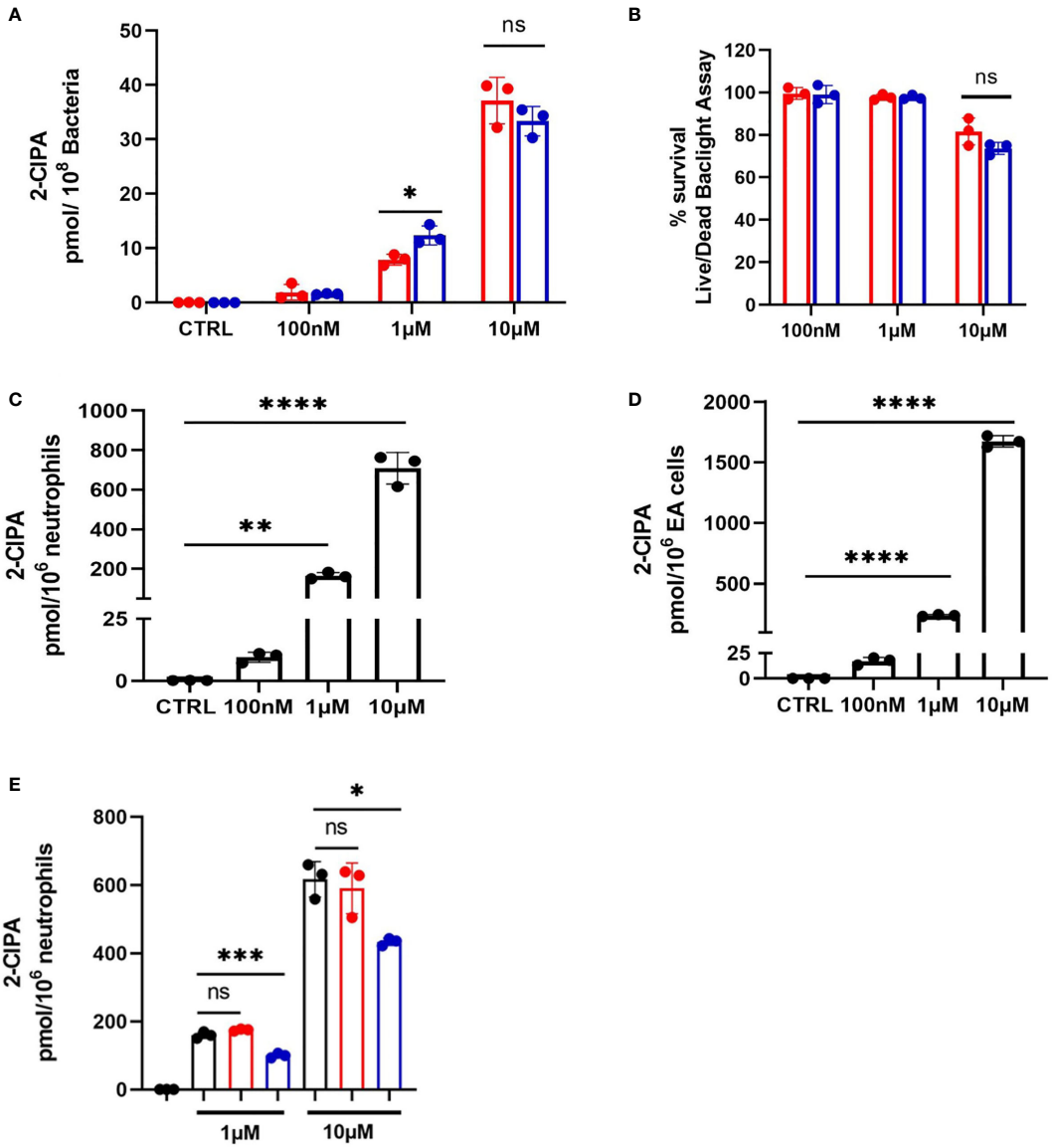

FIGURE 6 | 2-ClFALD metabolism in host cells and bacteria. **(A)** Indicated concentrations of the 2-ClFALD molecular species, 2-chlorohexadecanal, in 0.1% EtOH in HBSS media were exogenously provided to 50 x10^6/ml CFT073 (red) and JM109 (blue) cells for 1h at 37°C. Metabolized free 2-chloropalmitic acid (2-ClPA) was measured as described in "Material and Methods". **(B)** Following indicated 2-chlorohexadecanal treatments for 1h, CFT073 and JM109 viability was measured using Live/Dead Baclight Bacterial viability kit as described in "Material and Methods". Percent survival was calculated relative to the control bacteria. **(C)** Neutrophils (1x10^6/ml) or **(D)** EA hy296 cells (EA) were incubated with indicated concentrations 2-chlorohexadecanal for 1h at 37°C to determine conversion to 2-ClPA. **(E)** Neutrophils were cocultured with either CFT073 (red) or JM109 (blue) with exogenously provided 2-chlorohexadecanal for 30 min and 2-ClPA was measured. Control neutrophils are in black. Statistics were done using unpaired t-test **(A, B)** and one-way ANOVA with Tukey's multiple comparison test **(C–E)**. Error bars represents ± SD, n=3, p-value: ****< 0.0001; ***< 0.001; **< 0.01; * < 0.05. ns indicates not significant.

assembly of the NADPH oxidase complex at the phagosome membrane to generate superoxide and subsequently production of HOCl catalyzed by MPO. HOCl is a strong oxidizing agent that reacts with both microbe and host molecules (43–45). HOCl targets plasmalogen phospholipids to generate a family of chlorolipids. 2-ClFALD is the first product of the chlorolipid family, and it is subsequently oxidized to 2-ClFA, which is a stable, relatively long-lived chlorolipid (7, 12, 14). 2-ClFA and 2-ClFALD have profound effects on endothelial cells, monocytes, and neutrophils (7, 19, 22–25). Additionally, although chlorolipids are produced in both human and rodent sepsis (19, 20), the results herein are the first to show the production of 2-ClFALD and 2-ClFA by human neutrophils activated by exposure to bacteria.

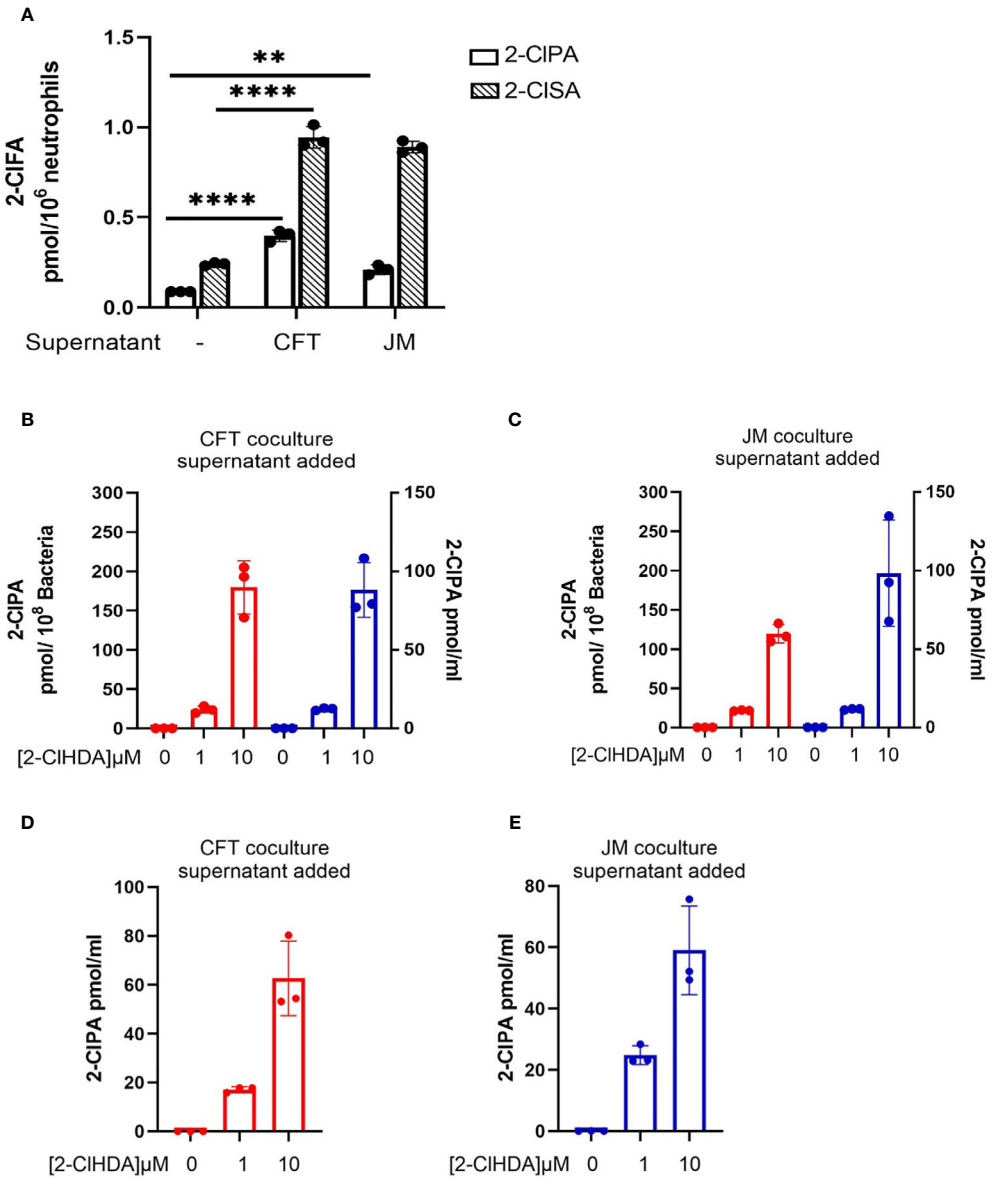

FIGURE 7 | Coculture supernatants amplify 2-ClFA production. 2x10^6/ml neutrophils were cocultured with 20x10^6/ml CFT073 or JM109 for 30 min at 37°C and the cells were pelleted. **(A)** The supernatants of CFT073 coculture or JM109 coculture were added to 1x10^6/ml neutrophils for 1hr at 37°C and free 2-chloropalmitic acid (2-ClPA) and 2-chlorostearic acid (2-ClSA) were measured. **(B, C)** CFT073 coculture supernatant or JM109 coculture supernatant was added to 50x10^6/ml of CFT073 (red) or JM109 (blue) and incubated with exogenous 2-chlorohexadecanal (2-ClHDA) for 1hr at 37°C and 2-ClPA was measured. **(D, E)** CFT073 or JM109 coculture supernatants were incubated with exogenous 2-ClHDA (0.1% EtOH) for 1 hour at 37°C without bacteria and 2-ClPA was measured. Each condition was performed with n=3 replicates. Statistics were done using one-way ANOVA with Tukey's multiple comparison test. Error bars represents ± SD, p-value: ****< 0.0001; **< 0.01.

Chlorolipid production was investigated in response to both the non-pathogenic K-12 laboratory *E. coli* strain, JM109, and the pathogenic EPEC *E. coli* strain, CFT073. 2-ClFALD, the first product of the chlorinated lipidome was increased in response to human neutrophil exposure to either of these *E. coli* strains. However, 2-ClFA was only increased with neutrophil exposure to the CFT073 *E. coli* strain. Chlorolipids were cell-associated and were not elevated in the cell culture media. Chlorolipid production elicited by JM109 and CFT073 cocultures with neutrophils was inhibited by ATZ. Additionally, these studies are the first to show chlorolipids are bactericidal and, in particular, the JM109 *E. coli* strain is much more susceptible to killing by chlorolipids compared to CFT073. The JM109 *E. coli* strain was very sensitive to killing by 2-ClFA.

The disparate production of 2-ClFA in coculture systems of human neutrophils with JM109 and CFT073 strains of *E. coli*

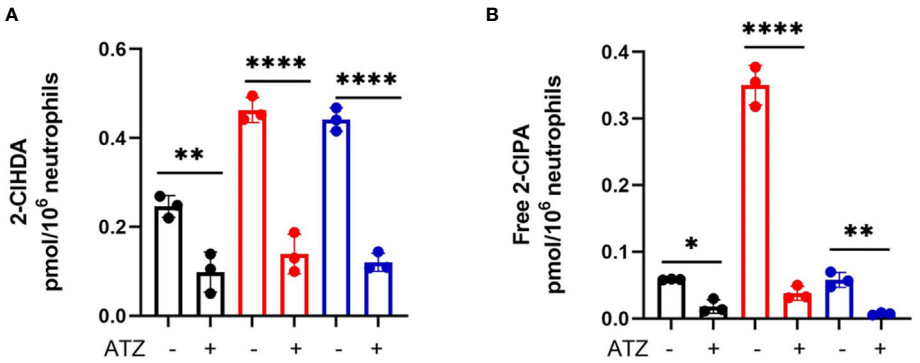

FIGURE 8 | Coculture 2-ClFALD and 2-ClFA production can be inhibited by blocking MPO. 2x10^6/ml neutrophils were pretreated with 10mM ATZ for 5min and incubated with either no bacteria (control, black), or, CFT073 (red) or JM109 (blue) strains of *E. coli* at a neutrophil: *E. coli* ratio of 1:10 for 30 min at 37°C. 2-Chlorohexadecanal (2-ClHDA, **A**) and 2-chloropalmitic acid (2-ClPA, **B**) were quantified as described in "Material and Methods. Multiple comparisons were performed using one-way ANOVA with Tukey's multiple comparison test. Data represents n=3, error bars for ± SD, p-value: ****< 0.0001; **< 0.01; *< 0.05.

may be due to the differences in the activation of mechanisms involved in neutrophil bacterial killing. Compared to JM109, the CFT073 strain possesses multiple virulence factors. CFT073 harbor pathogenic islands that carry clusters of virulence genes such as autotransporters, hemolysin that are crucial for pathogen survival, invasion, and colonization of human cells (28). In contrast, JM109 strain is devoid of all known virulence factors. Previous studies have also shown that CFT073 is more resistant to neutrophil killing and they are resistant to reactive oxygen species and oxidative stress (30, 40). EPEC strains have also exhibited intracellular survival in human neutrophils (46). Our studies also show the CFT073 modestly survives coculture with neutrophils better than cocultures of JM109. Additionally, considering the known differences in CFT073 and JM109 in resisting oxidative stress it is not surprising that CFT073 is more resilient to survival compared to JM109 when challenged with chlorinated lipids. Furthermore, the disparate resistance to oxidative stress may have a direct effect on 2-ClFALD conversion to 2-ClFA, which is dependent on NAD^+ (47).

E. coli killing and phagocytosis by neutrophils was suboptimal in the present studies in comparison to those of others (41, 42) since *E. coli* were not opsonized. The major goal of these studies was to examine changes in chlorolipids which would be complicated by the addition of chlorolipids and other lipids present in plasma. Under the conditions employed in this study, cyD treatment of neutrophils led to reduced killing of both strains of *E. coli*, which indicated phagocytosis mediates the bacterial killing process under the conditions employed in these studies. Phagocytosis, based on cyD inhibition of bacteria killing, appeared to be the predominant mechanism for killing in the coculture assays. Phagocytosis was also assessed using pHrodo-labeled *E. coli*, which was also cyD-sensitive. Although the pHrodo technique used in this study has been used by others (e.g., 48) to measure phagocytosis by neutrophils there is concern regarding the pHrodo assay in neutrophils based on studies focusing on the pH of the phagosome (49). Using pH-sensitive SNARF-1 labeled dead *C. albicans* the neutrophil phagosome was found to be alkaline for up to 30 min. Additionally, our studies show that in the absence of opsonization, bacteria killing was inhibited by ATZ. This contrast to the non-oxidative dependent killing of opsonized bacteria (41, 42). Based on the disparate requirement of oxidative killing of opsonized and non-opsonized bacteria it will be interesting to evaluate chlorolipid production in response to opsonized bacteria in future studies.

We also examined NETosis in cocultures. We previously found 2-ClFA can elicit NETosis (25). Interestingly, there was a significant increase in ecDNA formation within 30 min in CFT073 cocultures indicating NETosis activation. In comparison, NETosis in JM109 cocultures was delayed. Thus, it is possible that the disparate increase in 2-ClFA levels in CFT073 coculture compared to JM109 coculture may be responsible for the observed NETosis at 30 min in CFT073 cocultures compared to JM109 cocultures. Immunofluorescence images also showed bacterial trapping in NETs. Furthermore, NETs isolated from PMA-stimulated neutrophils had bactericidal activity toward both CFT073 and JM109. This shows NETs can kill these strains, but it should be appreciated that these studies were performed with NETs produced and isolated from PMA-stimulated neutrophils. While these findings are consistent with the concept that NETs prevent microbial dissemination by physically trapping bacteria and/or killing bacteria (50), data with cyD indicate *E. coli* killing in the absence of opsonization is by neutrophil phagocytosis. Although, the role of NETs in bacterial killing is controversial (51), the production of NETs by the uroseptic *E. coli* strain, CFT073, may indicate other roles of NETs in sepsis including detrimental effects on the host such as influencing thrombus formation and disseminated intravascular coagulation (52).

This is the first study to show the bactericidal activity of 2-ClFA and 2-ClFALD. Moreover, the antibacterial effect of chlorolipids is divergent for the two *E.coli* strains examined. It has previously been shown that saturated and unsaturated fatty

acids have bactericidal properties, and the antibacterial activity varies with the lipid species and the microorganism strain (53–55). Antibacterial activity of palmitic acid with *E.coli* has previously been shown at concentrations 12-24 higher than the highest concentrations tested in this study (i.e., 10 μM) (56). In comparison, the present studies show 2-chloropalmitic acid toxicity at concentrations as low as 100 nM in the JM109 strain of *E. coli*. It is possible that the α-carbon chlorine is reactive with nucleophiles in *E. coli* leading to the antibacterial activity. We have previously shown 2-ClFALD reacts with glutathione leading to a fatty aldehyde-glutathione adduct (13), and it is predicted that similar reactivity of 2-chloropalmitic acid or its acyl CoA derivative with nucleophiles could occur. Such targeting in *E. coli* needs to be further investigated.

To have a comparative perspective of 2-ClFALD metabolism by cells encountering 2-ClFALD *in vivo*, we examined the metabolism of exogenous 2-ClFALD in endothelial cells, neutrophils and bacteria. Comparisons based on cell number indicated endothelial cells metabolized 2-ClFALD to 2-ClFA about 2-fold greater than neutrophils, and neutrophil 2-ClFALD metabolism was over 1000-fold greater than that of either JM109 or CFT073 *E. coli* strains. Thus, it is likely that *in vivo* metabolism of 2-ClFALD is mediated predominantly by host cells including neutrophils and endothelial cells compared to *E. coli*. Also, an intriguing discovery was that coculture media from incubations of neutrophils with either strain of *E. coli* has activity capable of converting 2-ClFALD to 2-ClFA. The most logical explanation of these findings is that this activity is a result of neutrophil lysis. Future studies will further examine these properties, which might have a significant role in extracellular production of 2-ClFA.

We previously showed fatty aldehyde dehydrogenase mediates the oxidation of 2-ClFALD to 2-ClFA (12). Interestingly, in the present studies we found endogenous 2-ClFALD conversion to 2-ClFA was attenuated in cocultures with JM109 in comparison to cocultures with CFT073. Similarly, exogenous 2-ClFALD conversion to 2-ClFA was reduced in JM109 cocultures with neutrophils compared to CFT073 cocultures (**Figure 6E**). Based on the relative conversion of exogenous 2-ClFALD to 2-ClFA in *E. coli* compared to neutrophils it seems likely that the majority of the metabolism in coculture is mediated by neutrophil fatty aldehyde dehydrogenase. It is possible that factors are released from JM109 cocultures inhibit 2-ClFALD metabolism since media from JM109 cocultures with neutrophils applied to CFT073 cocultures with neutrophils slightly reduced exogenous 2-ClFALD metabolism while the opposite crossover experiment did not alter exogenous 2-ClFALD metabolism by JM109 cocultures with neutrophils. We speculate that the increased neutrophil killing of JM109 compared to CFT073 has a role in the difference in metabolism of endogenous 2-ClFALD to 2-ClFA. It is also possible that JM109 compared to CFT073 has a greater propensity to react 2-ClFALD with nucleophiles. Identifying these potential targets may provide additional insights into differences in neutrophil responses to specific bacteria.

Increased plasma 2-chlorofatty acid levels associate with ARDS-caused mortality in human sepsis (19). Although the origin of elevations in 2-chlorofatty acid in septic humans is likely due to neutrophil activation in response to bacteria, until now the direct production of 2-chlorofatty acid and 2-chlorofatty aldehyde in response to bacteria has not been shown. By comparing neutrophil responses to JM109 and CFT073 strains of *E. coli* we observed that while both strains led to 2-chlorofatty aldehyde, only the pathogenic uroseptic strain CFT073 produced significant amounts of 2-ClFA. Since 2-ClFA is associated with poor outcomes in sepsis and elicits potentially deleterious NET formation it will be important to further understand the mechanisms responsible for the disparate accumulation of 2-ClFA in neutrophils exposed to JM109 and CFT073 as well as the disparate sensitivity of JM109 cells to bactericidal effects of 2-ClFA.

DATA AVAILABILITY STATEMENT

The original contributions presented in the study are included in the article/supplementary material. Further inquiries can be directed to the corresponding author.

ETHICS STATEMENT

The studies involving human participants were reviewed and approved by Saint Louis University Institutional Review Board. The patients/participants provided their written informed consent to participate in this study.

AUTHOR CONTRIBUTIONS

KA performed all experiments, analyzed all data, prepared first draft, and contributed to final manuscript preparation. GK performed image analysis of NETs. DF was responsible for oversight of all aspects of studies, manuscript preparation, and final manuscript. All authors contributed to the article and approved the submitted version.

FUNDING

This study was supported (in part) by research funding from the National Institutes of Health R01 GM-115553, R01 GM129508 and S10OD025246 to DF. The content is solely the responsibility of the authors and does not necessarily represent the official views of the National Institutes of Health.

ACKNOWLEDGMENTS

The authors acknowledge the technical support of Carolyn J. Albert in these studies.

REFERENCES

1. Papayannopoulos V. Neutrophil Extracellular Traps in Immunity and Disease. *Nat Rev Immunol* (2018) 18(2):134–47. doi: 10.1038/nri.2017.105
2. Harrison JE, Schultz J. Studies on the Chlorinating Activity of Myeloperoxidase. *J Biol Chem* (1976) 251(5):1371–4. doi: 10.1016/S0021-9258(17)33749-3
3. Hazen SL, Hsu FF, Duffin K, Heinecke JW. Molecular Chlorine Generated by the Myeloperoxidase-Hydrogen Peroxide-Chloride System of Phagocytes Converts Low Density Lipoprotein Cholesterol Into a Family of Chlorinated Sterols. *J Biol Chem* (1996) 271(38):23080–8. doi: 10.1074/jbc.271.38.23080
4. Pattison DI, Davies MJ. Reactions of Myeloperoxidase-Derived Oxidants With Biological Substrates: Gaining Chemical Insight Into Human Inflammatory Diseases. *Curr Med Chem* (2006) 13(27):3271–90. doi: 10.2174/092986706778773095
5. Pattison DI, Hawkins CL, Davies MJ. What Are the Plasma Targets of the Oxidant Hypochlorous Acid? A Kinetic Modeling Approach. *Chem Res Toxicol* (2009) 22(5):807–17. doi: 10.1021/tx800372d
6. Albert CJ, Crowley JR, Hsu FF, Thukkani AK, Ford DA. Reactive Chlorinating Species Produced by Myeloperoxidase Target the Vinyl Ether Bond of Plasmalogens: Identification of 2-Chlorohexadecanal. *J Biol Chem* (2001) 276(26):23733–41. doi: 10.1074/jbc.M101447200
7. Thukkani AK, Hsu FF, Crowley JR, Wysolmerski RB, Albert CJ, Ford DA. Reactive Chlorinating Species Produced During Neutrophil Activation Target Tissue Plasmalogens: Production of the Chemoattractant, 2-Chlorohexadecanal. *J Biol Chem* (2002) 277(6):3842–9. doi: 10.1074/jbc.M109489200
8. Chilton FH, Connell TR. 1-Ether-Linked Phosphoglycerides. Major Endogenous Sources of Arachidonate in the Human Neutrophil. *J Biol Chem* (1988) 263(11):5260–5. doi: 10.1016/S0021-9258(18)60709-4
9. Ford DA, Gross RW. Plasmenylethanolamine is the Major Storage Depot for Arachidonic Acid in Rabbit Vascular Smooth Muscle and Is Rapidly Hydrolyzed After Angiotensin II Stimulation. *Proc Natl Acad Sci USA* (1989) 86(10):3479–83. doi: 10.1073/pnas.86.10.3479
10. Gross RW. High Plasmalogen and Arachidonic Acid Content of Canine Myocardial Sarcolemma: A Fast Atom Bombardment Mass Spectroscopic and Gas Chromatography-Mass Spectroscopic Characterization. *Biochemistry* (1984) 23(1):158–65. doi: 10.1021/bi00296a026
11. Murphy EJ, Joseph L, Stephens R, Horrocks LA. Phospholipid Composition of Cultured Human Endothelial Cells. *Lipids* (1992) 27(2):150–3. doi: 10.1007/BF02535816
12. Anbukumar DS, Shornick LP, Albert CJ, Steward MM, Zoeller RA, Neumann WL, et al. Chlorinated Lipid Species in Activated Human Neutrophils: Lipid Metabolites of 2-Chlorohexadecanal. *J Lipid Res* (2010) 51(5):1085–92. doi: 10.1194/jlr.M003673
13. Duerr MA, Aurora R, Ford DA. Identification of Glutathione Adducts of Alpha-Chlorofatty Aldehydes Produced in Activated Neutrophils. *J Lipid Res* (2015) 56(5):1014–24. doi: 10.1194/jlr.M058636
14. Wildsmith KR, Albert CJ, Anbukumar DS, Ford DA. Metabolism of Myeloperoxidase-Derived 2-Chlorohexadecanal. *J Biol Chem* (2006) 281(25):16849–60. doi: 10.1074/jbc.M602505200
15. Wildsmith KR, Albert CJ, Hsu FF, Kao JL-F, Ford DA. Myeloperoxidase-Derived 2-Chlorohexadecanal Forms Schiff Bases With Primary Amines of Ethanolamine Glycerophospholipids and Lysine. *Chem Phys Lipids* (2006) 139:157–70. doi: 10.1016/j.chemphyslip.2005.12.003
16. Thukkani AK, Martinson BD, Albert CJ, Vogler GA, Ford DA. Neutrophil-Mediated Accumulation of 2-ClHDA During Myocardial Infarction: 2-ClHDA-Mediated Myocardial Injury. *Am J Physiol-Heart Circ Physiol* (2005) 288:H2955–64. doi: 10.1152/ajpheart.00834.2004
17. Thukkani AK, McHowat J, Hsu FF, Brennan ML, Hazen SL, Ford DA. Identification of Alpha-Chloro Fatty Aldehydes and Unsaturated Lysophosphatidylcholine Molecular Species in Human Atherosclerotic Lesions. *Circulation* (2003) 108(25):3128–33. doi: 10.1161/01.CIR.0000104564.01539.6A
18. Brahmbhatt VV, Albert CJ, Anbukumar DS, Cunningham BA, Neumann WL, Ford DA. {Omega}-Oxidation of {Alpha}-Chlorinated Fatty Acids: Identification of {Alpha}-Chlorinated Dicarboxylic Acids. *J Biol Chem* (2010) 285(53):41255–69. doi: 10.1074/jbc.M110.147157
19. Meyer NJ, Reilly JP, Feng R, Christie JD, Hazen SL, Albert CJ, et al. Myeloperoxidase-Derived 2-Chlorofatty Acids Contribute to Human Sepsis Mortality *via* Acute Respiratory Distress Syndrome. *JCI Insight* (2017) 2:pii: 96432. doi: 10.1172/jci.insight.96432
20. Pike DP, Vogel MJ, McHowat J, Mikuzis PA, Schulte KA, Ford DA. 2-Chlorofatty Acids are Biomarkers of Sepsis Mortality and Mediators of Barrier Dysfunction in Rats. *J Lipid Res* (2020) 61(7):1115–27. doi: 10.1194/jlr.RA120000829
21. Yu H, Liu Y, Wang M, Restrepo RJ, Wang D, Kalogeris TJ, et al. Myeloperoxidase Instigates Proinflammatory Responses in a Cecal Ligation and Puncture Rat Model of Sepsis. *Am J Physiol Heart Circ Physiol* (2020) 319(3):H705–H21. doi: 10.1152/ajpheart.00440.2020
22. Hartman CL, Duerr MA, Albert CJ, Neumann WL, McHowat J, Ford DA. 2-Chlorofatty Acids Induce Weibel-Palade Body Mobilization. *J Lipid Res* (2018) 59:113–22. doi: 10.1194/jlr.M080200
23. McHowat J, Shakya S, Ford DA. 2-Chlorofatty Aldehyde Elicits Endothelial Cell Activation. *Front Physiol* (2020) 11:460. doi: 10.3389/fphys.2020.00460
24. Wang WY, Albert CJ, Ford DA. Alpha-Chlorofatty Acid Accumulates in Activated Monocytes and Causes Apoptosis Through Reactive Oxygen Species Production and Endoplasmic Reticulum Stress. *Arterioscler Thromb Vasc Biol* (2014) 34(3):526–32. doi: 10.1161/ATVBAHA.113.302544
25. Palladino END, Katunga LA, Kolar GR, Ford DA. 2-Chlorofatty Acids: Lipid Mediators of Neutrophil Extracellular Trap Formation. *J Lipid Res* (2018) 59(8):1424–32. doi: 10.1194/jlr.M084731
26. Schrag SJ, Farley MM, Petit S, Reingold A, Weston EJ, Pondo T, et al. Epidemiology of Invasive Early-Onset Neonatal Sepsis, 2005 to 2014. *Pediatrics* (2016) 138(6):e20162013. doi: 10.1542/peds.2016-2013
27. Dale AP, Woodford N. Extra-Intestinal Pathogenic Escherichia Coli (ExPEC): Disease, Carriage and Clones. *J Infect* (2015) 71(6):615–26. doi: 10.1016/j.jinf.2015.09.009
28. Luo C, Hu GQ, Zhu H. Genome Reannotation of Escherichia Coli CFT073 With New Insights Into Virulence. *BMC Genomics* (2009) 10:552. doi: 10.1186/1471-2164-10-552
29. Bokil NJ, Totsika M, Carey AJ, Stacey KJ, Hancock V, Saunders BM, et al. Intramacrophage Survival of Uropathogenic Escherichia Coli: Differences Between Diverse Clinical Isolates and Between Mouse and Human Macrophages. *Immunobiology* (2011) 216(11):1164–71. doi: 10.1016/j.imbio.2011.05.011
30. Hryckowian AJ, Welch RA. RpoS Contributes to Phagocyte Oxidase-Mediated Stress Resistance During Urinary Tract Infection by Escherichia Coli CFT073. *mBio* (2013) 4(1):e00023–13. doi: 10.1128/mBio.00023-13
31. Waldhuber A, Puthia M, Wieser A, Cirl C, Durr S, Neumann-Pfeifer S, et al. Uropathogenic Escherichia Coli Strain CFT073 Disrupts NLRP3 Inflammasome Activation. *J Clin Invest* (2016) 126(7):2425–36. doi: 10.1172/JCI81916
32. Bligh EG, Dyer WJ. A Rapid Method of Total Lipid Extraction and Purification. *Can J Biochem Physiol* (1959) 37:911–7. doi: 10.1139/y59-099
33. Wacker BK, Albert CJ, Ford BA, Ford DA. Strategies for the Analysis of Chlorinated Lipids in Biological Systems. *Free Radic Biol Med* (2013) 59:92–9. doi: 10.1016/j.freeradbiomed.2012.06.013
34. Wang WY, Albert CJ, Ford DA. Approaches for the Analysis of Chlorinated Lipids. *Anal Biochem* (2013) 443(2):148–52. doi: 10.1016/j.ab.2013.09.016
35. Parker HA, Magon NJ, Green JN, Hampton MB, Winterbourn CC. Analysis of Neutrophil Bactericidal Activity. *Methods Mol Biol* (2014) 1124:291–306. doi: 10.1007/978-1-62703-845-4_19
36. Najmeh S, Cools-Lartigue J, Giannias B, Spicer J, Ferri LE. Simplified Human Neutrophil Extracellular Traps (NETs) Isolation and Handling. *JoVE* (2015) (98):52687. doi: 10.3791/52687
37. Flores R, Dohrmann S, Schaal C, Hakkim A, Nizet V, Corriden R. The Selective Estrogen Receptor Modulator Raloxifene Inhibits Neutrophil Extracellular Trap Formation. *Front Immunol* (2016) 7:566. doi: 10.3389/fimmu.2016.00566
38. Kayganich K, Murphy R. Fast Atom Bombardment Tandem Mass Spectrometric Identification of Diacyl, Alkylacyl, and Alk-1-Enylacyl Molecular Species of Glycerophosphoethanolamine in Human Polymorphonuclear Leukocytes. *Anal Biochem* (1992) 64:2965–71. doi: 10.1021/ac00047a015
39. Sohlenkamp C, Geiger O. Bacterial Membrane Lipids: Diversity in Structures and Pathways. *FEMS Microbiol Rev* (2016) 40(1):133–59. doi: 10.1093/femsre/fuv008

40. Loughman JA, Hunstad DA. Attenuation of Human Neutrophil Migration and Function by Uropathogenic Bacteria. *Microbes Infect* (2011) 13(6):555–65. doi: 10.1016/j.micinf.2011.01.017
41. Hampton MB, Winterbourn CC. Modification of Neutrophil Oxidant Production With Diphenyleneiodonium and its Effect on Bacterial Killing. *Free Radic Biol Med* (1995) 18(4):633–9. doi: 10.1016/0891-5849(94)00181-I
42. Rosen H, Michel BR. Redundant Contribution of Myeloperoxidase-Dependent Systems to Neutrophil-Mediated Killing of Escherichia Coli. *Infect Immun* (1997) 65(10):4173–8. doi: 10.1128/iai.65.10.4173-4178.1997
43. Hurst JK. What Really Happens in the Neutrophil Phagosome? *Free Radic Biol Med* (2012) 53(3):508–20. doi: 10.1016/j.freeradbiomed.2012.05.008
44. Klebanoff SJ. Oxygen Metabolism and the Toxic Properties of Phagocytes. *Ann Intern Med* (1980) 93(3):480–9. doi: 10.7326/0003-4819-93-3-480
45. Klebanoff SJ, Waltersdorph AM, Rosen H. Antimicrobial Activity of Myeloperoxidase. *Methods Enzymol* (1984) 105:399–403. doi: 10.1016/S0076-6879(84)05055-2
46. Nazareth H, Genagon SA, Russo TA. Extraintestinal Pathogenic Escherichia Coli Survives Within Neutrophils. *Infect Immun* (2007) 75(6):2776–85. doi: 10.1128/IAI.01095-06
47. Rizzo WB, Craft DA, Dammann AL, Phillips MW. Fatty Alcohol Metabolism in Cultured Human Fibroblasts. Evidence for a Fatty Alcohol Cycle. *J Biol Chem* (1987) 262(36):17412–9. doi: 10.1016/S0021-9258(18)45394-X
48. Takahashi Y, Wake H, Sakaguchi M, Yoshii Y, Teshigawara K, Wang D, et al. Histidine-Rich Glycoprotein Stimulates Human Neutrophil Phagocytosis and Prolongs Survival Through CLEC1A. *J Immunol* (2021) 206(4):737–50. doi: 10.4049/jimmunol.2000817
49. Foote JR, Patel AA, Yona S, Segal AW. Variations in the Phagosomal Environment of Human Neutrophils and Mononuclear Phagocyte Subsets. *Front Immunol* (2019) 10:188. doi: 10.3389/fimmu.2019.00188
50. Barrientos L, Marin-Esteban V, de Chaisemartin L, Le-Moal VL, Sandre C, Bianchini E, et al. An Improved Strategy to Recover Large Fragments of Functional Human Neutrophil Extracellular Traps. *Front Immunol* (2013) 4:166. doi: 10.3389/fimmu.2013.00166
51. Nauseef WM, Kubes P. Pondering Neutrophil Extracellular Traps With Healthy Skepticism. *Cell Microbiol* (2016) 18(10):1349–57. doi: 10.1111/cmi.12652
52. Camicia G, Pozner R, de Larranaga G. Neutrophil Extracellular Traps in Sepsis. *Shock* (2014) 42(4):286–94. doi: 10.1097/SHK.0000000000000221
53. Desbois AP, Smith VJ. Antibacterial Free Fatty Acids: Activities, Mechanisms of Action and Biotechnological Potential. *Appl Microbiol Biotechnol* (2010) 85(6):1629–42. doi: 10.1007/s00253-009-2355-3
54. Kabara JJ, Swieczkowski DM, Conley AJ, Truant JP. Fatty Acids and Derivatives as Antimicrobial Agents. *Antimicrob Agents Chemother* (1972) 2(1):23–8. doi: 10.1128/AAC.2.1.23
55. Zheng CJ, Yoo JS, Lee TG, Cho HY, Kim YH, Kim WG. Fatty Acid Synthesis is a Target for Antibacterial Activity of Unsaturated Fatty Acids. *FEBS Lett* (2005) 579(23):5157–62. doi: 10.1016/j.febslet.2005.08.028
56. Stojanovic-Radic Z, Comic L, Radulovic N, Dekic M, Randelovic V, Stefanovic O. Chemical Composition and Antimicrobial Activity of Erodium Species: E. Coconium, E. Cicutarium L. And E. Absinthoides Willd. (Geraniaceae). *Chem Papers* (2010) 64:368–77. doi: 10.2478/s11696-010-0014-x

Conflict of Interest: The authors declare that the research was conducted in the absence of any commercial or financial relationships that could be construed as a potential conflict of interest.

Publisher's Note: All claims expressed in this article are solely those of the authors and do not necessarily represent those of their affiliated organizations, or those of the publisher, the editors and the reviewers. Any product that may be evaluated in this article, or claim that may be made by its manufacturer, is not guaranteed or endorsed by the publisher.

frontiers in Immunology

ORIGINAL RESEARCH
published: 13 August 2021
doi: 10.3389/fimmu.2021.703846

Identification of Novel Low-Density Neutrophil Markers Through Unbiased High-Dimensional Flow Cytometry Screening in Non-Small Cell Lung Cancer Patients

*Paulina Valadez-Cosmes[1], Kathrin Maitz[1], Oliver Kindler[1], Sofia Raftopoulou[1], Melanie Kienzl[1,2], Ana Santiso[1], Zala Nikita Mihalic[1], Luka Brcic[3], Jörg Lindenmann[4], Melanie Fediuk[4], Martin Pichler[5], Rudolf Schicho[1,2], A. McGarry Houghton[6,7,8], Akos Heinemann[1,2] and Julia Kargl[1,2]**

[1] Otto Loewi Research Center, Division of Pharmacology, Medical University of Graz, Graz, Austria, [2] BioTechMed, Graz, Austria, [3] Diagnostic and Research Institute of Pathology, Medical University of Graz, Graz, Austria, [4] Division of Thoracic and Hyperbaric Surgery, Department of Surgery, Medical University of Graz, Graz, Austria, [5] Division of Oncology, Department of Internal Medicine, Medical University of Graz, Graz, Austria, [6] Clinical Research Division, Fred Hutchinson Cancer Research Center, Seattle, WA, United States, [7] Human Biology Division, Fred Hutchinson Cancer Research Center, Seattle, WA, United States, [8] Division of Pulmonary and Critical Care Medicine, University of Washington, Seattle, WA, United States

OPEN ACCESS

Edited by:
Dragana Odobasic, Monash University, Australia

Reviewed by:
Anja Meissner, Lund University, Sweden
Tamás Laskay, University of Lübeck, Germany

***Correspondence:**
Julia Kargl
julia.kargl@medunigraz.at

Specialty section:
This article was submitted to Molecular Innate Immunity, a section of the journal Frontiers in Immunology

Received: *30 April 2021*
Accepted: *15 July 2021*
Published: *13 August 2021*

Citation:
Valadez-Cosmes P, Maitz K, Kindler O, Raftopoulou S, Kienzl M, Santiso A, Mihalic ZN, Brcic L, Lindenmann J, Fediuk M, Pichler M, Schicho R, Houghton AM, Heinemann A and Kargl J (2021) Identification of Novel Low-Density Neutrophil Markers Through Unbiased High-Dimensional Flow Cytometry Screening in Non-Small Cell Lung Cancer Patients. Front. Immunol. 12:703846. doi: 10.3389/fimmu.2021.703846

Neutrophils have been described as a phenotypically heterogeneous cell type that possess both pro- and anti-tumor properties. Recently, a subset of neutrophils isolated from the peripheral blood mononuclear cell (PBMC) fraction has been described in cancer patients. These low-density neutrophils (LDNs) show a heterogeneous maturation state and have been associated with pro-tumor properties in comparison to mature, high-density neutrophils (HDNs). However, additional studies are necessary to characterize this cell population. Here we show new surface markers that allow us to discriminate between LDNs and HDNs in non-small cell lung cancer (NSCLC) patients and assess their potential as diagnostic/prognostic tool. LDNs were highly enriched in NSCLC patients (median=20.4%, range 0.3-76.1%; n=26) but not in healthy individuals (median=0.3%, range 0.1-3.9%; n=14). Using a high-dimensional human cell surface marker screen, we identified 12 surface markers that were downregulated in LDNs when compared to HDNs, while 41 surface markers were upregulated in the LDN subset. Using flow cytometry, we confirmed overexpression of CD36, CD41, CD61 and CD226 in the LDN fraction. In summary, our data support the notion that LDNs are a unique neutrophil population and provide novel targets to clarify their role in tumor progression and their potential as diagnostic and therapeutic tool.

Keywords: low-density neutrophils, non-small cell lung cancer (NSCLC), high-dimensional flow cytometry, CD36, CD41, CD61, CD226

INTRODUCTION

Lung cancer is the leading cause of cancer deaths worldwide and kills more patients each year than does breast, colon, prostate and pancreatic cancer, combined (1). Most patients are diagnosed at advanced stage with limited treatment options and overall five-year survival rates are below 18% (2). Detection at early stage, when the disease is still localized, significantly increases five-year survival rates to 55%; however, only 16% of lung cancer cases are diagnosed at early stage. For late-stage diagnosis with distant metastases five-year survival rates are as low as 4% (2). The two main lung cancer types are small cell lung cancer (SCLC) and non-small cell lung cancer (NSCLC) (2). NSCLC comprises mainly of lung adenocarcinoma and lung squamous cell carcinoma, representing ~80% of all lung cancer cases (3). Although surgical intervention for early-stage NSCLC can be curative, traditional chemo-and radiotherapy on the one hand, and targeted- and immunotherapy on the other hand, are of limited effectiveness (3). Diagnosis at advanced stage and poor outcome for most patients, highlights the need for novel biomarkers to improve early lung cancer detection and tools to monitor therapy response.

Tumor initiation and progression are commonly accompanied by inflammation (4) and the role of neutrophils in the development of cancer has attracted interest over the last years. Multifaceted and opposing roles of neutrophils in lung cancer have been highlighted (5–7), although the bulk of clinical evidence mostly supports the idea that neutrophils promote cancer progression and have immunosuppressive properties (8). Therefore, our view of neutrophils as a uniform immune population of terminally differentiated cells has given way to the concept that neutrophils are plastic cells that can display distinct morphological, phenotypical and functional properties in health and disease (9, 10). Molecules involved in neutrophil homeostasis are often upregulated in tumors (11–15), leading to neutrophil release from the bone marrow, including immature cells identified by their nuclei shape (9, 13, 16–18). However, the phenotype, relevance and function of immature neutrophils in circulation of tumor patients is not well understood yet. Neutrophil to lymphocyte ratio (NLR) has been shown to correlate with outcome and has been proposed as biomarker for cancer risk assessment and treatment decisions (19, 20). Additional measurement of neutrophil-activating and polarization factors, or identifying neutrophil subpopulations in circulation, released from the bone marrow in response to tumor, would enhance the clinical potential of neutrophils as biomarker for cancer patients.

Low-density neutrophils (LDNs), a neutrophil subtype largely absent in healthy volunteers, have been reported in cancer patients (6, 9, 21, 22) but their function and potential as biomarkers for lung cancer has not been comprehensively evaluated. LDNs consist of mature and immature neutrophil subsets and have been associated with immunosuppressive functions, as opposed to the high-density neutrophils (HDNs) which have anti-tumorigenic properties (9). These findings raise the question which are the distinct features that truly characterize LDNs and separate them from HDNs in the same patient. LDNs have previously also been described as PMN-MDSC or granulocytic-MDSC (myeloid derived suppressor cells) (23), however, additional studies are necessary to define the phenotypic and functional properties of this cell populations in more detail.

In the current study, we focus on the identification of cellular markers that distinguish LDNs from HDNs in NSCLC patients which have the potential to act as novel biomarkers. We show that LDNs are increased in lung cancer patients. Using a high-dimensional flow cytometry screening panel we identified surface markers that are uniquely expressed by the LDN subset in NSCLC patients. Our data support the concept that neutrophils in cancer display diverse phenotypes. Moreover, we provide novel targets to identify and manipulate LDNs and thereby further understand their role in tumor progression and their potential as diagnostic tool.

MATERIAL AND METHODS

Study Design

NSCLC patients were recruited from the Department of Internal Medicine, Division of Oncology and Department of Surgery, Division of Thoracic and Hyperbaric Surgery, Medical University of Graz (Graz, Austria) (**Table 1**). Informed consent was obtained from all participants and blood samples were obtained prior to treatment. Healthy volunteers without a history of cancer were recruited as control group. Blood samples were processed within 4 hours after blood draw.

Study Approval

The study complied with the Declaration of Helsinki and was approved by the Ethics Committee of the Medical University of Graz (EK-numbers: 30-105 ex17/18, 29-593 ex 16/17 and 17-291 ex 05/06).

TABLE 1 | Participants characteristics.

	All NSCLC
N	n = 54
Age	66 (45 – 81)
Sex	Female n = 21
	Male n = 33
Smoking	Yes n = 44
	No n = 9
	Unknown n = 1
Stages	I-IIa n = 18
	IIIa n = 8
	Ib n = 6
	IIb n = 6
	IIIb n = 4
	IV n = 0
	Undefined n = 12
Histology	Adenocarcinoma n = 31
	Squamous cell carcinoma n = 15
	Undefined NSCLC n = 8
Therapy	No prior treatment n = 54
	Treatment n = 0

Density Centrifugation

Blood from NSCLC patients and healthy volunteers (10 ml) was collected in EDTA-containing tubes (Greiner). Platelet-rich plasma was removed by centrifugation (300 g, 20 min) and erythrocytes were removed by dextran sedimentation. An equal volume of 3% Dextran T-500 in saline (Sigma Aldrich) was added to the cells, and mixed. Erythrocytes were allowed to sediment for 30 min, and the upper phase containing leukocytes was slowly layered on top of Histopaque 1077 (Sigma Aldrich) in 15 ml tubes. High-density polymorphonuclear leukocytes (PMNL, containing high-density neutrophils (HDNs)) were then separated from low-density peripheral blood mononuclear cells (PBMC; comprising LDNs in cancer patients) by centrifugation (300 g, 20 min, no brake). PBMCs were carefully removed from the interphase to a fresh tube and washed in PBS without Ca^{2+} and Mg^{2+}. NH_4Cl was used to lyse erythrocytes in the high-density fraction (PMNLs). PMNLs were washed twice in PBS without Ca^{2+} and Mg^{2+}. PBMCs and PMNLs were resuspended in PBS. Whole blood samples were collected in EDTA-containing tubes, erythrocytes were lysed in NH_4Cl and cells were washed in PBS without Ca^{2+} and Mg^{2+}. Cell viability and cell numbers were determined using an EVE automated cell counter (NanoEntek).

Cytospins

Cytospins were prepared from the PBMC fractions by centrifugation of $1x10^5$ cells in PBS onto a glass slide (600 g, 5 min) using a Shandon Cytospin 3 and stained immediately using Hemacolor® rapid staining of blood smear according to manufacturer´s instructions (Merck).

Flow Cytometry

Flow cytometry staining was performed immediately after PMNL and PBMC fractions were obtained or on lysed whole blood samples. In brief, cells were pre-incubated with human TruStain FcX blocking solution (FcBlock, Biolegend) to reduce non-specific binding in staining buffer (SB, PBS + 2% FBS) and incubated at 4°C for 10 min. Subsequently, cells were stained for 20 min at 4°C with CD66b-APC (LDN identification) or CD45-AF700, CD66b-PeCy7, CD36-BV421, CD41-BV785, CD61-FITC, CD226-BV711 and Lox1-PE (marker validation) antibodies in SB. Cells were centrifuged (500 g, 5 min, 4°C), resuspended in 200 µL of SB and washed again with SB. Propidium iodide (PI, 5 min, RT) or fixable viability dye eFluor™ 780 (FVD, eBioscience) (30 min, 4°C) was used to stain dead cells. FVD stained cells were fixed with IC fixation buffer (eBioscience) (10 min, 4°C), centrifuged and resuspended in 100 µL SB. Samples were measured on a FACS Canto II or BD LSR II Fortessa (BD Biosciences).

Flow Cytometry – LEGENDScreen Neutrophil Surface Marker Screening

PBMC and PMNL fractions were isolated by density centrifugation and stained for flow cytometry analysis. Briefly, cells were incubated with FVD eFluor™ 780 (eBioscience) (30 min, 4°C), washed twice with SB and pre-incubated with FcBlock (Biolegend) (10 min, 4°C). Subsequently, cells were stained with the following antibody master mix (antibody and clone details, see **Supplementary Table 1**): PBMC panel; CD45-AF700, CD3-PECy5, CD4-BUV395, CD8-BUV496, CD19-FITC, CD14-BUV605, CD66b-APC, Siglec8-PECy7. PMNL panel; CD45-AF700, CD66b-APC, Siglec8-PeCy7 (30 min, 4°C). Cells were then distributed ($3x10^5$ cells/well) and stained according to the LEGENDScreen™ Human PE Kit (Biolegend) protocol. PBMCs and PMNLs from 6 NSCLC patients were isolated to acquire enough cells for all 361 markers (including 10 isotype controls). Cells were measured on a BD LSR II Fortessa (BD Biosciences). 33 markers were excluded from analysis due to low live neutrophil counts (<100 cells) or abnormal FSC/SSC properties. 328 samples were included in the final analysis based on their quality after data acquisition.

InfinityFlow Analysis

The R Package InfinityFlow without background correction was used for the prediction of marker co-expression and the two-dimensional projection of the data using Uniform Manifold Approximation and Projection (UMAP) plots (standard parameters as stated in the package description) (24). 328 fcs files of the LEGENDScreen were used as input. Graphs were drawn with the Packages ggplot2_3.3.3, pheatmap_1.0.12 and corrplot_0.84 (R-Version 4.0.3).

Statistical Analysis

Flow cytometry data were reported as % of cells, % of $CD45^+$ cells or % of $CD66b^+$ cells and as Geometric Mean (GeoMean) and Median Fluorescence Intensity (MFI). Compensation of flow cytometry data was performed using single stains. Cut-offs for background fluorescence were based on the 'fluorescence minus one' (FMO) strategy (25). Data were analyzed using FlowJo software (TreeStar).

Statistical analyses were performed using GraphPad Prism 6.1 (GraphPad Software). All data were tested for Gaussian distribution of variables using the Shapiro-Wilk normality test. Significant differences between healthy controls and patient samples with normal distribution were determined using unpaired student's t-tests with Welch´s correction, otherwise Mann-Whitney test was applied. For comparison between samples from the same patient, paired t-test (parametric) or Wilcoxon matched-pairs test (non-parametric) was applied. Results are expressed as the mean ± S.E.M. A p-value <0.05 was considered statistically significant.

RESULTS

Low-Density Neutrophils Are Expanded in Patients With NSCLC

The presence of granulocytes in the mononuclear fraction of peripheral blood has previously been reported in the blood of patients with cancer including renal carcinoma, head and neck cancer, pancreatic cancer, colon cancer and breast adenocarcinoma (26–28). More recently, LDNs have also been reported in lung cancer patients (6, 21, 22, 29).

To determine whether LDNs were also present in this NSCLC patient cohort, blood samples were collected from NSCLC patients, regardless of disease stage. PBMCs were isolated from peripheral blood of NSCLC patients and healthy controls by density gradient centrifugation. As controls, PBMCs and PMNLs from healthy donors were used.

LDNs were identified as $CD66b^+$ cells in the PBMC fraction of NSCLC patients (**Figures 1A–C** and **Supplementary Figures 1A, B**). We found that the LDN fraction was significantly increased in NSCLC patients (median=20.4%, range 0.3-76.1%; n=26) when compared to healthy volunteers. LDNs were almost absent in healthy controls (median=0.3%, range 0.1-3.9%; n=14) (**Figure 1B**). No differences were found in the percentage of $CD66b^+$ cells in the PMNL fraction of NSCLC patients and healthy donors (**Figure 1B**), however, the percentage of $CD66b^+$ cells was significantly increased in whole blood of patients (median=56.4%, range 15.1-81.5%) vs. controls (median=32.9%, range 10.9-59.1%) (**Figure 1B**) which might reflect the higher number of LDNs in patients.

In addition, morphological analyses showed that, LDNs were absent in the PBMC fraction of healthy volunteers, whereas in NSCLC patients, LDNs were heterogeneous and contained segmented as well as morphologically immature (banded and ring-shaped) neutrophils (**Figure 1C**) as has previously been reported (9).

Unbiased Surface Marker Screen to Identify LDN Specific Markers Using Flow Cytometry

We next aimed to characterize the phenotype of LDNs in NSCLC patients with the intention to find specific surface markers that discriminate LDNs and HDNs. Previous studies have mostly

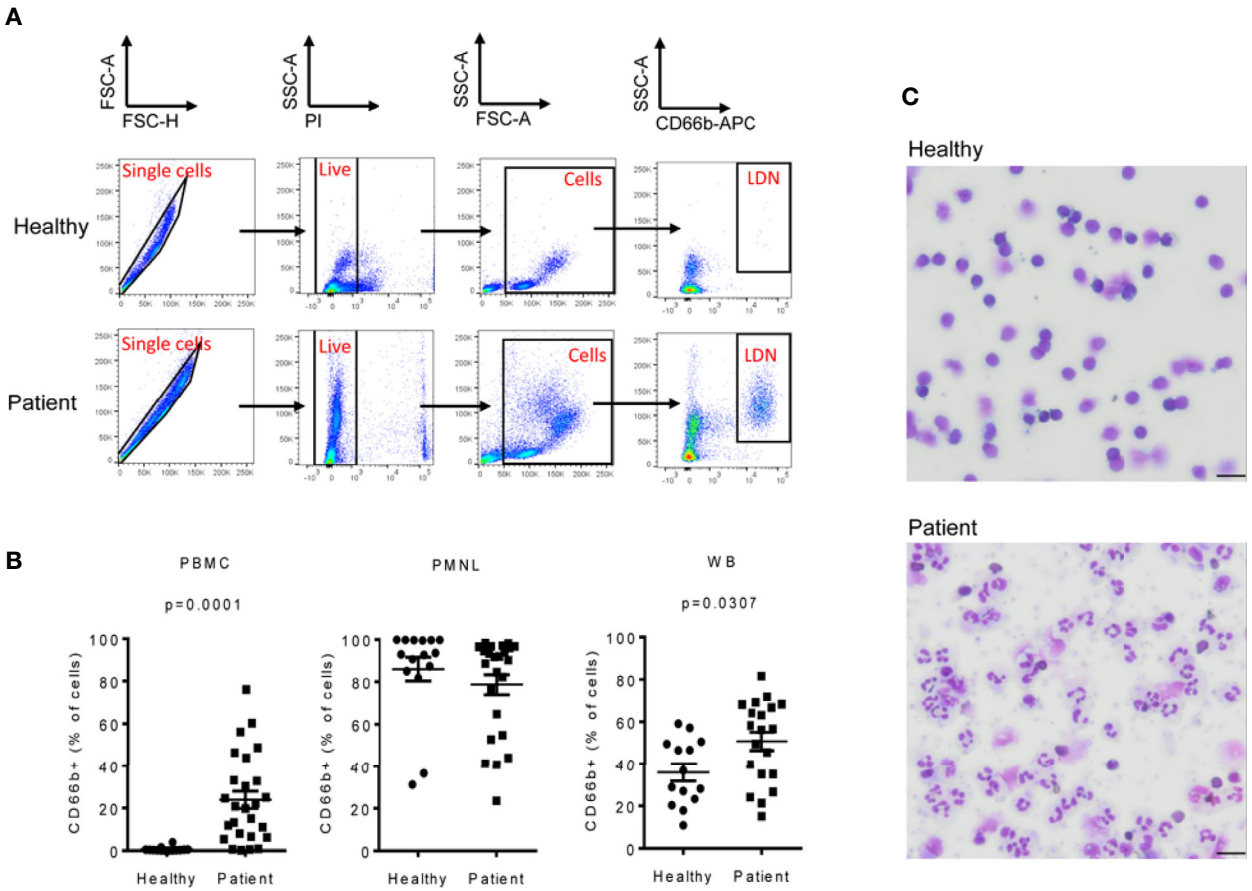

FIGURE 1 | Low-density neutrophils (LDNs) are elevated in patients with NSCLC. PBMC and PMNL fractions were isolated from peripheral blood of patients with NSCLC by density gradient centrifugation. Immediately after isolation, PBMCs, PMNLs and whole blood cells were stained with CD66b antibody to identify LDNs. **(A)** Representative polychromatic dot plots demonstrating the gating strategy employed to identify LDN cell content in the PBMC fraction of peripheral blood of healthy controls and NSCLC patients. Initial gate is to eliminate doublets from the analysis followed by gating on live (PI-). Total cells were gated based on their forward and side scatter properties and LDNs were identified as $CD66b^+$ cells. **(B)** LDNs were quantified as the percentage of $CD66b^+$ cells in the PBMC fraction of peripheral blood of 26 NSCLC patients and 14 healthy controls. Each symbol represents an individual donor. The percentage of $CD66b^+$ cells in the PMNL fraction and whole blood (WB) was also evaluated. **(C)** Representative cytospin images of the PMBC fractions of a healthy donor showing no LDNs and a NSCLC patient with heterogeneous LDNs including mature (segmented nucleus) and immature neutrophils (band cells). Pictures were acquired with a 40X objective, bar length 20μM. Statistical differences were assessed by using unpaired student´s t-test with Welch´s correction or Mann-Whitney test and data are expressed as the mean ± S.E.M.

separated LDNs from HDNs based on the expression of known myeloid cell and neutrophil maturation markers (30–33). Our study aimed to analyze a wider range of surface markers, most of which have not been previously reported to be expressed by neutrophils.

For this purpose, we used the human LEGENDScreen (Biolegend) and measured 328 surface markers in combination with 'backbone' markers that define neutrophils and performed InfinityFlow analysis (24). Briefly, the expression of PE-conjugated markers was used to predict the specific expression of each exploratory marker on all single cell events acquired through the LEGENDScreen *via* non-linear regression using the expression of the backbone markers. PBMCs and PMNLs were isolated from peripheral blood of NSCLC patients and live, $CD66b^+$ $Siglec8^-$ cells were identified as LDNs and HDNs in the PBMC and PMNL fractions, respectively (**Figure 2A**, Siglec8 was used to separate neutrophils ($Siglec8^-$) and eosinophils ($Siglec8^+$) within the $CD66b^+$ gate). 53 markers were up or downregulated (defined by LDN/HDN fold change in GeoMean - lower than 0.5 or higher than 2) in LDNs when compared to HDNs (**Figure 2B** and **Supplementary Table 2**) and the top four upregulated hits (CD36 fold change=31.1, CD41 fold change=6.7, CD61 fold change=20.1, CD226 fold change=27.8) showed a fold change above 5 (**Figures 3A, B** and **Supplementary Table 2**). UMAP plots of the LDN population confirmed the observations made by manual gating and moreover, revealed a heterogeneous expression of CD36, CD41, CD61 and CD226 (**Figure 3B**).

LDNs of NSCLC Patients Reveal Distinct Surface Marker Expression Profile

To validate the surface marker screening results, some of the highest expressed markers in the LDN fraction were selected, including CD36, CD41, CD61 and CD226 (**Figure 3A**) respectively. Unbiased InfinityFlow protein expression analysis revealed heterogenous expression patterns of all four markers within the LDN population (**Figure 3B**). Lox-1 was also included in the validation panel since it has been suggested to be a distinctive marker of the LDN population in cancer patients (34), although no difference in expression was observed between HDNs and LDNs in the surface marker screen (fold change=1.1, **Supplementary Figure 2**). Flow cytometry was used to evaluate the expression of the selected markers in the PBMC and PMNL fractions in a cohort of 13 NSCLC patients (**Figures 4A–D**). We confirmed that LDNs (defined as $CD66^+$ $Siglec8^-$ cells) showed a significantly higher proportion of CD36 (median=48.2%, range 5.1-87.4%), CD41 (median=29.2%, range 5.3-70.8%), CD61 (median=44.4%, range 16.8-90.2%) and Lox1 (median=22.1%, range 7.7-58.3%) when compared to HDNs (**Figures 4C, D**).

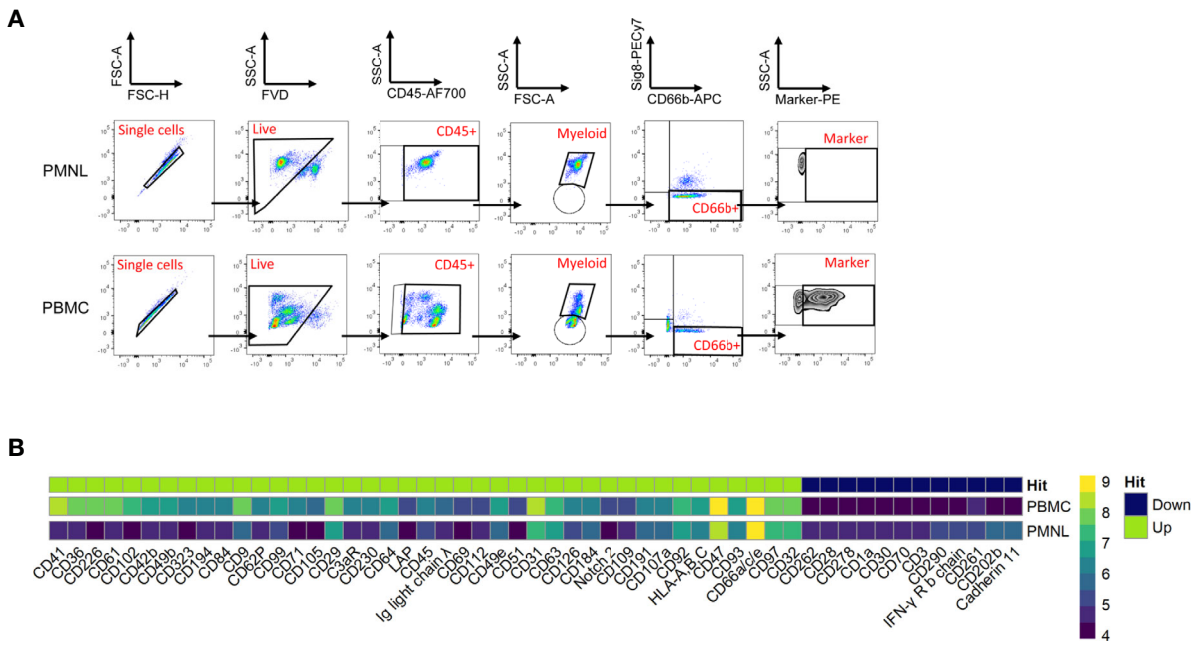

FIGURE 2 | Comprehensive surface marker screening in PMNLs and PBMCs from NSCLC patients. PBMCs and PMNLs were isolated from peripheral blood of NSCLC patients by density gradient centrifugation. Cells were initially stained with a backbone panel including antibodies against CD45, CD66b and Siglec8 and then distributed and stained with 361 anti-human PE-conjugated variable antibodies (Legend Screen, Biolegend). **(A)** Representative flow cytometry dot plots demonstrating the gating strategy employed to identify the PE-conjugated cell surface markers in the HDN and LDN fractions. Initial gate is to eliminate doublets from the analysis followed by gating on live (FVD) and $CD45^+$ cells. The myeloid population (containing neutrophils and eosinophils) was gated based on its forward and side scatter properties. Neutrophils (HDNs in PMNL fraction and LDNs in PBMC fraction) were identified as $CD66b^+$ $Siglec8^-$ cells and PE channel was used to analyze the individual surface markers. **(B)** Expression heatmap of marker hits. Hits were defined by fold change marker expression (GeoMean) with fold change > 2 and < 0.5 (ratio LDN/HDN) (see details **Supplementary Table 2**). Heatmap scale represents the GeoMean and 'hits' show the differentially regulated markers in the LDNs (PBMC gated) vs HDNs (PMNL gated); green-overexpressed, dark blue-downregulated.

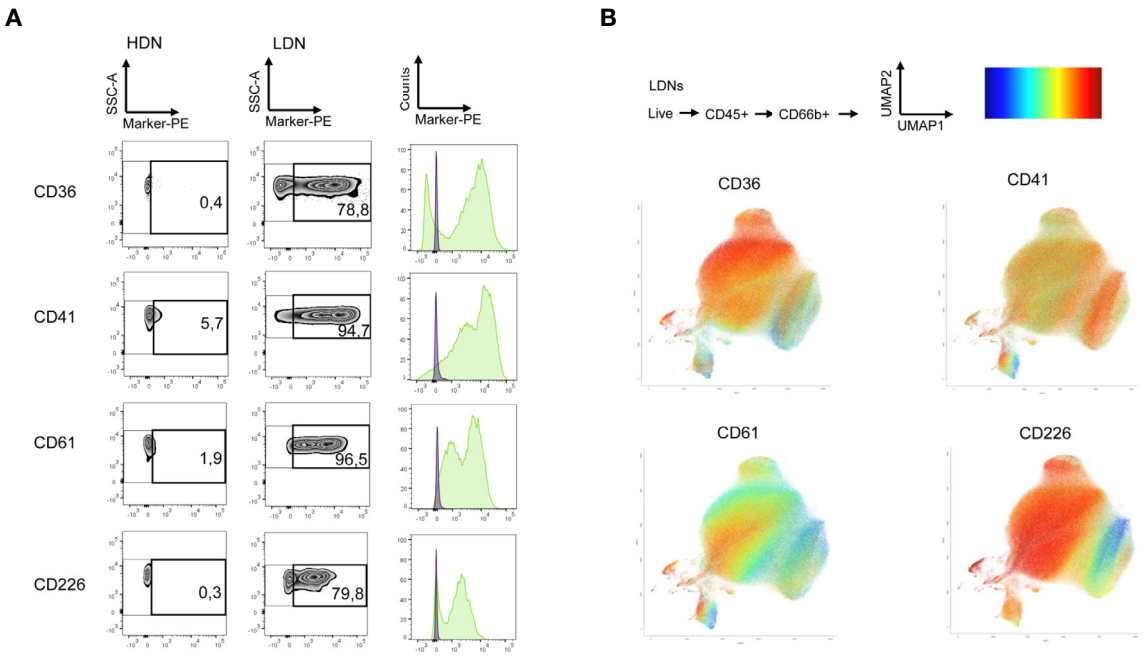

FIGURE 3 | LDNs show heterogenous expression of top screening hits. **(A)** Selected surface antigens with the most pronounced differences in expression between HDNs and LDNs. Zebra plots representing CD36, CD41, CD61 and CD226, respectively, in the HDN and LDN fractions are presented. Histograms showing the fluorescence intensity in the HDNs (violet) and LDNs (green) are also displayed. **(B)** The results of the LegendScreen were used as an input for the InfinityFlow pipeline. UMAP plots demonstrating heterogeneity of CD36, CD41, CD61 and CD226 expression in LDNs were created based on the predictions of the pipeline expression level high (red), low (blue).

These results were also reflected as an increase in the GeoMean of the selected markers in LDNs vs. HDNs (**Figure 4C**). CD226 (median=4.6%, range 0.6-35.2%, n=6) also showed increased expression on LDNs vs. HDNs, however this marker was excluded due to weak separation of negative and positive populations (**Supplementary Figure 3**). Further, we observed an increased LDN/HDN ratio of all respective markers expressed as % of $CD66b^+$ cells and GeoMean (**Figure 4D**). LDNs have been described as a population consisting of mature and immature neutrophil subsets. In order to address the maturation status of LDNs in our study cohort, we analyzed the expression of some myeloid and maturation markers including CD10, CD16, CD15 and CD11b in the LDN and HDN fractions of 7 NSCLC patients (**Supplementary Figure 4A**). We did not find significant differences in the expression of any of the markers when comparing HDNs vs LDNs (**Supplementary Figure 4A**). The analysis of the expression of CD10 in the LDNs and HDNs of 7 NSCLC patients, revealed that the vast majority of the HDN fraction expressed CD10, confirming the nature of mature neutrophils in this fraction (**Supplementary Figure 4B**). In contrast, LDNs presented more variability in the proportion of $CD10^-$ vs $CD10^+$ between different patients (**Supplementary Figure 4B**). Further studies analyzing the co-expression of neutrophil maturation markers and the surface markers CD36, CD41 and CD61 in larger patient cohorts are necessary. Taken together, these data suggest that expression levels of the surface markers CD36, CD41, CD61 and Lox-1 are significantly higher on LDNs when compared to HDNs.

LDN Markers Are Co-Expressed in LDNs of NSCLS Patients

In order to investigate whether the new identified LDN markers are co-expressed, we used t-distributed stochastic neighbor embedding (tSNE) plots and correlation analysis. tSNE plots were generated from the HDN and LDN populations of a representative healthy and NSCLC patient. We observed that none of the investigated markers was expressed in the HDNs of the healthy donor (**Figure 5A**). Moreover, when we compared HDNs and LDNs of a NSCLC patient we observed a heterogeneous expression of the markers in the LDN population, with some cells sharing expression of all the markers, other cells being positive for some of the markers and a subset of cells showing no positive signal for any of the antigens. No positive signal of CD36, CD41 and CD61 was observed in the HDNs (**Figure 5A**), however, it is important to note that Lox-1 showed expression in a subset of cells in the HDNs of the patient (**Figure 5A**).

Further analysis revealed a strong correlation between CD36, CD41 and CD61 expression while Lox-1 did not show correlation with any of the other markers (**Figure 5B**). Moreover, we observed that using the selected markers we can capture around 80% of all LDNs (**Figure 5C**).

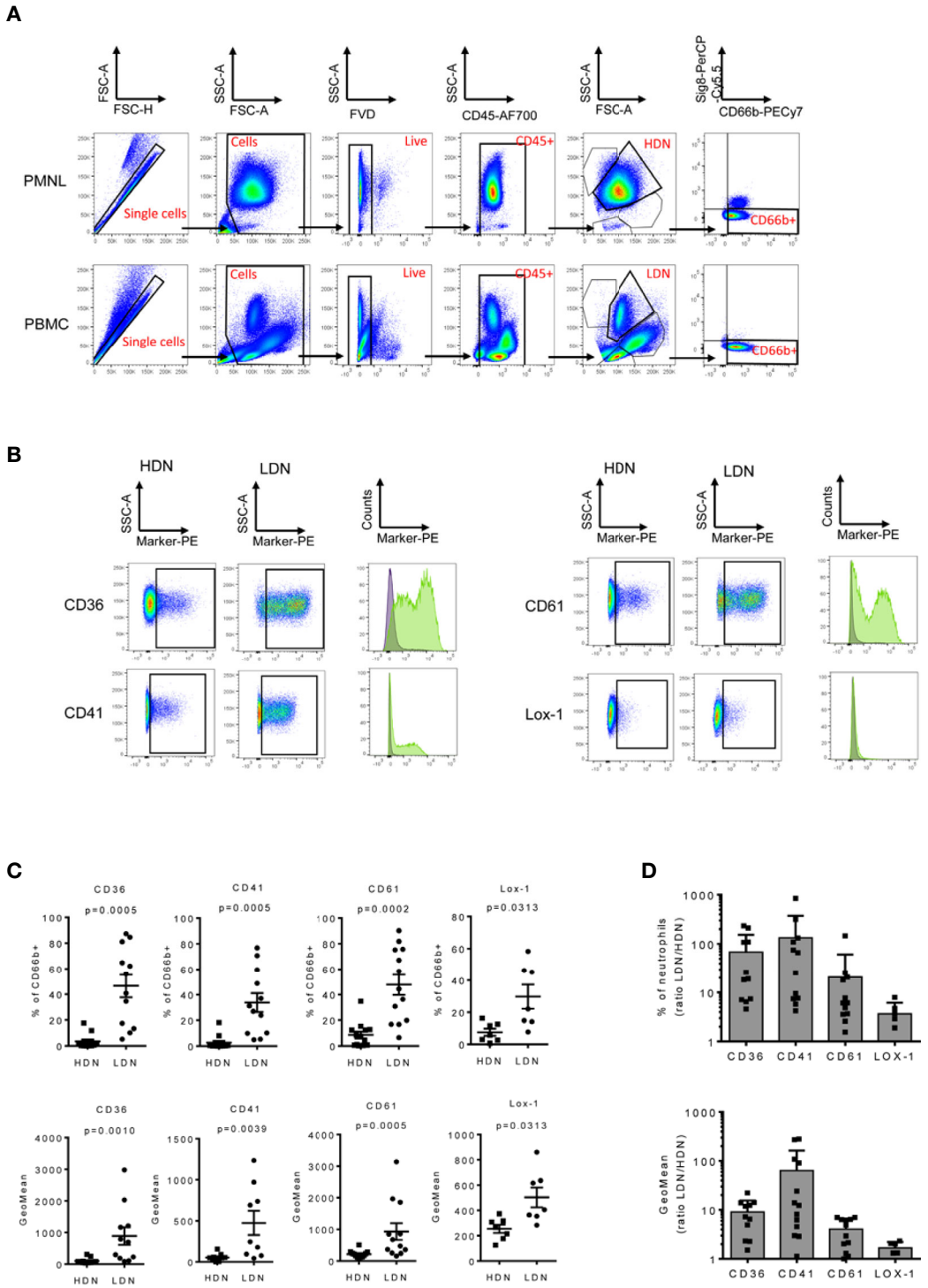

FIGURE 4 | LDNs overexpress CD36, CD41, CD61 and Lox1. PMBCs and PMNLs were isolated from 13 NSCLC patients and stained to validate the surface marker expression by flow cytometry. **(A)** Representative flow cytometry dot plots demonstrating the gating strategy. Initial gate is to eliminate doublets from the analysis followed by gating on total cells, live (FVD) and $CD45^+$ cells. HDNs and LDNs were gated base on its forward and side scatter properties. Neutrophils were identified as $CD66b^+$ $Siglec8^-$ cells **(B)** Representative dot plots and histograms showing an increased expression of $CD36^+$, $CD41^+$, $CD61^+$ and $Lox1^+$ in the LDN fraction of cancer patients. **(C)** Quantitative analysis of the marker expression as % of $CD66b^+$ cells and GeoMean in the HDN and LDN subsets in NSCLC patients. **(D)** The LDN/HDN ratio of the different markers was also analyzed. Statistical differences were assessed by using paired t-tests or Wilcoxon matched-pairs and data are expressed as the mean ± S.E.M.

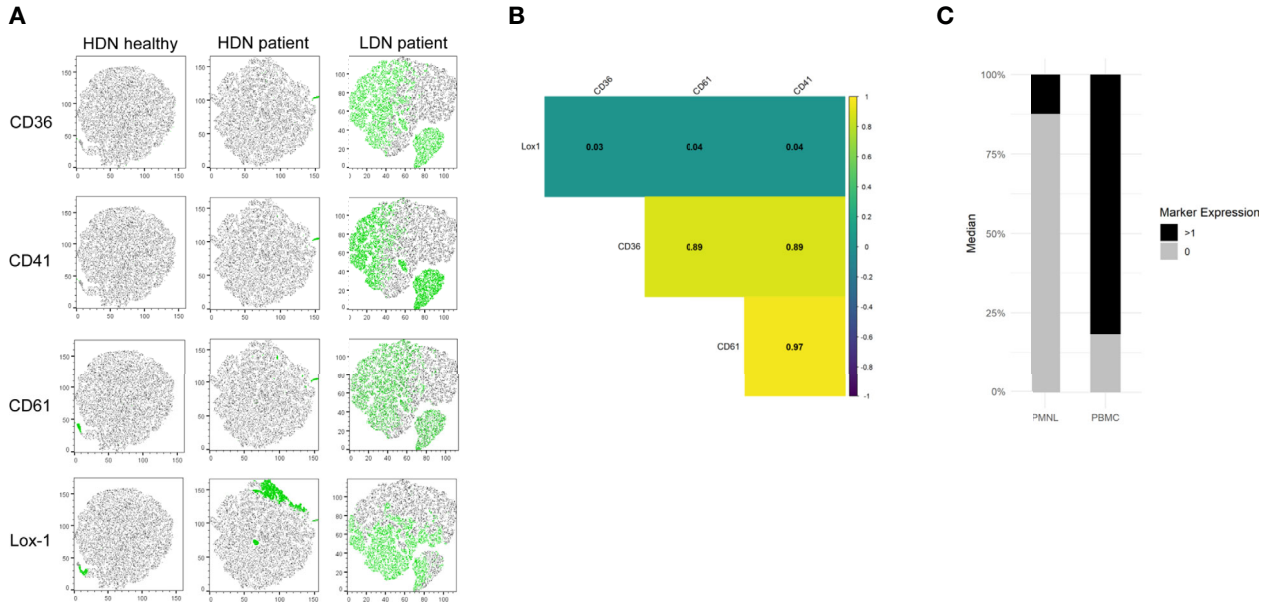

FIGURE 5 | CD36, CD41, CD61 and Lox-1 are co-expressed in LDNs from NSCLC patients. **(A)** Representative tSNE visualization of HDNs and LDNs demonstrates almost absent expression of CD36, CD41, CD61 and Lox-1 in HDNs from healthy donors and NSCLC patients while a heterogeneous expression of the markers was detected in LDNs from NSCLC patients. **(B)** Correlation analysis of the expression of the four studied markers indicating no correlation of Lox-1 with the rest of the markers and high correlation between CD36, CD41 and CD61 in one representative patient. (all results statistically significant/p<0.01). **(C)** Proportions of positive marker expression (black) and negative marker expression (grey) in the PMNL and PBMC fractions of NSCLC patient.

DISCUSSION

The presence of myeloid cells in the complex scenery of cancer has shown to have pivotal roles. In this context, neutrophils have recently attracted attention in terms of diversity and functionality. It is getting evident that neutrophils are heterogeneous and consist of diverse, dynamic subpopulations that have distinct phenotypes and can oppose or enhance cancer progression. It is possible that the ratio between the different neutrophil subpopulations, and the nature of their activity can define their overall role in cancer.

Here we report that LDNs are increased in NSCLC patients when compared to healthy individuals independent of stage. It has to be noted that within the sampled NSCLC patients, LDN presence ranges from 0.3-76.1% of all cells in the PBMC fraction. This indicates that LDN abundance is heterogenous and might correlate with tumor stage as previously reported (22, 29). The clinical significance of the presence of LDNs in the circulation of cancer patients is still unknown. Sagiv and colleagues have proposed that circulating neutrophils, besides their different density properties, might possess functional differences being the 'normal' HDNs anti-tumorigenic, whereas LDNs are associated with pro-tumor activity (9).

Current limitations to further exploit the power of LDNs as diagnostic and prognostic factor is the relatively high work load to isolate them (sucrose gradient centrifugation followed by flow cytometry staining) and the necessity to process the blood samples within a few hours after blood draw; main limitations to perform these experiments in a clinical setting. On this regard, some efforts have been made to further characterize different neutrophil subpopulations in circulation.

Most studies have been focused on myeloid and maturation markers (such as CD10, CD11b, CD15 and CD16, CXCR4, PDL-1) (22, 33, 35) and there is a lack of unbiased analysis of neutrophil heterogeneity in circulation in the setting of cancer. This is most likely because unbiased gene expression analysis is difficult to perform on neutrophils due to low RNA abundance in mature cells. One exception is the study by Condamine et al. identifying Lox1 as a LDN surface marker using a gene expression array (34). Although the immature status of neutrophils was initially thought to be directly related with their immunosuppressive and tumor-supportive role, in contrast with the cytotoxic function of mature neutrophils, multiple evidences collected in both human and animal models show that mature neutrophils can display immunosuppressive functions as well (9, 10).

We performed an unbiased high-dimensional flow cytometry surface marker screen on $CD66b^{+}Siglec8^{-}$ cells isolated from the PBMC (LDNs) and PMNL (HDNs) fractions of NSCLC patients with the aim to identify markers which distinguish LDNs and HDNs. Although the power of our screen analysis is limited due to sample size, UMAP and correlation analysis together with flow cytometry-based validation of the top hits, revealed new cellular markers that are significantly overexpressed in LDNs vs. HDNs. The top hits from the screen (CD36, CD41, CD61 and CD226) could be confirmed to be overexpressed in the LDN fraction of NSCLC patients when compared to HDNs.

CD36 is a widely studied transmembrane glycoprotein that functions as a scavenger receptor (36). It is involved in multiple cellular functions including lipid uptake, immunological recognition, inflammation, molecular adhesion, and apoptosis (36). CD36 is expressed on the cell surface of multiple cell types, including macrophages, monocytes, dendric cells, microvascular endothelial cells, retinal epithelial cells, adipocytes, platelets, enterocytes, microglial cells and podocytes (36, 37). CD36 expression has been also reported in tumor cells, stromal and immune cells in tumor tissues (37). In cancer, CD36 plays important roles in lipid homeostasis, immune response, angiogenesis, adhesion and metastasis (37). CD41, also known as αIIb integrin, is expressed on platelets and megakaryocytes (38, 39). Its expression has also been reported in hematopoietic progenitors in the embryo, fetus and adult of various species and during early stages of hematopoietic differentiation (40). CD61 (integrin β3) is expressed on megakaryocytes, besides its expression on human plasmacytoid dendritic cells. It is involved in the uptake of apoptotic cells and induction of immune tolerance (41, 42). CD41 and CD61 are often associated in a complex to form the integrin GPIIb/IIIa, which plays a major role in platelet function, acting as a receptor for several adhesion molecules, including fibronectin, fibrinogen, vitronectin and Willebrand factor (38, 40). The CD41/CD61 complex is required for platelet aggregation and clotting (38).

These novel LDN markers clearly describe this neutrophil subset in circulation of NSCLC patients. LDN presence has also been reported in the PBMCs of human patients suffering from other pathologies including autoimmune disorders and asthma, systemic and local infection, HIV, dermatomyelosis and malaria (43–53). Although the first evidence suggested that LDNs were a neutrophil subset present only under pathological conditions, LDNs have also been identified during pregnancy and in newborns (30, 54, 55). CD36, CD41 and CD61 has expression to be evaluated in LDNs in these pathologies and during pregnancy to further understand LDN heterogeneity and function. Further studies using larger cohorts and including patients in different stages of disease and under treatment will be necessary to confirm the potential use of these identified markers as prognostic biomarkers or to monitor treatment. Moreover, the development of whole blood-based protocols for the identification of the suggested markers is a crucial step towards future applications of the use of these markers as diagnostic and prognostic tools.

It has to be noted that, based on our data, low marker expression on HDNs was observed in some patients. This further supports the concept of neutrophil plasticity and the idea that HDNs and LDNs represent a continuum in the spectrum of phenotypes neutrophils can acquire. In this context, a recent report showed than HDNs from cancer patients can be retrieved in the LDN fraction and a fraction of the LDNs can be retrieved in the HDN fraction (22). This is in accordance with a previous study that described that in tumor-bearing mice HDNs can become LDNs and LDNs can switch toward HDNs, *in vivo* and *ex vivo* (9). Further studies including the new suggested LDN markers CD36, CD41 and CD61 in addition to neutrophil maturation markers would help to improve our knowledge regarding the origin and function of LDNs.

DATA AVAILABILITY STATEMENT

The original contributions presented in the study are included in the article/**Supplementary Material**. Further inquiries can be directed to the corresponding author.

ETHICS STATEMENT

The studies involving human participants were reviewed and approved by Ethics Committee of the Medical University of Graz. The patients/participants provided their written informed consent to participate in this study.

AUTHOR CONTRIBUTIONS

PV-C, JK and KM designed and supervised the research. PV-C and KM performed the experiments and analyzed the results. OK performed bioinformatic analysis. SR, MK, AS and ZNM assisted with the performance of the experiments. LB, JL, MF and MP provided the clinical samples and maintained the clinical database. PV-C and OK performed statistical analyses. PV-C and OK crafted the figures. PV-C, KM, OK, RS, AMH, AH and JK interpreted the data and provided technical support. PV-C and JK wrote the manuscript. All authors critically revised and commented on the manuscript. All authors contributed to the article and approved the submitted version.

FUNDING

This work was supported by the OENB Anniversary Fund (17584) and FFG-Bridge 1 grant (871284). PhD candidates PV-C, OK, SR, MK, AS, and ZNM received funding from the FWF [doctoral programs: DK-MOLIN (W1241) and DP-iDP (DOC-31)] or BioTechMed and were trained within the frame of the PhD Program Molecular Medicine of the Medical University of Graz. Work in the lab of RS is funded by FWF grants P33325 and KLI887.

ACKNOWLEDGMENTS

We are grateful to Sabine Kern, Iris Red, Stefanie Stanzer and the study nurses for their excellent technical assistance.

SUPPLEMENTARY MATERIAL

The Supplementary Material for this article can be found online at: https://www.frontiersin.org/articles/10.3389/fimmu.2021.703846/full#supplementary-material

REFERENCES

1. Sung H, Ferlay J, Siegel RL, Laversanne M, Soerjomataram I, Jemal A, et al. Global Cancer Statistics 2020: GLOBOCAN Estimates of Incidence and Mortality Worldwide for 36 Cancers in 185 Countries. *CA Cancer J Clin* (2021) 71:209–49. doi: 10.3322/caac.21660
2. Bade BC, Dela Cruz CS. Lung Cancer 2020: Epidemiology, Etiology, and Prevention. *Clin Chest Med* (2020) 41:1–24. doi: 10.1016/j.ccm.2019.10.001
3. Zappa C, Mousa SA. Non-Small Cell Lung Cancer: Current Treatment and Future Advances. *Transl Lung Cancer Res* (2016) 5:288–300. doi: 10.21037/tlcr.2016.06.07
4. Balkwill F, Charles KA, Mantovani A. Smoldering and Polarized Inflammation in the Initiation and Promotion of Malignant Disease. *Cancer Cell* (2005) 7:211–7. doi: 10.1016/j.ccr.2005.02.013
5. Eruslanov EB, Bhojnagarwala PS, Quatromoni JG, Stephen TL, Ranganathan A, Deshpande C, et al. Tumor-Associated Neutrophils Stimulate T Cell Responses in Early-Stage Human Lung Cancer. *J Clin Invest* (2014) 124:5466–80. doi: 10.1172/JCI77053
6. Kargl J, Busch SE, Yang GHY, Kim KH, Hanke ML, Metz HE, et al. Neutrophils Dominate the Immune Cell Composition in Non-Small Cell Lung Cancer. *Nat Commun* (2017) 8:14381. doi: 10.1038/ncomms14381
7. Ilie M, Hofman V, Ortholan C, Bonnetaud C, Coëlle C, Mouroux J, et al. Predictive Clinical Outcome of the Intratumoral CD66b-Positive Neutrophil-to-CD8-Positive T-Cell Ratio in Patients With Resectable Nonsmall Cell Lung Cancer. *Cancer* (2012) 118:1726–37. doi: 10.1002/cncr.26456
8. Coffelt SB, Wellenstein MD, De Visser KE. Neutrophils in Cancer: Neutral No More. *Nat Rev Cancer* (2016) 16:431–46. doi: 10.1038/nrc.2016.52
9. Sagiv JY, Michaeli J, Assi S, Mishalian I, Kisos H, Levy L, et al. Phenotypic Diversity and Plasticity in Circulating Neutrophil Subpopulations in Cancer. *Cell Rep* (2015) 10:562–73. doi: 10.1016/j.celrep.2014.12.039
10. Hsu BE, Tabariès S, Johnson RM, Andrzejewski S, Senecal J, Lehuédé C, et al. Immature Low-Density Neutrophils Exhibit Metabolic Flexibility That Facilitates Breast Cancer Liver Metastasis. *Cell Rep* (2019) 27:3902–15.e6. doi: 10.1016/j.celrep.2019.05.091
11. Acharyya S, Oskarsson T, Vanharanta S, Malladi S, Kim J, Morris PG, et al. A CXCL1 Paracrine Network Links Cancer Chemoresistance and Metastasis. *Cell* (2012) 150:165–78. doi: 10.1016/j.cell.2012.04.042
12. Casbon AJ, Reynau D, Park C, Khu E, Gan DD, Schepers K, et al. Invasive Breast Cancer Reprograms Early Myeloid Differentiation in the Bone Marrow to Generate Immunosuppressive Neutrophils. *Proc Natl Acad Sci USA* (2015) 112:E566–75. doi: 10.1073/pnas.1424927112
13. Coffelt SB, Kersten K, Doornebal CW, Weiden J, Vrijland K, Hau CS, et al. IL-17-Producing γδ T Cells and Neutrophils Conspire to Promote Breast Cancer Metastasis. *Nature* (2015) 522:345–8. doi: 10.1038/nature14282
14. Waight JD, Hu Q, Miller A, Liu S, Abrams SI. Tumor-Derived G-CSF Facilitates Neoplastic Growth Through a Granulocytic Myeloid-Derived Suppressor Cell-Dependent Mechanism. *PLoS One* (2011) 6(11):e27690. doi: 10.1371/journal.pone.0027690
15. Kowanetz M, Wu X, Lee J, Tan M, Hagenbeek T, Qu X, et al. Granulocyte-Colony Stimulating Factor Promotes Lung Metastasis Through Mobilization of Ly6G+Ly6C+ Granulocytes. *Proc Natl Acad Sci USA* (2010) 107:21248–55. doi: 10.1073/pnas.1015855107
16. Fridlender ZG, Sun J, Kim S, Kapoor V, Cheng G, Ling L, et al. Polarization of Tumor-Associated Neutrophil Phenotype by TGF-β: "N1" Versus "N2" TAN. *Cancer Cell* (2009) 16:183–94. doi: 10.1016/j.ccr.2009.06.017
17. Youn J-I, Collazo M, Shalova IN, Biswas SK, Gabrilovich DI. Characterization of the Nature of Granulocytic Myeloid-Derived Suppressor Cells in Tumor-Bearing Mice. *J Leukoc Biol* (2012) 91:167–81. doi: 10.1189/jlb.0311177
18. Ueda Y, Kondo M, Kelsoe G. Inflammation and the Reciprocal Production of Granulocytes and Lymphocytes in Bone Marrow. *J Exp Med* (2005) 201:1771–80. doi: 10.1084/jem.20041419
19. Guthrie GJK, Charles KA, Roxburgh CSD, Horgan PG, McMillan DC, Clarke SJ. The Systemic Inflammation-Based Neutrophil-Lymphocyte Ratio: Experience in Patients With Cancer. *Crit Rev Oncol Hematol* (2013) 88:218–30. doi: 10.1016/j.critrevonc.2013.03.010
20. Templeton AJ, McNamara MG, Šeruga B, Vera-Badillo FE, Aneja P, Ocaña A, et al. Prognostic Role of Neutrophil-to-Lymphocyte Ratio in Solid Tumors: A Systematic Review and Meta-Analysis. *J Natl Cancer Inst* (2014) 106(6): dju124. doi: 10.1093/jnci/dju124
21. Liu Y, Hu Y, Gu F, Liang J, Zeng Y, Hong X, et al. Phenotypic and Clinical Characterization of Low Density Neutrophils in Patients With Advanced Lung Adenocarcinoma. *Oncotarget* (2017) 8:90969–78. doi: 10.18632/oncotarget.18771
22. Shaul ME, Eyal O, Guglietta S, Aloni P, Zlotnik A, Forkosh E, et al. Circulating Neutrophil Subsets in Advanced Lung Cancer Patients Exhibit Unique Immune Signature and Relate to Prognosis. *FASEB J* (2020) 34:4204–18. doi: 10.1096/fj.201902467R
23. Bronte V, Brandau S, Chen SH, Colombo MP, Frey AB, Greten TF, et al. Recommendations for Myeloid-Derived Suppressor Cell Nomenclature and Characterization Standards. *Nat Commun* (2016) 7. doi: 10.1038/ncomms12150
24. Becht E, Tolstrup D, Dutertre CA, Ginhoux F, Newell EW, Gottardo R, et al. Infinity Flow: High-Throughput Single-Cell Quantification of 100s of Proteins Using Conventional Flow Cytometry and Machine Learning. *bioRxiv* (2020). doi: 10.2139/ssrn.3656603
25. Tung JW, Heydari K, Tirouvanziam R, Sahaf B, Parks DR, Herzenberg LA, et al. Modern Flow Cytometry: A Practical Approach. *Clin Lab Med* (2007) 27:453–68. doi: 10.1016/j.cll.2007.05.001
26. Brandau S, Trellakis S, Bruderek K, Schmaltz D, Steller G, Elian M, et al. Myeloid-Derived Suppressor Cells in the Peripheral Blood of Cancer Patients Contain a Subset of Immature Neutrophils With Impaired Migratory Properties. *J Leukoc Biol* (2011) 89:311–7. doi: 10.1189/jlb.0310162
27. Schmielau J, Finn OJ. Activated Granulocytes and Granulocyte-Derived Hydrogen Peroxide Are the Underlying Mechanism of Suppression of T-Cell Function in Advanced Cancer Patients. *Cancer Res* (2001) 61:4756–60.
28. Najjar YG, Rayman P, Jia X, Pavicic PG, Rini BI, Tannenbaum C, et al. Myeloid-Derived Suppressor Cell Subset Accumulation in Renal Cell Carcinoma Parenchyma Is Associated With Intratumoral Expression of IL1b, IL8, CXCL5, and Mip-1α. *Clin Cancer Res* (2017) 23:2346–55. doi: 10.1158/1078-0432.CCR-15-1823
29. Yamauchi Y, Safi S, Blattner C, Rathinasamy A, Umansky L, Juenger S, et al. Circulating and Tumor Myeloid-Derived Suppressor Cells in Resectable Non-Small Cell Lung Cancer. *Am J Respir Crit Care Med* (2018) 198:777–87. doi: 10.1164/rccm.201708-1707OC
30. Weinhage T, Kölsche T, Rieger-Fackeldey E, Schmitz R, Antoni A-C, Ahlmann M, et al. Cord Blood Low-Density Granulocytes Correspond to an Immature Granulocytic Subset With Low Expression of S100A12. *J Immunol* (2020) 205:56–66. doi: 10.4049/jimmunol.1901308
31. Elghetany MT. Surface Antigen Changes During Normal Neutrophilic Development: A Critical Review. *Blood Cells Mol Dis* (2002) 28:260–74. doi: 10.1006/bcmd.2002.0513
32. Marini O, Costa S, Bevilacqua D, Calzetti F, Tamassia N, Spina C, et al. Mature CD10+ and Immature CD10- Neutrophils Present in G-CSF-Treated Donors Display Opposite Effects on T Cells. *Blood* (2017) 129:1343–56. doi: 10.1182/blood-2016-04-713206
33. Singhal S, Bhojnagarwala PS, O'Brien S, Moon EK, Garfall AL, Rao AS, et al. Origin and Role of a Subset of Tumor-Associated Neutrophils With Antigen-Presenting Cell Features in Early-Stage Human Lung Cancer. *Cancer Cell* (2016) 30:120–35. doi: 10.1016/j.ccell.2016.06.001
34. Condamine T, Gabrilovich DI, Dominguez GA, Youn J-I, Kossenkov AV, Mony S, et al. Lectin-Type Oxidized LDL Receptor-1 Distinguishes Population of Human Polymorphonuclear Myeloid-Derived Suppressor Cells in Cancer Patients. *Sci Immunol* (2016) 1(2):aaf8943. doi: 10.1126/sciimmunol.aaf8943
35. Lang S, Bruderek K, Kaspar C, Höing B, Kanaan O, Dominas N, et al. Clinical Relevance and Suppressive Capacity of Human Myeloid-Derived Suppressor Cell Subsets. *Clin Cancer Res* (2018) 24:4834–44. doi: 10.1158/1078-0432.CCR-17-3726
36. Silverstein RL, Febbraio M. CD36, a Scavenger Receptor Involved in Immunity, Metabolism, Angiogenesis, and Behavior. *Sci Signal* (2009) 2 (72):re3. doi: 10.1126/scisignal.272re3
37. Wang J, Li Y. CD36 Tango in Cancer: Signaling Pathways and Functions. *Theranostics* (2019) 9:4893–908. doi: 10.7150/thno.36037
38. Gekas C, Graf T. CD41 Expression Marks Myeloid-Biased Adult Hematopoietic Stem Cells and Increases With Age. *Blood* (2013) 121:4463–72. doi: 10.1182/blood-2012-09-457929
39. Drissen R, Buza-Vidas N, Woll P, Thongjuea S, Gambardella A, Giustacchini A, et al. Distinct Myeloid Progenitor-Differentiation Pathways Identified Through

Single-Cell RNA Sequencing. *Nat Immunol* (2016) 17:666–76. doi: 10.1038/ni.3412
40. Mitjavila-Garcia MT, Cailleret M, Godin I, Nogueira MM, Cohen-Solal K, Schiavon V, et al. Expression of CD41 on Hematopoietic Progenitors Derived From Embryonic Hematopoietic Cells. *Development* (2002) 129:2003–13. doi: 10.1242/dev.129.8.2003
41. Parcina M, Schiller M, Gierschke A, Heeg K, Bekeredjian-Ding I. PDC Expressing CD36, CD61 and IL-10 may Contribute to Propagation of Immune Tolerance. *Autoimmunity* (2009) 42:353–5. doi: 10.1080/08916930902831969
42. Dejima H, Nakanishi H, Kuroda H, Yoshimura M, Sakakura N, Ueda N, et al. Detection of Abundant Megakaryocytes in Pulmonary Artery Blood in Lung Cancer Patients Using a Microfluidic Platform. *Lung Cancer* (2018) 125:128–35. doi: 10.1016/j.lungcan.2018.09.011
43. Fu J, Tobin MC, Thomas LL. Neutrophil-Like Low-Density Granulocytes Are Elevated in Patients With Moderate to Severe Persistent Asthma. *Ann Allergy Asthma Immunol* (2014) 113:635–40.e2. doi: 10.1016/j.anai.2014.08.024
44. Grayson PC, Carmona-Rivera C, Xu L, Lim N, Gao Z, Asare AL, et al. Neutrophil-Related Gene Expression and Low-Density Granulocytes Associated With Disease Activity and Response to Treatment in Antineutrophil Cytoplasmic Antibody-Associated Vasculitis. *Arthritis Rheumatol* (2015) 67:1922–32. doi: 10.1002/art.39153
45. Midgley A, Beresford MW. Increased Expression of Low Density Granulocytes in Juvenile-Onset Systemic Lupus Erythematosus Patients Correlates With Disease Activity. *Lupus* (2016) 25:407–11. doi: 10.1177/0961203315608959
46. Cloke T, Munder M, Taylor G, Müller I, Kropf P. Characterization of a Novel Population of Low-Density Granulocytes Associated With Disease Severity in HIV-1 Infection. *PLoS One* (2012) 7(11):e48939. doi: 10.1371/journal.pone.0048939
47. Hacbarth E, Kajdacsy-Balla A. Low Density Neutrophils in Patients With Systemic Lupus Erythematosus, Rheumatoid Arthritis, and Acute Rheumatic Fever. *Arthritis Rheum* (1986) 29:1334–42. doi: 10.1002/art.1780291105
48. Denny MF, Yalavarthi S, Zhao W, Thacker SG, Anderson M, Sandy AR, et al. A Distinct Subset of Proinflammatory Neutrophils Isolated From Patients With Systemic Lupus Erythematosus Induces Vascular Damage and Synthesizes Type I IFNs. *J Immunol* (2010) 184:3284–97. doi: 10.4049/jimmunol.0902199
49. Marini O, Spina C, Mimiola E, Cassaro A, Malerba G, Todeschini G, et al. Identification of Granulocytic Myeloid-Derived Suppressor Cells (G-MDSCs) in the Peripheral Blood of Hodgkin and Non-Hodgkin Lymphoma Patients. *Oncotarget* (2016) 7:27676–88. doi: 10.18632/oncotarget.8507
50. Deng Y, Ye J, Luo Q, Huang Z, Peng Y, Xiong G, et al. Low-Density Granulocytes Are Elevated in Mycobacterial Infection and Associated With the Severity of Tuberculosis. *PLoS One* (2016) 11(4):e0153567. doi: 10.1371/journal.pone.0153567
51. Drifte G, Dunn-Siegrist I, Tissières P, Pugin J. Innate Immune Functions of Immature Neutrophils in Patients With Sepsis and Severe Systemic Inflammatory Response Syndrome. *Crit Care Med* (2013) 41:820–32. doi: 10.1097/CCM.0b013e318274647d
52. Zhang S, Shen H, Shu X, Peng Q, Wang G. Abnormally Increased Low-Density Granulocytes in Peripheral Blood Mononuclear Cells Are Associated With Interstitial Lung Disease in Dermatomyositis. *Mod Rheumatol* (2017) 27:122–9. doi: 10.1080/14397595.2016.1179861
53. Rocha BC, Marques PE, Leoratti FMDS, Junqueira C, Pereira DB, Antonelli LRDV, et al. Type I Interferon Transcriptional Signature in Neutrophils and Low-Density Granulocytes Are Associated With Tissue Damage in Malaria. *Cell Rep* (2015) 13:2829–41. doi: 10.1016/j.celrep.2015.11.055
54. Ssemaganda A, Kindinger L, Bergin P, Nielsen L, Mpendo J, Ssetaala A, et al. Characterization of Neutrophil Subsets in Healthy Human Pregnancies. *PLoS One* (2014) 9(2):e85696. doi: 10.1371/journal.pone.0085696
55. Rieber N, Gille C, Köstlin N, Schäfer I, Spring B, Ost M, et al. Neutrophilic Myeloid-Derived Suppressor Cells in Cord Blood Modulate Innate and Adaptive Immune Responses. *Clin Exp Immunol* (2013) 174:45–52. doi: 10.1111/cei.12143

Conflict of Interest: The authors declare that the research was conducted in the absence of any commercial or financial relationships that could be construed as a potential conflict of interest.

Publisher's Note: All claims expressed in this article are solely those of the authors and do not necessarily represent those of their affiliated organizations, or those of the publisher, the editors and the reviewers. Any product that may be evaluated in this article, or claim that may be made by its manufacturer, is not guaranteed or endorsed by the publisher.

frontiers in Immunology

ORIGINAL RESEARCH
published: 06 October 2021
doi: 10.3389/fimmu.2021.701721

Stamp2 Protects From Maladaptive Structural Remodeling and Systolic Dysfunction in Post-Ischemic Hearts by Attenuating Neutrophil Activation

Martin Mollenhauer[1,2,3†], Senai Bokredenghel[1,2,3†], Simon Geißen[1,2,3†], Anna Klinke[1,3,4], Tobias Morstadt[1], Merve Torun[1,2,3], Sabrina Strauch[1], Wibke Schumacher[1,2,3], Martina Maass[1], Jürgen Konradi[1], Vera B. M. Peters[1,2,3], Eva Berghausen[1,2,3], Marius Vantler[1,2,3], Stephan Rosenkranz[1,2,3], Dennis Mehrkens[1,2,3], Simon Braumann[1,2,3], Felix Nettersheim[1,2,3], Alexander Hof[1,2,3], Sakine Simsekyilmaz[1,2], Holger Winkels[1,2,3], Volker Rudolph[1,3,4], Stephan Baldus[1,2,3], Matti Adam[1,2,3] and Henrik ten Freyhaus[1,2,3]*

[1] Department for Experimental Cardiology, Faculty of Medicine, University of Cologne, and Clinic III for Internal Medicine, University Hospital Cologne, Cologne, Germany, [2] Center for Molecular Medicine Cologne (CMMC), University of Cologne, Cologne, Germany, [3] Cologne Cardiovascular Research Center (CCRC), University of Cologne, Cologne, Germany, [4] Clinic for General and Interventional Cardiology/Angiology, Herz- und Diabeteszentrum Nordrhein-Westfalen, University Hospital Ruhr-Universität Bochum, Bad Oeynhausen, Germany

The six-transmembrane protein of prostate 2 (Stamp2) acts as an anti-inflammatory protein in macrophages by protecting from overt inflammatory signaling and Stamp2 deficiency accelerates atherosclerosis in mice. Herein, we describe an unexpected role of Stamp2 in polymorphonuclear neutrophils (PMN) and characterize Stamp2's protective effects in myocardial ischemic injury. In a murine model of ischemia and reperfusion (I/R), echocardiography and histological analyses revealed a pronounced impairment of cardiac function in hearts of Stamp2-deficient- (*Stamp2*$^{-/-}$) mice as compared to wild-type (WT) animals. This difference was driven by aggravated cardiac fibrosis, as augmented fibroblast-to-myofibroblast transdifferentiation was observed which was mediated by activation of the redox-sensitive p38 mitogen-activated protein kinase (p38 MAPK). Furthermore, we observed increased production of reactive oxygen species (ROS) in *Stamp2*$^{-/-}$ hearts after I/R, which is the likely cause for p38 MAPK activation. Although myocardial macrophage numbers were not affected by Stamp2 deficiency after I/R, augmented myocardial infiltration by polymorphonuclear neutrophils (PMN) was observed, which coincided with enhanced myeloperoxidase (MPO) plasma levels. Primary PMN isolated from *Stamp2*$^{-/-}$ animals exhibited a proinflammatory phenotype characterized by enhanced nuclear factor (NF)-κB activity and MPO secretion. To prove the critical role of PMN for the observed phenotype after I/R, antibody-mediated PMN depletion was performed in *Stamp2*$^{-/-}$ mice which reduced deterioration of LV function and adverse structural remodeling to WT levels. These data indicate a novel role of Stamp2 as an anti-inflammatory regulator of PMN and fibroblast-to-myofibroblast transdifferentiation in myocardial I/R injury.

Keywords: six-transmembrane protein of prostate 2, Stamp2, Steap4, myocardial infarction, ischemia and reperfusion damage, left ventricular dysfunction, inflammation, polymorphonuclear neutrophils (PMN)

OPEN ACCESS

Edited by:
Clare Hawkins, University of Copenhagen, Denmark

Reviewed by:
Paul Kenneth Witting, The University of Sydney, Australia
Sarah Lena Puhl, Ludwig Maximilian University of Munich, Germany

***Correspondence:**
Martin Mollenhauer
martin.mollenhauer@uk-koeln.de
Henrik ten Freyhaus
henrik.ten-freyhaus@uk-koeln.de

†*These authors have contributed equally to this work*

Specialty section:
This article was submitted to Molecular Innate Immunity, a section of the journal Frontiers in Immunology

Received: *28 April 2021*
Accepted: *31 August 2021*
Published: *06 October 2021*

Citation:
Mollenhauer M, Bokredenghel S, Geißen S, Klinke A, Morstadt T, Torun M, Strauch S, Schumacher W, Maass M, Konradi J, Peters VBM, Berghausen E, Vantler M, Rosenkranz S, Mehrkens D, Braumann S, Nettersheim F, Hof A, Simsekyilmaz S, Winkels H, Rudolph V, Baldus S, Adam M and ten Freyhaus H (2021) Stamp2 Protects From Maladaptive Structural Remodeling and Systolic Dysfunction in Post-Ischemic Hearts by Attenuating Neutrophil Activation. Front. Immunol. 12:701721. doi: 10.3389/fimmu.2021.701721

HIGHLIGHTS

Herein, we investigate the role of Stamp2 in hearts subjected to ischemia and reperfusion injury. Loss of Stamp2 enhances neutrophil activation, thereby aggravating maladaptive structural remodeling and systolic dysfunction.

INTRODUCTION

As the most severe manifestation of coronary artery disease (CAD), acute myocardial infarction (AMI) remains a leading cause of death in the western world despite an overall reduction in AMI mortality due to more aggressive approaches to coronary revascularization (1, 2). Revascularization is associated with inflammatory tissue injury at the site of ischemia and reperfusion (I/R) leading to subsequent ventricular fibrotic remodeling and heart failure (HF) (3). HF is the most common reason for hospitalization and affects around 26 million people worldwide (4).

I/R is a major trigger of polymorphonuclear neutrophils (PMN) recruitment and activation. PMN are among the first cells that infiltrate the ischemic area and accumulate in great numbers within the infarcted region. Intriguing data suggest that PMN's level of inflammatory activation determines the extent of fibrotic scar generation and thereby recovery or persistent deterioration of cardiac function (5–7). Whereas total antibody-mediated depletion of PMN impairs infarct healing (8), targeted and more sophisticated modulation, e.g. by inhibition of neutrophil-secreted inflammatory proteins like myeloperoxidase (MPO), improves cardiac repair and function (9).

Activation of PMN stimulates fibroblast-to-myofibroblast transdifferentiation, giving rise to the major collagen-producing cell type within the heart (10). This process can be mediated by oxidative activation and phosphorylation of the p38 mitogen-activated protein kinase (p38 MAPK) which is, among others, induced by MPO and subsequent release of hypochlorous acid (HOCl) (11, 12).

The six-transmembrane protein of the prostate 2 (Stamp2), also known as six-transmembrane epithelial antigen of prostate 4 (STEAP4), has emerged as a regulator of leukocyte-driven inflammation in metabolic syndrome (13) atherosclerosis (14), and pulmonary vascular remodeling (15). Containing an NADP-oxidoreductase motif (Rossman Fold), Stamp2 is able to oxidize NADPH to $NADP^+$, thereby transferring electrons through the plasma membrane to iron and copper ions (14, 16). Upon loss or dysfunction of Stamp2, NADPH accumulates within the cytosol and binds to the NADPH sensor and inhibitor of nuclear factor (NF)-κB activity NmrA-like family domain-containing protein 1 (NmRal), thereby preventing its nuclear translocation. In turn, nuclear NF-κB activity is enhanced, causing production and release of proinflammatory mediators (14).

Here, we show that Stamp2 is a novel anti-inflammatory regulator in myocardial I/R damage and omit closely related to the development of adverse ventricular remodeling and HF. *Stamp2*$^{-/-}$ mice subjected to I/R showed a pronounced inflammatory PMN activation and elevated fibroblast-to-myofibroblast transdifferentiation, revealing a role of Stamp2 as a potential target for upcoming anti-inflammatory therapies in myocardial injury.

METHODS AND MATERIALS

Animals and Neutrophil Depletion

The generation of *Stamp2*$^{-/-}$ mice was described by Wellen et al. (13). WT and *Stamp2*$^{-/-}$ mice were used as littermates for all animal studies. Animals were kindly provided by Prof. Gökhan S. Hotamisligil (Sabri Ülker Center, Department of Molecular Metabolism and Broad Institute of Harvard-MIT and Harvard T.H. Chan School of Public Health, Boston, US). 8- to 12-week old male mice (C57/Bl6 background) were used for all animal studies. Neutrophil depletion was performed by intraperitoneal (i.p.) injection of monoclonal antibody clone 1A8 (50 µg, Stemmcell, Cologne, Germany) 1 day prior to I/R and on day 3 after I/R (8).

Left Anterior Descending Artery Ligation

Mice were anaesthetized by intraperitoneal (i.p.) injection of 5 mg/kg bodyweight midazolam and 0.25 mg/kg bodyweight medetomidine. Analgesia was performed by i.p. injection of 0.05 mg/kg bodyweight fentanyl. Body temperature was kept constant using a rectal thermometer and an electric warming pad. To compensate evaporation, the animals received a continuous infusion of pre-warmed saline. Animals were placed in a supine position, intubated under direct laryngoscopy with a 22 gauge angiocath and ventilated using a small animal respirator (Harvard Apparatus, USA; tidal volume: 0.1 ml per 10g mouse body weight, ventilation rate: 170/min). Surgical procedures were carried out using a dissecting microscope (Leica MZ6, Leica Microsystems, Germany). After lateral thoracotomy of the fourth intercostal space, a suture (8/0 polypropylene suture, Polypro, CP Medical, USA) was placed around the left coronary artery after retraction of the left atrial appendage. The artery was ligated with a bow tie. The ligation was removed after 40 min to allow for reperfusion, the thorax was closed and the animals were allowed to recover on a warming pad.

Echocardiographic Studies

Transthoracic echocardiography was performed using the Vevo 3100 System (VisualSonics, Toronto, Canada) (17). B-mode and M-mode recordings were performed using a MX 550S transducer (25-55 MHz) with a frame rate of 230–400 frames/s to assess LV dimensions. All images were recorded digitally and analysis was performed using the Vevo 3100-software. Ejection fraction (EF), cardiac output (CO) and global longitudinal strain were calculated as described before (18). Echocardiography was performed before surgery (baseline) and 7 days after AMI.

Analysis of Fibrotic Area

Hearts were excised and cut along the long axis at the ligation position or, for non-infarcted animals, at the center of the left ventricle, fixed in 3.7% formaldehyde solution for 2 days and embedded in paraffin. Consecutive long axis sections of 4 µm were cut. Sections were stained

with Masson Trichrome solution following standard protocols. Images were acquired using a BZ-9000 microscope (Keyence, Germany). The area of fibrosis in percent of the left ventricle was quantified using Keyence analytic software (Keyence, Germany). Mean fibrotic area of 3 sections was calculated, respectively (12).

MPO Plasma Level

Blood was drawn into heparinized syringes in deep isoflurane anesthesia by heart puncture, followed by centrifugation for 10 min at 1,300 x g. Plasma was analyzed for MPO using a Mouse MPO ELISA (Hycult biotech, Uden, Netherlands) according to manufacturer's instructions (12).

DHE Staining of Ventricular Sections

Frozen heart sections were stained with dihydroethidium (DHE, 5 µM, diluted in DMSO and HBSS-buffer, ThermoFisher, Germany). The slides were incubated with DHE for 30 minutes at 37°C in the dark before pictures were taken.

Staining for Myocardial Macrophage and PMN Infiltration

Hearts were frozen in OCT compound and cut into 6 µm sections. Frozen heart specimens were fixed with acetone. Sections were incubated with rat anti-mouse F4/80 (1:100, Abcam plc, UK) or with neutrophil Ly6G primary antibody (1:40, Hycult biotech, NL) and endogenous peroxidase activity was blocked. Secondary antibody was horseradish peroxidase (HRP)-labeled rabbit anti-rat (1:100, Dako, Glostrup, Denmark) and tertiary antibody was HRP-labeled goat anti-rabbit (1:500, Vectorlabs, Burlingame, USA) in 3% normal mouse serum, respectively. Macrophages and PMN were stained with AEC solution and tissue was counterstained with hematoxylin. Images were acquired using a BZ-9000 microscope (Keyence, Germany). Results are shown as mean number of $F4/80^+$ or $Ly6G^+$ cells of the LV tissue area (12).

Immunofluorescence Staining for Myofibroblasts

Hearts were frozen in OCT compound and cut to 6 µm longitudinal sections. Sections were thawed, fixed with 3.7% formaldehyde solution and were blocked with 10% mouse serum. Slides were treated with 0.1% Triton X-100 and incubated with primary antibody against α–smooth muscle actin (α-SMA; 1:200, rabbit IgG, ab5694, Abcam, Cambridge, UK) and discoidin domain-containing receptor 2 (DDR-2; 1:50, goat IgG, sc7555, Santa Cruz, Texas, USA) respectively for 1 hr at room temperature in PBS with 0.1% Triton-X100 and 10% mouse serum. Secondary antibody was Alexa Fluor-594 chicken-anti-rabbit IgG and Alexa Fluor-488 chicken-anti-goat IgG (Invitrogen) and nuclei were stained with DAPI. Confocal imaging was performed using a TCS SP8 confocal microscope (Leica Microsystems, Germany).

Fibroblast Isolation and Characterization

Mice subjected to I/R were sacrificed, ventricles were removed and washed in sterile HEPES-buffered Tyrode's solution (135 mM NaCl, 4 mM KCl, 0.3 mM NaH2PO4, 1 mM MgCl2, 10 mM HEPES, 2 g/l glucose, pH = 7.3, Sigma-Aldrich, St. Louis, USA). Ventricles were minced and digested in 0.1 g/l Liberase/Tyrode solution (Liberase TM research grade, Roche, Basel, Switzerland) for 10 minutes at 37°C. The supernatant was collected and the digestion step repeated 6 times. The supernatant was filtered (40 µm cell strainer, Thermo Fisher Scientific, Waltham, USA), centrifuged and the fibroblasts were resuspended in DMEM supplemented with 10% FCS. The cells were again centrifuged and further processed for immunoblotting.

For mRNA investigations, hearts were isolated from 10-12 week old WT and *Stamp2*$^{-/-}$ mice. Ventricles were cut into 1-2 mm^2 pieces and digested in a semi-automated dissociation process following manufacturer's protocol (GentleMACS Dissociator and Multi Tissue Dissociation Kit 2, Miltenyi Biotec, Bergisch-Gladbach, Germany). Cell suspension was resuspended in DMEM+ Glutamax (PAN-Biotech, Aidenbach, Germany) supported by 10% fetal calf serum (FCS), 1% Penicillin/Streptomycin and 0,1% Fibroblast Growth Factor (Recombinant Human FGF-basic (154 a.a.) Peprotech, Rocky Hill, NJ, USA). Cells were transferred to 6-well plates pre-coated with 1% gelatin at 37°C and 5% CO_2. Cells were split at 70-80% confluency. In 3rd passage, cells were harvested by adding 800µl of RNA Lysis Buffer T to each well and Stamp2 mRNA expression analyses were performed.

PMN Isolation and Characterization

PMN isolation was performed following a modified standard protocol by English and Andersen (19). In short, murine EDTA blood was taken by cardiac puncture. Blood was applied on a double layer of Histopaque 1119/1077 (Sigma Aldrich, Germany) and centrifuged at 700g for 30 min without break. Granulocytes located between Histopaque 1119 and Histopaque 1077 were carefully isolated and washed two times with HBSS. Cell number was counted. For Stamp2 expression analyses 100,000 cells were used. For NF-κB activity analyses cells were lysed in RIPA buffer. For MPO secretion analyses 100,000 cells were treated with PMA (Sigma-Aldrich, Germany) 100ng/ml or with saline for 2 hours at 37°C in HBSS. Supernatants were collected and vaporized by SpeedVac Vacuum centrifugation for 24 hours. Residues were dissolved in 100µl H_2O and MPO levels were assessed (12).

Immunoblotting

Protein extraction and immunoblotting were performed according to standard protocols (20). Briefly, membranes were incubated with the following antibodies overnight at 4°C: anti-GAPDH (1:1000; Santa Cruz), anti-p65 (1:5000; Abcam ab7970), Phospho-NF-κB p65 (Ser536) (1:1000 CellSignaling), p38 MAP kinase (CellSignaling, 1:100, New England Biolabs, Frankfurt, Germany), p-p38 MAP kinase (CellSignaling, 1:100, New England Biolabs). After incubation with appropriate secondary antibodies for 1 hour, chemiluminescence was detected using a Fusion FX (Vilber Lourmat) imaging system and quantified with Quantity One (BioRad) (20).

mRNA Expression Analyses

RNA-Isolation was performed by using the peqGOLD Total RNA Kit (VWR, Darmstadt, Germany). mRNA was converted to cDNA. Stamp2 mRNA expression was investigated by quantitative real-time PCR using the following primers: Stamp2 (NM_054098.3) -fwd: TCAAATGCGGAATACCT TGCT, -rev: GCATCTAGTGTTCCTGACTGGA; 18S ribosomal RNA (NR_003278.3) -fwd: GTAACCCGTTGAA CCCCATT, -rev: CCATCCAATCGGTAGTAGCG.

White Blood Cell Count

EDTA blood was taken by cardiac puncture from untreated WT and *Stamp2*$^{-/-}$ male mice and immediately analyzed by the 5-Part hematology-system Sysmex XN (Sysmex, Gemany).

Infarct Size Determination

Hearts were excised and the aortic arch was cannulated to perform perfusion with PBS supplemented with 50I.U. heparin/ml in a retrograde manner. Consequently, the knot that had been used for initial ligation was closed and perfusion with Evan's blue dye was performed to stain healthy tissue. Afterwards, hearts were cut into 1mm slides and incubated in 2,3,5-triphenyl-tetrazolium chloride solution. Healthy tissue was identified as blue area, area at risk as red area and infarcted tissue as white area using the BZ2-Analyser software (Keyence).

Heart Digestion and Flow Cytometry

For flow cytometry analysis, hearts were perfused *via* the left ventricular cavity with 10ml of PBS supplemented with heparin (50I.E./ml), immediately mechanically disrupted in digestion buffer (450u/ml collagenase I (Sigma Aldrich, St. Loius, MO, USA), 125u/ml collagenase XI (Sigma Aldrich), 60u/ml hyaluronidase (Sigma Aldrich) and 60u/ml DNAse I (Thermo Fisher Scientific, Waltham, MA, USA) in HBSS) and digested for 1 hour at 30°C. The single cell suspension was stained with a cocktail of antibodies including CD45, CD11b, CD64, CCR2 and TIMD4 (an antibody list including clones, fluorescent dyes and manufacturer data can be found in the supplementary material). Fluorescence minus one controls (FMO) for each marker were used to assure correct compensation. The Zombie UV fixable kit (Biolegend, San Diego, CA, USA) was used to assure cell viability. Stained cells were analyzed with a Cytek Aurora flow cytometer (Cytek, Fremont, CA, USA). Cells were gated for single, viable leukocytes. After exclusion of lymphocytes and monocytes, macrophages were identified as $CD64^+$ $CD11b^+$ cells. Timd4 was used as a marker for long-term residual macrophages, CCR2 as marker for monocyte derived macrophages (21).

Statistical Analysis

In all cases, investigators were blinded for the genotype or treatment group of the respective animals or samples. Results are expressed as mean ± SEM. Normal distribution was tested for by either Kolmogorov-Smirnov- or Shapiro-Wilk-Test. For parametric data, comparative analysis was performed using Unpaired Student's t-test or Two-way ANOVA followed by Tukey *post-hoc* test. For nonparametric data, either Mann-Whitney- or Kruskal-Wallis-test followed by Dunn's *post-hoc* test was performed. A *P*-value of < 0.05 was considered statistically significant. Graphs were created with GraphPad Prism 7.0a. All statistical calculations were carried out using GraphPad Prism 7.0a (GraphPad). $^*P < 0.05$, $^{**}P < 0.01$, $^{***}P < 0.001$.

RESULTS

Stamp2 Deficiency Further Decreases Systolic Left Ventricular Function in a Murine Model of I/R

Given the abundance of Stamp2 in leukocytes and its potential anti-inflammatory role in atherosclerosis, we investigated the effects of Stamp2 deficiency on left ventricular (LV) function in a murine model of myocardial I/R injury. Thus, *Stamp2*$^{-/-}$ and WT mice were subjected to ligation of the left anterior descending artery (LAD) for 40 minutes followed by myocardial reperfusion for up to 7 days.

In *Stamp2*$^{-/-}$ mice, echocardiographic analyses (representative recordings are shown in **Figure 1A**, full echocardiographic recordings are provided as **Supplemental Videos 1** and **2** in the supplemental material) revealed a substantially stronger reduction of LV EF as compared to WT (mean reduction in **Figure 1B** and reduction within the same animal in **Figure 1C**) Accordingly, total CO (**Figure 1D**, change of CO in **Figure 1E**) was more significantly reduced in *Stamp2*$^{-/-}$ hearts. In line with these observations, global longitudinal strain reduction was more pronounced in *Stamp2*$^{-/-}$ hearts after I/R as compared to WT (**Figure 1F**). Moreover, thinning of the left ventricular wall was significantly more pronounced in *Stamp2*$^{-/-}$ animals (**Supplemental Figures S1A, B**). Of note, baseline characterization of heart function and vital parameters under isoflurane narcosis revealed a reduced heart rate in *Stamp2*$^{-/-}$ animals (**Supplemental Figure S2**). Altogether, this data indicates a prominent role of Stamp2 in LV function after ischemic injury.

Stamp2 Deficiency Promotes Left Ventricular Fibrotic Remodeling

Post-infarct LV remodeling includes fibrotic scar formation that promotes development of HF (22). To assess the impact of Stamp2 on fibrotic remodeling, Masson's trichrome staining was performed, which revealed significantly larger areas of collagen deposition in cardiac sections of *Stamp2*$^{-/-}$ mice as compared to WT (**Figures 2A, B**).

As myofibroblasts are the major source of collagen in the infarcted myocardium (23), myofibroblast accumulation was analyzed by immunoreactivity to the fibroblast marker DDR-2 and to the myofibroblast marker α-SMA 7 days post I/R. These experiments revealed that the number of myofibroblasts was significantly elevated in the peri-infarct region of *Stamp2*$^{-/-}$ hearts as compared to WT (**Figures 2C, D**). Fibroblast-to-myofibroblast transdifferentiation in the context of inflammation is driven by activation and phosphorylation of the p38 MAPK pathway (12, 24). To test whether this process is involved in the observed phenotype, we isolated primary cardiac fibroblasts from *Stamp2*$^{-/-}$ and WT hearts. Immunoblottings of isolated primary cardiac fibroblasts after I/R

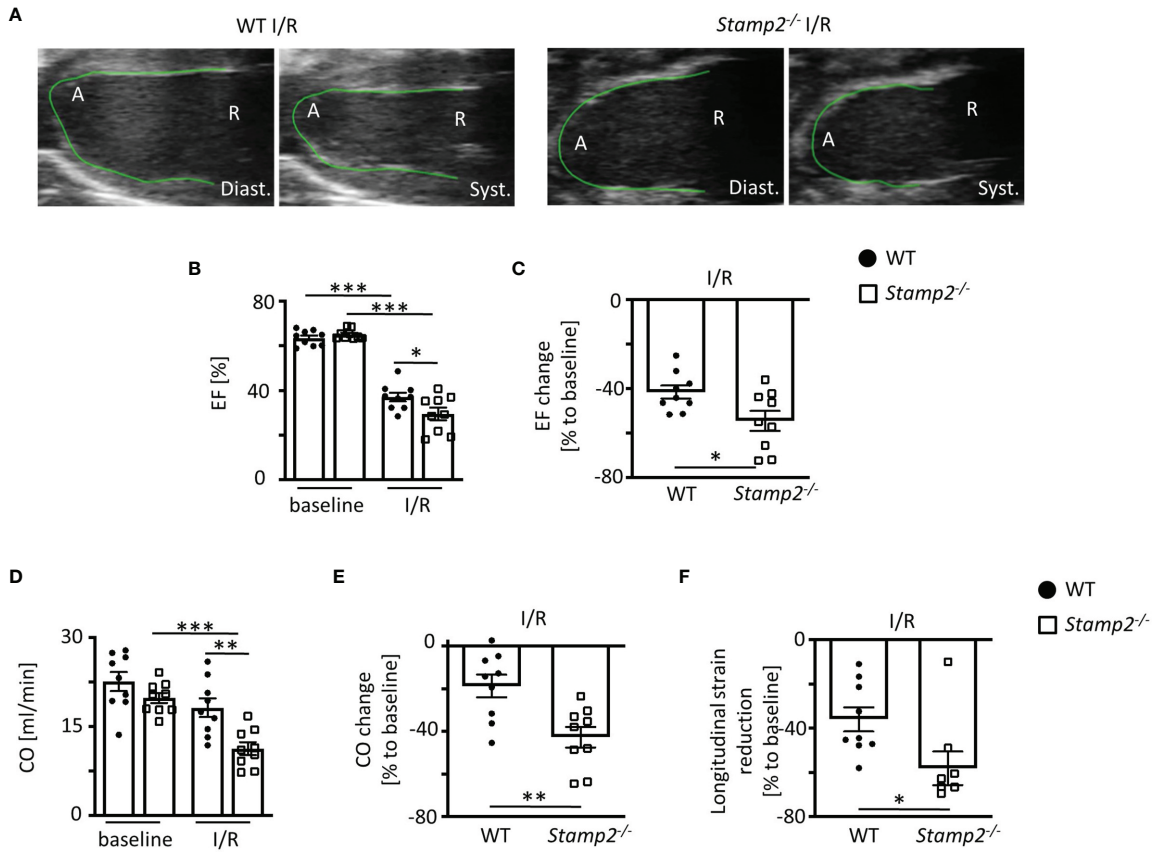

FIGURE 1 | Left ventricular (LV) function is impaired in *Stamp2*$^{-/-}$ mice when subjected to ischemia and reperfusion injury (I/R). **(A)** Representative echocardiographic recordings indicating enhanced reduction of LV function in *Stamp2*$^{-/-}$ hearts as compared to WT after 7 days of I/R (A=Apex, R= Aortic root; Diast.=diastole Syst.=systole). **(B)** Total ejection fraction (EF, n=9/9/9/9) and **(C)** change of EF in % to baseline (n=9/9). **(D)** Total cardiac output (CO, n=9/9/9/9) and **(E)** change of CO in % to baseline (n=9/9) as assessed by echocardiography. **(F)** Global longitudinal strain reduction after subjection to I/R (n=9/9). Baseline echocardiography was directly performed before MI induction and I/R echocardiography at day 7. Graphs show Mean ± SEM. Significance was determined by two-way ANOVA followed by Tukey *post-hoc* test **(B, D)** or by unpaired Student's t-test **(C, E, F)**. *P < 0.05, **P < 0.01, ***P < 0.001.

demonstrated increased p38 MAPK phosphorylation in *Stamp2*$^{-/-}$ cells as compared to WT controls (**Figure 2E**, *full unedited gel shown in* **Supplemental Figure S8**). Of note, total infarct size was unchanged in *Stamp2*$^{-/-}$ hearts (**Supplemental Figure S3**).

Stamp2 Deficiency Promotes Myocardial PMN Infiltration Upon I/R

Leukocyte activation upon myocardial I/R injury is associated with cardiac fibrotic remodeling and is the main contributor to profibrotic fibroblast-to-myofibroblast transdifferentiation (24). Apart from cytokines and growth factors, p38 MAPK signaling can be driven by PMN-derived reactive oxygen species (ROS) (12, 25). Thus, we analyzed the oxidation of dihydroethidium (DHE) in cardiac sections as an indicator for superoxide release. Fluorescence intensity of oxidized DHE was significantly elevated in *Stamp2*$^{-/-}$ *vs.* WT hearts after I/R, demonstrating increased ventricular ROS production (**Figures 3A, B**).

Given the anti-inflammatory role of Stamp2 in macrophages, we expected an increased abundance of these cells within the infarct region of *Stamp2*$^{-/-}$ mice. However, despite increased macrophage numbers upon I/R in both genotypes, numbers were not different in *Stamp2*$^{-/-}$ mice (**Figures 3C, D**). This could be further confirmed by flow cytometric analyses indicating equal numbers and proportions of macrophage populations in both genotypes 3 days after I/R induction (**Supplemental Figure S4**).

PMN are among the first ROS-producing cells invading the injured myocardium. Their inflammatory activation has been closely linked to ventricular remodeling (5). Consequently, we quantified LV PMN abundance by immunohistochemical stainings for the PMN marker Ly6G. Strikingly, PMN numbers were substantially increased in *Stamp2*$^{-/-}$ hearts *vs.* WT 3 days after I/R (**Figures 3E, F**).

Stamp2 Regulates Proinflammatory PMN Activation and Myeloperoxidase Secretion

Apart from controlling myocardial PMN infiltration in the context of I/R, Stamp2 may also directly alter cellular responses. Given that

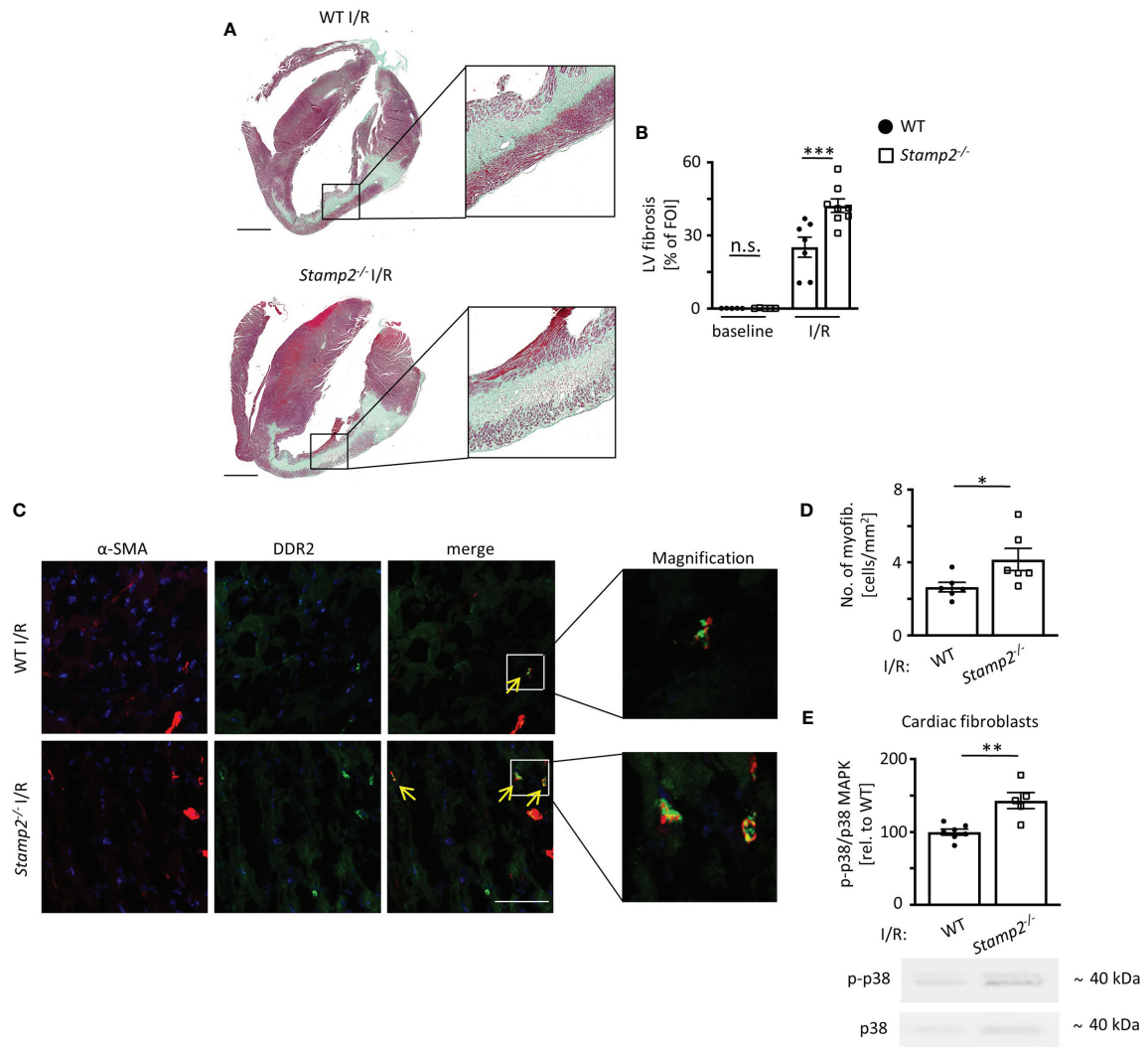

FIGURE 2 | Stamp2 deficiency aggravates I/R-induced LV fibrotic remodeling. **(A)** Representative images of Masson's trichrome-stained cardiac sections of WT and Stamp2$^{-/-}$animals 7 days after I/R. Scale bar=1mm. **(B)** Quantification of left ventricular fibrotic areas stained in green (n=5/5/7/8). **(C)** Representative immunofluorescence stainings imaged by confocal microscopy for the myofibroblast marker α-SMA (α-smooth muscle actin; red), for the fibroblast marker DDR-2 (discoidin domain-containing receptor 2; green) and for nuclei (DAPI, blue). Scale bar=50μm. **(D)** Quantitative analysis of myofibroblasts within the peri-infarct region (n=6/6). **(E)** Relative phosphorylation of p38 MAPK (p-p38/p38 MAPK) in isolated primary fibroblasts from hearts 3 days post I/R (n=7/5). Graphs show Mean ± SEM. Full blots are shown in **Supplemental Figure S4**. Significance was determined by two-way ANOVA followed by Tukey *post-hoc* test **(B)** or by unpaired Student's t-test **(D, E)**. *P < 0.05, **P < 0.01, ***P < 0.001. n.s., not significant.

Stamp2 is abundantly expressed in murine PMN (**Supplemental Figures S5, S6**), Stamp2-mediated PMN activation might be closely associated with myocardial infarction, subsequent post-infarct remodeling and scar formation (8, 26). To characterize cellular responses to Stamp2 deficiency, we isolated primary PMN from *Stamp2*$^{-/-}$ and WT mice. Stamp2 deficiency led to pronounced NF-κB activity in isolated PMN as demonstrated by enhanced phosphorylation of its subunit RelA (p65) (**Figure 4A**), which is closely associated with enhanced immune responses, leukocyte activation and cytokine secretion (27). Enhanced proinflammatory activation could be further confirmed *ex vivo* showing that Stamp2 deficiency elevated MPO secretion from primary isolated PMN, which reflects pro-inflammatory granule release (28) (**Figure 4B**, *full unedited gel shown in* **Supplemental Figure S9**).

Plasma levels of PMN-derived MPO were elevated in *Stamp2*$^{-/-}$ animals both at baseline conditions and after subjection to I/R (**Figure 4C**). To rule out pre-existing leukocytosis in *Stamp2*$^{-/-}$ animals, blood counts were analyzed. These demonstrated equal leukocyte numbers (white blood cell count, WBC, **Supplemental Figure S7**) in both genotypes indicating that enhanced myocardial PMN infiltration and systemic MPO levels after I/R were due to enhanced PMN activation.

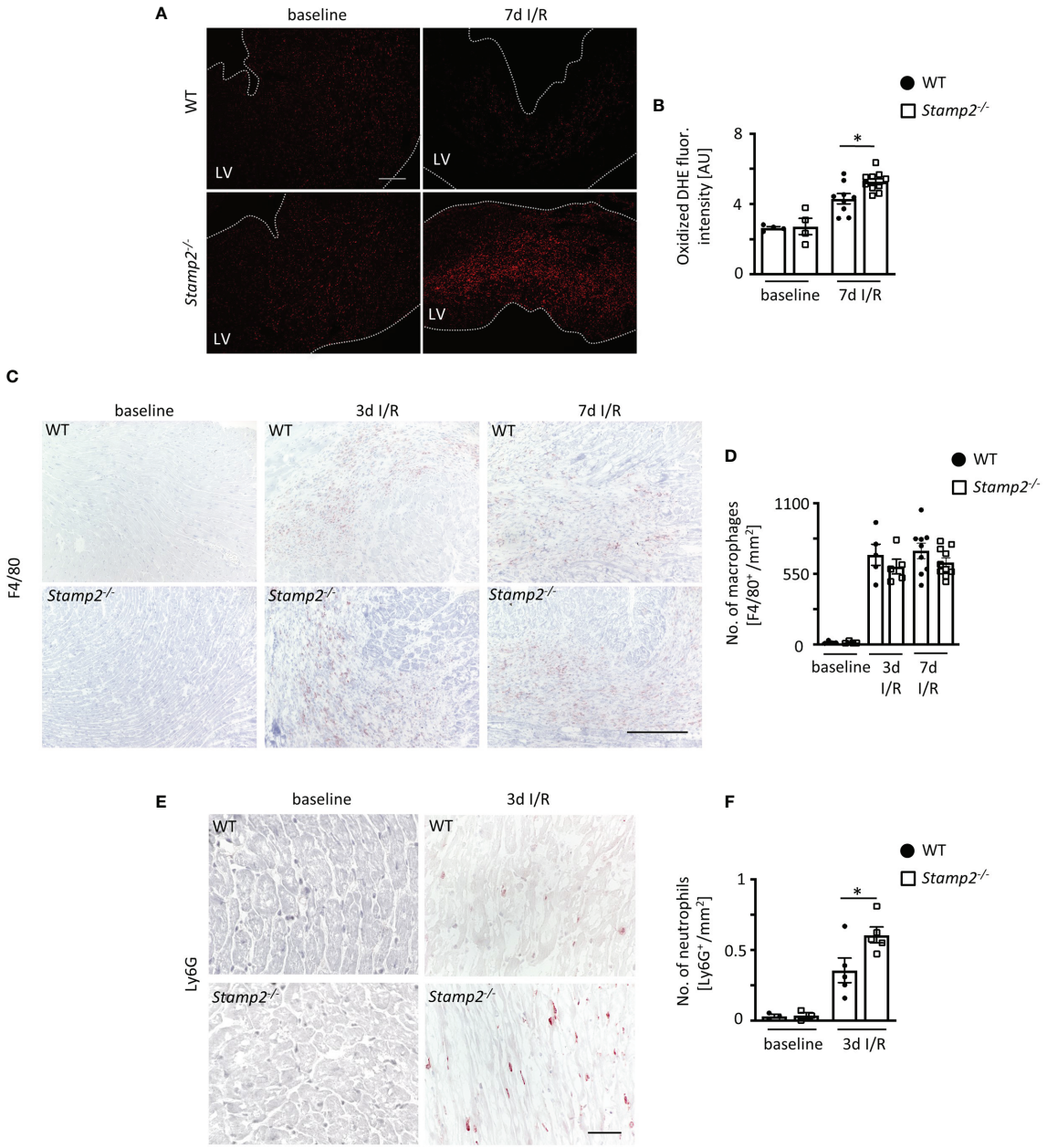

FIGURE 3 | Stamp2 regulates myocardial PMN infiltration after I/R. **(A)** Representative stainings of oxidized dihydroethidium (DHE) and **(B)** quantitative analysis of ROS production in myocardial sections 7 days after I/R induction (n=4/4/7/8). Scale bar=200 μm. **(C)** Representative left ventricular immunohistological stainings for the pan-macrophage marker F4/80 (brown) and **(D)** quantitative analysis of macrophage numbers within the infarct region (n=4/4/5/5/9/10). Scale bar= 200 μm. **(E)** Representative left ventricular immunohistological stainings for the PMN marker Ly6G (brown) and **(F)** quantitative analysis of neutrophil numbers within the infarct region 3 days after I/R induction (n=3/3/5/5). Scale bar = 50 μm. Graphs show Mean ± SEM. Significance was determined by two-way ANOVA followed by Tukey *post-hoc* test. *P < 0.05.

PMN Depletion Abolishes the Effect of Stamp2 Deficiency on I/R-Mediated Fibrotic Remodeling and LV Function

To investigate whether the impairment of LV function by Stamp2 deficiency is causally linked to enhanced PMN activation and infiltration, WT- and *Stamp2*$^{-/-}$ mice were subjected to Ly6G antibody-mediated PMN depletion (injection schematic is shown in **Figure 5A**) (8). Intriguingly, PMN depletion completely reversed the maladaptive phenotype of Stamp2 deficiency after I/R. This included attenuated LV fibrotic remodeling (**Figures 5B, C**) and LV function. In detail, the *Stamp2*$^{-/-}$mediated alterations in total EF (**Figure 5E**;

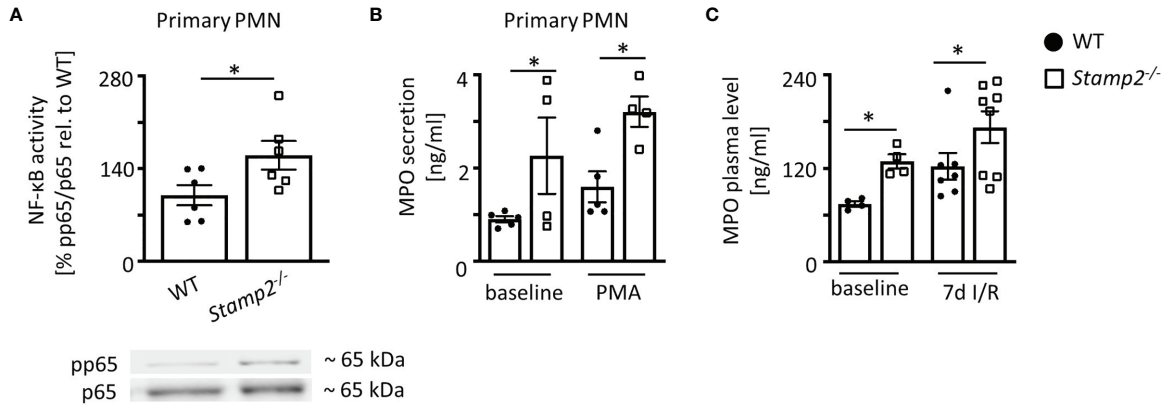

FIGURE 4 | Proinflammmatory activation of PMN by Stamp2 deficiency. **(A)** Immmunoblotting of p65-phosphorylation (pp65) *vs.* total p65 expresssion as an indicator of NF-κB activity (n=6/6). **(B)** Myeloperoxidase (MPO) secretion into the supernatant of isolated PMN as assessed by ELISA with and without inflammatory stimulation (PMA 100ng/ml; n=5/4/5/4). **(C)** MPO plasma levels in mice at baseline and subjected to 7 days of I/R as assessed by ELISA (n=4/4/7/8). Graphs show Mean ± SEM. Full blots are shown in **Supplemental Figure S5**. Significance was determined by two-way ANOVA followed by Tukey *post-hoc* test **(B, C)** or by unpaired Student's t-test **(A)**. *P < 0.05.

representative recordings are shown in **Figure 5D**, full echocardiographic recordings are provided as **Supplemental Videos 3** and **4** in the supplemental material), mean EF reduction (**Figure 5F**) as well as total CO (**Figure 5G**), mean CO reduction (**Figure 5H**) and global longitudinal strain reduction (**Figure 5I**) were blunted upon PMN depletion.

Taken together, we herein demonstrate that Stamp2 deficiency leads to enhanced inflammatory PMN activation upon I/R injury resulting in pronounced fibroblast-to-myofibroblast transdifferentiation. These cellular alterations promote maladaptive fibrotic remodeling, ultimately resulting in the loss of LV function (**Figure 6**). These data put Stamp2 in a central position controlling PMN functions to protect from adverse LV remodeling after I/R injury.

DISCUSSION

Herein, we show that Stamp2 deficiency promotes adverse LV structural remodeling after myocardial I/R injury by elevating proinflammatory PMN activation. Studies of a murine model of myocardial I/R injury reveal that loss of Stamp2 enhances (i) inflammatory activation of PMN in mice subjected to I/R damage resulting in (ii) enhanced ventricular fibrosis by transdifferentiation of fibroblasts to myofibroblasts ultimately causing (iii) reduced LV function.

The inflammatory activation of leukocytes, in particular neutrophils, has long been regarded as a crucial mechanistic component to myocardial I/R damage (29, 30). Although the underlying mechanisms are diverse and still not completely understood (31), clinical trials targeting pro-inflammatory pathways (COLCOT, LoDoCo, CANTOS) (32–34), emphasize the clinical need and the feasibility to target and modulate innate immune responses to prevent myocardial damage.

Stamp2 has emerged as an anti-inflammatory regulator of the innate immunity by suppressing inflammatory cytokine expression (13). Furthermore, endothelial expression of leukocyte-recruiting cell surface proteins like ICAM-1 und VCAM-1 is enhanced in Stamp2 deficiency (35), a mechanism which has been closely linked to myocardial infarct healing und -function (25). In particular, the role of macrophage activation in the context of Stamp2 deficiency was reported in various pathologies like atherosclerosis (14), pulmonary hypertension (15), adipose tissue insulin resistance (36) and prostate cancer (37). Hitherto, a role of Stamp2 in PMN activation in cardiovascular disease was unknown. We show for the first time, that Stamp2 is a regulator of PMN infiltration and myocardial healing after I/R injury by modulating NF-κB activation. So far, this mechanism has been described only in atherosclerotic macrophages due to Stamp2´s NADPH-oxidizing properties (14, 37) although NF-κB regulation differs between PMN and mononuclear cells (38).

Stamp2 deficiency induces PMN degranulation and secretion of MPO, a pro-inflammatory heme enzyme which is the most abundant protein in granules of PMN (28) and responsible for maladaptive ventricular remodeling after I/R injury (12). The molecular mechanisms of Stamp2 in regulating PMN degranulation remain elusive although it is tempting to speculate that, given the importance of NADPH-oxidases in PMN priming and degranulation (39), Stamp2-mediated oxidation of NADPH might be the driving factor (14). Of note, enhanced MPO secretion could be detected not only in unstimulated isolated PMN but also in untreated *Stamp2*$^{-/-}$ animals, indicating enhanced PMN activation even under baseline conditions.

Ventricular fibroblast activation and fibrotic remodeling are significantly pronounced in *Stamp2*$^{-/-}$ animals finally resulting in severe impairment of LV function. Myofibroblasts are the main cellular contributors to ventricular fibrosis (22). In *Stamp2*$^{-/-}$

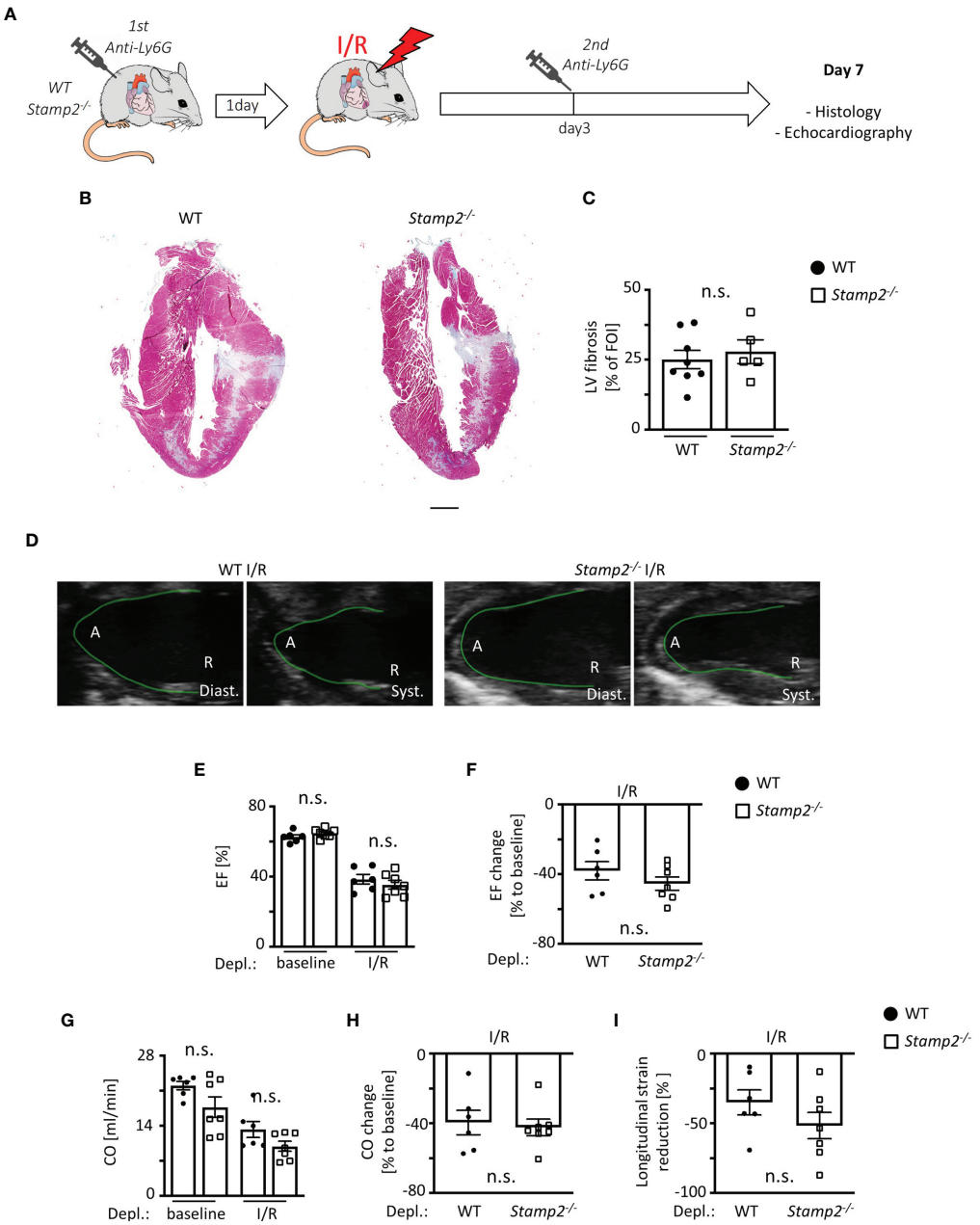

FIGURE 5 | PMN depletion rescues impaired LV function in *Stamp2*$^{-/-}$ mice after I/R. **(A)** Schematic overview of PMN depletion by i.p. injection of an anti-Ly6G antibody 1 day prior to- and 3 days after subjection to I/R (13). **(B)** Representative images of Masson's trichrome-stained cardiac sections of WT- and *Stamp2*$^{-/-}$ animals 7 days after I/R with **(C)** assessment of the LV fibrotic areas stained in green/grey (n=8/5). Scale bar=1mm **(D)** Representative echocardiographic recordings of WT- and *Stamp2*$^{-/-}$ hearts (A=Apex, R=Aortic root; Diast.=diastole, Syst.=systole). **(E)** Total ejection fraction (EF, n=6/7/6/7) and **(F)** change of EF in % to baseline (n=6/7). **(G)** Total cardiac output (CO, n=6/7/6/7) and **(H)** change of CO in % to baseline as assessed by echocardiography (n=6/7). **(I)** Longitudinal strain reduction after subjection to I/R (n=6/7). Baseline echocardiography was directly performed before MI induction and I/R echocardiography at day 7. Graphs show Mean ± SEM. Significance was determined by two-way ANOVA followed by Tukey *post-hoc* test **(E, G)** or by unpaired Student's t-test **(C, F, H, I)**. n.s., not significant.

animals, MPO plasma levels are significantly higher upon myocardial injury. We have shown previously that the major MPO-derived species hypochlorous acid (HOCl) (40) leads to activation of p38 MAPK that in turn promotes fibroblast transdifferentiation and results in enhanced ventricular fibrotic remodeling (11). The importance of these fibrotic mechanisms for heart function is further underlined by the unaltered infarct size in *Stamp2*$^{-/-}$ animals upon I/R injury.

As this study was performed in a small animal model, a number of limitations may apply when translating the present

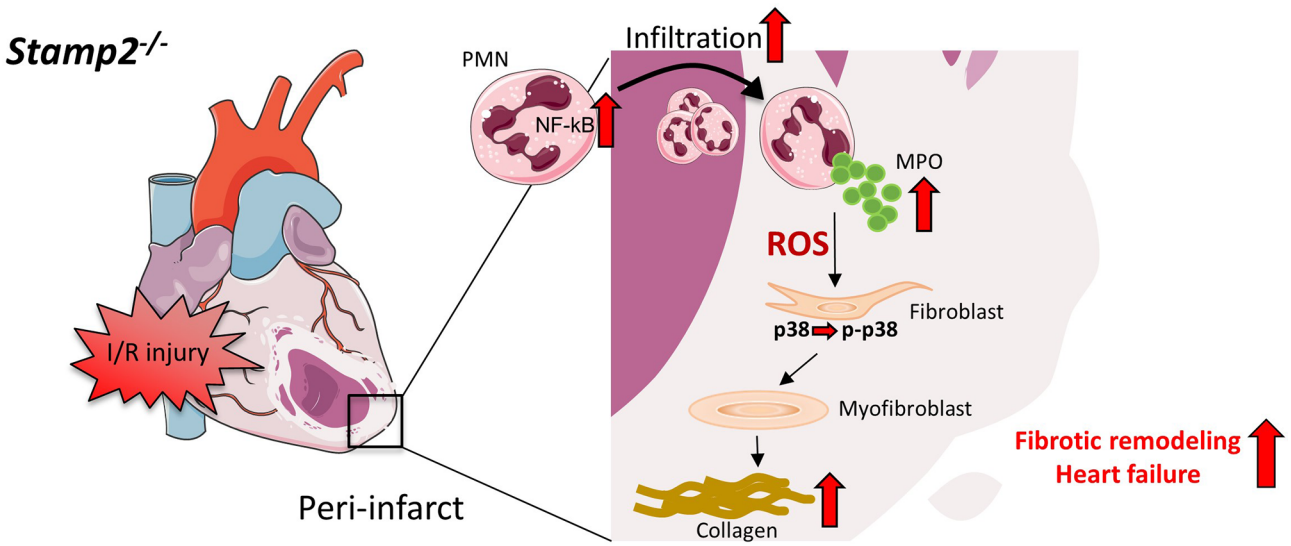

FIGURE 6 | Schematic overview of PMN activation and fibrotic remodeling in *Stamp2*$^{-/-}$ mice after I/R. Stamp2 deficiency results in NmRal-mediated proinflammatory NF-κB activation (11, 15) which subsequently induces enchanced myocardial PMN infiltration after I/R injury. PMN degranulation and MPO secretion are elevated in *Stamp2*$^{-/-}$ PMN, thereby activating the p38-MAPK pathway and inducing fibroblast-to-myofibroblast transdifferentiation. In turn, enchanced collagen deposition promotes maladaptive structural remodeling finally leading to loss of LV function. PMN: polymorphonuclear neutrophils, Stamp2: six transmembrane protein of prostate 2, NF-κB: nuclear factor 'kappa-light-chain-enchancer' of activated B-cells, NmRal: NmrA-like family domain- containing protein 1, MPO: myeloperoxidase, p-p38/p38: phosphor/ p38 MAP kinase. Figures were produced using Servier Medical Art (http://www.servier.com/).

findings to human pathology. Given the mechanistic complexity of involved cell types, inflammatory stimuli, growth factors, cell death- and hypertrophic signaling pathways in myocardial post-infarct healing, it has to be considered that PMN may not be the exclusive cellular mediators by which Stamp2 deficiency promotes fibrotic remodeling. Macrophages are important for structural remodeling post infarction (41) and it cannot be ruled out that Stamp2 influences macrophage activation in this regard (14). However, RNA-seq data revealed low Stamp2 expression in macrophages as compared to PMN at baseline levels and after myocardial infarction (7). Furthermore, infiltrating macrophage numbers and populations did not differ between WT- and *Stamp2*$^{-/-}$ hearts after I/R injury indicating a minor role of Stamp2 in macrophages in infarct healing.

Stamp2-mediated endogenous effects on fibroblasts could not be fully disclosed since Stamp2 mRNA is expressed in activated cardiac myofibroblasts. Nonetheless, in comparison, isolated cardiac fibroblasts showed lower Stamp2 expression than primary PMN. Accordingly, specific PMN depletion by Ly6G antibody injection, a well-established method for studying PMN in myocardial pathologies (8), completely reversed *Stamp2*$^{-/-}$ mediated functional LV impairment and enhanced fibrosis, underlining the prominent role of PMN for the observed phenotype in Stamp2 deficiency.

The reduction in heart rate in *Stamp2*$^{-/-}$ animals compared to WT animals at baseline conditions might furthermore suggest an unknown effect of Stamp 2 on the cardiac conduction system and demands further investigation.

Stamp2 expression has been inversely correlated with the pathological severity of atherosclerosis (14), pulmonary hypertension (15) and obesity (36). In view of a clinical translation, the assessment of Stamp2 expression in PMN might therefore emerge as a marker for clinical outcome in patients after myocardial infarction. Furthermore, anti-inflammatory effects of pharmacological Stamp2 activation or augmented expression may be beneficial as novel therapeutic strategies. Such an effect has been recently reported for the AMP-activated protein kinase (AMPK) activator cilostazol in nonalcoholic fatty liver disease (42). Moreover, in a setting of acute myocardial injury for 2 hours, treatment with the biguanide metformin reduced cardiomyocyte apoptosis in a Stamp2-dependent manner (43). The development of more specific compounds for pharmacological Stamp2 regulation in cardiovascular diseases is therefore an interesting goal for future studies.

In conclusion, the current data reveal that absence of Stamp2 adversely affects myocardial function after I/R injury. Mechanistically, deficiency of Stamp2 induces pro-inflammatory activation and degranulation of PMN which subsequently leads to enhanced LV fibrotic remodeling *via* activation of fibroblast-to-myofibroblast transdifferentiation (**Figure 6**). These results not only indicate that Stamp2 is a novel regulator of the inflammatory response in ischemic cardiomyopathy but also point to Stamp2 activation as a potential pharmacological target.

DATA AVAILABILITY STATEMENT

The original contributions presented in the study are included in the article/**Supplementary Material**. Further inquiries can be directed to the corresponding authors.

ETHICS STATEMENT

All animal studies were approved by the local Animal Care and Use Committees (Ministry for Environment, Agriculture, Conservation and Consumer Protection of the State of North Rhine-Westphalia: State Agency for Nature, Environment and Consumer Protection (LANUV), NRW, Germany) and follow ARRIVE (Animal Research: Reporting of In Vivo Experiments) guidelines.

AUTHOR CONTRIBUTIONS

The author contributions are as follows: MMo, SeB, MA, and HF designed the project, performed experiments and statistical analysis and prepared the manuscript. AK, TM, SSt, WS, EB, MV, SR, DM, SiB, SG, FN, AH, SSi and HW performed experiments and provided suggestions on the project. VR and StB provided substantial suggestions on the project and critically revised the manuscript. SeB and HF supervised the project. MT, MMa, JK and VP substantially performed revision experiments. SG substantially performed revision experiments and wrote the revised manuscript. MM supervised the project and wrote the manuscript. All authors contributed to the article and approved the submitted version.

FUNDING

This work was funded by the Deutsche Forschungsgemeinschaft DFG (RU 16783-3 and 360043781 - GRK 2407 to VR, 360043781 - GRK 2407 to SB, MO 3438/2-1 to MM and Grant. No. 397484323 - TRR259 to SB, HW and MA) and the Center for Molecular Medicine Cologne funding (Baldus B-02). HF was funded by the Köln Fortune Program of the University of Cologne (254/2014, 240/2017), and by the German Foundation of Heart Research (F/45/15, F37/17).

ACKNOWLEDGMENTS

We thank Lisa Remane, Christina Kerkenpaß and Simon Grimm for expert technical assistance. We thank the CECAD Imaging Facility and especially Dr. Astrid Schauss and Peter Zentis for their support in microscopy and image analysis.

SUPPLEMENTARY MATERIAL

The Supplementary Material for this article can be found online at: https://www.frontiersin.org/articles/10.3389/fimmu.2021.701721/full#supplementary-material

REFERENCES

1. McManus DD, Gore J, Yarzebski J, Spencer F, Lessard D, Goldberg RJ. Recent Trends in the Incidence, Treatment, and Outcomes of Patients With STEMI and NSTEMI. *Am J Med* (2011) 124:40–7. doi: 10.1016/j.amjmed.2010.07.023
2. Reed GW, Rossi JE, Cannon CP. Acute Myocardial Infarction. *Lancet (London England)* (2017) 389:197–210. doi: 10.1016/S0140-6736(16)30677-8
3. Suthahar N, Meijers WC, Silljé HHW, de Boer RA. From Inflammation to Fibrosis—Molecular and Cellular Mechanisms of Myocardial Tissue Remodelling and Perspectives on Differential Treatment Opportunities. *Curr Heart Fail Rep* (2017) 14:235–50. doi: 10.1007/s11897-017-0343-y
4. Ponikowski P, Anker SD, AlHabib KF, Cowie MR, Force TL, Hu S, et al. Heart Failure: Preventing Disease and Death Worldwide. *ESC Hear Fail* (2014) 1:4–25. doi: 10.1002/ehf2.12005
5. Puhl S-L, Steffens S. Neutrophils in Post-Myocardial Infarction Inflammation: Damage *vs*. Resolution? *Front Cardiovasc Med* (2019) 6:25. doi: 10.3389/fcvm.2019.00025
6. Swirski FK, Nahrendorf M. Leukocyte Behavior in Atherosclerosis, Myocardial Infarction, and Heart Failure. *Science* (2013) 339:161–6. doi: 10.1126/science.1230719
7. Vafadarnejad E, Rizzo G, Krampert L, Arampatzi P, Arias-Loza A-P, Nazzal Y, et al. Dynamics of Cardiac Neutrophil Diversity in Murine Myocardial Infarction. *Circ Res* (2020) 127:e232–e249. doi: 10.1161/CIRCRESAHA.120.317200
8. Horckmans M, Ring L, Duchene J, Santovito D, Schloss MJ, Drechsler M, et al. Neutrophils Orchestrate Post-Myocardial Infarction Healing by Polarizing Macrophages Towards a Reparative Phenotype. *Eur Heart J* (2016) 241:ehw002. doi: 10.1093/eurheartj/ehw002
9. Ali M, Pulli B, Courties G, Tricot B, Sebas M, Iwamoto Y, et al. Myeloperoxidase Inhibition Improves Ventricular Function and Remodeling After Experimental Myocardial Infarction. *JACC Basic to Transl Sci* (2016) 1:633–43. doi: 10.1016/j.jacbts.2016.09.004
10. Humeres C, Frangogiannis NG. Fibroblasts in the Infarcted, Remodeling, and Failing Heart. *JACC Basic to Transl Sci* (2019) 4:449–67. doi: 10.1016/j.jacbts.2019.02.006
11. Midwinter RG, Vissers MC, Winterbourn CC. Hypochlorous Acid Stimulation of the Mitogen-Activated Protein Kinase Pathway Enhances Cell Survival. *Arch Biochem Biophys* (2001) 394:13–20. doi: 10.1006/abbi.2001.2530
12. Mollenhauer M, Friedrichs K, Lange M, Gesenberg J, Remane L, Kerkenpaß C, et al. Myeloperoxidase Mediates Postischemic Arrhythmogenic Ventricular Remodeling. *Circ Res* (2017) 121(1):56–70. doi: 10.1161/CIRCRESAHA.117.310870
13. Wellen KE, Fucho R, Gregor MF, Furuhashi M, Morgan C, Lindstad T, et al. Coordinated Regulation of Nutrient and Inflammatory Responses by STAMP2 Is Essential for Metabolic Homeostasis. *Cell* (2007) 129:537–48. doi: 10.1016/J.CELL.2007.02.049
14. ten Freyhaus H, Calay ES, Yalcin A, Vallerie SN, Yang L, Calay ZZ, et al. Stamp2 Controls Macrophage Inflammation Through Nicotinamide Adenine Dinucleotide Phosphate Homeostasis and Protects Against Atherosclerosis. *Cell Metab* (2012) 16:81–9. doi: 10.1016/j.cmet.2012.05.009
15. Batool M, Berghausen EM, Zierden M, Vantler M, Schermuly RT, Baldus S, et al. The Six-Transmembrane Protein Stamp2 Ameliorates Pulmonary Vascular Remodeling and Pulmonary Hypertension in Mice. *Basic Res Cardiol* (2020) 115:68. doi: 10.1007/s00395-020-00826-8
16. Ohgami RS, Campagna DR, McDonald A, Fleming MD. The Steap Proteins Are Metalloreductases. *Blood* (2006) 108:1388–94. doi: 10.1182/blood-2006-02-003681
17. Carrier L, Schlossarek S, Willis MS, Eschenhagen T. The Ubiquitin-Proteasome System and Nonsense-Mediated mRNA Decay in Hypertrophic Cardiomyopathy. *Cardiovasc Res* (2010) 85:330–8. doi: 10.1093/cvr/cvp247
18. Kanno S, Lerner DL, Schuessler RB, Betsuyaku T, Yamada KA, Saffitz JE, et al. Echocardiographic Evaluation of Ventricular Remodeling in a Mouse Model of Myocardial Infarction. *J Am Soc Echocardiogr* (2002) 15:601–9. doi: 10.1067/mje.2002.117560
19. English D, Andersen BR. Single-Step Separation of Red Blood Cells, Granulocytes and Mononuclear Leukocytes on Discontinuous Density Gradients of Ficoll-Hypaque. *J Immunol Methods* (1974) 5:249–52. doi: 10.1016/0022-1759(74)90109-4
20. Vettel C, Lindner M, Dewenter M, Lorenz K, Schanbacher C, Riedel M, et al. Phosphodiesterase 2 Protects Against Catecholamine-Induced Arrhythmia and Preserves Contractile Function After Myocardial Infarction. *Circ Res* (2017) 120:120–32. doi: 10.1161/CIRCRESAHA.116.310069

21. Dick SA, Macklin JA, Nejat S, Momen A, Clemente-Casares X, Althagafi MG, et al. Self-Renewing Resident Cardiac Macrophages Limit Adverse Remodeling Following Myocardial Infarction. *Nat Immunol* (2019) 20:29–39. doi: 10.1038/s41590-018-0272-2
22. Travers JG, Kamal FA, Robbins J, Yutzey KE, Blaxall BC. Cardiac Fibrosis: The Fibroblast Awakens. *Circ Res* (2016) 118:1021–40. doi: 10.1161/CIRCRESAHA.115.306565
23. van den Borne SWM, Diez J, Blankesteijn WM, Verjans J, Hofstra L, Narula J. Myocardial Remodeling After Infarction: The Role of Myofibroblasts. *Nat Rev Cardiol* (2010) 7:30–7. doi: 10.1038/nrcardio.2009.199
24. Turner NA, Blythe NM. Cardiac Fibroblast P38 MAPK: A Critical Regulator of Myocardial Remodeling. *J Cardiovasc Dev Dis* (2019) 6(3):27. doi: 10.3390/jcdd6030027
25. Prabhu SD, Frangogiannis NG. The Biological Basis for Cardiac Repair After Myocardial Infarction: From Inflammation to Fibrosis. *Circ Res* (2016) 119:91–112. doi: 10.1161/CIRCRESAHA.116.303577
26. Ma Y, Yabluchanskiy A, Iyer RP, Cannon PL, Flynn ER, Jung M, et al. Temporal Neutrophil Polarization Following Myocardial Infarction. *Cardiovasc Res* (2016) 110:51–61. doi: 10.1093/cvr/cvw024
27. Liu T, Zhang L, Joo D, Sun S-C. Nf-κb Signaling in Inflammation. *Signal Transduct Target Ther* (2017) 2:17023. doi: 10.1038/sigtrans.2017.23
28. Odobasic D, Kitching AR, Holdsworth SR. Neutrophil-Mediated Regulation of Innate and Adaptive Immunity: The Role of Myeloperoxidase. *J Immunol Res* (2016) 2016:2349817. doi: 10.1155/2016/2349817
29. Baxter GF. The Neutrophil as a Mediator of Myocardial Ischemia-Reperfusion Injury: Time to Move on. *Basic Res Cardiol* (2002) 97:268–75. doi: 10.1007/s00395-002-0366-7
30. Vinten-Johansen J. Involvement of Neutrophils in the Pathogenesis of Lethal Myocardial Reperfusion Injury. *Cardiovasc Res* (2004) 61:481–97. doi: 10.1016/j.cardiores.2003.10.011
31. Eltzschig HK, Eckle T. Ischemia and Reperfusion–From Mechanism to Translation. *Nat Med* (2011) 17:1391–401. doi: 10.1038/nm.2507
32. Bouabdallaoui N, Tardif J-C, Waters DD, Pinto FJ, Maggioni AP, Diaz R, et al. Time-to-Treatment Initiation of Colchicine and Cardiovascular Outcomes After Myocardial Infarction in the Colchicine Cardiovascular Outcomes Trial (COLCOT). *Eur Heart J* (2020) 41(42):4092–9. doi: 10.1093/eurheartj/ehaa659
33. Tardif J-C, Kouz S, Waters DD, Bertrand OF, Diaz R, Maggioni AP, et al. Efficacy and Safety of Low-Dose Colchicine After Myocardial Infarction. *N Engl J Med* (2019) 381:2497–505. doi: 10.1056/NEJMoa1912388
34. Ridker PM, Everett BM, Thuren T, MacFadyen JG, Chang WH, Ballantyne C, et al. Antiinflammatory Therapy With Canakinumab for Atherosclerotic Disease. *N Engl J Med* (2017) 377:1119–31. doi: 10.1056/NEJMoa1707914
35. Wang F, Han L, Qin R, Zhang Y, Wang D, Wang Z-H, et al. Overexpressing STAMP2 Attenuates Adipose Tissue Angiogenesis and Insulin Resistance in Diabetic Apoe $^{-/-}$ /LDLR $^{-/-}$ Mouse. *via PPARγ/CD36 pathway. J Cell Mol Med* (2017) 21:3298–308. doi: 10.1111/jcmm.13233
36. Han L, Tang M-X, Ti Y, Wang Z-H, Wang J, Ding W-Y, et al. Overexpressing STAMP2 Improves Insulin Resistance in Diabetic Apoe–/–/LDLR–/– Mice *via* Macrophage Polarization Shift in Adipose Tissues. *PloS One* (2013) 8:e78903. doi: 10.1371/journal.pone.0078903
37. Jin Y, Wang L, Qu S, Sheng X, Kristian A, Mælandsmo GM, et al. STAMP 2 Increases Oxidative Stress and is Critical for Prostate Cancer. *EMBO Mol Med* (2015) 7:315–31. doi: 10.15252/emmm.201404181
38. Castro-Alcaraz S, Miskolci V, Kalasapudi B, Davidson D, Vancurova I. NF-Kappa B Regulation in Human Neutrophils by Nuclear I Kappa B Alpha: Correlation to Apoptosis. *J Immunol* (2002) 169:3947–53. doi: 10.4049/jimmunol.169.7.3947
39. Lacy P. Mechanisms of Degranulation in Neutrophils. *Allergy Asthma Clin Immunol* (2006) 2:98–108. doi: 10.1186/1710-1492-2-3-98
40. Davies MJ. Myeloperoxidase-Derived Oxidation: Mechanisms of Biological Damage and Its Prevention. *J Clin Biochem Nutr* (2011) 48:8–19. doi: 10.3164/jcbn.11-006FR
41. O'Rourke SA, Dunne A, Monaghan MG. The Role of Macrophages in the Infarcted Myocardium: Orchestrators of ECM Remodeling. *Front Cardiovasc Med* (2019) 6:101. doi: 10.3389/fcvm.2019.00101
42. Oh YJ, Kim HY, Lee MH, Suh SH, Choi Y, Nam T, et al. Cilostazol Improves HFD-Induced Hepatic Steatosis by Upregulating Hepatic STAMP2 Expression Through AMPK. *Mol Pharmacol* (2018) 94:1401–11. doi: 10.1124/mol.118.113217
43. Luo T, Zeng X, Yang W, Zhang Y. Treatment With Metformin Prevents Myocardial Ischemia-Reperfusion Injury *via* STEAP4 Signaling Pathway. *Anatol J Cardiol* (2019) 21:261–71. doi: 10.14744/AnatolJCardiol.2019.11456

Conflict of Interest: The authors declare that the research was conducted in the absence of any commercial or financial relationships that could be construed as a potential conflict of interest.

frontiers in Immunology

REVIEW
published: 23 December 2021
doi: 10.3389/fimmu.2021.782495

Antimicrobial Activity of Neutrophils Against Mycobacteria

Heather A. Parker, Lorna Forrester, Christopher D. Kaldor, Nina Dickerhof and Mark B. Hampton *

Centre for Free Radical Research, Department of Pathology and Biomedical Science, University of Otago, Christchurch, New Zealand

The mycobacterium genus contains a broad range of species, including the human pathogens *M. tuberculosis* and *M. leprae*. These bacteria are best known for their residence inside host cells. Neutrophils are frequently observed at sites of mycobacterial infection, but their role in clearance is not well understood. In this review, we discuss how neutrophils attempt to control mycobacterial infections, either through the ingestion of bacteria into intracellular phagosomes, or the release of neutrophil extracellular traps (NETs). Despite their powerful antimicrobial activity, including the production of reactive oxidants such as hypochlorous acid, neutrophils appear ineffective in killing pathogenic mycobacteria. We explore mycobacterial resistance mechanisms, and how thwarting neutrophil action exacerbates disease pathology. A better understanding of how mycobacteria protect themselves from neutrophils will aid the development of novel strategies that facilitate bacterial clearance and limit host tissue damage.

Keywords: phagosomes, neutrophil extracellular traps, oxidative stress, tuberculosis, leprosy

OPEN ACCESS

Edited by:
Clare Hawkins, University of Copenhagen, Denmark

Reviewed by:
William Michael Nauseef, The University of Iowa, United States
Nathalie Winter, Institut National de recherche pour l'agriculture, l'alimentation et l'environnement (INRAE), France

***Correspondence:**
Mark B. Hampton
mark.hampton@otago.ac.nz

Specialty section:
This article was submitted to Molecular Innate Immunity, a section of the journal Frontiers in Immunology

Received: *24 September 2021*
Accepted: *06 December 2021*
Published: *23 December 2021*

Citation:
Parker HA, Forrester L, Kaldor CD, Dickerhof N and Hampton MB (2021) Antimicrobial Activity of Neutrophils Against Mycobacteria. Front. Immunol. 12:782495. doi: 10.3389/fimmu.2021.782495

INTRODUCTION

Mycobacterium is a diverse genus comprising almost 200 species (1). The most well-known members are the human pathogens *Mycobacterium tuberculosis* and *Mycobacterium leprae*, which are the causative agents of tuberculosis and leprosy, respectively. Tuberculosis is a pulmonary disease that has plagued humans for thousands of years, and while global prevalence was reduced in the early 20th century due to the development of vaccines and antibiotics, the incidence has increased again such that it is estimated that a quarter of the world's population is currently infected with *M. tuberculosis* with more than 4,000 deaths per day (2). The prevalence of leprosy is still of significant concern in endemic areas (3), and while curable the age-old stigma associated with leprosy still persists, creating fear and a reluctance to seek medical help. The mycobacterium genus also contains obligate and opportunistic pathogenic mycobacteria, which are grouped together as non-tuberculous mycobacteria (NTM). The incidence of NTM infection is increasing, such that in the USA the prevalence of pulmonary disease due to NTM is now greater than that of tuberculosis (4). The appearance of multi-drug resistant mycobacteria is of major concern, and new treatments are urgently required.

Mycobacteria can be remarkably successful intracellular pathogens that not only survive the initial assault of the innate immune system, but eventually take up residence within macrophages

(5, 6). Neutrophils are also prominent in the lungs of patients with active pulmonary tuberculosis (7). They migrate to sites of infection in response to chemotactic signals, where they ingest pathogens into intracellular phagosomes (**Figure 1**). Neutrophil cytoplasmic granules fuse with the phagosomal membrane and empty antimicrobial peptides and proteins onto the pathogen, in a process termed degranulation. At the same time, an NADPH oxidase (NOX) complex assembles on the phagosomal membrane, transferring electrons from cytosolic NADPH to molecular oxygen in the phagosome. The initial product is superoxide, which dismutates to hydrogen peroxide and is converted to the potent bactericidal oxidant hypochlorous acid (HOCl) by another granule constituent, myeloperoxidase (MPO) (8). Pathogens that survive the initial oxidative burst may take up residence inside neutrophils. However, the neutrophil is a short-lived cell, providing a transport route into resident macrophages that are charged with clearing apoptotic neutrophils.

While the internalization of pathogens limits exposure of host tissue to the toxic compounds produced by neutrophils, extracellular release can occur (**Figure 1**). This includes the ejection of strands of chromatin coated with neutrophil proteins, which form a meshwork termed neutrophil extracellular traps (NETs) (9–11). NETs have been shown to trap bacteria and fungi and are thought to contribute towards containment of infection (9, 12) and antimicrobial activity (9, 13, 14). However, NETs can cause damage to host cells and tissue, and NETs are linked with various pathological conditions and diseases (15, 16). Unresolved inflammation will damage lung tissue and provide further opportunity for bacterial expansion.

In recent years it has become clear that neutrophils have more complex roles in immune regulation, with their ability to produce and modify cytokines, and release extracellular vesicles (17), enabling significant crosstalk with adaptive immune cells (18). This review focuses, however, on the early interactions between mycobacteria and neutrophils, and we ask the question of how pathogenic mycobacteria avoid destruction by neutrophils. Insight into their underlying survival mechanisms may provide therapeutic strategies that tilt this balance in favour of the neutrophil, and enable the early resolution of infection.

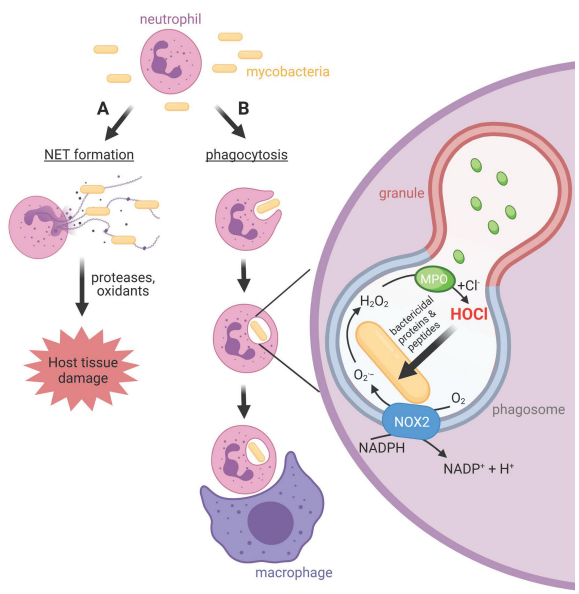

FIGURE 1 | Neutrophil activities at sites of mycobacterial infections. **(A)** Neutrophils release neutrophil extracellular traps (NETs), chromatin structures decorated with neutrophil bactericidal peptides and proteins, in response to mycobacteria. Whether NETs contribute to bacterial clearance or predominantly promote host tissue damage is unclear. **(B)** Neutrophils phagocytose mycobacteria, albeit slower than other bacteria. The phagosomal membrane fuses with cytoplasmic granules to release antimicrobial peptides and proteins including myeloperoxidase (MPO) into the phagosome. The NOX2 assembles on the phagosomal membrane resulting in the production of superoxide and hydrogen peroxide, which MPO uses to produce the strong antimicrobial oxidant HOCl. Unlike other bacteria, and for reasons as yet unknown, mycobacteria do not succumb to HOCl produced in the phagosome. Neutrophils and their resident mycobacteria are ingested by macrophages. This may augment macrophage killing of mycobacteria *via* delivery of neutrophil antimicrobial agents, or provide transfer of live bacteria to a longer-lived host cell.

NEUTROPHILS IN MYCOBACTERIAL INFECTION AND DISEASE

Neutrophils in Tuberculosis

Lung resident macrophages are the first immune cells to encounter inhaled *M. tuberculosis*, and they contribute towards bacterial clearance (19, 20). Neutrophils are subsequently recruited to the site of infection. The number of circulating neutrophils increases in patients with active tuberculosis (21–23), and a rise in neutrophil-derived transcriptional signatures has been observed in blood from patients with active tuberculosis (24). A study of close contacts of patients with active pulmonary tuberculosis showed an inverse correlation between peripheral blood neutrophil counts and risk of *M. tuberculosis* infection (21), and depletion of neutrophils from whole blood *in vitro* increased *M. tuberculosis* growth (25), suggesting that neutrophils can play an active role in limiting infection. Indeed, more neutrophils than macrophages were observed to have intracellular *M. tuberculosis* in sputum, bronchoalveolar lavage (BAL) fluid and granulomas from patients with active pulmonary tuberculosis (7). However, the fate of *M. tuberculosis* phagocytosed by neutrophils is not clear.

M. tuberculosis can survive and replicate within macrophages (26–28), where they are hidden from the immune system (29). Neutrophils have been proposed to play a similar "Trojan horse" role for *M. tuberculosis* (30, 31). Some bacteria and parasites, including *Yersinia pestis* (32), *Chlamydia pneumoniae* (33) and *Leishmania major* (34) can survive within neutrophils, and the length of *M. tuberculosis* bacilli observed in BAL fluid and sputum from patients with active tuberculosis was noted to be similar to lengths observed in logarithmic phase cultures (7), consistent with bacterial survival.

Neutrophils undergo apoptosis at sites of infection and can be cleared by macrophages. In these cases, any viable intracellular

bacteria in neutrophils will be transferred to macrophages, where they can replicate and modulate macrophage responses and function. While it has been shown that neutrophils provide a source of antimicrobial agents that potentiate macrophage killing of *M. tuberculosis* by delivery of their granule contents (35), the survival of *M. tuberculosis* within macrophages has been shown to be enhanced after ingestion of neutrophils containing the bacterium (36). Further evidence that neutrophils play a permissive role in *M. tuberculosis* transmission was recently demonstrated in a report showing that dead neutrophils have the capacity to mediate short range, aerosol transmission of viable *M. tuberculosis* aggregates (37).

Disease severity in tuberculosis-sensitive mice has been linked to the survival of *M. tuberculosis* within neutrophils (31, 38). Neutrophil phagocytosis of *M. tuberculosis* was greater in genetically-susceptible mice than in those more resistant to tuberculosis, but the majority of the bacteria remained viable within the neutrophils (31). Furthermore, in a study of *M. bovis* BCG infection following inoculation of bacteria into the ears of C57BL/6 mice, neutrophils were observed to transport BCG to the auricular draining lymph nodes early in infection (30). BCG-laden neutrophils penetrated the paracortex, an area that is rich in T-cells (39). Notably, the bacilli load at the infection site did not decrease, indicating that in this model neutrophils do not clear the infection. Neutrophils are reported to be capable of functioning as antigen presenting cells (40), and others have suggested that while neutrophils may not directly control *M. tuberculosis* growth, they promote migration of dendritic cells to the lung draining mediastinal lymph node, facilitating priming of the adaptive immune response (41). However, neutrophils may protect the phagocytosed bacteria from recognition by the immune system thus delaying the adaptive immune response. In a study by Abadie et al. live BCG were recovered from the lymph nodes in numbers that remained stable over two weeks, lending support to this scenario (30).

The host response to pulmonary *M. tuberculosis* infection involves formation of nodule-like structures in the lung called granulomas, which comprise an assemblage of various immune cells, including neutrophils (42). Granulomas contain infection by preventing dissemination of bacteria; however, they may also provide a niche for *M. tuberculosis* survival (43–45). Neutrophils in zebrafish infected with *M. marinum* have been shown to work in conjunction with macrophages in developing granulomas to contain infection (46). However, in active disease the granulomas develop into large inflammatory lesions, and neutrophil accumulation may play an important part of this process. In a non-human primate model of tuberculosis, greater neutrophil accumulation was observed in the larger granulomas associated with active tuberculosis compared with the smaller granulomas of a latent infection (47). In a mouse model, interleukin (IL)-17 neutralization decreased neutrophil accumulation in lung granulomas but there was no difference in bacterial burden (47), while neutrophil depletion in C57BL/6J mice during the chronic phase of infection improved control of *M. tuberculosis* (48).

Several studies suggest that neutrophil accumulation is associated with a dysregulated immune response and a poor prognosis in tuberculosis. Even after bacterial clearance, neutrophil accumulation is linked with post-TB lung disease (49). Levels of calprotectin, the most abundant neutrophil cytoplasmic protein, and neutrophil chemokines are increased in patients with active tuberculosis compared to healthy controls and those with latent infection, and this is correlated with lung damage (47). Increased neutrophil accumulation was shown to be mediated, at least in part, *via* calprotectin-dependent upregulation of the neutrophil integrin CD11b (48). Calprotectin has antimicrobial activity, however improved control of infection was observed when a subunit of calprotectin was knocked out (48). Mice infected by aerosol with a low dose of *M. tuberculosis* were grouped into three different classes: resistant, susceptible and super-susceptible mice; reflecting the variation observed in humans (50). Lungs of super-susceptible mice showed the highest numbers of infiltrating neutrophils, had the largest granulomas with areas of necrosis, and the highest bacterial burden. Another mouse study found that neutrophil depletion significantly increased survival following *M. tuberculosis* infection (51). Using several different models, Mishra et al. concluded that neutrophil accumulation in the lungs correlated with increased bacterial burden and animal weight loss, and that inhibition of neutrophil recruitment decreased bacterial numbers (52).

In summary, current evidence indicates that neutrophils play an important role during in bacterial clearance the acute stages of human TB. This is supported by several animal studies (53, 54). However, if the infection continues, accumulating evidence indicates that neutrophils contribute towards disease pathology and a negative prognosis. Investigation of the suitability of neutrophils as a marker for poor outcome in TB is ongoing (55).

Neutrophils in Leprosy

M. leprae infects macrophages (56) and Schwann cells (57), and it is these cells that are traditionally thought to be important players in infection (58, 59). Peripheral blood neutrophils from lepromatous leprosy patients have, however, also been shown to harbor *M. leprae* (60). The course of lepromatous leprosy can involve periods of acute inflammation called reactions, the most common of which is erythema nodosum leprosum (ENL). Neutrophil infiltration is a feature of the skin lesions associated with this reaction, although neutrophils are not always present (61–63). ENL can occur as a single acute episode, several discrete acute episodes or as a chronic condition, and can occur before, during or after multi-drug therapy (64, 65). Importantly, ENL is a major contributor towards nerve damage in leprosy patients and contributes significantly towards mortality (66). Despite the fact that neutrophils are the hallmark of ENL in histological samples (67), few studies have examined their role, but the evidence indicates neutrophils may make a significant contribution to the pathogenesis of ENL [reviewed in (63, 68, 69)].

Two early studies examined neutrophil activation in ENL by measuring reduction of nitroblue tetrazolium (NBT) (70, 71), which is reduced by superoxide to dark formazan precipitates (72). In the first study, spontaneous reduction of NBT was significantly increased in blood from patients with reactional lepromatous leprosy (RLL), of which ENL is a major subset,

compared with blood from healthy controls and patients with other forms of leprosy (70). RLL patient sera did not increase neutrophil activation in blood from healthy controls, suggesting that the activating stimulus was not present in the circulation (70). In contrast, the second study that used isolated neutrophils reported no increase in spontaneous NBT reduction in neutrophils from ENL patients, and ENL patient sera induced a large increase in NBT reduction in neutrophils from healthy controls and ENL patients (71). The difference between studies may have been due to the use of heparin at higher concentrations, which can form particles with NBT that activate neutrophils (73), and/or the presence of an inhibitory factor that is absent from ENL sera.

Activated neutrophils express the Fcγ-receptor I (Fcγ-R1) (also known as CD64), a high affinity receptor for IgG (74). Fcγ-R1 expression was observed on neutrophils within ENL skin lesions and expression was significantly higher in the peripheral blood of ENL patients compared to lepromatous leprosy patients without ENL (62). The presence of Fcγ-R1 expressing neutrophils in peripheral blood increased with disease severity, and treatment of ENL with thalidomide, which improved symptoms, decreased Fcγ-R1 expression and the level of neutrophils in skin lesions (62). In addition, the neutrophil granule protein pentraxin-3 (PTX-3) was found to be increased in the blood of multibacillary leprosy patients, in particular, levels were higher in those that went on to develop ENL (75). PTX-3 levels correlated with Fcγ-R1 expression in the circulation and PTX-3 was also increased in ENL skin lesions and correlated with neutrophils (myeloperoxidase) (75). More studies on the relationship of neutrophils to more severe forms of leprosy are needed.

Neutrophils in Other Mycobacterial Infections

M. avium complex (MAC) are the most common cause of NTM-induced pulmonary disease, predominately, but not exclusively, in those with pre-existing lung conditions (76). They are also a leading cause of disseminated NTM infection (76). Mouse studies examining the role of neutrophils in MAC infection show differences in their role dependent on the form of infection, pulmonary or systemic. C57BL/6 mice with the beige mutation, whose neutrophils are defective in chemotaxis and killing (77), have increased susceptibility to MAC infection (78, 79). In a study of disseminated infection, neutrophil transfusion from WT mice improved the resistance of beige mice to intravenous *M. avium* infection while neutrophil depletion in WT mice increased their susceptibility (78). This implies a protective role for neutrophils in systemic MAC infection in this mouse model. However, in lung infection of C57BL/6 mice, Saunders et al. found that a 95% decrease in neutrophils in the lungs had no effect on bacterial numbers, indicating neutrophils are dispensable in controlling MAC lung infection in these mice (79). Further support that neutrophils are ineffective in controlling MAC infection was provided by a study of mice over-expressing the transcription factor RAR-related orphan receptor gamma t (RORγt), which regulates Th17 responses and increased pulmonary neutrophil infiltration, yet bacterial burden was similar to that in WT mice (80).

In humans, a study of MAC-infected patients with no pre-existing lung disease found that the level of neutrophils in patient BAL fluid was significantly higher than that of control patients (81), with higher neutrophil counts subsequently correlated with worsening disease (82). Similarly, in a more recent retrospective study of pulmonary MAC infection, BAL fluid from patients whose disease progressed had higher numbers of neutrophils than those who had stable infection (83). Together these studies provide evidence that neutrophils are ineffective in preventing MAC-induced pulmonary disease.

Slow growing *M. kansasii* are considered to be the most pathogenic of the NTM, as when isolated they are almost always associated with disease (84, 85). *M. kansasii* most frequently cause pulmonary disease that is clinically similar to tuberculosis (86), but infections at other sites are also reported (87). In humans, abundant neutrophils have been observed at sites of *M. kansasii* infection (87–89). In CD-1 mice, peritoneal inoculation with *M. kansasii* or *M. avium* was found to lead to chronic neutrophil infiltration, with bacterial numbers gradually decreased during this time (90). Neutrophil ingestion of *M. kansasii* and *M. avium* was not examined, however neutrophil uptake of non-pathogenic *M. aurum* only occurred during the first two days (90). Macrophages were present at the infection site and ingested dying neutrophils (90). Lactoferrin, present in neutrophils but not macrophages, was detected within peritoneal macrophages suggesting transfer from neutrophils to macrophages either by neutrophil degranulation and subsequent uptake of granule components by resident macrophages, or through uptake of the intact neutrophil. Macrophage antibacterial activity *in vitro* was enhanced when the macrophages were pre-incubated with neutrophils, leading the authors to conclude that neutrophils do not directly control NTM infection but participate indirectly *via* transfer of macromolecules that enhance macrophage killing of these bacteria (90).

M. abscessus are rapidly growing NTM that cause pulmonary disease in both healthy individuals and those with underlying lung disease, disseminated infections, and skin and soft tissue infections (91–93). Of note, *M. abscessus* are particularly recalcitrant to antibiotic therapy (94, 95). Extensive numbers of neutrophils are reported within patient granulomas or at the site of infection (96–98). In addition, human lung tissue infected with *M. abscessus ex vivo* showed bacteria within neutrophils at the site of infection (99). *M. abscessus*, like several other NTM (91), exist in one of two colony morphological forms. A smooth, non-cording form and a rough cording form, that differ in their concentration of cell wall glycopeptidolipid (100). The rough form is associated with more severe pulmonary disease (101). Greater neutrophil numbers were measured in BAL fluid from C57BL/6 mice infected with the rough form (102). In a zebrafish model of *M. abscessus* infection, ingestion of the rough form by macrophages was associated with increased macrophage apoptosis, release of viable bacteria and intense cording growth, which neither macrophages nor neutrophils could

engulf because of the size of the cords (103). However, in a subsequent study both rough and smooth forms induced a large influx of neutrophils early at the infection site that was dependent on IL-8 and macrophage-secreted TNF (104). Both forms were engulfed equally by neutrophils, and neutrophil depletion resulted in uncontrolled bacterial growth and zebrafish larvae death with either (104). Neutrophils were found to be essential for the development and maintenance of protective granuloma in the infected zebrafish (104).

M. smegmatis is a rapidly growing NTM that is ubiquitous in the environment and is generally considered to be non-pathogenic. Due to its fast replication rate (relative to other mycobacteria), amenability to genetic manipulation, and the fact that it can be grown under normal Biosafety Level 2 laboratory conditions, *M. smegmatis* is often used as a model to study *M. tuberculosis* infection and virulence factors. Occasionally *M. smegmatis* causes skin and soft tissue infections, and very rarely disseminated infection (105–108). Hospital-acquired infections also occur, resulting from a variety of procedures including catheterization, cardiac and plastic surgery (109). Although infrequent, these infections can be difficult to treat requiring surgical debridement and long term antibiotic therapy (105). Neutrophils are recruited to the site of infection in humans (106, 110), and in mice infected with *M. smegmatis* intratracheally (111). *M. smegmatis* has been shown to induce neutrophil exocytosis of gelatinase granules releasing active matrix metalloproteinase-9 that degrades the extracellular matrix (112). Release of these granules may contribute towards the tissue degradation observed in soft tissue infections caused by this bacteria. Neutrophil exocytosis of azurophilic granules has also been reported in response to *M. smegmatis* and constituents of these granules can also cause host tissue damage (113).

Much work remains to be done to gain a better understanding of the role of neutrophils in mycobacterial infection and disease. The plethora of studies implicating neutrophils in the pathogenesis of mycobacterial infections strongly suggests that the capacity of neutrophils to control infection by intra- and extra-cellular killing mechanisms is either insufficient, defective or thwarted by mycobacteria. In the next sections of this review we discuss the current evidence for neutrophil phagocytosis and killing of mycobacteria (both phagosomal and NET-mediated) and evidence for resistance of mycobacteria to neutrophil oxidants.

NEUTROPHIL PHAGOCYTOSIS OF MYCOBACTERIA

The major antimicrobial strategy employed by neutrophils involves the ingestion of pathogens into phagosomes, followed by the degranulation of antimicrobial peptides and proteins and the production of toxic reactive oxygen species inside the phagosome (8, 114). Neutrophils are known to phagocytose both pathogenic and non-pathogenic mycobacteria (7, 30, 36, 112, 115–121), with ingestion of mycobacteria increasing in the presence of serum (112, 115–117). The mechanism of phagocytosis differs depending on whether neutrophils bind opsonized or non-opsonized mycobacteria. Neutrophil complement receptor 3 (CR3) binds *M. leprae* phenolic glycolipid-I resulting in bacterial phagocytosis and activation of the Syk tyrosine kinase, which leads to activation of the transcription factor NFATc and Il-10 production (122). Phagocytosis of non-opsonized *M. kansasii* has also been shown to occur *via* CR3 in a cholesterol-dependent and glycosylphosphatidylinositol (GPI) anchored protein-dependent manner, while cholesterol was not required with opsonized bacteria (123). Phagocytosis of non-opsonized *M. smegmatis* was also dependent on CR3 and cholesterol (113). GPI-anchored proteins and cholesterol accumulate in lipid rafts (124) suggesting that the localization of CR3 to lipid rafts is required for neutrophil internalization of non-opsonized mycobacteria. The glycosphingolipid lactosylceramide (LacCer), enriched in lipid rafts (125), is also required for non-opsonic internalization of mycobacteria (126). Binding to LacCer is mediated by lipoarabinomannan (LAM) on the mycobacterial surface. Interestingly, the mannose cap on LAM (ManLAM) of pathogenic mycobacteria, but not the phosphoinositol cap (PILAM) of non-pathogenic mycobacteria, appears to prevent fusion of azurophil granules with the phagosome (126), which will have a significant impact on the antimicrobial activity of neutrophils.

While most studies report that neutrophils phagocytose mycobacteria, a few have reported impaired phagocytosis. In zebrafish infected with *M. marium*, neutrophils were absent from the initial infection site but were recruited to the developing granuloma by dying macrophages (46). Neutrophils then phagocytosed *M. marium* indirectly by taking them up from macrophages. The investigators observed a small increase in direct neutrophil phagocytosis of *M. marium* when inoculum numbers were increased (46). Neutrophil uptake in BALB/c mice was shown to be negligible after intravenous injection of a relatively low dose of *M. tuberculosis* (53). However, Abadie et al. observed abundant neutrophil phagocytosis of BCG in C57BL/6 mice after inoculation with a similar low dose of bacteria as present in the BCG vaccine (30).

Recently we measured the rate of phagocytosis of *M. smegmatis* and found that it was five times slower than the phagocytosis of *Staphylococcus aureus* and 3.5 times slower than that for *Escherichia coli* (127, 128). Phagocytosis of *M. abscessus* was also found to be slower than that of *S. aureus* when examined by counting the number of neutrophils containing fluorescently labelled bacteria (129). In another study, approximately half of a population of *M. fortuitum* was phagocytosed within 30 min (130), only slightly faster than the 43 min we measured for *M. smegmatis*, and still considerably slower than the 9 min for *S. aureus* and 12 min for *E. coli* (127, 131). As far as we are aware no *in vitro* studies have directly compared phagocytosis of different mycobacteria by the same neutrophils; however, neutrophils were found to ingest *M. abscessus* more frequently than either *M. tuberculosis* or *M. avium* in an *ex vivo* infection of human lung tissue (99).

Evidence from tuberculosis patients indicates that patient neutrophils are primed for phagocytosis. Surface expression of

the Ig receptor FcγR1 (CD64) was found to be increased on peripheral blood neutrophils from patients with tuberculosis pleuritis compared to healthy controls, and neutrophils obtained from pleural fluid showed further enhanced FcγR1 expression and increased expression of the pattern recognition receptor TLR2 (132). An increase in expression of FcγR1, TLR2 and TLR4 was also observed in neutrophils from the peripheral blood of patients with active pulmonary tuberculosis prior to treatment (133). Despite the evidence for increased receptor expression, studies examining the phagocytic activity of neutrophils from patients with active pulmonary tuberculosis generally show their capacity for phagocytosis is decreased. Hilda et al. measured significantly reduced phagocytic activity in blood neutrophils from patients prior to treatment (133), and Shalekoff et al. also found peripheral blood neutrophil function impaired in patients with active pulmonary tuberculosis (134). Patient neutrophils showed a reduced capacity for phagocytosis compared to healthy controls and this was observed both soon after the start of treatment and when treatment had been undertaken for almost 30 weeks (134). Similarly, another study found peripheral blood neutrophils from tuberculosis patients had reduced phagocytic activity compared to healthy controls (135). In these studies, phagocytic capacity was measured in patient neutrophils by assessing phagocytosis of *E. coli* or yeast to rule out *M. tuberculosis* factors that may interfere with neutrophil uptake.

Mycobacteria are able to directly inhibit neutrophil phagocytosis. *M. abscessus* rough morphotypes prevent phagocytosis by formation of serpentine cords that are too large for neutrophils to ingest, with these large aggregates linked to pathogenesis (103). *M. leprae* cell wall lipids inhibit macrophage phagocytic activity (136), but to our knowledge there are no reports on whether these lipids affect neutrophil phagocytosis. Exposure of *M. tuberculosis* to human alveolar lining fluid results in changes to the bacterial cell wall and release of cell wall fragments (137). Macrophage phagocytosis of *M. tuberculosis* decreased when the bacteria were pre-exposed to alveolar lining fluid, however, neutrophil phagocytosis was found to increase (138, 139). This increase in phagocytosis was due to bacterial alveolar lining fluid exposure rather than *M. tuberculosis* cell wall fragments released by treatment with alveolar lining fluid (139).

PHAGOSOMAL KILLING OF MYCOBACTERIA

The ability of neutrophils to kill *M. tuberculosis* is controversial with some studies observing killing (116, 140–142) while others do not (115, 143–145). Neutrophils have been reported to kill 50-70% of *M. tuberculosis* within 90-120 minutes (116, 140); however, Corleis et al. found neutrophils did not kill *M. tuberculosis* even after six hours co-incubation (115) and others found no killing after incubation with neutrophils for 24 hours (144, 145). While Hartman et al. reported near complete killing of *M. avium* by neutrophils in two hours (120), only around 40% of populations of *M. abscessus* and *M. fortuitum* were killed after two hours incubation with neutrophils (146). We have previously reported half-lives for *E. coli* and *S. aureus* inside the neutrophil phagosome of 2 min and 6 min, respectively (128), and recently measured a half-life for *M. smegmatis* of 30 min inside the neutrophil phagosome, which indicates that even though killing occurs, it is slow (127).

In terms of bactericidal mechanisms, the neutrophil oxidative burst is activated upon uptake of various mycobacteria, including *M. tuberculosis*, *M. canettii*, *M. abscessus*, *M. kansaii*, *M. phlei*, *M. fortuitum* and *M. smegmatis* (115, 117, 130, 144, 146–148). Contrary to this, *M. gordonae* did not stimulate neutrophil oxidant production (144) and *M. bovis* induced a weak oxidative burst in comparison to *Listeria monocytogenes* (118). Interestingly, *M. tuberculosis* were found to induce a stronger oxidative burst than *M. smegmatis*, yet *M. smegmatis* was killed while *M. tuberculosis* was not (115). Rough morphotypes of *M. abscessus* induced a stronger oxidative burst in comparison to smooth morphotypes, yet neutrophil killing of both was unaffected by inhibition of oxidant production (146).

The purified $MPO/H_2O_2/Cl^-$ system is capable of killing *M. tuberculosis* and *M. leprae* (149, 150); however, it has been reported that the complete system did not augment killing of *M. tuberculosis* over that observed by H_2O_2 alone (141). Reagent HOCl killed *M. smegmatis*, but approximately seven times more HOCl was required to kill *M. smegmatis* than *S. aureus* suggesting mycobacteria may be innately more resistant to HOCl (127). Further studies are required to determine if other mycobacteria are similarly resistant to HOCl. We recently sought to examine whether HOCl plays a role in killing of *M. smegmatis* in the neutrophil phagosome. The amount of reagent HOCl required to kill a bacterium cannot be directly translated to the phagosome as neutrophil oxidants are produced in a flux in the phagosome, and a flux of HOCl may be less harmful to the bacteria than a single high dose. Additionally, the neutrophil phagosome contains many proteins and amines that can react with phagosomal HOCl before it reaches the bacterium (151, 152). Using a fluorescent probe we observed HOCl production in the phagosome and that MPO inhibition abrogated HOCl production (127). By modelling the data obtained in our study we estimated that it would take 30-40 minutes at full MPO capacity for sufficient HOCl to be produced to kill a single ingested *M. smegmatis*. Sustained MPO activity for that length of time is unlikely and therefore we concluded that insufficient HOCl is produced in the neutrophil phagosome to directly kill this bacterium. In support of this conclusion, inhibition of MPO had no effect on neutrophil killing of *M. smegmatis* (127).

Inhibition of the NADPH oxidase had no effect on the ability of human neutrophils to kill *M. tuberculosis* and *M. abscessus* (142, 146). Defective killing by neutrophils from patients with chronic granulomatous disease (CGD), who have mutations that lead to a non-functional NADPH oxidase (153), is often used as evidence for the requirement for oxidants in bacterial killing. Jones et al. showed that CGD neutrophils killed *M. tuberculosis* as effectively as neutrophils from healthy donors (140). However, in countries where tuberculosis is endemic, the incidence of tuberculosis is greater in CGD patients than the rest of the

population (154–156), though it is important to consider that NOX2 has other roles during inflammation (157). X-linked CGD mice showed increased bacterial growth and an increase in granuloma size in their lungs compared to C57BL/6 mice (158). A high incidence of complications due to BCG vaccination has also been reported in CGD patients (155, 156, 159–161). Neutrophil killing of *M. marinum* was found to depend on an active NADPH oxidase in a zebrafish model of early tuberculosis disease using morphant larvae with neutrophils deficient in two subunits of the NADPH oxidase ($gp91^{phox}$ and $pg22^{phox}$) (46). In a zebrafish model of cystic fibrosis, transmembrane conductance regulator morphants showed reduced neutrophil oxidant production and reduced intracellular control of *M. abscessus* that was linked to a reduction in NADPH oxidase activity (147).

Neutrophil killing of mycobacteria can occur *via* non-oxidative processes. Defensins, components of azurophil granules, have been shown to have anti-mycobacterial activity (21, 162, 163). Defensin-depleted granules have also been shown to kill *M. tuberculosis*, *M. bovis* BCG and *M. smegmatis* although *M. tuberculosis* were more resistant to killing (164). The azurophil granule proteins elastase, azurocidin, and lysozyme, and the specific granule protein lactoferrin were shown to kill *M. smegmatis* (164). In addition, conditioned media from neutrophils incubated with *M. abscessus* for 90 minutes showed bactericidal activity towards this bacterium (146). This was most likely due to degranulation of cytotoxic agents. *In vitro*, *M. tuberculosis* induced neutrophils to release MPO and elastase (165) and neutrophils were found to release elastase and cathepsin G, another major azurophil granule protein, into the bronchoalveolar space in mice infected with *M. bovis* BCG (166). Released neutrophil granule proteins have been shown to be taken up by infected macrophages and to increase macrophage killing of *M. tuberculosis* and *M. bovis* BCG (35, 164). Efferocytosis also potentiates macrophage killing of ingested *M. tuberculosis* through delivery of granule proteins to early endosomes and fusion of these with the phagosome (35). Augmented macrophage killing due to uptake of neutrophil granule proteins has been demonstrated in other bacteria (167, 168). When neutrophils struggle to control a mycobacterial infection through intracellular killing, degranulation and efferocytosis could be an important mechanism by which neutrophils contribute towards host defense.

In the early stages of *M. tuberculosis* infection, and when they escape from phagocytic cells, *M. tuberculosis* are exposed to a variety of agents in alveolar lining fluid (ALF) that can alter the bacterial cell wall (137). Exposure of neutrophils to *M. tuberculosis* pre-treated with human ALF increased phagocytosis and neutrophil killing of *M. tuberculosis* while dampening the oxidative burst response (138). The increase in intracellular killing corresponded with an increase in granule/phagosome fusion and was mediated by a protein component in ALF, as the observed increase in killing was lost when ALF was heat-inactivated (138). Incubation with ALF also reduced extracellular degranulation in response to *M. tuberculosis* (138). Of note, neutrophils infected with ALF-treated *M. tuberculosis* did not activate macrophages and infection with ALF-treated *M. tuberculosis* had no significant effect on neutrophil apoptosis or necrosis. This study shows that exposure of *M. tuberculosis* to ALF alters the interaction of the bacteria with neutrophils in a way that facilitates neutrophils to kill the bacteria intracellularly without release of damaging neutrophil proteins.

Taken together, the evidence so far indicates that neutrophil oxidants are dispensable for killing of some mycobacteria. By dispensable we mean that oxidants are likely to contribute when they are being produced, but in their absence the non-oxidative mechanisms are able to compensate. More studies are required, ideally using neutrophils from CGD patients, to examine neutrophil killing of a wider range of mycobacteria. To our knowledge the question of whether neutrophils kill *M. leprae* is unanswered, and more studies are also needed to examine neutrophil killing of the more significant NTM, particularly MAC, *M. kansaii* and *M. abscessus*.

NEUTROPHIL EXTRACELLULAR TRAP-MEDIATED KILLING OF MYCOBACTERIA

NETs contain proteins with antimicrobial activities, including MPO, calprotectin and elastase (12, 13, 169). Histones on NETs have also been shown to mediate microbial killing as has NET-DNA (9, 14, 170). The prolonged presence of cytotoxic NET constituents as a result of excessive NET release or impaired clearance can also be detrimental to the host.

In vivo, NET markers have been measured in the plasma of patients with active tuberculosis (171, 172) and observed to decrease with antibiotic therapy (171). NETs have also been observed in BALF samples from mice 3 – 4 weeks after aerosol challenge with *M. tuberculosis* (119) and in skin samples from guinea pigs within several hours following intradermal *M. tuberculosis* inoculation (173), indicating that NETs may participate in both early and late stages of infection. Whether their presence is important in control of *M. tuberculosis* infection or if they contribute towards pathogenesis remains to be determined. Recently, NETs have been observed in lung lesions resected from patients with persistent pulmonary TB and from TB-susceptible mice lending support to their role in TB pathogenesis (174). Increased human DNA-histone complexes associated with NETs have been measured in ENL sera compared with lepromatous and borderline lepromatous leprosy patients (175). NET components (DNA/histone/MPO) were observed in ENL skin lesions, and DNA-histone complexes in patient sera were significantly higher than those with lepromatous and borderline lepromatous leprosy and healthy controls (176). This data is suggestive of NETs contributing towards more severe leprosy disease. A recent review discusses the potential for NETs as a putative prognostic tool in ENL to direct medical treatment (177).

Several mycobacteria, including *M. tuberculosis*, *M. bovis* BCG, *M. abscessus, M. avium* subsp. *paratuberculosis* and *M. leprae*, have been shown to induce NETs *in vitro* (121, 129, 146, 148, 176, 178–181). How the interaction of mycobacteria with neutrophils leads to the formation of NETs appears to differ

depending on the bacterial species. The early secreted antigen-6 (ESAT-6) of *M. tuberculosis* has been shown to induce neutrophils to release NETs (148, 181, 182), as has secreted sphingomyelinase Rv088 (182, 183). Rv088 has both sphingomyelinase (184) and nuclease (185) activity but it is the sphingomyelinase activity that is required for neutrophils to form NETs (183). Phagocytosis is also a prerequisite for the induction of NETs in response to *M. tuberculosis* and *M. abscessus*, as NET formation did not occur when phagocytosis was inhibited with cytochalasin D (146, 181). In contrast, Branzk et al. found with *M. bovis* BCG that NETs only occurred in response to small non-phagocytosed aggregates (179). Single bacteria were phagocytosed and neutrophils containing these bacteria did not go on to form NETs, at least not over the four hours of this study (179).

Neutrophil oxidants are required for NET formation in response to various stimuli (186–188), and *M. bovis* BCG NET induction was shown to be dependent on neutrophil oxidants (189). In addition, NETs were not formed under hypoxia in response to *M. tuberculosis* (190). Both rough and smooth morphotypes of *M. abscessus* were found to induce NETs, though the mechanism differed between morphotypes (146). Early NET induction (up to one hour) was independent of neutrophil oxidant production, while NETs formed after four hours co-incubation with bacteria did depend on oxidants, similar to that which has been reported for *S. aureus* (191).

Despite increasing evidence that mycobacteria induce neutrophils to form NETs, there is relatively little information on whether NETs contribute to killing of mycobacteria or control of infection. Evidence suggests that *M. abscessus* are killed by NETs whereas *M. tuberculosis* are not (146, 148, 173). In a study by Ramos-Kichik et al., *M. tuberculosis* was not killed by NETs formed by PMA (148). NET constituents as well as their post-translation modifications can vary depending on the stimulus (11, 181) potentially altering their bactericidal activity. Therefore, it is important to examine NETs induced either by the bacterium studied or host/bacterial factors that may be present at the infection site. In a guinea pig model of extra-pulmonary tuberculosis, NETs induced by *M. tuberculosis in vivo* were not bactericidal (173). This provides good evidence that NETs do not contribute towards killing of *M. tuberculosis*, but further studies are required to corroborate this in human disease.

NET-mediated killing of *M. abscessus*, as with NET induction, appears to differ with the morphotype studied. Neutrophil killing of the smooth morphotype was found to occur predominately *via* NETs, as removal with DNase resulted in only slight killing (146). In contrast, approximately half the rough morphotype were still killed when NETs were degraded, indicating other neutrophil killing mechanisms are more important for this morphotype. Notably in this study, neutrophil killing was only measured over the first hour of co-incubation when NET release was relatively low making it difficult to gain a full appreciation of the effect of NETs on *M. abscessus* viability. As the mechanism of NET formation differed between early and later formed NETs, it is conceivable that later-formed NETs may contain different constituents and therefore different antimicrobial activity.

There is evidence that NETs may increase the anti-mycobacterial capacity of macrophages. In one study, NETs produced in response to *M. tuberculosis* were shown to activate macrophages, leading to production of pro-inflammatory cytokines (181). In another study, *M. bovis* BCG was shown to induce NETs that contain the antimicrobial cathelicidin LL37, and macrophages were observed to ingest NET fragments containing this cathelicidin (189). By creating DNA : LL37 complexes to mimic NET fragments, Stephan et al. monitored the intracellular localization of these complexes in macrophages that had already phagocytosed BCG. Following uptake, the DNA was degraded in lysosomes releasing LL37 in close proximity to the internalized bacteria and inhibiting bacterial growth (189). Interestingly, significantly greater growth inhibition was observed when infected macrophages were incubated with DNA : LL37 complexes rather than LL37 alone. The authors speculated that the binding and internalization of DNA may increase killing by activating intrinsic antimicrobial pathways within the macrophage.

NETs may play a beneficial role in mycobacterial infection simply by capturing bacteria and preventing dissemination, and by facilitating activation of macrophages and other immune cells. Indeed, NETs have been shown to prime T cells (192). NETs are observed in the leprosy reaction ENL. However, evidence of free bacteria in ENL patient sera suggests that NETs are not capable of containing *M. leprae*. Moreover, NETs may also be detrimental. They may bind other immune cells inhibiting their function, and may also directly damage host tissue. NETs are linked to lung injury in respiratory conditions such as cystic fibrosis, chronic obstructive pulmonary disease, and pneumonia-associated acute respiratory distress syndrome (193–195). They have also been linked to lung injury in mice infected with *M. smegmatis* expressing the sphingomyelinase/nuclease Rv088 from *M. tuberculosis* (183). Lung injury was largely mediated by MPO (183), which is present and active on NETs (13). If NETs are proven ineffective at limiting infection, then there may be an advantage in blocking production or removing them to help protect damage to lung tissue.

MYCOBACTERIAL RESISTANCE TO NEUTROPHIL OXIDANTS

Killing of mycobacteria by neutrophils appears to be much slower than other pathogens, suggesting that these bacteria possess an innate resistance to the fast-acting oxidative killing mechanisms in the phagosome. In support of this, we have shown that *M. smegmatis* can cope with relatively high doses of the most bactericidal oxidant produced in the neutrophil phagosome, HOCl (LD_{50} of 90 nmol/10^8 CFU) (127). HOCl reacts rapidly with a wide range of biomolecules, and the relative resistance may be related to the larger size of these microbes i.e. more HOCl is required to damage enough critical targets in the bacterium. A rod-shape *M. smegmatis* 10 μm in length and 0.8 μm in diameter has a volume of $5x10^{-12}$ mL. In contrast, *S. aureus*, *P. aeruginosa* and *E. coli* (rod- or sphere-shaped with 1-2

μm in length and 0.5–1 μm diameter) have approximately 10% that volume. The susceptibility of these bacteria to HOCl ranges from 2.5-3 nmol/10^8 CFU for *P. aeruginosa* and *E. coli* (196, 197), to approximately 10 nmol/10^8 CFU for *S. aureus* (151, 197, 198).

The presence of protective compounds will also contribute to HOCl resistance. Mycothiol (MSH), the main low molecular weight thiol (LMWT) in mycobacteria, has been proposed to play a role in defending against neutrophil oxidants. Mycothiol carries out many of the cellular functions performed by glutathione in eukaryotic cells and gram-negative bacteria, including the detoxification of electrophilic compounds and maintaining redox homeostasis (199). Interestingly, MSH levels in *M. tuberculosis* and *M. smegmatis* are much higher than those of the main LMWT in other bacteria such as bacillithiol (BSH) in *S. aureus* or glutathione in *Pseudomonas aeruginosa* (9–19, 0.7 and 1.1 μmol/g residual dry weight, respectively) (200). Since HOCl reacts very rapidly with thiol moieties (201), the higher LMWT content in mycobacteria might protect them from killing by HOCl. Consistent with a role for mycothiol in HOCl resistance, mycobacteria lacking the ability to synthesize this LMWT are significantly more sensitive to reagent HOCl and its secondary oxidants, chloramines (127, 202, 203). However, the amount of HOCl required to kill *M. smegmatis* (200-300 nmol/10^8 bacteria) greatly exceeds that of mycothiol (5 nmol/10^8 bacteria) (127), suggesting that mycothiol exerts its protective role not by scavenging the oxidant directly, but by forming mixed disulfides with critical cysteine residues in proteins in a process termed S-mycothiolation. Because S-mycothiolated proteins can be reduced by mycoredoxin-1 (203), this modification protects cysteine residues from irreversible oxidation. S-mycothiolation occurs in *M. smegmatis* exposed to hypochlorous acid (202). We recently observed that neutrophils killed mycothiol-deficient *M. smegmatis* at the same rate as wild type bacteria, indicating that mycothiol itself is not responsible for the ability of *M. smegmatis* to cope with HOCl or other oxidants produced in the phagosome (127).

Mycobacteria also contain other LMWTs such as gamma-glutamylcysteine, coenzyme A, cysteine and ergothioneine, albeit at much lower levels than mycothiol (127, 204). Interestingly, unlike mycothiol, ergothioneine is known to be actively exported suggesting an extracellular function for this LMWT (205), which may provide greater protection against HOCl. Also, ergothioneine, which is upregulated in mycothiol-deficient mutants, can compensate for the loss of mycothiol in protecting against organic hydroperoxides and is essential for survival of *M. tuberculosis* in macrophages and mice (205). The contribution of ergothioneine and other LMWTs to surviving neutrophil phagocytosis remains unexplored and future investigations are needed to establish their role in mycobacterial resistance to neutrophil oxidants. Apart from thiol groups, HOCl also reacts rapidly with methionine residues on proteins (201) resulting in the formation of methionine sulfoxide. Methionine sulfoxides are reduced by methionine sulfoxide reductases, the lack of which in *M. tuberculosis* made the bacteria more susceptible to HOCl (206). Whether or not methionine sulfoxide reductase activity protects mycobacteria from oxidative killing by neutrophils remains to be investigated.

Bacterial superoxide dismutase (SOD), which catalyzes the conversion of superoxide to hydrogen peroxide, is another candidate for conferring resistance of mycobacteria to neutrophil killing. SOD is exported in large amounts by *M. tuberculosis* and production increases further under hydrogen peroxide stress (207, 208). A role for SOD in the virulence of *M. tuberculosis* was established in a mouse infection model (207). Superoxide is the most-upstream of the oxidants produced by the neutrophil, and while SOD will facilitate conversion to hydrogen peroxide, the superoxide itself can modulate MPO activity (209). The addition of SOD to the surface of *S. aureus* slowed the rate at which they were killed by neutrophils (210). Non-pathogenic *M. smegmatis* express almost 100-fold less SOD than *M. tuberculosis* and export a smaller fraction (208). However, we could not slow the killing of *M. smegmatis* by genetically-modifying them to express large amounts of *M. tuberculosis* SOD, albeit as noted above, wild-type *M. smegmatis* are already killed very slowly (127).

CONCLUSIONS AND FUTURE PERSPECTIVES

While neutrophils attempt to control mycobacterial infection, the bulk of the evidence indicates that the effectiveness of their phagosomal and extracellular killing mechanisms is thwarted by the microbes. Rather than destroy mycobacteria, the neutrophils appear to provide a safe haven and transport them into macrophages, while retaining the potential to damage host tissue. With regards to the latter, it will be valuable to determine if NETs play a significant role in the control of infection by preventing the spread or directly killing mycobacteria, or if they simply cause tissue damage and contribute towards a pro-inflammatory environment.

It is important to note the limitations of current experimental models (211). *In vitro* studies of neutrophil and mycobacteria interactions occur using neutrophils isolated from circulating blood; they have not been exposed to the plethora of signals and cell interactions that occur during migration and upon arrival at a site of infection. Human tuberculosis granulomas are highly hypoxic (212), which will suppress the oxidative burst, yet little is known about how hypoxia affects the response of neutrophils to mycobacteria (213). There is considerable heterogeneity in neutrophil populations, and certain subpopulations may be more effective at ingesting and destroying mycobacteria. Also, a significant amount of information has been derived from animal models, but neutrophils function differently between species, particularly mouse and human (214).

The current challenge is to apply our knowledge of neutrophil-mycobacteria interactions to improving treatments. The appearance of multi-drug resistance strains of *M. tuberculosis* is of major concern. Treatment for drug-susceptible *M. tuberculosis* involves six months of antibiotic therapy provided by four front line drugs:

isoniazid, rifampicin, ethambutol and pyrazinamide. Treatment of infections with multi-drug resistant (MDR) strains takes longer, costs considerably more and uses second generation drugs with greater side effects and more complex drug delivery (2). Extensively drug-resistant strains have also arisen that are resistant to at least one second-line drug used to treat MDR (fluoroquinolone) and one second-line injectable drug (2). Infections with NTM can also be difficult to treat (215, 216).

In terms of bacterial resistance, the mycobacteria tested so far appear to be phagocytosed and killed more slowly than other pathogenic bacteria, with resistance to neutrophil oxidants likely to be an important factor. While a number of mechanisms have been shown to underwrite the resistance of mycobacteria to individual oxidants, none of these have yet been conclusively demonstrated to play a role in resistance to neutrophils. Better understanding of how these microbes survive oxidant exposure in the phagosome may provide therapeutic targets for sensitizing pathogenic mycobacteria to killing by the immune system. Pharmacological interventions might also be useful in limiting any adverse effects of NETs during mycobacterial infection.

AUTHOR CONTRIBUTIONS

HP compiled the first draft of the review, using additional content provided by LF, CK, and ND. MH edited the article and generated the final version. All authors contributed to the article and approved the submitted version.

FUNDING

This work was supported by the Canterbury Medical Research Foundation, the Health Research Council of New Zealand (15/479), and the Travis Trust of New Zealand.

REFERENCES

1. Tortoli E, Meehan CJ, Grottola A, Serpini GF, Fabio A, Trovato A, et al. Genome-Based Taxonomic Revision Detects a Number of Synonymous Taxa in the Genus Mycobacterium. *Infect Genet Evol* (2019) 75:103983. doi: 10.1016/j.meegid.2019.103983
2. World Health Organisation. *Global Tuberculosis Report 2020*. Geneva: World Health Organization (2020). p. 1–232.
3. World Health Organisation. Global Leprosy (Hansen Disease) Update, 2019: Time to Step-Up Prevention Initiatives. *Wkly Epidemiol Rec*. (2020) 95:417–40.
4. Daniel-Wayman S, Abate G, Barber DL, Bermudez LE, Coler RN, Cynamon MH, et al. Advancing Translational Science for Pulmonary Nontuberculous Mycobacterial Infections. A Road Map for Research. *Am J Respir Crit Care Med* (2019) 199(8):947–51. doi: 10.1164/rccm.201807-1273PP
5. Hmama Z, Pena-Diaz S, Joseph S, Av-Gay Y. Immunoevasion and Immunosuppression of the Macrophage by *Mycobacterium Tuberculosis*. *Immunol Rev* (2015) 264(1):220–32. doi: 10.1111/imr.12268
6. Houben EN, Nguyen L, Pieters J. Interaction of Pathogenic Mycobacteria With the Host Immune System. *Curr Opin Microbiol* (2006) 9(1):76–85. doi: 10.1016/j.mib.2005.12.014
7. Eum S-Y, Kong J-H, Hong M-S, Lee Y-J, Kim J-H, Hwang S-H, et al. Neutrophils Are the Predominant Infected Phagocytic Cells in the Airways of Patients With Active Pulmonary TB. *Chest* (2010) 137(1):122–8. doi: 10.1378/chest.09-0903
8. Winterbourn CC, Kettle AJ, Hampton MB. Reactive Oxygen Species and Neutrophil Function. *Annu Rev Biochem* (2016) 85(1):765–92. doi: 10.1146/annurev-biochem-060815-014442
9. Brinkmann V, Reichard U, Goosmann C, Fauler B, Uhlemann Y, Weiss DS, et al. Neutrophil Extracellular Traps Kill Bacteria. *Science* (2004) 303 (5663):1532–5. doi: 10.1126/science.1092385
10. Chapman EA, Lyon M, Simpson D, Mason D, Beynon RJ, Moots RJ, et al. Caught in a Trap? Proteomic Analysis of Neutrophil Extracellular Traps in Rheumatoid Arthritis and Systemic Lupus Erythematosus. *Front Immunol* (2019) 10:423. doi: 10.3389/fimmu.2019.00423
11. Petretto A, Bruschi M, Pratesi F, Croia C, Candiano G, Ghiggeri G, et al. Neutrophil Extracellular Traps (NET) Induced by Different Stimuli: A Comparative Proteomic Analysis. *PloS One* (2019) 14(7):e0218946. doi: 10.1371/journal.pone.0218946
12. Urban CF, Ermert D, Schmid M, Abu-Abed U, Goosmann C, Nacken W, et al. Neutrophil Extracellular Traps Contain Calprotectin, a Cytosolic Protein Complex Involved in Host Defense Against *Candida Albicans*. *PloS Pathog* (2009) 5(10):e1000639. doi: 10.1371/journal.ppat.1000639
13. Parker H, Albrett AM, Kettle AJ, Winterbourn CC. Myeloperoxidase Associated With Neutrophil Extracellular Traps Is Active and Mediates Bacterial Killing in the Presence of Hydrogen Peroxide. *J Leukoc Biol* (2012) 91(3):369–76. doi: 10.1189/jlb.0711387
14. Guimarães-Costa AB, Nascimento MT, Froment GS, Soares RP, Morgado FN, Conceição-Silva F, et al. *Leishmania Amazonensis* Promastigotes Induce and Are Killed by Neutrophil Extracellular Traps. *Proc Natl Acad Sci USA* (2009) 106(16):6748–53. doi: 10.1073/pnas.0900226106
15. Saffarzadeh M, Juenemann C, Queisser MA, Lochnit G, Barreto G, Galuska SP, et al. Neutrophil Extracellular Traps Directly Induce Epithelial and Endothelial Cell Death: A Predominant Role of Histones. *PloS One* (2012) 7: e32366. doi: 10.1371/journal.pone.0032366
16. Wang L, Zhou X, Yin Y, Mai Y, Wang D, Zhang X. Hyperglycemia Induces Neutrophil Extracellular Traps Formation Through an NADPH Oxidase-Dependent Pathway in Diabetic Retinopathy. *Front Immunol* (2019) 9:3076. doi: 10.3389/fimmu.2018.03076
17. Alvarez-Jimenez VD, Leyva-Paredes K, Garcia-Martinez M, Vazquez-Flores L, Garcia-Paredes VG, Campillo-Navarro M, et al. Extracellular Vesicles Released From *Mycobacterium Tuberculosis*-Infected Neutrophils Promote Macrophage Autophagy and Decrease Intracellular Mycobacterial Survival. *Front Immunol* (2018) 9:272. doi: 10.3389/fimmu.2018.00272
18. Rosales C. Neutrophils at the Crossroads of Innate and Adaptive Immunity. *J Leukoc Biol* (2020) 108(1):377–96. doi: 10.1002/JLB.4MIR0220-574RR
19. Cambier C, O'Leary SM, O'Sullivan MP, Keane J, Ramakrishnan L. Phenolic Glycolipid Facilitates Mycobacterial Escape From Microbicidal Tissue-Resident Macrophages. *Immunity* (2017) 47(3):552–65. doi: 10.1016/j.immuni.2017.08.003
20. Huang L, Nazarova EV, Tan S, Liu Y, Russell DG. Growth of *Mycobacterium tuberculosis In Vivo* Segregates With Host Macrophage Metabolism and Ontogeny. *J Exp Med* (2018) 215(4):1135–52. doi: 10.1084/jem.20172020
21. Martineau AR, Newton SM, Wilkinson KA, Kampmann B, Hall BM, Nawroly N, et al. Neutrophil-Mediated Innate Immune Resistance to Mycobacteria. *J Clin Invest* (2007) 117(7):1988–94. doi: 10.1172/jci31097
22. Estévez O, Anibarro L, Garet E, Martínez A, Pena A, Barcia L, et al. Multi-Parameter Flow Cytometry Immunophenotyping Distinguishes Different Stages of Tuberculosis Infection. *J Infect* (2020) 81:57–71. doi: 10.1016/j.jinf.2020.03.064
23. Olaniyi J, Aken'Ova Y. Haematological Profile of Patients With Pulmonary Tuberculosis in Ibadan, Nigeria. *Afr J Med Med Sci* (2003) 32(3):239–42.
24. Berry MP, Graham CM, McNab FW, Xu Z, Bloch SA, Oni T, et al. An Interferon-Inducible Neutrophil-Driven Blood Transcriptional Signature in Human Tuberculosis. *Nature* (2010) 466(7309):973–7. doi: 10.1038/nature09247

25. Lowe DM, Demaret J, Bangani N, Nakiwala JK, Goliath R, Wilkinson KA, et al. Differential Effect of Viable Versus Necrotic Neutrophils on *Mycobacterium Tuberculosis* Growth and Cytokine Induction in Whole Blood. *Front Immunol* (2018) 9:903. doi: 10.3389/fimmu.2018.00903
26. Jayachandran R, Sundaramurthy V, Combaluzier B, Mueller P, Korf H, Huygen K, et al. Survival of Mycobacteria in Macrophages Is Mediated by Coronin 1-Dependent Activation of Calcineurin. *Cell* (2007) 130(1):37–50. doi: 10.1016/j.cell.2007.04.043
27. Sundaramurthy V, Korf H, Singla A, Scherr N, Nguyen L, Ferrari G, et al. Survival of *Mycobacterium Tuberculosis* and *Mycobacterium Bovis* BCG in Lysosomes *In Vivo*. *Microbes Infect* (2017) 19(11):515–26. doi: 10.1016/j.micinf.2017.06.008
28. Levitte S, Adams KN, Berg RD, Cosma CL, Urdahl KB, Ramakrishnan L. Mycobacterial Acid Tolerance Enables Phagolysosomal Survival and Establishment of Tuberculous Infection. *vivo. Cell Host Microbe* (2016) 20 (2):250–8. doi: 10.1016/j.chom.2016.07.007
29. BoseDasgupta S, Pieters J. Macrophage-Microbe Interaction: Lessons Learned From the Pathogen *Mycobacterium Tuberculosis*. *Sem Immunopath* (2018) 40(6):577–91. doi: 10.1007/s00281-018-0710-0.
30. Abadie V, Badell E, Douillard P, Ensergueix D, Leenen PJ, Tanguy M, et al. Neutrophils Rapidly Migrate *via* Lymphatics After *Mycobacterium Bovis* BCG Intradermal Vaccination and Shuttle Live Bacilli to the Draining Lymph Nodes. *Blood* (2005) 106(5):1843–50. doi: 10.1182/blood-2005-03-1281
31. Eruslanov EB, Lyadova IV, Kondratieva TK, Majorov KB, Scheglov IV, Orlova MO, et al. Neutrophil Responses to *Mycobacterium Tuberculosis* Infection in Genetically Susceptible and Resistant Mice. *Infect Immun* (2005) 73(3):1744–53. doi: 10.1128/iai.73.3.1744-1753.2005
32. Spinner JL, Winfree S, Starr T, Shannon JG, Nair V, Steele-Mortimer O, et al. *Yersinia Pestis* Survival and Replication Within Human Neutrophil Phagosomes and Uptake of Infected Neutrophils by Macrophages. *J Leukoc Biol* (2014) 95(3):389–98. doi: 10.1189/jlb.1112551
33. Rupp J, Pfleiderer L, Jugert C, Moeller S, Klinger M, Dalhoff K, et al. *Chlamydia Pneumoniae* Hides Inside Apoptotic Neutrophils to Silently Infect and Propagate in Macrophages. *PloS One* (2009) 4:e6020. doi: 10.1371/journal.pone.0006020
34. van Zandbergen G, Klinger M, Mueller A, Dannenberg S, Gebert A, Solbach W, et al. Cutting Edge: Neutrophil Granulocyte Serves as a Vector for Leishmania Entry Into Macrophages. *J Immunol* (2004) 173(11):6521–5. doi: 10.4049/jimmunol.173.11.6521
35. Tan BH, Meinken C, Bastian M, Bruns H, Legaspi A, Ochoa MT, et al. Macrophages Acquire Neutrophil Granules for Antimicrobial Activity Against Intracellular Pathogens. *J Immunol* (2006) 177(3):1864–71. doi: 10.4049/jimmunol.177.3.1864
36. Dallenga T, Repnik U, Corleis B, Eich J, Reimer R, Griffiths GW, et al. *M. Tuberculosis*-Induced Necrosis of Infected Neutrophils Promotes Bacterial Growth Following Phagocytosis by Macrophages. *Cell Host Microbe* (2017) 22(4):519–30. doi: 10.1016/j.chom.2017.09.003
37. Pfrommer E, Dreier C, Gabriel G, Dallenga T, Reimer R, Schepanski K, et al. Enhanced Tenacity of Mycobacterial Aerosols From Necrotic Neutrophils. *Sci Rep* (2020) 10(1):1–14. doi: 10.1038/s41598-020-65781-9
38. Sánchez F, Radaeva TV, Nikonenko BV, Persson A-S, Sengul S, Schalling M, et al. Multigenic Control of Disease Severity After Virulent *Mycobacterium Tuberculosis* Infection in Mice. *Infect Immun* (2003) 71(1):126–31. doi: 10.1128/IAI.71.1.126-131.2003
39. Bogle G, Dunbar PR. Simulating T-Cell Motility in the Lymph Node Paracortex With a Packed Lattice Geometry. *Immunol Cell Biol* (2008) 86 (8):676–87. doi: 10.1038/icb.2008.60
40. Vono M, Lin A, Norrby-Teglund A, Koup RA, Liang F, Loré K. Neutrophils Acquire the Capacity for Antigen Presentation to Memory CD4+ T Cells. *Vitro ex vivo. Blood* (2017) 129(14):1991–2001. doi: 10.1182/blood-2016-10-744441
41. Blomgran R, Ernst JD. Lung Neutrophils Facilitate Activation of Naive Antigen-Specific CD4+ T Cells During *Mycobacterium Tuberculosis* Infection. *J Immunol* (2011) 186(12):7110–9. doi: 10.4049/jimmunol.1100001
42. Chai Q, Lu Z, Liu CH. Host Defense Mechanisms Against *Mycobacterium Tuberculosis*. *Cell Mol Life Sci* (2019) 77:1859–78. doi: 10.1007/s00018-019-03353-5
43. Cambier C, Falkow S, Ramakrishnan L. Host Evasion and Exploitation Schemes of *Mycobacterium Tuberculosis*. *Cell* (2014) 159(7):1497–509. doi: 10.1016/j.cell.2014.11.024
44. Cosma CL, Humbert O, Ramakrishnan L. Superinfecting Mycobacteria Home to Established Tuberculous Granulomas. *Nat Immunol* (2004) 5 (8):828–35. doi: 10.1038/ni1091
45. Saunders BM, Cooper AM. Restraining Mycobacteria: Role of Granulomas in Mycobacterial Infections. *Immunol Cell Biol* (2000) 78(4):334–41. doi: 10.1046/j.1440-1711.2000.00933.x
46. Yang C-T, Cambier CJ, Davis JM, Hall CJ, Crosier PS, Ramakrishnan L. Neutrophils Exert Protection in the Early Tuberculous Granuloma by Oxidative Killing of Mycobacteria Phagocytosed From Infected Macrophages. *Cell Host Microbe* (2012) 12(3):301–12. doi: 10.1016/j.chom.2012.07.009
47. Gopal R, Monin L, Torres D, Slight S, Mehra S, McKenna KC, et al. S100A8/A9 Proteins Mediate Neutrophilic Inflammation and Lung Pathology During Tuberculosis. *Am J Respir Crit Care Med* (2013) 188(9):1137–46. doi: 10.1164/rccm.201304-0803OC
48. Scott NR, Swanson RV, Al-Hammadi N, Domingo-Gonzalez R, Rangel-Moreno J, Kriel BA, et al. S100A8/A9 Regulates CD11b Expression and Neutrophil Recruitment During Chronic Tuberculosis. *J Clin Invest* (2020) 130:3098–112. doi: 10.1172/JCI130546
49. Jones TPW, Dabbaj S, Mandal I, Cleverley J, Cash C, Lipman MCI, et al. The Blood Neutrophil Count After 1 Month of Treatment Predicts the Radiologic Severity of Lung Disease at Treatment End. *Chest* (2021) 160 (6):2030–41.. doi: 10.1016/j.chest.2021.07.041
50. Niazi MK, Dhulekar N, Schmidt D, Major S, Cooper R, Abeijon C, et al. Lung Necrosis and Neutrophils Reflect Common Pathways of Susceptibility to *Mycobacterium Tuberculosis* in Genetically Diverse, Immune-Competent Mice. *Dis Model Mech* (2015) 8(9):1141–53. doi: 10.1242/dmm.020867
51. Nandi B, Behar SM. Regulation of Neutrophils by Interferon-γ Limits Lung Inflammation During Tuberculosis Infection. *J Exp Med* (2011) 208 (11):2251–62. doi: 10.1084/jem.20110919
52. Mishra BB, Lovewell RR, Olive AJ, Zhang G, Wang W, Eugenin E, et al. Nitric Oxide Prevents a Pathogen-Permissive Granulocytic Inflammation During Tuberculosis. *Nat Microbiol* (2017) 2(7):1–11. doi: 10.1038/nmicrobiol.2017.72
53. Pedrosa J, Saunders BM, Appelberg R, Orme IM, Silva MT, Cooper AM. Neutrophils Play a Protective Nonphagocytic Role in Systemic *Mycobacterium Tuberculosis* Infection of Mice. *Infect Immun* (2000) 68 (2):577–83. doi: 10.1128/IAI.68.2.577-583.2000
54. Sugawara I, Udagawa T, Yamada H. Rat Neutrophils Prevent the Development of Tuberculosis. *Infect Immun* (2004) 72(3):1804–6. doi: 10.1128/IAI.72.3.1804-1806.2004
55. Carvalho ACC, Amorim G, Melo MGM, Silveira AKA, Vargas PHL, Moreira ASR, et al. Pre-Treatment Neutrophil Count as a Predictor of Antituberculosis Therapy Outcomes: A Multicenter Prospective Cohort Study. *Front Immunol* (2021) 12:661934. doi: 10.3389/fimmu.2021.661934
56. McDougall A, Rees R, Weddell A, Wajdi Kanan M. The Histopathology of Lepromatous Leprosy in the Nose. *J Path* (1975) 115(4):215–26. doi: 10.1002/path.1711150406
57. Kumar V, Sachan T, Natrajan M, Sharma A. High Resolution Structural Changes of Schwann Cell and Endothelial Cells in Peripheral Nerves Across Leprosy Spectrum. *Ultrastruct Path* (2014) 38(2):86–92. doi: 10.3109/01913123.2013.870273
58. Montoya D, Cruz D, Teles RM, Lee DJ, Ochoa MT, Krutzik SR, et al. Divergence of Macrophage Phagocytic and Antimicrobial Programs in Leprosy. *Cell Host Microbe* (2009) 6(4):343–53. doi: 10.1016/j.chom.2009.09.002
59. Spierings E, De Boer T, Zulianello L, Ottenhoff T. The Role of Schwann Cells, T Cells and *Mycobacterium Leprae* in the Immunopathogenesis of Nerve Damage in Leprosy. *Lepr Rev* (2000) 71(Suppl):S121–S9.
60. Drutz DJ, Chen TS, Lu W-H. The Continuous Bacteremia of Lepromatous Leprosy. *N Eng J Med* (1972) 287(4):159–64. doi: 10.1056/NEJM197207272870402
61. Sarita S, Muhammed K, Najeeba R, Rajan GN, Anza K, Binitha MP, et al. A Study on Histological Features of Lepra Reactions in Patients Attending the Dermatology Department of the Government Medical College, Calicut, Kerala, India. *Lepr Rev* (2013) 84(1):51–64.

62. Schmitz V, Prata R, Barbosa M, Mendes MA, Brandão SS, Amadeu TP, et al. Expression of CD64 on Circulating Neutrophils Favoring Systemic Inflammatory Status in Erythema Nodosum Leprosum. *PloS Negl Trop Dis* (2016) 10(8):e0004955. doi: 10.1371/journal.pntd.0004955
63. Polycarpou A, Walker SL, Lockwood DN. A Systematic Review of Immunological Studies of Erythema Nodosum Leprosum. *Front Immunol* (2017) 8:233. doi: 10.3389/fimmu.2017.00233
64. Pocaterra L, Jain S, Reddy R, Muzaffarullah S, Torres O, Suneetha S, et al. Clinical Course of Erythema Nodosum Leprosum: An 11-Year Cohort Study in Hyderabad, India. *Am J Trop Med Hyg* (2006) 74(5):868–79.
65. Walker SL, Balagon M, Darlong J, Doni SN, Hagge DA, Halwai V, et al. ENLIST 1: An International Multi-Centre Cross-Sectional Study of the Clinical Features of Erythema Nodosum Leprosum. *PloS Negl Trop Dis* (2015) 9(9):e0004065. doi: 10.1371/journal.pntd.0004065
66. Walker SL, Lebas E, Doni SN, Lockwood DN, Lambert SM. The Mortality Associated With Erythema Nodosum Leprosum in Ethiopia: A Retrospective Hospital-Based Study. *PloS Negl Trop Dis* (2014) 8(3):e2690. doi: 10.1371/journal.pntd.0002690
67. Mabalay M, Helwig E, Tolentino J, Binford C. The Histopathology and Histochemistry of Erythema Nodosum Leprosum. *Int J Lepr* (1965) 33 (1):28–49.
68. Schmitz V, Tavares IF, Pacheco F, dos Santos JB, dos Santos CO, Sarno EN. Neutrophils in Leprosy. *Front Immunol* (2019) 10:495. doi: 10.3389/fimmu.2019.00495
69. Pinheiro RO, Schmitz V, Silva B, Dias AA, De Souza BJ, de Mattos Barbosa MG, et al. Innate Immune Responses in Leprosy. *Front Immunol* (2018) 9:518. doi: 10.3389/fimmu.2018.00518
70. Goihman-Yahr M, Rodriguez-Ochoa G, Aranzazu N, Convit J. Polymorphonuclear Activation in Leprosy. I. Spontaneous and Endotoxin-Stimulated Reduction of Nitroblue Tetrazolium: Effects of Serum and Plasma on Endotoxin-Induced Activation. *Clin Exp Immunol* (1975) 20(2):257.
71. Sher R, Anderson R, Glover A, Wadee AA. Polymorphonuclear Cell Function in the Various Polar Types of Leprosy and Erythema Nodosum Leprosum. *Infect Immun* (1978) 21(3):959–65. doi: 10.1128/iai.21.3.959-965.1978
72. Park BH, Fikrig SM, Smithwick EM. Infection and Nitroblue-Tetrazolium Reduction by Neutrophils: A Diagnostic Aid. *Lancet* (1968) 292(7567):532–4. doi: 10.1016/S0140-6736(68)92406-9
73. Hohn DC, Lehrer RI. Mechanism of the Heparin Effect on the Nitroblue-Tetrazolium Slide Test. *Infect Immun* (1974) 10(4):772–5. doi: 10.1128/iai.10.4.772-775.1974
74. Schiff DE, Rae J, Martin TR, Davis BH, Curnutte JT. Increased Phagocyte Fc gammaRI Expression and Improved Fc Gamma-Receptor-Mediated Phagocytosis After in Vivo Recombinant Human Interferon-Gamma Treatment of Normal Human Subjects. *Blood* (1997) 90(8):3187–94. doi: 10.1182/blood.V90.8.3187
75. Mendes MA, de Carvalho DS, Amadeu TP, Silva B, Prata R, da Silva CO, et al. Elevated Pentraxin-3 Concentrations in Patients With Leprosy: Potential Biomarker of Erythema Nodosum Leprosum. *J Infect Dis* (2017) 216(12):1635–43. doi: 10.1093/infdis/jix267
76. Daley C. *Mycobacterium Avium* Complex Disease. *Microbiol Spectr* (2017) 5: TNMI7–0045-2017. doi: 10.1128/microbiolspec.TNMI7-0045-2017
77. Gallin JI, Bujak JS, Patten E, Wolff SM. Granulocyte Function in the Chediak-Higashi Syndrome of Mice. *Blood* (1974) 43(2):201–6. doi: 10.1182/blood.V43.2.201.201
78. Appelberg R, Castro AG, Gomes S, Pedrosa J, Silva MT. Susceptibility of Beige Mice to *Mycobacterium Avium*: Role of Neutrophils. *Infect Immun* (1995) 63(9):3381–7. doi: 10.1128/iai.63.9.3381-3387.1995
79. Saunders BM, Cheers C. Intranasal Infection of Beige Mice With *Mycobacterium Avium* Complex: Role of Neutrophils and Natural Killer Cells. *Infect Immun* (1996) 64(10):4236–41. doi: 10.1128/iai.64.10.4236-4241.1996
80. Matsuyama M, Ishii Y, Sakurai H, Ano S, Morishima Y, Yoh K, et al. Overexpression of Rorγt Enhances Pulmonary Inflammation After Infection With *Mycobacterium Avium*. *PloS One* (2016) 11(1):e0147064. doi: 10.1371/journal.pone.0147064
81. Yamazaki Y, Kubo K, Sekiguchi M, Honda T. Analysis of BAL Fluid in *M. Avium*-Intracellulare Infection in Individuals Without Predisposing Lung Disease. *Eur Respir J* (1998) 11(6):1227–31. doi: 10.1183/09031936.98.11061227
82. Yamazaki Y, Kubo K, Takamizawa A, Yamamoto H, Honda T, Sone S. Markers Indicating Deterioration of Pulmonary *Mycobacterium Avium*-Intracellulare Infection. *Am J Respir Crit Care Med* (1999) 160(6):1851–5. doi: 10.1164/ajrccm.160.6.9902019
83. Inomata T, Konno S, Nagai K, Suzuki M, Nishimura M. Neutrophil Predominance in Bronchoalveolar Lavage Fluid Is Associated With Disease Severity and Progression of HRCT Findings in Pulmonary *Mycobacterium Avium* Infection. *PloS One* (2018) 13(2):e0190189. doi: 10.1371/journal.pone.0190189
84. Gommans EPAT, Even P, Linssen CFM, van Dessel H, van Haren E, de Vries GJ, et al. Risk Factors for Mortality in Patients With Pulmonary Infections With Non-Tuberculous Mycobacteria: A Retrospective Cohort Study. *Respir Med* (2015) 109(1):137–45. doi: 10.1016/j.rmed.2014.10.013
85. Van Ingen J, Bendien SA, De Lange WCM, Hoefsloot W, Dekhuijzen PNR, Boeree MJ, et al. Clinical Relevance of Non-Tuberculous Mycobacteria Isolated in the Nijmegen-Arnhem Region, The Netherlands. *Thorax* (2009) 64(6):502–6. doi: 10.1136/thx.2008.110957
86. Johnston JC CL, Elwood K. *Mycobacterium Kansasii*. *Microbiol Spectr* (2017) 5:TNMI7–0011-2016. doi: 10.1128/microbiolspec.TNMI7-0011-2016
87. Smith MB, Molina CP, Schnadig VJ, Boyars MC, Aronson JF. Pathologic Features of *Mycobacterium Kansasii* Infection in Patients With Acquired Immunodeficiency Syndrome. *Arch Path Lab Med* (2003) 127(5):554–60. doi: 10.5858/2003-127-0554-PFOMKI
88. Domfeh AB, Nodit L, Gradowski JF, Bastacky S. *Mycobacterium Kansasii* Infection Diagnosed by Pleural Fluid Cytology. *Acta Cytol* (2007) 51(4):627–30. doi: 10.1159/000325813
89. Schnadig VJ, Quadri SF, Boyvat F, Borucki M. *Mycobacterium Kansasii* Osteomyelitis Presenting as a Solitary Lytic Lesion of the Ulna: Fine-Needle Aspiration Findings and Morphologic Comparison With Other Mycobacteria. *Diagn Cytopathol* (1998) 19(2):94–7. doi: 10.1002/(SICI)1097-0339(199808)19:2<94::AID-DC4>3.0.CO;2-N
90. Silva MT, Silva MNT, Appelberg R. Neutrophil-Macrophage Cooperation in the Host Defence Against Mycobacterial Infections. *Microb Pathog* (1989) 6 (5):369–80. doi: 10.1016/0882-4010(89)90079-X
91. Johansen MD, Herrmann J-L, Kremer L. Non-Tuberculous Mycobacteria and the Rise of *Mycobacterium Abscessus*. *Nat Rev Microbiol* (2020) 18:392–407. doi: 10.1038/s41579-020-0331-1
92. Dedrick RM, Guerrero-Bustamante CA, Garlena RA, Russell DA, Ford K, Harris K, et al. Engineered Bacteriophages for Treatment of a Patient With a Disseminated Drug-Resistant *Mycobacterium Abscessus*. *Nat Med* (2019) 25 (5):730–3. doi: 10.1038/s41591-019-0437-z
93. Griffith DE, Aksamit T, Brown-Elliott BA, Catanzaro A, Daley C, Gordin F, et al. An Official ATS/IDSA Statement: Diagnosis, Treatment, and Prevention of Nontuberculous Mycobacterial Diseases. *Am J Respir Crit Care Med* (2007) 175(4):367–416. doi: 10.1164/rccm.200604-571ST
94. Kwak N, Dalcolmo MP, Daley CL, Eather G, Gayoso R, Hasegawa N, et al. *Mycobacterium Abscessus* Pulmonary Disease: Individual Patient Data Meta-Analysis. *Eur Respir J* (2019) 54(1):1801991. doi: 10.1183/13993003.01991-2018
95. Nessar R, Cambau E, Reyrat JM, Murray A, Gicquel B. *Mycobacterium Abscessus*: A New Antibiotic Nightmare. *J Antimicrob Chemother* (2012) 67 (4):810–8. doi: 10.1093/jac/dkr578
96. Chuang A-Y, Tsou M-H, Chang S-J, Yang L-Y, Shih C-C, Tsai M-P, et al. *Mycobacterium Abscessus* Granulomatous Prostatitis. *Am J Surg Pathol* (2012) 36(3):418–22. doi: 10.1097/PAS.0b013e31823dafad
97. Rodriguez G, Ortegon M, Camargo D, Orozco L. Iatrogenic *Mycobacterium Abscessus* Infection: Histopathology of 71 Patients. *Brit J Dermatol* (1997) 137(2):214–8. doi: 10.1046/j.1365-2133.1997.18081891.x
98. Choi H, Kim YI, Na CH, Kim MS, Shin BS. *Mycobacterium Abscessus* Skin Infection Associated With Shaving Activity in a 75-Year-Old Man. *Ann Geriatr Med Res* (2018) 22(4):204–7. doi: 10.4235/agmr.18.0034
99. Ganbat D, Seehase S, Richter E, Vollmer E, Reiling N, Fellenberg K, et al. Mycobacteria Infect Different Cell Types in the Human Lung and Cause

Species Dependent Cellular Changes in Infected Cells. *BMC Pulmon Med* (2016) 16(1):1–16. doi: 10.1186/s12890-016-0185-5

100. Pawlik A, Garnier G, Orgeur M, Tong P, Lohan A, Le Chevalier F, et al. Identification and Characterization of the Genetic Changes Responsible for the Characteristic Smooth-to-Rough Morphotype Alterations of Clinically Persistent *Mycobacterium Abscessus*. *Mol Microbiol* (2013) 90(3):612–29. doi: 10.1111/mmi.12387
101. Catherinot E, Roux A-L, Macheras E, Hubert D, Matmar M, Dannhoffer L, et al. Acute Respiratory Failure Involving an R Variant of *Mycobacterium Abscessus*. *J Clin Microbiol* (2009) 47(1):271–4. doi: 10.1128/JCM.01478-08
102. Caverly LJ, Caceres SM, Fratelli C, Happoldt C, Kidwell KM, Malcolm KC, et al. *Mycobacterium Abscessus* Morphotype Comparison in a Murine Model. *PloS One* (2015) 10(2):e0117657. doi: 10.1371/journal.pone.0117657
103. Bernut A, Herrmann J-L, Kissa K, Dubremetz J-F, Gaillard J-L, Lutfalla G, et al. *Mycobacterium Abscessus* Cording Prevents Phagocytosis and Promotes Abscess Formation. *Proc Natl Acad Sci USA* (2014) 111(10): E943–52. doi: 10.1073/pnas.1321390111
104. Bernut A, Nguyen-Chi M, Halloum I, Herrmann J-L, Lutfalla G, Kremer L. *Mycobacterium Abscessus*-Induced Granuloma Formation Is Strictly Dependent on TNF Signaling and Neutrophil Trafficking. *PloS Pathog* (2016) 12(11):1005986. doi: 10.1371/journal.ppat.1005986
105. Best CA, Best TJ. *Mycobacterium Smegmatis* Infection of the Hand. *Hand* (2009) 4(2):165–6. doi: 10.1007/s11552-008-9147-6
106. Newton JAJr., Weiss PJ, Bowler WA, Oldfield ECIII. Soft-Tissue Infection Due to *Mycobacterium Smegmatis*: Report of Two Cases. *Clin Infect Dis* (1993) 16(4):531–3. doi: 10.1093/clind/16.4.531
107. Wallace RJJr., Nash DR, Tsukamura M, Blacklock ZM, Silcox VA. Human Disease Due to *Mycobacterium Smegmatis*. *J Infect Dis* (1988) 158(1):52–9. doi: 10.1093/infdis/158.1.52
108. Sevrin A, Reboli AC. Disseminated *Mycobacterium Smegmatis* Infection Associated With an Implantable Cardioverter Defibrillator. *Infect Dis Clin Pract* (2009) 17(5):349–51. doi: 10.1097/IPC.0b013e31819b8a9b
109. Brown-Elliott BA, Wallace RJ. Clinical and Taxonomic Status of Pathogenic Nonpigmented or Late-Pigmenting Rapidly Growing Mycobacteria. *Clin Microbiol Rev* (2002) 15(4):716–46. doi: 10.1128/CMR.15.4.716-746.2002
110. Saffo Z, Ognjan A. *Mycobacterium Smegmatis* Infection of a Prosthetic Total Knee Arthroplasty. *IDCases* (2016) 5:80–2. doi: 10.1016/j.idcr.2016.07.007
111. Wang J, Zhu X, Peng Y, Zhu T, Liu H, Zhu Y, et al. *Mycobacterium Tuberculosis* YrbE3A Promotes Host Innate Immune Response by Targeting NF-κb/JNK Signaling. *Microorganisms* (2020) 8(4):584. doi: 10.3390/microorganisms8040584
112. Miralda I, Klaes CK, Graham JE, Uriarte SM. Human Neutrophil Granule Exocytosis in Response to *Mycobacterium Smegmatis*. *Pathogens* (2020) 9 (2):123. doi: 10.3390/pathogens9020123
113. Cougoule C, Constant P, Etienne G, Daffé M, Maridonneau-Parini I. Lack of Fusion of Azurophil Granules With Phagosomes During Phagocytosis of *Mycobacterium Smegmatis* by Human Neutrophils Is Not Actively Controlled by the Bacterium. *Infect Immun* (2002) 70(3):1591–8. doi: 10.1128/iai.70.3.1591-1598.2002
114. Nauseef WM. How Human Neutrophils Kill and Degrade Microbes: An Integrated View. *Immunol Rev* (2007) 219(1):88–102. doi: 10.1111/j.1600-065X.2007.00550.x
115. Corleis B, Korbel D, Wilson R, Bylund J, Chee R, Schaible UE. Escape of *Mycobacterium Tuberculosis* From Oxidative Killing by Neutrophils. *Cell Microbiol* (2012) 14(7):1109–21. doi: 10.1111/j.1462-5822.2012.01783.x
116. Majeed M, Perskvist N, Ernst JD, Orselius K, Stendahl O. Roles of Calcium and Annexins in Phagocytosis and Elimination of an Attenuated Strain of *Mycobacterium Tuberculosis* in Human Neutrophils. *Microb Pathog* (1998) 24(5):309–20. doi: 10.1006/mpat.1997.0200
117. N'Diaye E-N, Darzacq X, Astarie-Dequeker C, Daffé M, Calafat J, Maridonneau-Parini I. Fusion of Azurophil Granules With Phagosomes and Activation of the Tyrosine Kinase Hck Are Specifically Inhibited During Phagocytosis of Mycobacteria by Human Neutrophils. *J Immunol* (1998) 161 (9):4983–91.
118. Seiler P, Aichele P, Raupach B, Odermatt B, Steinhoff U, Kaufmann SHE. Rapid Neutrophil Response Controls Fast-Replicating Intracellular Bacteria But Not Slow-Replicating *Mycobacterium Tuberculosis*. *J Infect Dis* (2000) 181(2):671–80. doi: 10.1086/315278
119. Repasy T, Lee J, Marino S, Martinez N, Kirschner DE, Hendricks G, et al. Intracellular Bacillary Burden Reflects a Burst Size for *Mycobacterium Tuberculosis In Vivo*. *PloS Pathog* (2013) 9(2):e1003190. doi: 10.1371/journal.ppat.1003190
120. Hartmann P, Becker R, Franzen C, Schell-Frederick E, Römer J, Jacobs M, et al. Phagocytosis and Killing of *Mycobacterium Avium* Complex by Human Neutrophils. *J Leuk Biol* (2001) 69(3):397–404. doi: 10.1189/jlb.69.3.397
121. Ladero-Aunon I, Molina E, Holder A, Kolakowski J, Harris H, Urkitza A, et al. Bovine Neutrophils Release Extracellular Traps and Cooperate With Macrophages in *Mycobacterium Avium Subsp. Paratuberculosis* Clearance *In Vitro*. *Front Immunol* (2021) 12:645304. doi: 10.3389/fimmu.2021.645304
122. Doz-Deblauwe E, Carreras F, Arbues A, Remot A, Epardaud M, Malaga W, et al. CR3 Engaged by PGL-I Triggers Syk-Calcineurin-NFATc to Rewire the Innate Immune Response in Leprosy. *Front Immunol* (2019) 10:2913. doi: 10.3389/fimmu.2019.02913
123. Peyron P, Bordier C, Elsa-Noah N, Maridonneau-Parini I. Nonopsonic Phagocytosis of *Mycobacterium Kansasii* by Human Neutrophils Depends on Cholesterol and is Mediated by CR3 Associated With Glycosylphosphatidylinositol-Anchored Proteins. *J Immunol* (2000) 165 (9):5186–91. doi: 10.4049/jimmunol.165.9.5186
124. Garner AE, Smith DA, Hooper NM. Sphingomyelin Chain Length Influences the Distribution of GPI-Anchored Proteins in Rafts in Supported Lipid Bilayers. *Mol Memb Biol* (2007) 24(3):233–42. doi: 10.1080/09687860601127770
125. Iwabuchi K. Involvement of Glycosphingolipid-Enriched Lipid Rafts in Inflammatory Responses. *Front Biosci* (2015) 20(2):325–34. doi: 10.2741/4312
126. Nakayama H, Kurihara H, Morita YS, Kinoshita T, Mauri L, Prinetti A, et al. Lipoarabinomannan Binding to Lactosylceramide in Lipid Rafts Is Essential for the Phagocytosis of Mycobacteria by Human Neutrophils. *Sci Signal* (2016) 9(449)::ra101. doi: 10.1126/scisignal.aaf1585
127. Parker HA, Dickerhof N, Forrester L, Ryburn H, Smyth L, Messens J, et al. *Mycobacterium Smegmatis* Resists the Bactericidal Activity of Hypochlorous Acid Produced in Neutrophil Phagosomes. *J Immunol* (2021) 206(8):1901–12. doi: 10.4049/jimmunol.2001084
128. Hampton MB, Vissers MCM, Winterbourn CC. A Single Assay for Measuring the Rates of Phagocytosis and Bacterial Killing by Neutrophils. *J Leukoc Biol* (1994) 55(2):147–52. doi: 10.1002/jlb.55.2.147
129. Malcolm KC, Nichols EM, Caceres SM, Kret JE, Martiniano SL, Sagel SD, et al. *Mycobacterium Abscessus* Induces a Limited Pattern of Neutrophil Activation That Promotes Pathogen Survival. *PloS One* (2013) 8(2):e57402. doi: 10.1371/journal.pone.0057402
130. Geertsma MF, Nibbering PH, Pos O, Van Furth R. Interferon-γ-Activated Human Granulocytes Kill Ingested *Mycobacterium Fortuitum* More Efficiently Than Normal Granulocytes. *Eur J Immunol* (1990) 20(4):869–73. doi: 10.1002/eji.1830200423
131. Hampton MB, Winterbourn CC. Modification of Neutrophil Oxidant Production With Diphenyleneiodonium and Its Effect on Bacterial Killing. *Free Radic Biol Med* (1995) 18(4):633–9. doi: 10.1016/0891-5849(94)00181-i
132. Alemán M, de la Barrera SS, Schierloh PL, Alves L, Yokobori N, Baldini M, et al. In Tuberculous Pleural Effusions, Activated Neutrophils Undergo Apoptosis and Acquire a Dendritic Cell–Like Phenotype. *J Infect Dis* (2005) 192(3):399–409. doi: 10.1086/431680
133. Hilda JN, Das S. Neutrophil CD64, TLR2 and TLR4 Expression Increases But Phagocytic Potential Decreases During Tuberculosis. *Tuberculosis* (2018) 111:135–42. doi: 10.1016/j.tube.2018.06.010
134. Shalekoff S, Tiemessen CT, Gray CM, Martin DJ. Depressed Phagocytosis and Oxidative Burst in Polymorphonuclear Leukocytes From Individuals With Pulmonary Tuberculosis With or Without Human Immunodeficiency Virus Type 1 Infection. *Clin Diagn Lab Immunol* (1998) 5(1):41–4. doi: 10.1128/CDLI.5.1.41-44
135. da Glória Bonecini-Almeida M, Werneck-Barroso E, Carvalho PB, de Moura CP, Andrade EF, Hafner A, et al. Functional Activity of Alveolar and Peripheral Cells in Patients With Human Acquired Immunodeficiency Syndrome and Pulmonary Tuberculosis. *Cell Immunol* (1998) 190(2):112–20. doi: 10.1006/cimm.1998.1399
136. Moura ACN, Modolell M, Mariano M. Down-Regulatory Effect of Mycobacterium Leprae Cell Wall Lipids on Phagocytosis, Oxidative

Respiratory Burst and Tumour Cell Killing by Mouse Bone Marrow Derived Macrophages. *Scand J Immunol* (1997) 46(5):500–5. doi: 10.1046/j.1365-3083.1997.d01-158.x
137. Arcos J, Sasindran SJ, Fujiwara N, Turner J, Schlesinger LS, Torrelles JB. Human Lung Hydrolases Delineate *Mycobacterium Tuberculosis*–Macrophage Interactions and the Capacity to Control Infection. *J Immunol* (2011) 187(1):372–81. doi: 10.4049/jimmunol.1100823
138. Arcos J, Diangelo LE, Scordo JM, Sasindran SJ, Moliva JI, Turner J, et al. Lung Mucosa Lining Fluid Modification of *Mycobacterium Tuberculosis* to Reprogram Human Neutrophil Killing Mechanisms. *J Infect Dis* (2015) 212:948–58. doi: 10.1093/infdis/jiv146
139. Scordo JM, Arcos J, Kelley HV, Diangelo L, Sasindran SJ, Youngmin E, et al. *Mycobacterium Tuberculosis* Cell Wall Fragments Released Upon Bacterial Contact With the Human Lung Mucosa Alter the Neutrophil Response to Infection. *Front Immunol* (2017) 8:307. doi: 10.3389/fimmu.2017.00307
140. Jones GS, Amirault HJ, Andersen BR. Killing of *Mycobacterium Tuberculosis* by Neutrophils: A Nonoxidative Process. *J Infect Dis* (1990) 162(3):700–4. doi: 10.1093/infdis/162.3.700
141. Brown AE, Holzer TJ, Andersen BR. Capacity of Human Neutrophils to Kill *Mycobacterium Tuberculosis*. *J Infect Dis* (1987) 156(6):985–9. doi: 10.1093/infdis/156.6.985
142. Kisich KO, Higgins M, Diamond G, Heifets L. Tumor Necrosis Factor Alpha Stimulates Killing of *Mycobacterium Tuberculosis* by Human Neutrophils. *Infect Immun* (2002) 70(8):4591–9. doi: 10.1128/iai.70.8.4591-4599.2002
143. Denis M. Human Neutrophils, Activated With Cytokines or Not, do Not Kill Virulent *Mycobacterium Tuberculosis*. *J Infect Dis* (1991) 163(4):919–20. doi: 10.1093/infdis/163.4.919
144. González-Cortés C, Reyes-Ruvalcaba D, Diez-Tascón C, Rivero-Lezcano OM. Apoptosis and Oxidative Burst in Neutrophils Infected With Mycobacterium Spp. *Immunol Lett* (2009) 126(1–2):16–21. doi: 10.1016/j.imlet.2009.07.006
145. Reyes-Ruvalcaba D, González-Cortés C, Rivero-Lezcano OM. Human Phagocytes Lack the Ability to Kill *Mycobacterium Gordonae*, a Non-Pathogenic Mycobacteria. *Immunol Lett* (2008) 116(1):72–8. doi: 10.1016/j.imlet.2007.11.010
146. Malcolm KC, Caceres SM, Pohl K, Poch KR, Bernut A, Kremer L, et al. Neutrophil Killing of Mycobacterium Abscessus by Intra-and Extracellular Mechanisms. *PloS One* (2018) 13(4):e0196120. doi: 10.1371/journal.pone.0196120
147. Bernut A, Dupont C, Ogryzko NV, Neyret A, Herrmann J-L, Floto RA, et al. CFTR Protects Against *Mycobacterium Abscessus* Infection by Fine-Tuning Host Oxidative Defenses. *Cell Rep* (2019) 26(7):1828–40. doi: 10.1016/j.celrep.2019.01.071
148. Ramos-Kichik V, Mondragón-Flores R, Mondragón-Castelán M, Gonzalez-Pozos S, Muñiz-Hernandez S, Rojas-Espinosa O, et al. Neutrophil Extracellular Traps Are Induced by *Mycobacterium Tuberculosis*. *Tuberculosis* (2009) 89(1):29–37. doi: 10.1016/j.tube.2008.09.009
149. Borelli V, Banfi E, Perrotta MG, Zabucchi G. Myeloperoxidase Exerts Microbicidal Activity Against *Mycobacterium Tuberculosis*. *Infect Immun* (1999) 67(8):4149–52. doi: 10.1128/IAI.67.8.4149-4152.1999
150. Klebanoff SJ, Shepard CC. Toxic Effect of the Peroxidase-Hydrogen Peroxide-Halide Antimicrobial System on *Mycobacterium Leprae*. *Infect Immun* (1984) 44(2):534. doi: 10.1128/iai.44.2.534-536.1984
151. Chapman ALP, Hampton MB, Senthilmohan R, Winterbourn CC, Kettle AJ. Chlorination of Bacterial and Neutrophil Proteins During Phagocytosis and Killing of *Staphylococcus Aureus*. *J Biol Chem* (2002) 277(12):9757–62. doi: 10.1074/jbc.M106134200
152. Green JN, Kettle AJ, Winterbourn CC. Protein Chlorination in Neutrophil Phagosomes and Correlation With Bacterial Killing. *Free Radic Biol Med* (2014) 77:49–56. doi: 10.1016/j.freeradbiomed.2014.08.013
153. Segal BH, Leto TL, Gallin JI, Malech HL, Holland SM. Genetic, Biochemical, and Clinical Features of Chronic Granulomatous Disease. *Medicine* (2000) 79(3):170–200. doi: 10.1097/00005792-200005000-00004
154. Lau Y, Chan G, Ha S, Hui Y, Yuen K. The Role of Phagocytic Respiratory Burst in Host Defense. *Clin Infect Dis* (1998) 26(1):226–7. doi: 10.1086/517036
155. Conti F, Lugo-Reyes SO, Galicia LB, He J, Aksu G, de Oliveira EBJr., et al. Mycobacterial Disease in Patients With Chronic Granulomatous Disease: A Retrospective Analysis of 71 Cases. *J Allergy Clin Immunol* (2016) 138 (1):241–8. doi: 10.1016/j.jaci.2015.11.041
156. Fattahi F, Badalzadeh M, Sedighipour L, Movahedi M, Fazlollahi MR, Mansouri SD, et al. Inheritance Pattern and Clinical Aspects of 93 Iranian Patients With Chronic Granulomatous Disease. *J Clin Immunol* (2011) 31 (5):792. doi: 10.1007/s10875-011-9567-x
157. Giardino G, Cicalese MP, Delmonte O, Migliavacca M, Palterer B, Loffredo L, et al. NADPH Oxidase Deficiency: A Multisystem Approach. *Oxid Med Cell Longev* (2017) 2017:4590127. doi: 10.1155/2017/4590127
158. Adams LB, Dinauer MC, Morgenstern DE, Krahenbuhl JL. Comparison of the Roles of Reactive Oxygen and Nitrogen Intermediates in the Host Response to *Mycobacterium Tuberculosis* Using Transgenic Mice. *Tubercle Lung Dis* (1997) 78(5):237–46. doi: 10.1016/S0962-8479(97)90004-6
159. Lee PPW, Chan K-W, Jiang L, Chen T, Li C, Lee T-L, et al. Susceptibility to Mycobacterial Infections in Children With X-Linked Chronic Granulomatous Disease: A Review of 17 Patients Living in a Region Endemic for Tuberculosis. *Pediatr Infect Dis J* (2008) 27(3):224–30. doi: 10.1097/INF.0b013e31815b494c
160. AlKhater SA, Deswarte C, Casanova JL, Bustamante J. A Novel Variant in the Neutrophil Cytosolic Factor 2 (NCF2) Gene Results in Severe Disseminated BCG Infectious Disease: A Clinical Report and Literature Review. *Mol Genet Genomic Med* (2020) 2020:e1237. doi: 10.1002/mgg3.1237
161. Li T, Zhou X, Ling Y, Jiang N, Ai J, Wu J, et al. Genetic and Clinical Profiles of Disseminated Bacillus Calmette-Guérin Disease and Chronic Granulomatous Disease in China. *Front Immunol* (2019) 10:73. doi: 10.3389/fimmu.2019.00073
162. Kalita A, Verma I, Khuller GK. Role of Human Neutrophil Peptide-1 as a Possible Adjunct to Antituberculosis Chemotherapy. *J Infect Dis* (2004) 190 (8):1476–80. doi: 10.1086/424463
163. Ogata K, Linzer BA, Zuberi RI, Ganz T, Lehrer RI, Catanzaro A. Activity of Defensins From Human Neutrophilic Granulocytes Against *Mycobacterium Avium-Mycobacterium Intracellulare*. *Infect Immun* (1992) 60(11):4720–5. doi: 10.1128/iai.60.11.4720-4725.1992
164. Jena P, Mohanty S, Mohanty T, Kallert S, Morgelin M, Lindstrøm T, et al. Azurophil Granule Proteins Constitute the Major Mycobactericidal Proteins in Human Neutrophils and Enhance the Killing of Mycobacteria in Macrophages. *PloS One* (2012) 7(12):e50345. doi: 10.1371/journal.pone.0050345
165. Hilda JN, Narasimhan M, Das SD. *Mycobacterium Tuberculosis* Strains Modify Granular Enzyme Secretion and Apoptosis of Human Neutrophils. *Mol Immunol* (2015) 68(2):325–32. doi: 10.1016/j.molimm.2015.09.019
166. Steinwede K, Maus R, Bohling J, Voedisch S, Braun A, Ochs M, et al. Cathepsin G and Neutrophil Elastase Contribute to Lung-Protective Immunity Against Mycobacterial Infections in Mice. *J Immunol* (2012) 188(9):4476–87. doi: 10.4049/jimmunol.1103346
167. Ribeiro-Gomes FL, Moniz-de-Souza MCA, Alexandre-Moreira MS, Dias WB, Lopes MF, Nunes MP, et al. Neutrophils Activate Macrophages for Intracellular Killing of Leishmania Major Through Recruitment of TLR4 by Neutrophil Elastase. *J Immunol* (2007) 179(6):3988–94. doi: 10.4049/jimmunol.179.6.3988
168. Mathy-Hartert M, Deby-Dupont G, Melin P, Lamy M, Deby C. Bactericidal Activity Against *Pseudomonas Aeruginosa* Is Acquired by Cultured Human Monocyte-Derived Macrophages After Uptake of Myeloperoxidase. *Experientia* (1996) 52(2):167–74. doi: 10.1007/BF01923364
169. Barrientos L, Marin-Esteban V, de Chaisemartin L, Sandre C, Bianchini E, Nicolas V, et al. An Improved Strategy to Recover Large Fragments of Functional Human Neutrophil Extracellular Traps. *Front Immunol* (2013) 4:166. doi: 10.3389/fimmu.2013.00166
170. Halverson TWR, Wilton M, Poon KKH, Petri B, Lewenza S. DNA Is an Antimicrobial Component of Neutrophil Extracellular Traps. *PloS Pathog* (2015) 11(1):e1004593. doi: 10.1371/journal.ppat.1004593
171. Schechter MC, Buac K, Adekambi T, Cagle S, Celli J, Ray SM, et al. Neutrophil Extracellular Trap (NET) Levels in Human Plasma Are Associated With Active TB. *PloS One* (2017) 12(8):e0182587. doi: 10.1371/journal.pone.0182587
172. van der Meer AJ, Zeerleder S, Blok DC, Kager LM, Lede IO, Rahman W, et al. Neutrophil Extracellular Traps in Patients With Pulmonary Tuberculosis. *Respir Res* (2017) 18(1):181. doi: 10.1186/s12931-017-0663-1

173. Filio-Rodríguez G, Estrada-García I, Arce-Paredes P, Moreno-Altamirano MM, Islas-Trujillo S, Ponce-Regalado MD, et al. *In Vivo* Induction of Neutrophil Extracellular Traps by *Mycobacterium Tuberculosis* in a Guinea Pig Model. *Innate Immun* (2017) 23(7):625–37. doi: 10.1177/1753425917732406
174. Moreira-Teixeira L, Stimpson PJ, Stavropoulos E, Hadebe S, Chakravarty P, Ioannou M, et al. Type I IFN Exacerbates Disease in Tuberculosis-Susceptible Mice by Inducing Neutrophil-Mediated Lung Inflammation and NETosis. *Nat Commun* (2020) 11(1):5566. doi: 10.1038/s41467-020-19412-6
175. Dias AA, Silva CO, Santos JPS, Batista-Silva LR, Acosta CCD, Fontes AN, et al. DNA Sensing *via* TLR-9 Constitutes a Major Innate Immunity Pathway Activated During Erythema Nodosum Leprosum. *J Immunol* (2016) 197 (5):1905–13. doi: 10.4049/jimmunol.1600042
176. Da Silva CO, Dias AA, da Costa Nery JA, de Miranda Machado A, Ferreira H, Rodrigues TF, et al. Neutrophil Extracellular Traps Contribute to the Pathogenesis of Leprosy Type 2 Reactions. *PloS Negl Trop Dis* (2019) 13(9): e0007368. doi: 10.1371/journal.pntd.0007368
177. Sahu S, Sharma K, Sharma M, Narang T, Dogra S, Minz RW, et al. Neutrophil NETworking in ENL: Potential as a Putative Biomarker: Future Insights. *Front Med (Lausanne)* (2021) 8:697804. doi: 10.3389/fmed.2021.697804
178. Liu K, Sun E, Lei M, Li L, Gao J, Nian X, et al. BCG-Induced Formation of Neutrophil Extracellular Traps Play an Important Role in Bladder Cancer Treatment. *Clin Immunol* (2019) 201:4–14. doi: 10.1016/j.clim.2019.02.005
179. Branzk N, Lubojemska A, Hardison SE, Wang Q, Gutierrez MG, Brown GD, et al. Neutrophils Sense Microbe Size and Selectively Release Neutrophil Extracellular Traps in Response to Large Pathogens. *Nat Immunol* (2014) 15 (11):1017–25. doi: 10.1038/ni.2987
180. Tenland E, Håkansson G, Alaridah N, Lutay N, Rönnholm A, Hallgren O, et al. Innate Immune Responses After Airway Epithelial Stimulation With Mycobacterium Bovis Bacille-Calmette Guérin. *PloS One* (2016) 11(10): e0164431. doi: 10.1371/journal.pone.0164431
181. Braian C, Hogea V, Stendahl O. *Mycobacterium Tuberculosis*-Induced Neutrophil Extracellular Traps Activate Human Macrophages. *J Innate Immun* (2013) 5(6):591–602. doi: 10.1159/000348676
182. Francis RJ, Butler RE, Stewart GR. *Mycobacterium Tuberculosis* ESAT-6 Is a Leukocidin Causing Ca(2+) Influx, Necrosis and Neutrophil Extracellular Trap Formation. *Cell Death Dis* (2014) 5(10):e1474. doi: 10.1038/cddis.2014.394
183. Dang G, Cui Y, Wang L, Li T, Cui Z, Song N, et al. Extracellular Sphingomyelinase Rv0888 of *Mycobacterium Tuberculosis* Contributes to Pathological Lung Injury of *Mycobacterium Smegmatis* in Mice *via* Inducing Formation of Neutrophil Extracellular Traps. *Front Immunol* (2018) 9:677. doi: 10.3389/fimmu.2018.00677
184. Speer A, Sun J, Danilchanka O, Meikle V, Rowland JL, Walter K, et al. Surface Hydrolysis of Sphingomyelin by the Outer Membrane Protein R V0888 Supports Replication of *Mycobacterium Tuberculosis* in Macrophages. *Mol Microbiol* (2015) 97(5):881–97. doi: 10.1111/mmi.13073
185. Dang G, Cao J, Cui Y, Song N, Chen L, Pang H, et al. Characterization of Rv0888, a Novel Extracellular Nuclease From *Mycobacterium Tuberculosis*. *Sci Rep* (2016) 6(1):1–11. doi: 10.1038/srep19033
186. Parker H, Dragunow M, Hampton MB, Kettle AJ, Winterbourn CC. Requirements for NADPH Oxidase and Myeloperoxidase in Neutrophil Extracellular Trap Formation Differ Depending on the Stimulus. *J Leuk Biol* (2012) 92:841–9. doi: 10.1189/jlb.1211601
187. Bianchi M, Hakkim A, Brinkmann V, Siler U, Seger RA, Zychlinsky A, et al. Restoration of NET Formation by Gene Therapy in CGD Controls Aspergillosis. *Blood* (2009) 114:2619–22. doi: 10.1182/blood-2009-05-221606
188. Lood C, Blanco LP, Purmalek MM, Carmona-Rivera C, De Ravin SS, Smith CK, et al. Neutrophil Extracellular Traps Enriched in Oxidized Mitochondrial DNA Are Interferogenic and Contribute to Lupus-Like Disease. *Nat Med* (2016) 22:146–53. doi: 10.1038/nm.4027
189. Stephan A, Batinica M, Steiger J, Hartmann P, Zaucke F, Bloch W, et al. LL37: DNA Complexes Provide Antimicrobial Activity Against Intracellular Bacteria in Human Macrophages. *Immunol* (2016) 148(4):420–32. doi: 10.1111/imm.12620
190. Ong CWM, Fox K, Ettorre A, Elkington PT, Friedland JS. Hypoxia Increases Neutrophil-Driven Matrix Destruction After Exposure to *Mycobacterium Tuberculosis*. *Sci Rep* (2018) 8(1):1–11. doi: 10.1038/s41598-018-29659-1
191. Pilsczek FH, Salina D, Poon KKH, Fahey C, Yipp BG, Sibley CD, et al. A Novel Mechanism of Rapid Nuclear Neutrophil Extracellular Trap Formation in Response to *Staphylococcus Aureus*. *J Immunol* (2010) 185 (12):7413–25. doi: 10.4049/jimmunol.1000675
192. Tillack K, Breiden P, Martin R, Sospedra M. T Lymphocyte Priming by Neutrophil Extracellular Traps Links Innate and Adaptive Immune Responses. *J Immunol* (2012) 188(7):3150–9. doi: 10.4049/jimmunol.1103414
193. Marcos V, Zhou-Suckow Z, Önder Yildirim A, Bohla A, Hector A, Vitkov L, et al. Free DNA in Cystic Fibrosis Airway Fluids Correlates With Airflow Obstruction. *Mediat Inflamm* (2015) 2015:408935. doi: 10.1155/2015/408935
194. Grabcanovic-Musija F, Obermayer A, Stoiber W, Krautgartner W-D, Steinbacher P, Winterberg N, et al. Neutrophil Extracellular Trap (NET) Formation Characterises Stable and Exacerbated COPD and Correlates With Airflow Limitation. *Respir Res* (2015) 16(1):59. doi: 10.1186/s12931-015-0221-7
195. Adrover JM, Aroca-Crevillén A, Crainiciuc G, Ostos F, Rojas-Vega Y, Rubio-Ponce A, et al. Programmed 'Disarming'of the Neutrophil Proteome Reduces the Magnitude of Inflammation. *Nat Immunol* (2020) 21:135–44. doi: 10.1038/s41590-019-0571-2
196. Bonvillain RW, Painter RG, Ledet EM, Wang G. Comparisons of Resistance of CF and Non-CF Pathogens to Hydrogen Peroxide and Hypochlorous Acid Oxidants *In Vitro*. *BMC Microbiol* (2011) 11(1):112. doi: 10.1186/1471-2180-11-112
197. Dickerhof N, Isles V, Pattemore P, Hampton MB, Kettle AJ. Exposure of *Pseudomonas Aeruginosa* to Bactericidal Hypochlorous Acid During Neutrophil Phagocytosis Is Compromised in Cystic Fibrosis. *J Biol Chem* (2019) 294(36):13502–14. doi: 10.1074/jbc.RA119.009934
198. Coker MS, Forbes LV, Plowman-Holmes M, Murdoch DR, Winterbourn CC, Kettle AJ. Interactions of Staphyloxanthin and Enterobactin With Myeloperoxidase and Reactive Chlorine Species. *Arch Biochem Biophys* (2018) 646:80–9. doi: 10.1016/j.abb.2018.03.039
199. Reyes AM, Pedre B, De Armas MI, Tossounian M-A, Radi R, Messens J, et al. Chemistry and Redox Biology of Mycothiol. *Antioxid Redox Signal* (2018) 28 (6):487–504. doi: 10.1089/ars.2017.7074
200. Newton GL, Arnold K, Price MS, Sherrill C, Delcardayre SB, Aharonowitz Y, et al. Distribution of Thiols in Microorganisms: Mycothiol Is a Major Thiol in Most Actinomycetes. *J Bacteriol* (1996) 178(7):1990–5. doi: 10.1128/jb.178.7.1990-1995.1996
201. Storkey C, Davies MJ, Pattison DI. Reevaluation of the Rate Constants for the Reaction of Hypochlorous Acid (HOCl) With Cysteine, Methionine, and Peptide Derivatives Using a New Competition Kinetic Approach. *Free Radic Biol Med* (2014) 73:60–6. doi: 10.1016/j.freeradbiomed.2014.04.024
202. Hillion M, Bernhardt J, Busche T, Rossius M, Maaß S, Becher D, et al. Monitoring Global Protein Thiol-Oxidation and Protein S-Mycothiolation in *Mycobacterium Smegmatis* Under Hypochlorite Stress. *Sci Rep* (2017) 7 (1):1195. doi: 10.1038/s41598-017-01179-4
203. Van Laer K, Buts L, Foloppe N, Vertommen D, Van Belle K, Wahni K, et al. Mycoredoxin-1 Is One of the Missing Links in the Oxidative Stress Defence Mechanism of Mycobacteria. *Mol Microbiol* (2012) 86(4):787–804. doi: 10.1111/mmi.12030
204. Sao Emani C, Williams MJ, Van Helden PD, Taylor MJC, Wiid IJ, Baker B. Gamma-Glutamylcysteine Protects Ergothioneine-Deficient *Mycobacterium Tuberculosis* Mutants Against Oxidative and Nitrosative Stress. *Biochem Biophys Res Comm* (2018) 495(1):174–8. doi: 10.1016/j.bbrc.2017.10.163
205. Sao Emani C, Williams MJ, Wiid IJ, Hiten NF, Viljoen AJ, Pietersen R-DD, et al. Ergothioneine Is a Secreted Antioxidant in *Mycobacterium Smegmatis*. *Antimicrob Agents Chemother* (2013) 57:3202–7. doi: 10.1128/AAC.02572-12
206. Lee WL, Gold B, Darby C, Brot N, Jiang X, De Carvalho LPS, et al. *Mycobacterium Tuberculosis* Expresses Methionine Sulphoxide Reductases A and B That Protect From Killing by Nitrite and Hypochlorite. *Mol Microbiol* (2009) 71:583–93. doi: 10.1111/j.1365-2958.2008.06548.x
207. Edwards KM, Cynamon MH, Voladri RK, Hager CC, DeSTEFANO MS, Tham KT, et al. Iron-Cofactored Superoxide Dismutase Inhibits Host

Responses to *Mycobacterium Tuberculosis*. *Am J Respir Crit Care Med* (2001) 164(12):2213–9. doi: 10.1164/ajrccm.164.12.2106093
208. Harth G, Horwitz MA. Export of Recombinant Mycobacterium Tuberculosis Superoxide Dismutase Is Dependent Upon Both Information in the Protein and Mycobacterial Export Machinery. A Model for Studying Export of Leaderless Proteins by Pathogenic Mycobacteria. *J Biol Chem* (1999) 274 (7):4281–92. doi: 10.1074/jbc.274.7.4281
209. Kettle AJ, Anderson RF, Hampton MB, Winterbourn CC. Reactions of Superoxide With Myeloperoxidase. *Biochemistry* (2007) 46(16):4888–97. doi: 10.1021/bi602587k
210. Hampton MB, Kettle AJ, Winterbourn CC. Involvement of Superoxide and Myeloperoxidase in Oxygen-Dependent Killing of *Staphylococcus Aureus* by Neutrophils. *Infect Immun* (1996) 64(9):3512–7. doi: 10.1128/iai.64.9.3512-3517.1996
211. Fonseca KL, Rodrigues PNS, Olsson IAS, Saraiva M. Experimental Study of Tuberculosis: From Animal Models to Complex Cell Systems and Organoids. *PloS Pathog* (2017) 13(8):e1006421. doi: 10.1371/journal.ppat.1006421
212. Belton M, Brilha S, Manavaki R, Mauri F, Nijran K, Hong YT, et al. Hypoxia and Tissue Destruction in Pulmonary TB. *Thorax* (2016) 71(12):1145–53. doi: 10.1136/thoraxjnl-2015-207402
213. Remot A, Doz E, Winter N. Neutrophils and Close Relatives in the Hypoxic Environment of the Tuberculous Granuloma: New Avenues for Host-Directed Therapies? *Front Immunol* (2019) 10:417. doi: 10.3389/fimmu.2019.00417
214. Mestas J, Hughes CC. Of Mice and Not Men: Differences Between Mouse and Human Immunology. *J Immunol* (2004) 172(5):2731–8. doi: 10.4049/jimmunol.172.5.2731
215. van der Werf TS, Stienstra Y, Johnson RC, Phillips R, Adjei O, Fleischer B, et al. *Mycobacterium Ulcerans* Disease. *Bull World Health Organ* (2005) 83:785–91.
216. Degiacomi G, Sammartino JC, Chiarelli LR, Riabova O, Makarov V, Pasca MR. *Mycobacterium Abscessus*, an Emerging and Worrisome Pathogen Among Cystic Fibrosis Patients. *Int J Mol Sci* (2019) 20(23):5868. doi: 10.3390/ijms20235868

Conflict of Interest: The authors declare that the research was conducted in the absence of any commercial or financial relationships that could be construed as a potential conflict of interest.

Publisher's Note: All claims expressed in this article are solely those of the authors and do not necessarily represent those of their affiliated organizations, or those of the publisher, the editors and the reviewers. Any product that may be evaluated in this article, or claim that may be made by its manufacturer, is not guaranteed or endorsed by the publisher.

frontiers | Frontiers in Immunology

ORIGINAL RESEARCH
published: 06 June 2022
doi: 10.3389/fimmu.2022.823121

Neutrophil-Specific Knockdown of β2 Integrins Impairs Antifungal Effector Functions and Aggravates the Course of Invasive Pulmonal Aspergillosis

Maximilian Haist[1], Frederic Ries[2], Matthias Gunzer[3,4], Monika Bednarczyk[1], Ekkehard Siegel[5], Michael Kuske[1], Stephan Grabbe[1], Markus Radsak[2†], Matthias Bros[1†] and Daniel Teschner[2,6†]*

[1] Department of Dermatology, University Medical Center of the Johannes Gutenberg University, Mainz, Germany, [2] Department of Hematology, Medical Oncology and Pneumology, University Medical Center of the Johannes Gutenberg University, Mainz, Germany, [3] Institute for Experimental Immunology and Imaging, University Hospital, University Duisburg-Essen, Essen, Germany, [4] Leibniz-Institut für Analytische Wissenschaften ISAS -e.V, Dortmund, Germany, [5] Institute for Medical Microbiology and Hygiene, University Medical Center of the Johannes Gutenberg University, Mainz, Germany, [6] Department of Internal Medicine II, University Hospital Würzburg, Würzburg, Germany

OPEN ACCESS

Edited by:
Marko Radic,
University of Tennessee College of Medicine, United States

Reviewed by:
Rodrigo Tinoco Figueiredo,
Federal University of Rio de Janeiro, Brazil
Meiqing Shi,
University of Maryland, College Park, United States

***Correspondence:**
Maximilian Haist
Maximilian.Haist@unimedizin-mainz.de

†These authors have contributed equally to this work

Specialty section:
This article was submitted to Molecular Innate Immunity, a section of the journal Frontiers in Immunology

Received: 26 November 2021
Accepted: 28 April 2022
Published: 06 June 2022

Citation:
Haist M, Ries F, Gunzer M, Bednarczyk M, Siegel E, Kuske M, Grabbe S, Radsak M, Bros M and Teschner D (2022) Neutrophil-Specific Knockdown of β2 Integrins Impairs Antifungal Effector Functions and Aggravates the Course of Invasive Pulmonal Aspergillosis. Front. Immunol. 13:823121. doi: 10.3389/fimmu.2022.823121

β2-integrins are heterodimeric surface receptors that are expressed specifically by leukocytes and consist of a variable α (CD11a-d) and a common β-subunit (CD18). Functional impairment of CD18, which causes leukocyte adhesion deficiency type-1 results in an immunocompromised state characterized by severe infections, such as invasive pulmonary aspergillosis (IPA). The underlying immune defects have largely been attributed to an impaired migratory and phagocytic activity of polymorphonuclear granulocytes (PMN). However, the exact contribution of β2-integrins for PMN functions *in-vivo* has not been elucidated yet, since the mouse models available so far display a constitutive CD18 knockout ($CD18^{-/-}$ or $CD18^{hypo}$). To determine the PMN-specific role of β2-integrins for innate effector functions and pathogen control, we generated a mouse line with a Ly6G-specific knockdown of the common β-subunit ($CD18^{Ly6G}$ cKO). We characterized $CD18^{Ly6G}$ cKO mice *in-vitro* to confirm the PMN-specific knockdown of β2-integrins. Next, we investigated the clinical course of IPA in *A. fumigatus* infected $CD18^{Ly6G}$ cKO mice with regard to the fungal burden, pulmonary inflammation and PMN response towards *A. fumigatus*. Our results revealed that the β2-integrin knockdown was restricted to PMN and that $CD18^{Ly6G}$ cKO mice showed an aggravated course of IPA. In accordance, we observed a higher fungal burden and lower levels of proinflammatory innate cytokines, such as TNF-α, in lungs of IPA-infected $CD18^{Ly6G}$ cKO mice. Bronchoalveolar lavage revealed higher levels of CXCL1, a stronger PMN-infiltration, but concomitantly elevated apoptosis of PMN in lungs of $CD18^{Ly6G}$ cKO mice. E*x-vivo* analysis further unveiled a strong impairment of PMN effector function, as reflected by an attenuated phagocytic activity, and a diminished generation of reactive oxygen species (ROS) and neutrophil-extracellular traps (NET) in CD18-deficient PMN. Overall, our study

demonstrates that β2-integrins are required specifically for PMN effector functions and contribute to the clearance of *A. fumigatus* by infiltrating PMN, and the establishment of an inflammatory microenvironment in infected lungs.

Keywords: β2 integrins, CD18, CD11b, polymorphonuclear neutrophils, *Aspergillus fumigatus*, pneumonia, complement receptor 3, phagocytosis

1 INTRODUCTION

Humans are constantly exposed to spores of the ubiquitous environmental mould *Aspergillus fumigatus* (*A. fumigatus*) (1, 2). Although *A. fumigatus* is usually well controlled in healthy individuals, *A. fumigatus* can cause lethal invasive pulmonary aspergillosis (IPA) in immunocompromised patients, e.g., due to chemotherapeutic treatment of malignant diseases or immunosuppressive therapy after allogeneic hematopoietic stem cell transplantation, with mortality varying between 30% and 90% (1, 3). Commonly, disease follows the inhalation of airborne conidia, which germinate in the lung of immunocompromised hosts, sprouting there as hyphae (4). Despite the clinical application of potent antifungal drugs for prophylaxis and treatment of invasive fungal diseases in patients with severe immune deficiency, IPA continues to be a highly relevant health issue in daily clinical care (5).

The small size of *A. fumigatus* conidia (2-3μm) allows them to bypass the physiological epithelial defence of the nasal and bronchial cavities and to reach the lung alveoli without being cleared by the ciliated bronchial epithelium (6, 7). Although several *in-vitro* studies indicated that epithelial cells may internalize and subject conidia to phagolysosomal degradation (8), an engulfment of conidia by bronchial epithelium has not been observed *in-vivo* so far (9). Hence, the clearance of *A. fumigatus* conidia requires effective cellular and humoral immune responses.

The innate immune system is considered the key player in the clearance of conidia and the defence against the outgrowth of *A. fumigatus* conidia. Here, resident leukocytes present in the alveolar lung tissue, such as alveolar macrophages and dendritic cells (DC) initiate an early response against invasive aspergillosis (10, 11). However, the recruitment of polymorphonuclear neutrophils (PMN) to the lung tissue is essential for an efficient clearing of *A. fumigatus* (5, 6, 12). The importance of PMN for an effective protection against IPA was inferred from the observation, that quantitative [i.e., in neutropenic patients (13)] or qualitative [i.e., patients with chronic granulomatous disease (14)] defects of PMN are critical predisposing factors for IPA (13, 15). PMN mediate the killing of *A. fumigatus via* different effector mechanisms dependent on the size of conidia and hyphae:

Since the size of hyphae prevents phagocytosis, hyphal killing is mainly conferred by oxidative and non-oxidative PMN effector functions. These include the generation of reactive oxygen species (ROS), the formation of neutrophil extracellular traps (NET) and the release of neutrophil granular content (6, 16, 17). In the context of oxidative PMN functions, it has been observed, that the common beta subunit of β2 integrins (CD18) is critical for the recognition of *A. fumigatus* and the subsequent generation of ROS (18, 19).

By contrast, the small-size of *A. fumigatus* conidia allows for the phagocytosis by PMN, which is either mediated by direct recognition *via* complement receptor 3 (CR3, i.e., CD11b/CD18), Dectin-1 or indirectly *via* complement-dependant opsonization (6, 18, 19). The importance of β2 integrins in PMN-functions has been confirmed in more recent reports, which revealed that an antibody-mediated blockade of CD11b prevents the generation of ROS (20) and phagocytosis of *A. fumigatus* conidia by PMN (21).

The ß2 integrin-family consists of four members, which are formed by heterodimerization of the common beta subunit (CD18) with a variable alpha subunit (CD11a-CD11d) (22, 23). The integrin receptor CR-3 is primarily expressed by leukocytes of the myeloid lineage, which was name-giving (macrophage antigen 1, MAC-1) (22). MAC-1 serves as an adhesion receptor for various ligands, including intercellular adhesion molecule 1 (ICAM-1), which is necessary for the transendothelial migration of macrophages and PMN (5, 24). MAC1/CR3 also binds complement-opsonized pathogens, and immune complexes, non-opsonized pathogens, and numerous serum factors (25). In addition, MAC-1 serves as a coreceptor for the Fc-receptor-mediated uptake of antibody-opsonized pathogens (26). It has further been shown that MAC-1 acts as a regulator of LPS-induced signaling in macrophages and DC, and that the engagement of MAC-1 with yet unrecognized T cell receptors mediates T cell activation (27, 28). Last, MAC-1 is a modifier of various signaling pathways (29), such as TLR-induced inflammatory signaling (27), which is involved in the innate immune response to invasive aspergillosis (10).

In accordance with the importance of β2 integrins for immune responses, loss-of-function mutations of the CD18 gene in humans result in the so-called leukocyte adhesion deficiency type 1 (LAD1) syndrome, being characterized by severe, recurrent bacterial and fungal infections in patients, which require extensive treatment with anti-infective agents (30). Several studies have indicated that an impaired migration and phagocytic activity of CD18-deficient PMN might be largely causative for the spreading of pathogens in LAD1 patients (31).

However, the exact contribution of β2 integrins for PMN functions *in-vivo* has not been fully elucidated yet, since the mouse models available so far either display a constitutive CD18-knockdown ($CD18^{hypo}$) or knockout ($CD18^{-/-}$), which complicates to delineate the cell-type specific role of CD18. In order to reveal the PMN-specific role of β2-integrins for the control of infectious diseases such as IPA, we established a

transgenic mouse with a floxed CD18 gene ($CD18^{fl/fl}$ $Ly6G^{Cre-}$). By crossing $CD18^{fl/fl}$ mice with transgenic mice expressing *Cre* recombinase under control of the PMN-specific ($Ly6G^{Cre+}$) promoter, offspring with a PMN-specific knockdown of CD18 have been generated, thus allowing to analyze the PMN-specific role in IPA.

In this study, we show that mice with a Ly6G-specific knockdown of CD18 ($CD18^{Ly6G}$ conditional knockout, in the following termed $CD18^{Ly6G}$ cKO) display an impaired survival during IPA as compared to control-mice ($CD18^{fl/fl}$). The impaired survival of $CD18^{Ly6G}$ cKO mice is reflected by a higher fungal burden in the lung of these mice during the early phase of pulmonary infection and lower amounts of proinflammatory innate mediators, such as TNF-α in the bronchoalveolar lavage fluid (BALF). By contrast, we detected an enhanced bronchial infiltration of PMN and elevated levels of the PMN-chemoattractant CXCL-1 in BALF derived from infected $CD18^{Ly6G}$ cKO mice, which might reflect a compensatory mechanism. Moreover, we could observe that CD18-deficient PMN showed a strong attenuation of effector functions *in-vitro*, which might explain the higher fungal burden in the lungs of infected $CD18^{Ly6G}$ cKO mice. In particular, we observed an impaired phagocytic uptake of *A. fumigatus* conidia, and a diminished generation of ROS and NET in CD18-deficient PMN.

2 MATERIALS AND METHODS

2.1 Fungal Strains and Cultivation Conditions

The wild type (WT; ATCC 46645) and the GFP-modified (AfS148) *A. fumigatus* strains (32) were cultured in Aspergillus minimal medium (AMM) with 1% (w/v) glucose, 1% Hutner´s trace element solution and 1M $MgSO_4$ (Carl Roth, Karlsruhe, Germany) as described earlier (16). Briefly, conidia were incubated on AMM agar plates for 4 days at 37°C and 5% CO_2. For preparation of spore suspensions, plates were washed with sterile water containing a small amount of glass pearls (Ø 4mm; Carl Roth, Karlsruhe, Germany) to detach conidia from agar plates. The obtained spore suspension was filtered twice through a sterile 40 µm nylon mesh and stored in sterile water at 4°C.

2.2 Mice

In order to allow for the assessment of the importance of β2-integrins specifically for PMN, we generated a transgenic mouse strain with a floxed CD18 gene ($CD18^{fl/fl}$ $Ly6G^{Cre-}$; B6.Cg-$Itgb2^{tm2.GrabS}$), which enabled a conditional knockout of β2 integrins in a cell-type specific manner (**Supplementary Figure 1**). The generation of mice with floxed exon 3 of the CD18 gene locus will be described in detail elsewhere. $CD18^{fl/fl}$ mice were bred with transgenic mice expressing *Cre* recombinase under control of the PMN-specific *Ly6G* promoter (33, 34) as described by Hasenberg and coworkers ($Ly6G^{Cre+}$, C57BL/6-*Ly6g*(tm2621(Cre-tdTomato)Arte mice) (35), yielding a mouse strain with diminished levels of CD18 on neutrophils ($CD18^{Ly6G}$ cKO). Resulting $CD18^{wt/fl}$ $Ly6G^{Cre-}$ offspring were crossed back to $CD18^{fl/fl}$ background. Derived male $CD18^{fl/fl}$ $Ly6G^{Cre-}$ mice were paired with $CD18^{fl/fl}$ Ly6GCre- females, yielding mice with diminished levels of CD18 on neutrophils ($CD18^{fl/fl}$ $Ly6G^{Cre-}$, in the following termed CD18Ly6G cKO) and $CD18^{fl/fl}$ $Ly6G^{Cre-}$ mice at the same ratio.

The mouse strains ($CD18^{fl/fl}$ $Ly6G^{Cre-}$ and $CD18^{Ly6G}$ cKO) were maintained in the Translational Animal Research Center of the University Medical Center Mainz under pathogen-free conditions on a standard diet. All animal procedures were performed in accordance with the institutional guidelines and approved by the responsible national authority (National Investigation Office Rhineland-Pfalz, Approval ID: 23177-07/G16-1-020). For the experiments, mice of both sexes were used, although most experiments were done with female mice. Mice used in the experiments were aged between 6-18 weeks unless stated otherwise.

2.3 Mouse Genotyping

Gene-targeted animals were verified by PCR (**Supplementary Figure 1**). To this end, ear biopsies of mice (2–6 weeks) were incubated with lysis buffer containing 100µl Direct PCR Ear Buffer (Viagen Biotec, Los Angeles, CA, USA) and 2µl proteinase K (ThermoFisher Scientific, Waltham, MA). Samples were incubated at 56°C for 1-3h under shaking. Subsequently the suspension was heated to 95°C for 5 min to inactivate proteinase K, and the lysate was put on ice until further processing. The typical PCR reaction contained a 25-µl volume containing 5µl PCR Reaction Mix (Sigma Aldrich, Merck, Darmstadt, Germany), 17,3µl H_2O, 0,2µl of myTaq-Polymerase (Roche, Mannheim, Germany) and 1µl of the primers (10pmol/µl) for PCR 1 (Mix of 2 primers: CD18 ex3_s2, B2 (s): 5´-GTGACACTTTAC TTGCGACCA-3´; CD18 loxp_as1,B3 (as): 5´-TGCCAATAAAGAATTTCAGAGCC-3´, suspended 1:10 in H_2O) or for PCR 2 (Mix of 3 primers: Ly6G [78]-s for 5´-CCTGCA ACCTGGTCAGAGAG-3´, and 5064_61_rev for 5´-G AGGTCCAAGAGACTTTCTGG-3´, and 2240_31 for 5´-ACGTCCAGACACAGCATAGG-3´ suspended 1:10 in H_2O). In PCR 2 we also included a control pair of primers for amplifying Actin as a wild-type allele (Actin FW: 5´-TGTTACCAACTGGG ACGACA-3´ and Actin REV: 5´-GACATGCAAGGAGTGC AAGA. The following PCR conditions were applied for PCR 1:initial146denaturation (3 min, 95°C), followed by 35 cycles (denaturation: 30 s, 95°C; annealing: 30 s, 58°C; elongation: 45 s, 72°C) and by a final elongation step (2 min 72°C). For PCR 2 the following PCR conditions were applied: initial denaturation (5 min, 95°C), followed by 35 cycles (denaturation: 30 s, 95°C; annealing: 30 s, 60°C; elongation: 1 min, 72°C) and by a final elongation step (10 min 72°C). PCR products were analyzed by agarose gel electrophoresis (**Supplementary Figure 1**).

2.4 Mouse Model of Invasive Aspergillosis

Mice were anesthetized with 14.5% Ketamin (50mg/ml)/5.7% Xylazin (0.2%) and were subsequently challenged with 10^7 *A. fumigatus* conidia (strain ATCC 46645) applied intratracheally as described (35, 36). In brief, a 22G indwelling venous catheter (Vasofix, B. Braun AG, Melsungen, Germany) was inserted into

the trachea and 100 µl sterile fungal suspension was administered through the catheter. To enhance dispersion in the lungs, mice were ventilated mechanically with 250 breaths/min, 300 µl/breath for 2 min using an animal respirator (MiniVent, Hugo Sachs, March-Hugstetten, Germany) as previously described (16). In order to characterize the early immune response to fungal infection, 10 mice/group were sacrificed 24h after infection. In two additional groups (n=5-8 mice/group) the course of systemic infection was daily examined by evaluation of weight, activity, breathing, overall appearance (as assessed by posture, skin, and fur appearance), and survival was monitored for 14 days. Mice with severe symptoms as determined by clinical scoring were immediately euthanized as required by the institutional animal ethics guidelines. Where indicated, PMN depletion was induced by i.p. injection of anti-Gr-1 antibody (150 µg, clone RB6-8C5; BioXCell, Lebanon, NH) 1 day prior to inoculation with fungal suspension.

2.5 Flow Cytometric Analysis

Blood samples, spleens and bone marrow were prepared from sacrificed mice, and lungs were flushed with 1 ml PBS. Spleen cell suspensions were generated *via* mechanical homogenization on a 40µm nylon mesh, washed twice with cold PBS, and red blood cells (RBC) were lysed with hypotonic Gey´s solution (155mM NH_4Cl, 10mM $KHCO_3$, 10µM EDTA at pH 7,4). RBC from blood samples were lysed in the same way. Cells derived from blood, spleen, bone marrow and bronchoalveolar lavage fluid (BALF) were analyzed by flow cytometry. To this end, cells were washed with staining buffer (PBS/2% FCS), and Fc receptors were blocked by incubation with rat anti-mouse CD16/CD32 antibody (clone 2.4G2) for 15 min at 4°C. Then, cells were incubated with FITC-conjugated anti-CD86 (GL-1), anti-CD45 (30F11), and anti-Annexin-V (Biolegend), PerCP-conjugated anti-Ly6C (HK1.4), APC-conjugated anti-CD18 (C71/16), anti-CD14 (Sa14-2), anti-Gr-1 (RB6-8C5) and anti-CD40 (1C10), APC-eFluor 780 conjugated anti-CD11c (N418), eFluor450-conjugated anti-MHCII (M5/114 15.2) and anti-F4/80 (BM8), eFluor506-conjugated anti-CD3 (500A2), Super Bright 600-conjugated anti-CD11b (M1/70), PE-conjugated anti-CD11a (M17/4), anti-CD80 (1610A1) and anti-Ly6G (1A8), PE-eFluor610-conjugated anti-Ly6G (1A8), PE-Cyanine7-conjugated anti-CD68 (FA11) and anti-CD62L (MEL-14). All antibodies were obtained from Biolegend (San Diego, CA) or Thermo Fisher (Waltham, MA). Viability was assessed using Fixable-viability-dye (FVD), conjugated either with APC eFluor 780, eFluor 450 or eFluor 506 (ThermoFisher). Samples were analyzed using a flow cytometer (Attune™ NxT Acoustic Focusing Cytometer, Thermo Fisher), and data were processed using FlowJo software V8.8.7 (Tree Star Inc., Ashland, OR, USA). The gating strategy is shown in **Supplementary Figure 2**.

2.6 Quantification of Fungal Burden

The right lungs of euthanized mice were removed, mechanically homogenized and serial dilutions were plated on Sabouraud-4% Glucose agar (Carl Roth, Karlsruhe, Germany), and cultivated at 37°C and 5% CO_2. Colony-forming units (CFU) were counted after 24h and 48h.

Moreover, a D-Galactomannan assay based on the Platelia *Aspergillus* EIA (Bio-Rad Laboratories, Marne-La-Coquette, France) was employed to quantify the fungal load in BALF and serum derived from IPA-infected mice. This enzyme immunoassay is used in clinical routine and validated for the detection of *A. fumigatus* antigen. The test uses the rat monoclonal antibody EBA-2 directed against *Aspergillus* galactomannan. In brief, the antigen is first bound to the wells of the microplate coated with the EBA-2 antibody and then revealed by binding to the peroxidase-linked EBA-2 antibody resulting in a colorimetric reaction, which is measured *via* optical density on a Plate Reader as described previously (37).

2.7 Histopathologic Analysis

For histopathological analysis the left lungs of euthanized mice were filled with 10% formalin *via* the trachea. Paraffin-embedded blocks were prepared, and derived sections (5 µm) were stained with H&E to assess inflammatory responses. For this, H&E-stained sections were examined by microscopy in a blinded fashion for peribronchial, perivascular and tissue inflammation, using a scoring system (0–3). Furthermore, sections of lungs were stained with Grocott Gomori's methenamine silver to assess the fungal burden of the lungs. Grocott stained sections were examined in a blinded fashion similar to H&E sections using a scoring system (0–3). In general, 3 randomly selected areas on each slide were analyzed with a BX40 microscope equipped with a CCD camera (Olympus, Hamburg, Germany).

2.8 Cytospin Analysis

For detection of lung infiltrating PMN, 100 µl of BALF containing 0.5-2x10^5 cells (see above) were cytospun onto microscope slides (3,500 rpm for 5 min; Cytospin 3, Thermo Fisher), treated with the Diff Quick Staining Set (Microptic, Barcelona, Spain), air-dried, and fixed as recommended. Samples were analyzed using a BX50WI microscope, equipped with a CCD camera (Olympus, Hamburg, Germany). PMN were identified based on their characteristic segmented nuclei.

2.9 Cytokine Detection

Serum and BALF were subjected to cytokine detection by Cytometric bead array (CBA) using the mouse CBA flex sets following the manufacturer's instructions (BD Bioscience, San Jose, CA). Similarly, *in-vitro* cytokine generation by $Ly6G^+$ PMN (10^5/100µl) immunomagnetically sorted from bone marrow of $CD18^{fl/fl}$ and $CD18^{Ly6G}$ cKO mice (see below) was quantified. Isolated PMN were incubated in Iscove's medium (Thermo Fisher Scientific) supplemented with 5% (v/v) FCS, 2 mM l-glutamine, 50 µM ß-mercaptoethanol and 1 mM Na-pyruvate (SERVA Electrophoresis, Heidelberg, Germany) in 96-well plates (Greiner Bio One, Frickenhausen, Germany) and treated overnight with PBS, recombinant murine GM-CSF (100ng/ml; Miltenyi Biotec, Bergsich-Gladbach, Germany), LPS (1µg/ml, Merck-Millipore, Darmstadt, Germany), CpG (1µg/ml, *In vivo*gen, Toulouse, France) or R8/48 (1µg/ml, *In vivo*gen). Supernatants were taken 3h and 24h later from PMN aliquots generated in n=3 independent experiments.

2.10 Fungal Uptake by PMN

PMN were purified from bone marrow of $CD18^{fl/fl}$ and $CD18^{Ly6G}$ cKO mice by magnetic cell sorting (MACS) using biotin-labeled Ly6G-specific antibodies and streptavidin-conjugated beads (both from Miltenyi Biotec) according to the manufacturer's protocol. The cell purity ($Ly6G^+$) exceeded 90% as assessed by flow cytometry. Freshly isolated PMN were resuspended (10^6 cells/ml) in cell culture medium (see above), seeded into 96-well plates (100µl/well) and were incubated with GFP-fluorescent *A. fumigatus* conidia (5) at the indicated ratios in parallel at 4°C and 37°C to differentiate mere adhesion and energy-dependent uptake. After 1h of incubation PMN were washed twice with 500µl cold PBS and stained with anti-CD11b, anti-Ly6G, anti-MHCII and anti-CD62L specific antibodies, and FVD eFluor 506 to determine the uptake and activation status of GFP-labeled conidia by flow cytometry (**Supplementary Figure 8** shows the gating strategy applied during the experiments).

2.11 Uptake of Inert Particles by PMN

To assess uptake of inert particles, we employed Cy5-labeled nanoparticles (Ø 50nm) and PE-labeled microBeads (Ø 2µm) (both Miltenyi Biotec). Immunomagnetically sorted PMN (10^6 cells/ml) were incubated in cell culture medium in 96-well plates (100µl) and treated over-night (12h) with GM-CSF (100ng/ml) or LPS (1µg/ml). Subsequently, PMN were washed once with 500µl cold PBS and were either left untreated, or incubated in parallel settings with particles, and particles pre-treated with native or heat-inactivated mouse serum (hiS; 56°C, 30min) at 4°C and 37°C for various periods of time (15-60 min). Pretreatment of particles with native versus heat-inactivated mouse serum served to elucidate the complement-dependent particle uptake. Subsequently PMN were washed twice with 500µl cold PBS and incubated with anti-CD11b, anti-Ly6G, anti-MHCII, anti-CD86, anti-Ly6C and anti-CD62L antibodies and FVD eFluor 506 to determine the PMN-specific uptake of inert particles by flow cytometry.

2.12 Assessment of Neutrophil Apoptosis

Freshly isolated PMN ($1x10^6$/ml) derived from bone marrow of either mouse strain were incubated in cell culture medium in 24-well plates and treated over-night (12h) in parallel w/o and with GM-CSF (100ng/ml), LPS (1µg/ml) and with GM-CSF plus LPS in order to differentiate spontaneous apoptosis (PBS-treated control), late-onset apoptosis (GM-CSF) and apoptosis upon LPS-treatment. Following over-night incubation, samples were washed twice with 1ml PBS and incubated with anti-Annexin V (FITC) and FVD (eFluor 506) according to the manufacturer´s protocol (ThermoFisher) to differentiate apoptosis and necrosis. Frequencies of apoptotic and necrotic PMN were determined by flow cytometry as described previously (38).

2.13 Analysis of ROS Production

To assess the rate of ROS production, PMN were isolated from bone marrow, were seeded into 96-well-plates (10^6/ml; 100µl/well) washed once with 200µl PBS and resuspended in 100 µl ROS-detection solution (2 µM 2´-7´Dichlorodihydrofluorescein [DCFDA] in PBS; Alexis Biochemicals, Lausen, CHE). After 20 min of incubation at 37°C the cells were washed with 200µl PBS, centrifuged, and the sedimented cells were dispersed in 200 µl PBS. Subsequently, PMN were stimulated with GM-CSF (100ng/ml), LPS (1µg/ml), *A. fumigatus* conidia (1:1), or 100 nM PMA (Sigma-Aldrich), respectively at 37°C, 5% CO2 in triplicates. Median fluorescence intensities (MFI) were measured using a SPARK multimode microplate-reader (TECAN Trading AG, CHE) at an excitation of 485nm and an emission of 530nm for 90min (intervals of 15min). After 90min cells were analyzed by flow cytometry for DCFDA-positive events.

2.14 Analysis of Neutrophil-Extracellular Traps Formation

To induce the release of neutrophil extracellular traps (NET) DNA, we isolated PMN from bone marrow as described previously and seeded PMN (10^5/100 µl) in 96-well plates with 100µl RPMI 1640 medium without phenol red (ThermoFisher, Waltham, CA). PMN were treated either with GM-CSF (100ng/ml), LPS (1µg/ml), *A. fumigatus* conidia (1:1), PMA (100 nM), or calcium ionophore (2,5µM; Sigma, Darmstadt, Germany), respectively. After incubation at 37°C for 3h, 5µM of Sytox orange nucleic stain (Invitrogen, Carlsbad, CA) was added and samples were incubated for 10min at room temperature in the dark. Subsequently, PMN were centrifugated and washed twice with 300µl cold PBS. MFI of Sytox orange was measured using a SPARK multimode microplate reader with an excitation of 547nm and an emission of 580nm. Then, cells were incubated with an anti-Ly6G antibody and analyzed by flow cytometry for Ly6G/Sytox orange double-positive cells.

2.15 RNA-Sequencing and Bioinformatical Analysis

First, PMN were isolated from bone marrow of $CD18^{fl/fl}$ and $CD18^{Ly6G}$ cKO mice (n=3). Each 10^6 PMN were either lysed directly after isolation or cultured overnight with GM-CSF (10ng/ml) plus LPS (1µg/ml). RNA was purified with the RNeasy Plus Micro Kit according to the manufacturer's protocol (Qiagen). RNA was quantified with a Qubit 2.0 fluorometer (Invitrogen) and the quality was assessed on a Bioanalyzer 2100 (Agilent) using a RNA 6000 Pico chip (Agilent). Samples with an RNA integrity number (RIN) of > 8 were used for library preparation. Barcoded mRNA-seq cDNA libraries were prepared from 10ng of total RNA using NEBNext® Poly(A) mRNA Magnetic Isolation Module and NEBNext® Ultra™ II RNA Library Prep Kit for Illumina® according to the manual with a final amplification of 15 PCR cycles. Quantity was assessed using Invitrogen's Qubit HS assay kit and library size was determined using Agilent's 2100 Bioanalyzer HS DNA assay. Barcoded RNA-Seq libraries were onboard clustered using HiSeq® Rapid SR Cluster Kit v2 using 8pM and 59bps were sequenced on the Illumina HiSeq2500 using HiSeq® Rapid SBS Kit v2 (59 Cycle). The raw output data of the HiSeq was preprocessed according to the Illumina standard protocol. Sequence reads were trimmed for adapter sequences and further processed using Qiagen's software CLC Genomics

Workbench (v20.0 with CLC's default settings for RNA-Seq analysis). Reads were aligned to GRCm38 genome. Sequencing data were first analyzed with CLC Genomics Work Bench (Qiagen). Further processing was performed in R using the DESeq2 package for calling differential gene expression (39, 40). To determine the most up- or downregulated genes, genes were sorted on the basis of $\log_2$ [fold change] maximum-likelihood estimation, and the *P*-value cut-off was set to 0.05. Results were illustrated using the pheatmap package. Functional interaction networks were visualized using the STRING package in the open-source platform Cytoscape.

2.16 Statistical Analysis

Statistical analysis was conducted with GraphPad Prism (version 5.0a; GraphPad Software, San Diego, CA, USA). Comparison of two different parameters was performed using paired Student's *t*-test. In case of comparison of more than two groups we employed one-way ANOVA and posthoc Tukey test. For survival analysis, Kaplan-Meier plots and hazard ratios have been calculated. For all analyses, $p < 0.05$ was considered as statistically significant. Abbreviations: *p<0.05, **p<0.005, ***p<0,001.

3 RESULTS

3.1 Phenotype and Impairment of PMN Effector Functions of CD18^{Ly6G} cKO Mice Assessed by *In-Vitro* Experiments

In murine leukocytes Ly6G is selectively expressed by PMN (41). To obtain mice with a diminished CD18 expression specifically on PMN (CD18^{Ly6G} cKO), we crossed a mice with a floxed CD18 gene (CD18$^{fl/fll}$) that was generated in our lab (will be described in detail elsewhere) with transgenic mice expressing the Cre recombinase under control of the Ly6G promoter (CD18$^{wt/wt}$ Ly6G^{Cre+}). Resulting offspring (CD18$^{wt/fl}$ Ly6G^{Cre+} and CD18$^{wt/fl}$ Ly6G^{Cre-}) were fertile and showed no obvious phenotype. These mice were crossed back to CD18$^{fl/fl}$ background yielding CD18^{Ly6G} cKO and CD18$^{fl/fl\ Cre-}$ mice at expected Mendelian ratios (not shown). All gene-targeted animals were verified by PCR (**Supplementary Figure 1**).

We could observe a downregulation of CD18 and accordingly of the β2 integrin alpha subunits (CD11a and CD11b) on PMN of CD18^{Ly6G} cKO mice. The extent of downregulation varied between 30-50% compared to CD18$^{fl/fl}$ mice depending on the investigated compartment (blood, spleen or bone marrow) (**Figure 1A**), which is in accordance with the extent of Ly6G *Cre*-mediated downregulation of targeted genes previously shown by Gunzer and coworkers (35). Notably, CD18-reduction was restricted to Ly6G$^+$ PMN, and was not observed for CD3$^+$ lymphocytes, F4/80$^+$ macrophages and Ly6C$^+$ monocytic cells, thus confirming the cell-type specific targeting of CD18 (**Supplementary Figures 2, 3**). Absolute PMN counts and relative amounts of PMN in both spleen and blood were found to be slightly higher, whereas PMN counts in the bone marrow did not show significant differences (**Figure 1B**). The percentages of monocytic and lymphocytic cells did not differ significantly between CD18^{Ly6G} cKO mice and CD18$^{fl/fl}$ mice in spleen (**Figure 1C**, left panel) and blood (**Figure 1C**, right panel).

As β2 integrins have also been implicated in the differentiation and in survival signaling of myeloid cells (42), we next investigated whether the PMN-restricted CD18-knockdown affected PMN apoptosis *in-vitro*. Here, we did not find significant differences in the apoptosis of PMN after treatment with GM-CSF or LPS, as assessed by Annexin-V/FVD negative and Annexin-V positive/FVD negative PMN derived from spleens and bone marrow (not shown).

3.2 PMN-Specific Knockdown of β2-Integrins Results in an Aggravated Course of IPA

To assess the relevance of β2 integrins for PMN-specific clearance of pulmonary infection with *A. fumigatus*, we examined the course of disease in CD18^{Ly6G} cKO and CD18$^{fl/fl}$ mice. In some mice an anti-Gr-1 antibody was applied prior to infection with *A. fumigatus* (d0) to deplete PMN as an internal control for the success of infection. As expected, all PMN-depleted mice died during the first days of infection (**Figure 2**), underlining the pivotal role of PMN to limit the spread of *A. fumigatus*. By contrast, all non-depleted CD18$^{fl/fl}$ mice survived infection monitored over 2 weeks, whereas 25% of CD18^{Ly6G} cKO mice died within the first week of infection. This finding is consistent with the observation that clinical signs of IPA infection were more aggravated in case of CD18^{Ly6G} cKO mice in the first days after inoculation. Furthermore, recovery of from clinical symptoms was delayed in CD18^{Ly6G} cKO mice as compared to CD18$^{fl/fl}$ mice (**Figure 2**).

3.3 CD18^{Ly6G} cKO Mice Show a Higher Fungal Burden

Next, we focused on the course of the early innate immune response towards *A. fumigatus* infection, which is known to be driven by PMN (12). For this, lungs, BALF, and serum of infected mice were analyzed 24h after infection in more detail. Lung homogenates of CD18^{Ly6G} cKO mice showed an enhanced amount of fungal conidia as compared to lungs from CD18$^{fl/fl}$ mice (**Figure 3**). Histopathological analysis confirmed a higher fungal burden and aggravated lung damage in in lungs of CD18^{Ly6G} cKO mice as assessed by Grocott-silver and Hematoxylin & Eosin (H&E) staining. Notably, sprouting of hyphae has only been observed in CD18^{Ly6G} cKO mice. Despite the strong differences in terms of fungal burden, H&E staining of lung tissues showed comparable levels of cellular inflammation, largely irrespective of the genotype (**Figures 3A**). D-Galactomannan-assays revealed that BALF derived from both mice strains contained *A. fumigatus* antigen above detection levels (>5.0), whereas serum analysis showed a higher fungal load in CD18^{Ly6G} cKO mice (mean= 5.8 ± 0.14 vs. 4.7 ± 0.33, p=0.01).

3.4 CD18^{Ly6G} cKO Mice Reveal a Decreased Pulmonary Inflammation

In contrast to the increased fungal burden found in lung tissues of CD18^{Ly6G} cKO mice, these mice displayed no significant differences in cellular inflammation as assessed by H&E

staining (**Figure 3**). However, as depicted in **Figure 4**, BALF derived from infected CD18^{Ly6G} cKO mice contained lower levels of pro-inflammatory cytokines (TNF-α), and chemokines (CCL2) compared to CD18$^{fl/fl}$ mice, albeit the reduction was below statistical significance in some cases (IL-1α, IL-1β and CCL5). Levels of IL-5, IL-6, IL-10, and GM-CSF were largely comparable. In contrast, BALF obtained from CD18^{Ly6G} cKO mice contained higher levels of the chemokine CXCL-1 known as a relevant chemoattractant for PMN (43).

In contrast, cytokine and chemokine levels in serum were largely comparable between *A. fumigatus* infected CD18$^{fl/fl}$ and CD18^{Ly6G} cKO mice (**Supplementary Figure 5**).

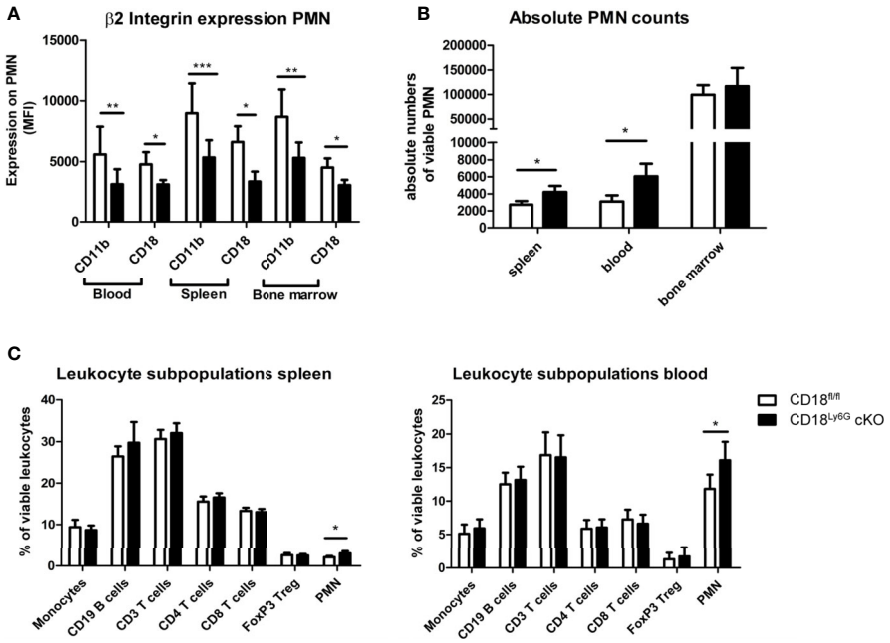

FIGURE 1 | Phenotypical and functional characteristics of CD18^{Ly6G} cKO mice compared to CD18$^{fl/fl}$ mice. We found a significant reduction of β2-integrin surface marker expression (CD11b, CD18) on PMN derived from blood, spleen, and bone marrow **(A)**. Data depict the results of *in-vitro* experiments from n=7-17 mice/genotype. In the same set of experiments we further observed higher absolute and relative counts of PMN in CD18^{Ly6G} cKO mice as compared to CD18$^{fl/fl}$ mice **(B,C)**, whereas the proportions of other leukocyte subpopulations did not differ significantly **(C)** (n=10/genotype). Legend in **(C)** applies to all panels. Statistically significant differences between groups are indicated (*p<0.05, **p<0.005, ***p<0.001).

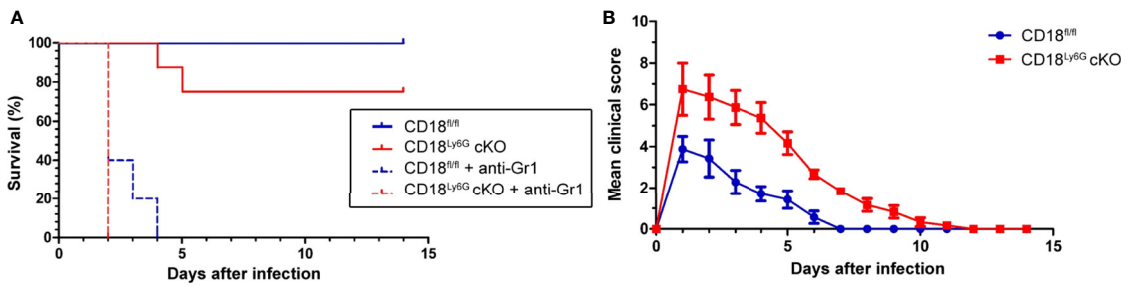

FIGURE 2 | Infection with IPA caused an impaired survival **(A)** and an aggravated course of the disease **(B)** in CD18^{Ly6G} cKO as compared to CD18$^{fl/fl}$ mice. CD18$^{fl/fl}$ and CD18^{Ly6G} cKO mice were infected i.t. with *A fumigatus* (each 10^7 conidia/mouse) in 2 independent experiments. **(A)** Survival was monitored daily for 2 weeks and is presented in a Kaplan-Meier survival curve. In parallel settings PMN were depleted in some mice *via* injection of an anti-Gr-1 antibody one day before infection. Data show the cumulative results of two independent experiments with a total of 12 (CD18$^{fl/fl}$) and 13 (CD18^{Ly6G} cKO) mice/group. 5 mice/group received an anti-Gr-1 antibody in order to deplete PMN in these mice. All Gr-1 depleted mice died within the first days after IPA infection, whereas all non-depleted CD18$^{fl/fl}$ mice survived. By contrast, some non-depleted CD18^{Ly6G} cKO mice (n=2) deceased within the first week after IPA infection. **(B)** The clinical course of IPA of monitoring was assessed in CD18$^{fl/fl}$ (n=7) and CD18^{Ly6G} cKO mice (n=8) for 14 days. Parameters comprised breathing, reaction to pain overall appearance, hypothermia, strong weight loss, motoric disabilities and apathy (each 0-2).

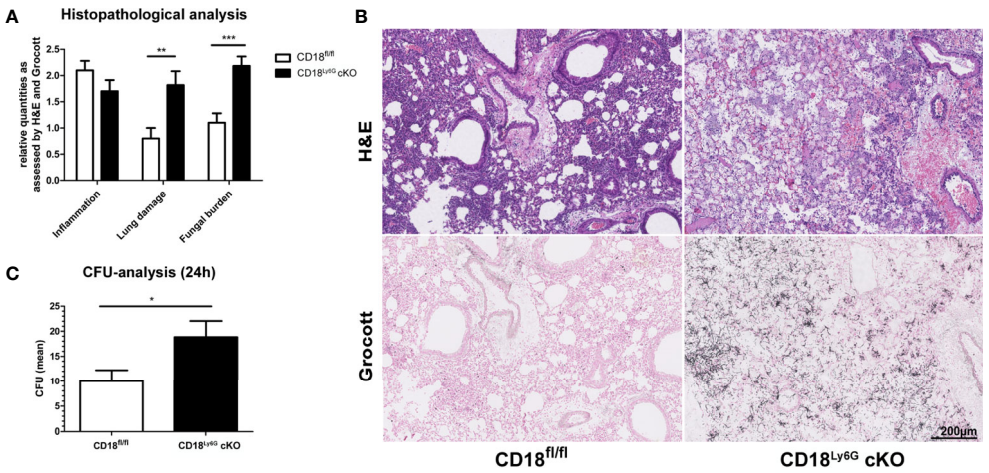

FIGURE 3 | CD18^{Ly6G} cKO mice show a higher pulmonary fungal burden. Histopathological analysis of H&E and Grocott-stained lungs derived from IPA-infected mice 24h upon *A.fumigatus* inoculation revealed a higher fungal burden and a stronger lung damage (i.e., hyaline membranes, fibrin-exudate within the alveoli) in CD18^{Ly6G} cKO mice **(A)**. Cellular inflammation did not show significant genotype-dependent differences. Representative examples of histological analysis are shown in **(B)** (Magnification 10x). Data in **(A)** denote results of histopathological analysis of n=9-10 mice/genotype. We further observed higher CFU counts in serial dilutions of lung homogenates (1:500) after incubation for 24h on Sabouraud-4% Glucose agar plates **(C)**. Data show the mean ± SEM of 6 mice/group. Statistically significant differences between groups are indicated (*p<0.05, **p<0.005, ***p<0.001).

3.5 Pulmonary PMN Infiltrates Are Increased in CD18^{Ly6G} cKO Mice Upon IPA

In accordance with elevated CXCL-1 levels, we observed higher numbers of PMN in the BALF of infected CD18^{Ly6G} cKO as compared to CD18$^{fl/fl}$ mice (**Figure 5A**). In contrast, PMN counts in spleen and blood remained comparable. Higher PMN numbers were also found in cytospin analysis (**Figure 5B**). Here, we could additionally observe lower counts of mononuclear cells in CD18^{Ly6G} cKO mice. Consistent with this observation, results of FACS-analysis revealed lower macrophage counts in the BALF of CD18^{Ly6G} cKO mice (**Figure 5B**).

Notably, a higher frequency of PMN in BALF (**Figure 5C**, left panel) and blood (**Figure 5C**, center panel) obtained from IPA-infected CD18^{Ly6G} cKO mice expressed the early apoptosis marker Annexin-V as compared to CD18$^{fl/fl}$ mice, indicating that CD18-deficient PMN might be more susceptible to apoptosis in response to *A. fumigatus*. In accordance, we

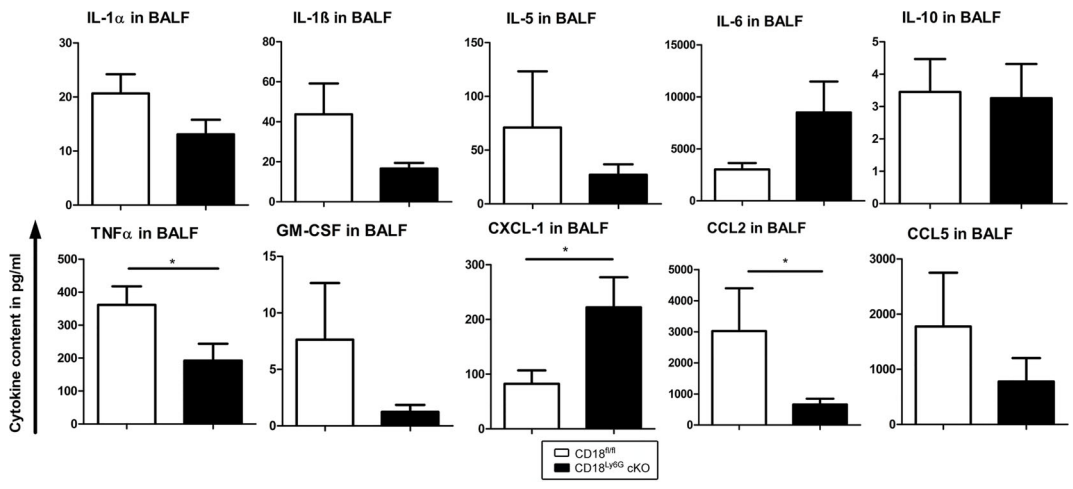

FIGURE 4 | The BAL fluid of *A. fumigatus* infected CD18^{Ly6G} cKO mice contains lower levels of proinflammatory cytokines. CD18$^{fl/fl}$ and CD18^{Ly6G} cKO mice were infected i.t. with *A. fumigatus*. On the next day, mice were euthanized, and cytokines in BAL fluid were analyzed. Data denote the mean ± SEM of 6-10 samples analyzed per group. Statistically significant differences between groups are indicated (*p< 0.05).

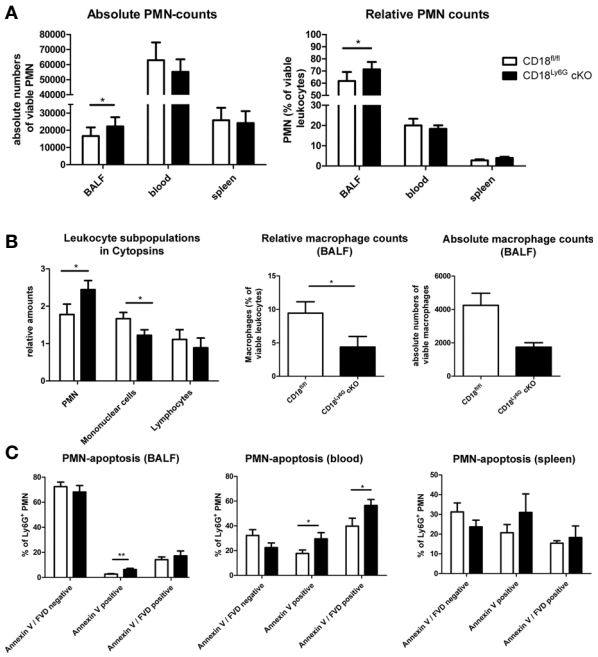

FIGURE 5 | CD18^{Ly6G} cKO mice infected with *A. fumigatus* are characterized by elevated lung infiltration of PMN, but not in spleens and blood (n=10/genotype) **(A)**. Elevated PMN counts have also been found in Cytospins (bars depict the mean ± SEM of n=8 cytospins/genotype; cell infiltration has been assessed using a scoring system; 0=missing - 3=strongest infiltration) **(B)**. Here, we could additionally observe higher numbers of mononuclear cells **(B)**. This is consistent with the finding of higher macrophage counts in the BALF of CD18$^{fl/fl}$ mice as compared to CD18^{Ly6G} cKO mice observed in FACS-analysis **(B)**. Assessment of PMN apoptosis revealed a stronger expression of apoptosis marker Annexin V in PMN derived from BALF and blood of CD18^{Ly6G} cKO mice **(C)**. Bars depict the mean ± SEM of the relative cell counts found in n=8 cytospins/genotype. Legend in A applies to all panels. Statistically significant differences between groups are indicated (*p<0.05)

observed a higher frequency of Annexin-V positive PMN in spleens of CD18^{Ly6G} cKO mice, albeit the differences here were found to be below statistical significance (**Figure 5C**, right panel).

Besides, our data show that a smaller fraction of PMN derived from BALF of CD18^{Ly6G} cKO mice expressed MHCII (1,6% vs. 4,6% of MHCII^{high} PMN), and CD80 (16.4% vs. 20.1% of CD80^{+} PMN) and showed a lower degree of degranulation as assessed by a low expression of CD62L (88.0% vs. 90.8% CD62L^{low} PMN) than observed for CD18$^{fl/fl}$ mice. BALF-derived PMN of both mice strains expressed the mouse DC marker CD11c at a moderate extent (**Supplementary Figure 6**). Infection-induced *de novo* expression of CD11c by PMN has been reported previously in different mouse infectious disease models (5).

Numbers of PMN, lymphocytes, and monocytes in the peripheral blood of *A. fumigatus* infected mice did not differ in a genotype-dependent manner (**Supplementary Figure 7**). In accordance with our *in-vitro* experiments, we could confirm that the knockdown of CD18 was restricted to Ly6G positive cells (**Supplementary Figure 3**). Similarly, we could observe a knockdown of the corresponding alpha subunits CD11a and CD11b on Ly6G positive PMN of IPA-infected mice (**Supplementary Figure 4**), which is consistent with the physiological role of CD18 as the rate-limiting subunit of β2-integrin surface expression.

3.6 Knockdown of CD18 Affects PMN Innate Effector Functions

3.6.1 Phagocytosis

Although PMN were able to infiltrate *A. fumigatus* infected lungs in CD18^{Ly6G} cKO mice, we observed an impaired ability to limit fungal spreading. Hence, we analyzed whether the knockdown of CD18, and thereby β2 integrins, affected the commonly known pathogen-induced immune responses of PMN.

As phagocytosis is a major effector mechanism of PMN to clear *A. fumigatus* conidia, we analyzed purified bone marrow-derived Ly6G^{+} PMN to assess potential genotype-dependent differences in this regard. Here, we first investigated the uptake of inert nanoparticles (NP, Ø 50nm) and microBeads (Ø 2μm). In order to dichotomize mere adhesion and energy-dependent uptake we investigated the uptake in parallel settings at 4°C and 37°C. Since MAC-1 has been attributed to serve as a receptor to facilitate complement-opsonized phagocytosis of pathogens we further examined whether the addition of murine serum might enhance the uptake of particles. Heat-inactivated serum which lacks complement activity served as an internal negative control. We could observe for both kinds of particles that their uptake was strongly impaired in case of PMN with a β2 integrin knockdown. This effect was predominantly observed for serum-opsonized particles, indicating that the recognition of complement- opsonized particles might have been diminished

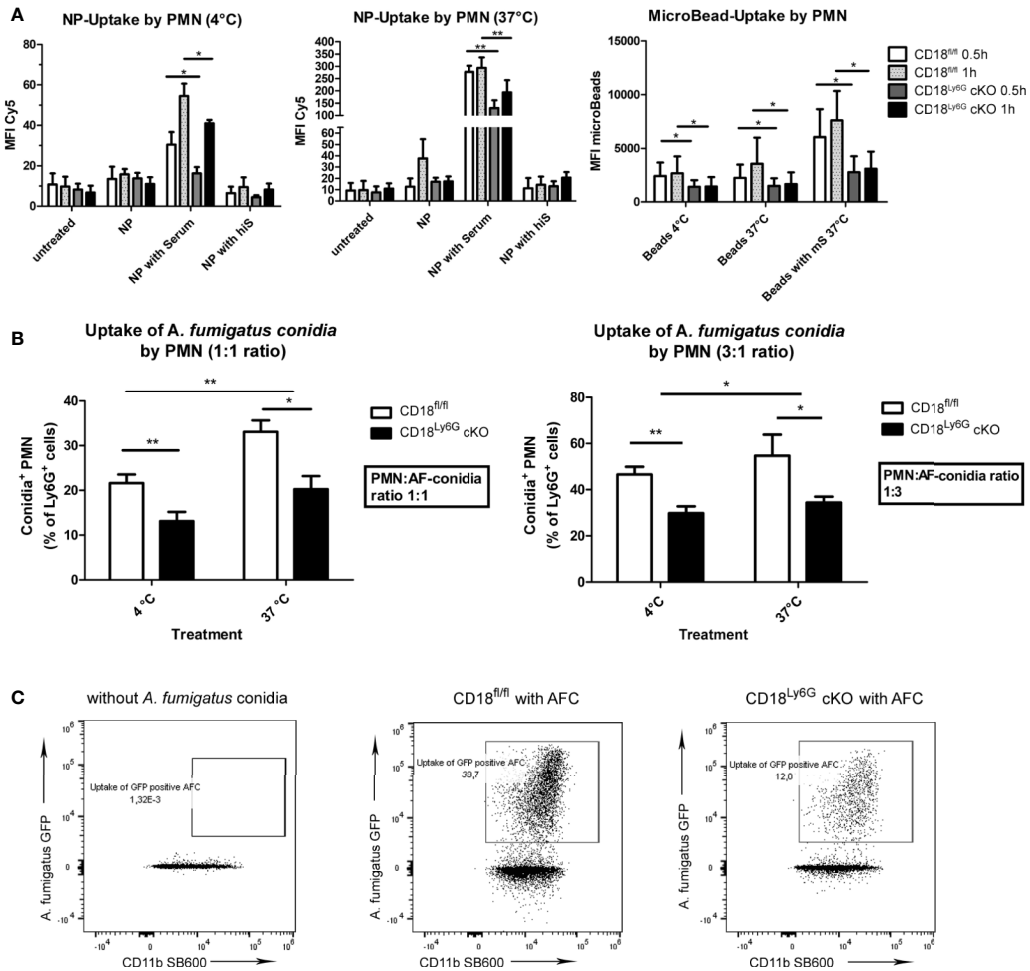

FIGURE 6 | Phagocytosis of inert particles and fungal conidia is less effective in PMN of CD18^{Ly6G} cKO mice. Freshly isolated PMN were co-incubated either with nanoparticles (NP), microBeads **(A)** or with GFP-fluorescent *A. fumigatus* conidia (AFC) at 37°C with indicated ratios **(B)**. Simultaneous co-incubation at 4°C served to differentiate mere adhesion from temperature-dependent binding. After 30 min and 60 min the frequency of either Cy5 positive NP, PE-positive microBeads **(A)**, or GFP-positive PMN **(B)** was determined by flow cytometry. Data represent the mean ± SEM of 3 samples analyzed/group. Exemplary flow cytometry data depicting the diminished uptake of GFP-fluorescent conidia by PMN from CD18^{Ly6G} cKO mice are shown in **(C)**. Statistically significant differences between groups are indicated (*p<0.05, **p<0.005).

in case of CD18 downregulation on PMN (**Figures 6A**). In accordance with the well-known role of MAC-1 (CD11b/CD18) for the binding and uptake of complement-opsonized material, we further observed a significant correlation between CD11b surface marker expression on PMN and the engagement of the aforementioned particles (Pearson´s r: 0.65; p= 0.0007).

Subsequently, we analyzed the phagocytic capacity of PMN after incubation with *A. fumigatus* conidia. Similar to previous experiments with inert particles, we observed a significantly lower phagocytic uptake of *A. fumigatus* conidia by PMN derived from CD18^{Ly6G} cKO mice (**Figure 6B, C**).

3.6.2 NETosis

We also investigated the rate of NET-formation of freshly isolated PMN after differential stimulation. Here, we could observe that the formation of NET by PMN derived from CD18^{Ly6G} cKO mice was significantly impaired after treatment with PMA or *A. fumigatus* conidia, as assessed by Sytox orange staining. After treatment with GM-CSF or LPS the differences in the formation of NET by PMN derived from CD18^{Ly6G} cKO vs CD18$^{fl/fl}$ mice were below statistical significance (**Figure 7A**).

3.6.3 ROS-Production

Next, we analyzed the generation of ROS as another important effector mechanism in the innate pathogen defense of PMN. To this end, we incubated freshly isolated PMN with GM-CSF, LPS, PMA or *A. fumigatus* conidia and assessed the generation of ROS *via* DCFDA staining in time intervals of 15min for a total period of 90min. Our results revealed that PMN isolated from CD18^{Ly6G} cKO mice generated significantly lower amounts of ROS after

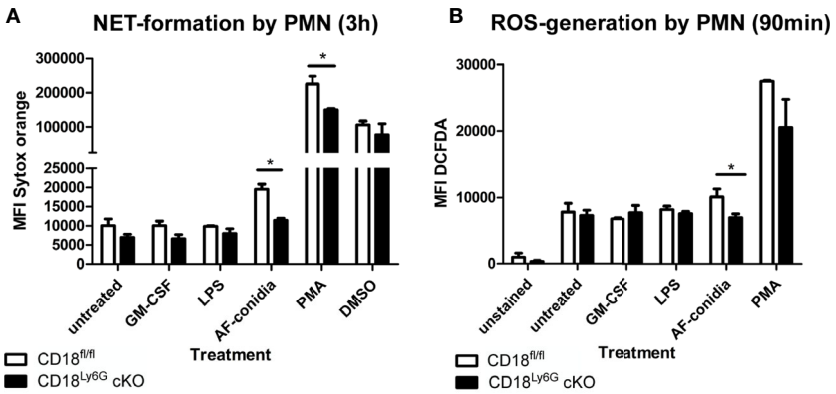

FIGURE 7 | Impaired oxidative and non-oxidative effector functions of CD18-deficient PMN. We could observe that the formation of NET after 3h of incubation **(A)** and ROS-generation **(B)** were significantly lower in PMN derived from $CD18^{Ly6G}$ cKO mice, particularly after stimulation with *A. fumigatus* conidia. Data represent the mean ± SEM of 3 samples analyzed/group. Statistically significant differences between groups are indicated (*p<0.05)

incubation with *A. fumigatus* conidia, suggesting that a CD18 knockdown might impair the ability of PMN to exercise this important effector mechanisms in pathogen-defense (**Figure 7B**). Referring particularly to the time kinetics of ROS-generation we could further observe that the ability to generate ROS was mainly impaired in the course of the first 60min, which indicates that β2 integrins might be implicated in the early generation of ROS (not shown).

3.6.4 Cytokine Secretion

β2 integrins have been found to regulate various signaling pathways in myeloid cells, which modulate the secretion of inflammatory cytokines (27). Hence, we have investigated the generation of cytokines by PMN after *in-vitro* stimulation with GM-CSF, LPS (TLR4 agonist), CpG (TLR9 agonist), and R8/48 (TLR7/8 agonist): Here, we could observe that PMN derived from $CD18^{Ly6G}$ cKO mice generated significantly less amounts of TNF-α upon treatment with LPS (**Figure 8**). On the other hand, we detected significant concentrations of IL-1β, IL-6 and IL-10 upon PMN stimulation, although genotype-dependent differences were largely below statistical significance (**Supplementary Figure 9**). Other cytokines (IL-12, IL-23 or IFN-γ) showed very low concentrations (not shown), suggesting that these cytokines might not be secreted by PMN under the conditions applied. These *in-vitro* data are consistent with our observations from *in-vivo* analysis, showing that BALF and

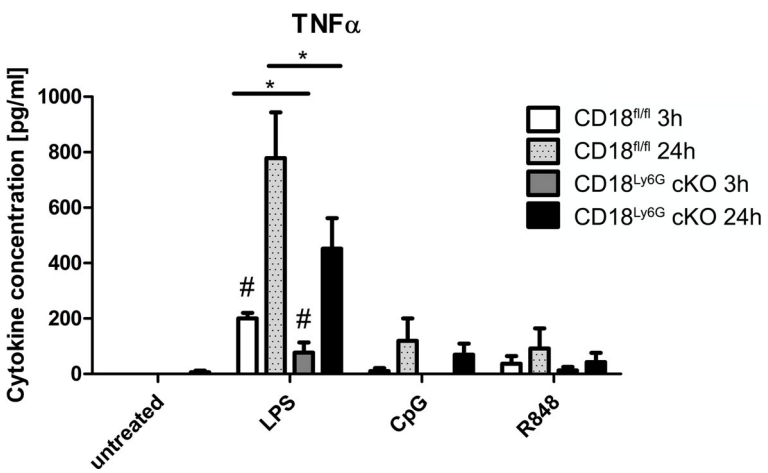

FIGURE 8 | PMN derived from $CD18^{Ly6G}$ cKO mice generate lower amounts of TNF-α after previous stimulation with LPS, CpG or R848. We have purified PMN from $CD18^{fl/fl}$ (n=3) mice and $CD18^{Ly6G}$ cKO (n=3) mice and incubated them for 24h at the indicated conditions. After 3h and 24h supernatants have been taken and were analyzed using a CBA. Results show significantly lower levels of TNF-α in supernatants derived from $CD18^{Ly6G}$ cKO mice. *p<0.05, #p<0.05 when comparing cytokine concentrations from supernatants at 3 vs 24h.

blood derived from CD18^{Ly6G} cKO mice contained lower amounts of TNF-α or IL-1.

3.6.5 RNA-Sequencing Analysis

Last, we have analyzed the impact of the β2 integrin knockdown on the transcriptome of PMN. To this end, we performed RNA-sequencing analysis of either freshly isolated PMN from CD18^{Ly6G} cKO and CD18$^{fl/fl}$ mice or treated aliquots of isolated PMN over-night with LPS (1μg/ml). This genome-wide gene expression analysis confirmed that both, freshly isolated and LPS-treated CD18-deficient PMN showed a significant downregulation of *Itgb2* and *Ly6G*. Referring to the expression of other integrin genes, we could further observe a downregulation *Itgb3* and *Itgb7*, whereas the CD11c encoding gene *Itgax*, and *Itgb2l* were found to be upregulated in CD18^{Ly6G} cKO PMN. Moreover, RNA-sequencing data revealed that CD18-deficient PMN showed a higher expression of genes implicated in NFκB signaling, such as *CD180*, *Ly86*, *CD14*, *Bach2* or the LPS antagonistic neutrophilic granule protein *Ngp* (44). On the other hand, we could observe a downregulation of genes involved in the inhibition of oxidative effector functions in PMN, such as *S100a9* (45), and a downregulation of genes being implicated in PMN chemotaxis and microbicidal functions (i.e., *Defb40*) in CD18^{Ly6G} cKO PMN (**Figure 9**).

4 DISCUSSION

The critical role of β2 integrins for immunological functions is confirmed by the severe immunocompromised state of LAD1 patients, which regularly results in reoccurring invasive bacterial and fungal infections (22, 30). PMN are considered the first line of defense to prevent the spread of inhaled pathogens in the lung (46), and were shown to require β2-integrins for transendothelial migration (24), phagocytosis of opsonized pathogens (21), as well as oxidative, and non-oxidative effector mechanisms (16). Due to the importance of β2-integrins for PMN effector functions and the frequent observation of IPA in LAD1 patients, we aimed to investigate the cell-type specific role of β2 integrins for PMN antifungal effector functions in the early innate immune response to IPA.

Here, we have obtained several key findings that corroborate previous concepts of the pathophysiological role of β2-integrins in the context of severe infections. Our results put these observations into a cell-type specific context and

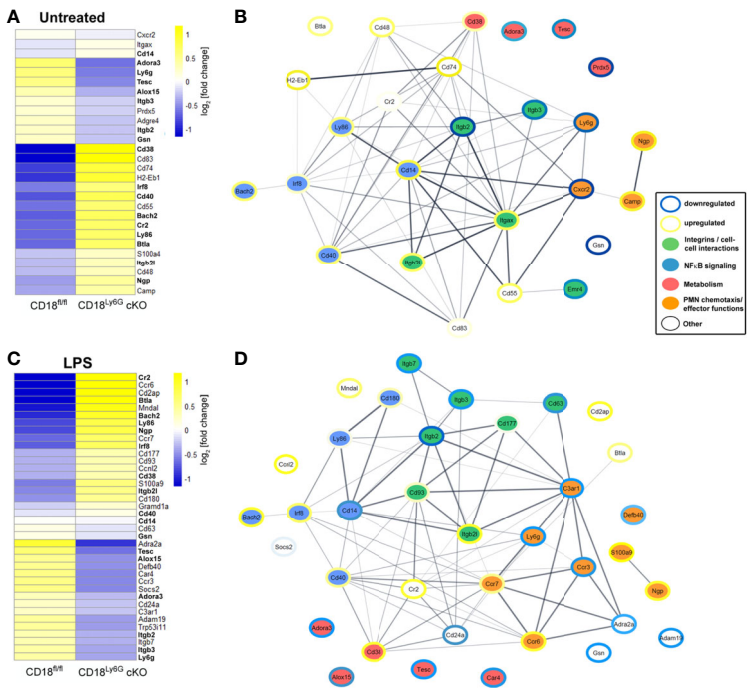

FIGURE 9 | Transcriptomes and functional interaction networks of PMN-associated genes directly after isolation or upon over-night treatment with LPS. PMN were sorted from CD18$^{fl/fl}$ and CD18^{Ly6G} cKO mice (each n=3) and RNA-seq was performed from untreated PMN **(A)** or LPS-treated PMN **(C)**. Expression of indicated PMN-associated genes was analyzed using CLC Genomics Workbench. Genes being differentially regulated both in LPS-treated and freshly isolated PMN are shown in bold **(A, C)**. Predicted interaction networks of the encoded proteins were being visualized using the STRING package in Cytoscape. Genes shown in the interaction networks of untreated PMN **(B)** or LPS-treated PMN **(D)** were categorized into 4 groups affecting either PMN cell-cell interactions, NFκB singaling, PMN metabolism or PMN chemotaxis and PMN effector functions. Colored borders illustrate the degree of the up- or downregulation (log fold change) found for the genes of PMN isolated from CD18^{Ly6G} cKO mice as compared to PMN isolated from CD18$^{fl/fl}$ mice. Legend in **(B, D)**.

allow insights into the role of CD18 for antifungal effector mechanisms of PMN in the course of IPA, which have not been shown previously.

First, we could observe that the fungal clearance and the early innate immune response in $CD18^{Ly6G}$ cKO mice are significantly impaired. In particular, we found that 24 hours after infection, lungs derived from $CD18^{Ly6G}$ cKO mice showed an enhanced fungal burden and a lower bronchial inflammation as compared to those of $CD18^{fl/fl}$ mice. When PMN are activated upon contact with pathogens and by various danger signals (i.e., the *A. fumigatus* cell wall component ß-glucan), they contribute to the inflammatory immune response in infected tissues by secreting proinflammatory cytokines and chemokines (47). We observed lower levels of innate proinflammatory mediators, such as TNF-α, IL-1α, IL-1ß, and chemokines, like CCL2 and CCL5 in BALF derived from $CD18^{Ly6G}$ cKO mice, suggesting that the knockdown of β2-integrins might have impaired the ability of PMN to generate these inflammatory mediators. Moreover, we observed lower expression levels of markers for PMN degranulation (CD62L) and activation (MHCII, CD80) in PMN derived from $CD18^{Ly6G}$ cKO mice, indicating that the inflammatory signaling pathways in PMN might have also been impaired by CD18 deficiency. In agreement, we found that *A. fumigatus* infected $CD18^{Ly6G}$ cKO mice showed an aggravated course of IPA.

Despite, the significant impairment of the early innate immune response mediated by PMN, the overall survival of *A. fumigatus* infected $CD18^{Ly6G}$ cKO mice was not significantly impaired, suggesting that CD18 despite its pivotal immunoregulatory function might not be critical for the long-term control of IPA or that the residual β2-integrin expression found on PMN of $CD18^{Ly6G}$ cKO mice was sufficient for PMN-mediated pathogen clearance in some mice. Additionally, our results revealed several mechanisms, which may serve to compensate for the impaired effector functions of PMN in $CD18^{Ly6G}$ cKO mice upon infection: Particularly, we could observe a higher level of the PMN-attracting chemokine CXCL-1 in BALF obtained from $CD18^{Ly6G}$ cKO mice. Accordingly, a significantly higher bronchial infiltration by PMN has been found in these mice. These findings were unexpected as β2 integrins were reported to be necessary for the firm adhesion of PMN to vessel endothelium as a prerequisite of PMN migration into the extravascular space (48). In this regard, it has been suggested, that the requirement of CD18 for PMN infiltration might depend on the type of pathogen used in $CD18^{-/-}$ mice (49) and the disease specific context investigated (50). Also, it has been suggested by Mackarel and coworkers, that PMN migration into inflamed lungs might occur either *via* a CD18-dependent or CD18-independent route, which is selected depending on whether inflammation is acute or chronic (51). In particular, Mizgerd and coworkers reported that intratracheal instillation with *E. coli* or *Ps. aeruginosa* resulted in a limited pulmonary PMN-infiltration, whereas infection with *S. pneumonia* yielded a stronger PMN-infiltration in a CD18-independent manner (49). These observations are consistent with previous reports, which have demonstrated that $CD11b^{-/-}$mice infected with either *S. pneumoniae* (52) or *A. fumigatus* (5), showed an elevated PMN infiltration 24 hours upon infection. However, also in these disease models a higher pulmonary burden and a diminished cellular inflammation have been reported. Similarly, a stronger pulmonary infiltration by PMN has been observed in LAD1 patients suffering from pneumonia (53), suggesting that MAC-1 might not be essential for PMN migration. Rather β2 integrin deficiency may be compensated by other adhesion receptors in a disease specific manner (22). In this context, some studies have reported that LFA-1 (CD11a/CD18) may play a dominant role for transendothelial migration of PMN (51, 54). Our results could however not reveal an upregulation of CD11a on PMN, but rather showed a significant downregulation of CD11a in the context of CD18-deficiency. This is in line with the physiological regulation of β2-integrins on PMN. In particular, the downregulation of CD18 in our knock-out mouse model limits the amount of intracellular available CD18 protein and thus heterodimerization with the corresponding alpha subunits on the cell surface is also being restricted, resulting in lower expression levels of LFA-1 (CD11a/CD18) and MAC-1 (CD11b/CD18) on PMN. On the other hand, RNA-sequencing results indicated that other β2 integrin-associated genes (such as the CD11c coding *Itgax* or *Itgb2l*) and genes coding for chemokine receptors (i.e., *Ccr7*) might be upregulated in PMN isolated from $CD18^{Ly6G}$ cKO mice potentially revealing another compensatory mechanism (**Figure 9**). Altogether, our results suggest that the knockdown of β2 integrins (LFA-1, MAC-1) might not significantly impair the pulmonary migration of PMN. However, when interpreting the results of our analysis, it has to be taken into account that a significant residual expression of CD18 was still being observed on PMN, which might allow for the CD18-dependent migration of PMN into inflamed pulmonary tissue.

Furthermore, we could demonstrate that PMN isolated from $CD18^{Ly6G}$ cKO mice showed an impaired phagocytic activity towards opsonized *A. fumigatus* conidia and inert particles as compared to $CD18^{fl/fl}$ PMN, which is consistent with the enhanced pulmonary fungal burden found in *A. fumigatus* infected $CD18^{Ly6G}$ cKO mice. This finding is in agreement with previous observations that MAC-1 is required in human PMN to recognize ß-glucan containing structures (55), such as *A. fumigatus* conidia, and thus to kill conidia by phagocytic uptake (21, 56).

In contrast to small-sized conidia, recognition of *A. fumigatus* hyphae has been largely attributed to IgG and Fcγ receptors (21). However, cross-linking of MAC-1 upon pathogen-recognition, also results in an NADPH-oxidase-dependent oxidative burst by PMN, which is required for an efficient fungal clearance of both *A. fumigatus* conidia and hyphae (19, 21, 57–59). Oxidative burst protects against invasive fungal infections, because it induces apoptosis-like cell death in fungal conidia (60) and contributes to the formation of NET (61, 62). The latter is considered a mechanism of extracellular killing of hyphae, being too large to be phagocytosed (63). The proposed role of MAC-1 for the induction of ROS and the formation of NET by PMN upon incubation with *A. fumigatus* conidia indicates that both antifungal killing-mechanisms might be impaired in $CD18^{Ly6G}$ cKO mice. These findings are again consistent with previous

reports, which demonstrated that $CD11b^{-/-}$ mice displayed an attenuated PMN killing activity and increased fungal burdens in a mouse model of candidiasis, thus underpinning the pivotal role of β2 integrins for antifungal effector mechanisms (64), such as CR3-mediated phagocytosis, NETosis (65) and ROS-generation (20, 66). Interestingly, Yakubenko and coworkers have more recently observed that neutrophil oxidative burst might further contribute to a positive feedback loop with β2 integrins by enhancing the affinity of MAC-1 ligands to MAC-1 on macrophages, thus stimulating their migratory activity (67).

Next to the direct cytotoxic effects exerted by PMN, some studies reported that the engagement of MAC-1 with extracellular pathogens also promotes proinflammatory signaling pathways in PMN *via* activation of members of the NF-κB transcription factor family, thus yielding an elevated production of proinflammatory cytokines such as IL-1 and TNF-α (68, 69). In agreement we observed that a knockdown of β2 integrins impaired the secretion of TNF-α. Moreover, it has been found that CD11b facilitates TLR-4 mediated proinflammatory immune responses by promoting MyD88 signaling pathways (27). Hence, the impaired induction of an inflammatory milieu in the lungs of $CD18^{Ly6G}$ cKO mice might be a consequence of the attenuated PMN activation, resulting from a reduced activity of CD18-deficient PMN to recognize and phagocytose *A. fumigatus* conidia and to promote TLR-4-induced signaling pathways.

Besides the diminished levels of proinflammatory cytokines found in BALF obtained from $CD18^{Ly6G}$ cKO mice, we could also observe lower levels of macrophage attracting chemokines CCL2 and CCL5 therein. CCL5 is known to attract many leukocyte populations, such as macrophages and PMN (70–72). Early in the course of inhalative inflammation, CCL5 is generated by various activated cell types, including airway epithelial cells (73) or lung fibroblasts (74). Moreover, *A. fumigatus* was reported to induce CCL5 in platelets (75), and activated PMN were demonstrated to produce CCL5 when incubated with *Toxoplasma gondii* (76). Therefore, it is conceivable that a reduced level of β2 integrins on PMN might impair their ability to generate CCL5.

CCL2, also known as monocyte chemoattractant protein (MCP)-1 is an important regulator of monocyte and macrophage trafficking during infection and in the presence of inflammation (77–79). CCL2 is generated by pulmonary epithelium (80), endothelial cells (81), fibroblasts and T cells upon induction with inflammatory stimuli such as LPS or IFN-γ (82). Notably, also PMN contribute to CCL2 generation, which can be induced upon TLR2-/TLR4-activation (82, 83). CCL2 mainly serves as a chemoattractant for monocytes and macrophages (82, 84–86). Beyond its role as a monocyte chemoattractant CCL2 has been implicated in various molecular and cellular processes impacting myeloid cell functions and their response to pathogens. In particular, it has been shown that CCL2 induces β2 integrin expression on monocytes, thus promoting their migration into inflamed tissues (82, 87) Moreover an enhanced survival and an augmented generation of proinflammatory cytokines by $CD11b^{+}$ cells has been demonstrated upon CCL2 treatment (88). CCL2 treatment has further been shown to induce respiratory burst in monocytes, thus contributing to myeloid cell effector functions in response to pathogens (82, 89). In agreement, increased CCL2 levels have been reported to improve the clearance of pathogens and the survival of *S. pneumonia* infected mice (90). These studies are consistent with our observations that $CD18^{fl/fl}$ mice show higher levels of CCL2, a lower fungal burden and a stronger pulmonary infiltration with macrophages, which might exert critical antifungal effector mechanisms in the early innate response to *A. fumigatus* infection (90). Due to impaired signaling in CD18-deficient PMN it also seems conceivable, that PMN might generate less CCL2 and CCL5 in $CD18^{Ly6G}$ cKO mice. However, as for the multiple sources of these chemokines, further studies are required to elucidate which cell types are responsible for the different concentrations of CCL2 and CCL5 in the lungs of *A. fumigatus* infected $CD18^{Ly6G}$ cKO mice and which cells are most likely to be attracted in response to these chemokines.

In addition to migration, pathogen recognition/phagocytosis, and the regulation of cell signaling, MAC-1 has also been implicated in myeloid cell survival. Referring particularly to PMN apoptosis, we could observe that PMN derived from *A. fumigatus* infected $CD18^{Ly6G}$ cKO mice showed a stronger expression of apoptosis marker Annexin-V, suggesting that a knockdown of β2 integrins might impair PMN survival. This is in contrast to previous *in-vitro* experiments from Coxon and coworkers, which suggested that CD11b contributes to PMN survival, as $CD11b^{-/-}$ PMN isolated from the peritoneum after injection of thioglycollate were characterized by lower apoptosis than their wild-type counterparts (42). However, the contribution of MAC-1 signaling to apoptosis of activated PMN is still subject to controversial discussion. For example, another report by Zhang *et al.* showed that phagocytosis of pathogens by PMN promoted apoptosis of the latter, which was associated with the induction of reactive oxygen species and was enhanced by TNF-α (91). In contrast, $CD11b^{-/-}$ PMN were not found to undergo phagocytosis-induced apoptosis. Similar findings were reported for human PMN (92). On the contrary, Yan and coworkers showed that antibody-mediated blockade of β2 integrins on human PMN elevated apoptosis after their activation by TNF-α or microbial stimuli (93). Since $CD18^{Ly6G}$ cKO mice only showed a moderate, PMN-restricted, LAD1 phenotype with a residual β2-integrin expression on PMN it seems conceivable that apoptosis may not have been significantly impaired, whereas the same moderate reduction of CD18 on PMN might yet affect other PMN effector functions, as well as the overall course of the disease. Hence, further studies are warranted to elucidate the exact role of MAC-1 on PMN viability during pathogen control.

Although our study focused on the role of β2 integrins for PMN effector mechanisms during early innate immune responses towards inhalative infection with *A. fumigatus*, it is likely that a knockdown of β2 integrins might not only impair PMN functions but may also modulate their interaction with

other immune cells implicated in IPA-resolution, such as DC (94), macrophages, lymphocytes or eosinophils (95, 96). Here, a report by Park and coworkers could show that PMN contribute to pulmonary infiltration of $CD11b^+$ conventional DC in IPA by activating $CD11b^+$ DC *via* DC-SIGN (94). This C-type lectin receptor expressed by DC and macrophages mediates the phagocytic uptake of *A. fumigatus* conidia (97) and engages with PMN-bound MAC-1 upon DC-PMN interaction (98). Hence, MAC-1 on PMN may further contribute to the activation of infiltrating DC, which produce IL-12 and IL-23, thus inducing Th_1 immunity in IPA (99). Notably, IL-23 has also been reported to stimulate IL-17 production in PMN, and IL-17 induced ROS production by PMN (100), contributing to the killing of *A. fumigatus* conidia and hyphae. Thus, the diminished expression of CD18 on PMN might further impair their interaction with DC, contributing to an impaired antifungal immune response in $CD18^{Ly6G}$ cKO mice. However, we could not find significant differences neither in IL-17 nor IL-23 secretion in BALF and serum. An important limitation of our experiments is the residual expression of β2-integrins on PMN derived from $CD18^{dLy6G}$ mice which may only result in a moderate impairment of PMN effector. On first sight, an adoptive transfer of PMN from $CD11b^{-/-}$ mice into infected WT mice after depletion of WT PMN may be suitable to give more comprehensive insights into the PMN-specific role of β2-integrins during invasive *A. fumigatus* infections and exclude compensatory effects that might result from an intermediate PMN phenotype. In this context it would also be interesting to evaluate whether the addition of WT PMN into $CD18^{Ly6G}$ cKO mice might reverse a severe course of the disease. However, such adoptive transfer studies might be subject to methodological bias, including the rather short life span of PMN in general, the influence of β2 integrins on PMN viability and the possibility of artificial PMN activation during adoptive transfer procedures. In conclusion, our results demonstrate, that the PMN-specific downregulation of CD18 allows for a distinct cell-type specific analysis of the role of β2 integrins for PMN effector functions, PMN signaling, survival and the role of β2 integrins as regulators within the immune cell network (47). We could further show that CD18 deficiency on PMN particularly affects the early course of IPA, which might be attributed to the critical role of MAC−1 for PMN antifungal effector mechanisms, such as phagocytosis and ROS-generation (5). However, we cannot rule out that the CD18-knockdown might cause additional unrecognized effects in PMN effector functions, such as the release of primary granules or MPO-activity contributing to the clearance of *A. fumigatus* or that residual CD18 expression might compensate some impaired effector functions. Taking into account that previous PMN-specific knock-out models, such as the $Syk^{fl/-}$ $MRP8Cre^{Tg}$ mice reported by van Ziffle and Lowell (101), also showed a residual expression of the targeted proteins on PMN, further work is necessary to generate knock-out models which might allow for a complete knock-out of β2-integrins on PMN. Also, additional studies will be necessary to elucidate the long-term course of IPA in $CD18^{Ly6G}$ cKO mice with regard to the interplay of PMN with DC, the efficacy of adaptive immune responses and the contribution of chemokines such as CCL2 and CCL5.

DATA AVAILABILITY STATEMENT

The datasets presented in this study can be found in online repositories. The names of the repository/repositories and accession number(s) can be found below: Gene Expression Omnibus, GSE195444.

ETHICS STATEMENT

The animal study was reviewed and approved by the National State Investigation Office Rhineland-Palatinate, Approval ID: 23177-07/G16-1-020.

AUTHOR CONTRIBUTIONS

MH designed methods for *in-vitro* and *ex-vivo* experiments, carried out experiments, performed image analysis, carried out data analysis, calculated statistics, designed and generated figures, compiled tables, and wrote the manuscript. MBro designed experiments, designed methods for *in-vitro* experiments, performed image analyses, edited and designed figures and tables, and helped writing the manuscript. FR, DT and MK helped to design and carry out the *in-vivo* experiments, helped writing the manuscript and edited the manuscript. MK and ES helped carrying out the experiments. SG and MR helped designing the experiments, as well as writing and editing the manuscript. MBed (Monika Bednarczyk) generated the $CD18^{fl/fl}$ and $CD18^{Ly6G}$ cKO mouse. MG helped generating the $CD18^{Ly6G}$ cKO mouse strain, provided C57BL/6-*Ly6g* (tm2621(Cre-tdTomato)Arte mice and AF strains (ATCC 46645 and Afs148) and helped editing the manuscript. All authors contributed to the article and approved the submitted version.

FUNDING

MH was supported by the Clinician Scientist Fellowship "TransMed Jumpstart Program: 2019_A72" supported by the Else Kröner Fresenius Foundation and by an intramural research funding of the UMC Mainz. MR is funded by the TRR156 KS01 and SFB1066 TPB10. SG is funded by the DFG (TRR156, B11; SFB1066, B04).

ACKNOWLEDGMENTS

The authors would like to thank C. Braun, F. Zarate, I. Tubbe, S. Hamdi and E. Montermann for excellent technical

assistance. Also, we gratefully acknowledge the support by Matthias Klein, the Forschungszentrum Immunologie (FZI) and the FZI sequencing core facility at the University Medical Center Mainz for the generation and analysis of RNA-sequencing data.

SUPPLEMENTARY MATERIAL

The Supplementary Material for this article can be found online at: https://www.frontiersin.org/articles/10.3389/fimmu.2022.823121/full#supplementary-material

REFERENCES

1. Gresnigt MS, Rekiki A, Rasid O, Savers A, Jouvion G, Dannaoui E, et al. Reducing Hypoxia and Inflammation During Invasive Pulmonary Aspergillosis by Targeting the Interleukin-1 Receptor. *Sci Rep* (2016) 6 (1):26490. doi: 10.1038/srep26490
2. O'Gorman CM, Fuller HT. Prevalence of Culturable Airborne Spores of Selected Allergenic and Pathogenic Fungi in Outdoor Air. *Atmos Environ* (2008) 42(18):4355–68. doi: 10.1016/j.atmosenv.2008.01.009
3. Brown GD, Denning DW, Gow NA, Levitz SM, Netea MG, White TC. Hidden Killers: Human Fungal Infections. *Sci Transl Med* (2012) 4 (165):165rv13. doi: 10.1126/scitranslmed.3004404
4. Feldmesser M. Role of Neutrophils in Invasive Aspergillosis. *Infect Immun* (2006) 74(12):6514–6. doi: 10.1128/IAI.01551-06
5. Teschner D, Cholaszczynska A, Ries F, Beckert H, Theobald M, Grabbe S, et al. CD11b Regulates Fungal Outgrowth But Not Neutrophil Recruitment in a Mouse Model of Invasive Pulmonary Aspergillosis. *Front Immunol* (2019) 10:123. doi: 10.3389/fimmu.2019.00123
6. Braem SG, Rooijakkers SH, van Kessel KP, de Cock H, Wosten HA, van Strijp JA, et al. Effective Neutrophil Phagocytosis of Aspergillus Fumigatus Is Mediated by Classical Pathway Complement Activation. *J Innate Immun* (2015) 7(4):364–74. doi: 10.1159/000369493
7. Latge JP. The Pathobiology of Aspergillus Fumigatus. *Trends Microbiol* (2001) 9(8):382–9. doi: 10.1016/S0966-842X(01)02104-7
8. Botterel F, Gross K, Ibrahim-Granet O, Khoufache K, Escabasse V, Coste A, et al. Phagocytosis of Aspergillus Fumigatus Conidia by Primary Nasal Epithelial Cells *In Vitro*. *BMC Microbiol* (2008) 8(1):97. doi: 10.1186/1471-2180-8-97
9. Rammaert B, Jouvion G, de Chaumont F, Garcia-Hermoso D, Szczepaniak C, Renaudat C, et al. Absence of Fungal Spore Internalization by Bronchial Epithelium in Mouse Models Evidenced by a New Bioimaging Approach and Transmission Electronic Microscopy. *Am J Pathol* (2015) 185(9):2421–30. doi: 10.1016/j.ajpath.2015.04.027
10. Luther K, Torosantucci A, Brakhage AA, Heesemann J, Ebel F. Phagocytosis of Aspergillus Fumigatus Conidia by Murine Macrophages Involves Recognition by the Dectin-1 Beta-Glucan Receptor and Toll-Like Receptor 2. *Cell Microbiol* (2007) 9(2):368–81. doi: 10.1111/j.1462-5822.2006.00796.x
11. Braedel S, Radsak M, Einsele H, Latge JP, Michan A, Loeffler J, et al. Aspergillus Fumigatus Antigens Activate Innate Immune Cells *via* Toll-Like Receptors 2 and 4. *Br J Haematol* (2004) 125(3):392–9. doi: 10.1111/j.1365-2141.2004.04922.x
12. Mircescu MM, Lipuma L, van Rooijen N, Pamer EG, Hohl TM. Essential Role for Neutrophils But Not Alveolar Macrophages at Early Time Points Following Aspergillus Fumigatus Infection. *J Infect Dis* (2009) 200(4):647–56. doi: 10.1086/600380
13. Post MJ, Lass-Floerl C, Gastl G, Nachbaur D. Invasive Fungal Infections in Allogeneic and Autologous Stem Cell Transplant Recipients: A Single-Center Study of 166 Transplanted Patients. *Transpl Infect Dis* (2007) 9 (3):189–95. doi: 10.1111/j.1399-3062.2007.00219.x
14. Cohen MS, Isturiz RE, Malech HL, Root RK, Wilfert CM, Gutman L, et al. Fungal Infection in Chronic Granulomatous Disease. The Importance of the Phagocyte in Defense Against Fungi. *Am J Med* (1981) 71(1):59–66. doi: 10.1016/0002-9343(81)90259-X
15. Gerson SL, Talbot GH, Hurwitz S, Strom BL, Lusk EJ, Cassileth PA. Prolonged Granulocytopenia: The Major Risk Factor for Invasive Pulmonary Aspergillosis in Patients With Acute Leukemia. *Ann Intern Med* (1984) 100(3):345–51. doi: 10.7326/0003-4819-100-3-345
16. Prufer S, Weber M, Stein P, Bosmann M, Stassen M, Kreft A, et al. Oxidative Burst and Neutrophil Elastase Contribute to Clearance of Aspergillus Fumigatus Pneumonia in Mice. *Immunobiology* (2014) 219(2):87–96. doi: 10.1016/j.imbio.2013.08.010
17. Diamond RD, Clark RA. Damage to Aspergillus Fumigatus and Rhizopus Oryzae Hyphae by Oxidative and Nonoxidative Microbicidal Products of Human Neutrophils *In Vitro*. *Infect Immun* (1982) 38(2):487–95. doi: 10.1128/iai.38.2.487-495.1982
18. Leal SMJr., Vareechon C, Cowden S, Cobb BA, Latge JP, Momany M, et al. Fungal Antioxidant Pathways Promote Survival Against Neutrophils During Infection. *J Clin Invest* (2012) 122(7):2482–98. doi: 10.1172/JCI63239
19. Boyle KB, Gyori D, Sindrilaru A, Scharffetter-Kochanek K, Taylor PR, Mocsai A, et al. Class IA Phosphoinositide 3-Kinase Beta and Delta Regulate Neutrophil Oxidase Activation in Response to Aspergillus Fumigatus Hyphae. *J Immunol* (2011) 186(5):2978–89. doi: 10.4049/jimmunol.1002268
20. Aarts CEM, Hiemstra IH, Beguin EP, Hoogendijk AJ, Bouchmal S, van Houdt M, et al. Activated Neutrophils Exert Myeloid-Derived Suppressor Cell Activity Damaging T Cells Beyond Repair. *Blood Adv* (2019) 3 (22):3562–74. doi: 10.1182/bloodadvances.2019031609
21. Gazendam RP, van Hamme JL, Tool AT, Hoogenboezem M, van den Berg JM, Prins JM, et al. Human Neutrophils Use Different Mechanisms To Kill Aspergillus Fumigatus Conidia and Hyphae: Evidence From Phagocyte Defects. *J Immunol* (2016) 196(3):1272–83. doi: 10.4049/jimmunol.1501811
22. Bednarczyk M, Stege H, Grabbe S, Bros M. Beta2 Integrins-Multi-Functional Leukocyte Receptors in Health and Disease. *Int J Mol Sci* (2020) 21(4):6. doi: 10.3390/ijms21041402
23. Arnaout MA. Biology and Structure of Leukocyte Beta 2 Integrins and Their Role in Inflammation. *F1000Res* (2016) 5(2433):1. doi: 10.12688/f1000research.9415.1
24. Basoni C, Nobles M, Grimshaw A, Desgranges C, Davies D, Perretti M, et al. Inhibitory Control of TGF-Beta1 on the Activation of Rap1, CD11b, and Transendothelial Migration of Leukocytes. *FASEB J* (2005) 19(7):822–4. doi: 10.1096/fj.04-3085fje
25. Ehlers MR. CR3: A General Purpose Adhesion-Recognition Receptor Essential for Innate Immunity. *Microbes Infect* (2000) 2(3):289–94. doi: 10.1016/S1286-4579(00)00299-9
26. Huang ZY, Hunter S, Chien P, Kim MK, Han-Kim TH, Indik ZK, et al. Interaction of Two Phagocytic Host Defense Systems: Fcgamma Receptors and Complement Receptor 3. *J Biol Chem* (2011) 286(1):160–8. doi: 10.1074/jbc.M110.163030
27. Ling GS, Bennett J, Woollard KJ, Szajna M, Fossati-Jimack L, Taylor PR, et al. Integrin CD11b Positively Regulates TLR4-Induced Signalling Pathways in Dendritic Cells But Not in Macrophages. *Nat Commun* (2014) 5(1):3039. doi: 10.1038/ncomms4039
28. Varga G, Balkow S, Wild MK, Stadtbaeumer A, Krummen M, Rothoeft T, et al. Active MAC-1 (CD11b/CD18) on DCs Inhibits Full T-Cell Activation. *Blood* (2007) 109(2):661–9. doi: 10.1182/blood-2005-12-023044
29. Lim J, Hotchin NA. Signalling Mechanisms of the Leukocyte Integrin Alphambeta2: Current and Future Perspectives. *Biol Cell* (2012) 104 (11):631–40. doi: 10.1111/boc.201200013
30. Harris ES, Weyrich AS, Zimmerman GA. Lessons From Rare Maladies: Leukocyte Adhesion Deficiency Syndromes. *Curr Opin Hematol* (2013) 20 (1):16–25. doi: 10.1097/MOH.0b013e32835a0091
31. Anderson DC, Schmalsteig FC, Finegold MJ, Hughes BJ, Rothlein R, Miller LJ, et al. The Severe and Moderate Phenotypes of Heritable Mac-1, LFA-1 Deficiency: Their Quantitative Definition and Relation to Leukocyte Dysfunction and Clinical Features. *J Infect Dis* (1985) 152(4):668–89. doi: 10.1093/infdis/152.4.668
32. Lother J, Breitschopf T, Krappmann S, Morton CO, Bouzani M, Kurzai O, et al. Human Dendritic Cell Subsets Display Distinct Interactions With the

Pathogenic Mould Aspergillus Fumigatus. *Int J Med Microbiol* (2014) 304 (8):1160–8. doi: 10.1016/j.ijmm.2014.08.009
33. Lee PY, Wang JX, Parisini E, Dascher CC, Nigrovic PA. Ly6 Family Proteins in Neutrophil Biology. *J Leukoc Biol* (2013) 94(4):585–94. doi: 10.1189/jlb.0113014
34. Becher B, Schlitzer A, Chen J, Mair F, Sumatoh HR, Teng KW, et al. High-Dimensional Analysis of the Murine Myeloid Cell System. *Nat Immunol* (2014) 15(12):1181–9. doi: 10.1038/ni.3006
35. Hasenberg A, Hasenberg M, Mann L, Neumann F, Borkenstein L, Stecher M, et al. Catchup: A Mouse Model for Imaging-Based Tracking and Modulation of Neutrophil Granulocytes. *Nat Methods* (2015) 12(5):445–52. doi: 10.1038/nmeth.3322
36. Alflen A, Prufer S, Ebner K, Reuter S, Aranda Lopez P, Scharrer I, et al. ADAMTS-13 Regulates Neutrophil Recruitment in a Mouse Model of Invasive Pulmonary Aspergillosis. *Sci Rep* (2017) 7(1):7184. doi: 10.1038/s41598-017-07340-3
37. Lamoth F. Galactomannan and 1,3-Beta-D-Glucan Testing for the Diagnosis of Invasive Aspergillosis. *J Fungi (Basel)* (2016) 2(3):22. doi: 10.3390/jof2030022
38. Majewska E, Sulowska Z, Baj Z. Spontaneous Apoptosis of Neutrophils in Whole Blood and Its Relation to Apoptosis Gene Proteins. *Scand J Immunol* (2000) 52(5):496–501. doi: 10.1046/j.1365-3083.2000.00802.x
39. Team RC. R Core Team R: A Language and Environment for Statistical Computing, *Foundation for Statistical Computing*, 2020.
40. Love MI, Huber W, Anders S. Moderated Estimation of Fold Change and Dispersion for RNA-Seq Data With Deseq2. *Genome Biol* (2014) 15(12):550. doi: 10.1186/s13059-014-0550-8
41. Wang JX, Bair AM, King SL, Shnayder R, Huang YF, Shieh CC, et al. Ly6G Ligation Blocks Recruitment of Neutrophils *via* a Beta2-Integrin-Dependent Mechanism. *Blood* (2012) 120(7):1489–98. doi: 10.1182/blood-2012-01-404046
42. Coxon A, Rieu P, Barkalow FJ, Askari S, Sharpe AH, von Andrian UH, et al. A Novel Role for the β2 Integrin CD11b/CD18 in Neutrophil Apoptosis: A Homeostatic Mechanism in Inflammation. *Immunity* (1996) 5(6):653–66. doi: 10.1016/S1074-7613(00)80278-2
43. Girbl T, Lenn T, Perez L, Rolas L, Barkaway A, Thiriot A, et al. Distinct Compartmentalization of the Chemokines CXCL1 and CXCL2 and the Atypical Receptor ACKR1 Determine Discrete Stages of Neutrophil Diapedesis. *Immunity* (2018) 49(6):1062–76.e6. doi: 10.1016/j.immuni.2018.09.018
44. Hong J, Qu P, Wuest T, Lin PC. Neutrophilic Granule Protein Is a Novel Murine LPS Antagonist. *J Immunol* (2020) 204(1):60.21–1. doi: 10.4110/in.2019.19.e34
45. Sroussi HY, Lu Y, Zhang QL, Villines D, Marucha PT. S100A8 and S100A9 Inhibit Neutrophil Oxidative Metabolism *In-Vitro*: Involvement of Adenosine Metabolites. *Free Radic Res* (2010) 44(4):389–96. doi: 10.3109/10715760903431434
46. Baddley JW, Andes DR, Marr KA, Kontoyiannis DP, Alexander BD, Kauffman CA, et al. Factors Associated With Mortality in Transplant Patients With Invasive Aspergillosis. *Clin Infect Dis* (2010) 50(12):1559–67. doi: 10.1086/652768
47. Yang F, Feng C, Zhang X, Lu J, Zhao Y. The Diverse Biological Functions of Neutrophils, Beyond the Defense Against Infections. *Inflammation* (2017) 40(1):311–23. doi: 10.1007/s10753-016-0458-4
48. Langer HF, Chavakis T. Leukocyte-Endothelial Interactions in Inflammation. *J Cell Mol Med* (2009) 13(7):1211–20. doi: 10.1111/j.1582-4934.2009.00811.x
49. Mizgerd JP, Horwitz BH, Quillen HC, Scott ML, Doerschuk CM. Effects of CD18 Deficiency on the Emigration of Murine Neutrophils During Pneumonia. *J Immunol* (1999) 163(2):995–9.
50. Cunin P, Lee PY, Kim E, Schmider AB, Cloutier N, Pare A, et al. Differential Attenuation of Beta2 Integrin-Dependent and -Independent Neutrophil Migration by Ly6G Ligation. *Blood Adv* (2019) 3(3):256–67. doi: 10.1182/bloodadvances.2018026732
51. Mackarel AJ, Russell KJ, Ryan CM, Hislip SJ, Rendall JC, FitzGerald MX, et al. CD18 Dependency of Transendothelial Neutrophil Migration Differs During Acute Pulmonary Inflammation. *J Immunol* (2001) 167(5):2839–46. doi: 10.4049/jimmunol.167.5.2839
52. Rijneveld AW, de Vos AF, Florquin S, Verbeek JS, van der Poll T. CD11b Limits Bacterial Outgrowth and Dissemination During Murine Pneumococcal Pneumonia. *J Infect Dis* (2005) 191(10):1755–60. doi: 10.1086/429633
53. Hawkins HK, Heffelfinger SC, Anderson DC. Leukocyte Adhesion Deficiency: Clinical and Postmortem Observations. *Pediatr Pathol* (1992) 12(1):119–30. doi: 10.3109/15513819209023288
54. Ding ZM, Babensee JE, Simon SI, Lu H, Perrard JL, Bullard DC, et al. Relative Contribution of LFA-1 and Mac-1 to Neutrophil Adhesion and Migration. *J Immunol* (1999) 163(9):5029–38.
55. van Bruggen R, Drewniak A, Jansen M, van Houdt M, Roos D, Chapel H, et al. Complement Receptor 3, Not Dectin-1, Is the Major Receptor on Human Neutrophils for Beta-Glucan-Bearing Particles. *Mol Immunol* (2009) 47(2-3):575–81. doi: 10.1016/j.molimm.2009.09.018
56. Moalli F, Doni A, Deban L, Zelante T, Zagarella S, Bottazzi B, et al. Role of Complement and Fc{gamma} Receptors in the Protective Activity of the Long Pentraxin PTX3 Against Aspergillus Fumigatus. *Blood* (2010) 116 (24):5170–80. doi: 10.1182/blood-2009-12-258376
57. Nilsson M, Weineisen M, Andersson T, Truedsson L, Sjobring U. Critical Role for Complement Receptor 3 (CD11b/CD18), But Not for Fc Receptors, in Killing of Streptococcus Pyogenes by Neutrophils in Human Immune Serum. *Eur J Immunol* (2005) 35(5):1472–81. doi: 10.1002/eji.200424850
58. Futosi K, Fodor S, Mocsai A. Neutrophil Cell Surface Receptors and Their Intracellular Signal Transduction Pathways. *Int Immunopharmacol* (2013) 17(3):638–50. doi: 10.1016/j.intimp.2013.06.034
59. Dekker LV, Leitges M, Altschuler G, Mistry N, McDermott A, Roes J, et al. Protein Kinase C-Beta Contributes to NADPH Oxidase Activation in Neutrophils. *Biochem J* (2000) 347 Pt 1(Pt 1):285–9. doi: 10.1042/bj3470285
60. Shlezinger N, Irmer H, Dhingra S, Beattie SR, Cramer RA, Braus GH, et al. Sterilizing Immunity in the Lung Relies on Targeting Fungal Apoptosis-Like Programmed Cell Death. *Science* (2017) 357(6355):1037–41. doi: 10.1126/science.aan0365
61. Fuchs TA, Abed U, Goosmann C, Hurwitz R, Schulze I, Wahn V, et al. Novel Cell Death Program Leads to Neutrophil Extracellular Traps. *J Cell Biol* (2007) 176(2):231–41. doi: 10.1083/jcb.200606027
62. Clark HL, Abbondante S, Minns MS, Greenberg EN, Sun Y, Pearlman E. Protein Deiminase 4 and CR3 Regulate Aspergillus Fumigatus and Beta-Glucan-Induced Neutrophil Extracellular Trap Formation, But Hyphal Killing Is Dependent Only on CR3. *Front Immunol* (2018) 9:1182. doi: 10.3389/fimmu.2018.01182
63. Urban CF, Ermert D, Schmid M, Abu-Abed U, Goosmann C, Nacken W, et al. Neutrophil Extracellular Traps Contain Calprotectin, a Cytosolic Protein Complex Involved in Host Defense Against Candida Albicans. *PloS Pathog* (2009) 5(10):e1000639. doi: 10.1371/journal.ppat.1000639
64. Soloviev DA, Jawhara S, Fonzi WA. Regulation of Innate Immune Response to Candida Albicans Infections by Alphambeta2-Pra1p Interaction. *Infect Immun* (2011) 79(4):1546–58. doi: 10.1128/IAI.00650-10
65. O'Brien XM, Reichner JS. Neutrophil Integrins and Matrix Ligands and NET Release. *Front Immunol* (2016) 7:363. doi: 10.3389/fimmu.2016.00363
66. Gazendam RP, van Hamme JL, Tool AT, van Houdt M, Verkuijlen PJ, Herbst M, et al. Two Independent Killing Mechanisms of Candida Albicans by Human Neutrophils: Evidence From Innate Immunity Defects. *Blood* (2014) 124(4):590–7. doi: 10.1182/blood-2014-01-551473
67. Yakubenko VP, Cui K, Ardell CL, Brown KE, West XZ, Gao D, et al. Oxidative Modifications of Extracellular Matrix Promote the Second Wave of Inflammation *via* Beta2 Integrins. *Blood* (2018) 132(1):78–88. doi: 10.1182/blood-2017-10-810176
68. Kim CH, Lee K-H, Lee C-T, Kim YW, Han SK, Shim Y-S, et al. Aggregation of β2integrins Activates Human Neutrophils Through the Iκb/NF-κb Pathway. *J Leukoc Biol* (2004) 75(2):286–92. doi: 10.1189/jlb.0103038
69. Kettritz R, Choi M, Rolle S, Wellner M, Luft FC. Integrins and Cytokines Activate Nuclear Transcription factor-kappaB in Human Neutrophils. *J Biol Chem* (2004) 279(4):2657–65. doi: 10.1074/jbc.M309778200
70. Keophiphath M, Rouault C, Divoux A, Clement K, Lacasa D. CCL5 Promotes Macrophage Recruitment and Survival in Human Adipose Tissue. *Arterioscler Thromb Vasc Biol* (2010) 30(1):39–45. doi: 10.1161/ATVBAHA.109.197442
71. Culley FJ, Pennycook AM, Tregoning JS, Dodd JS, Walzl G, Wells TN, et al. Role of CCL5 (RANTES) in Viral Lung Disease. *J Virol* (2006) 80(16):8151–7. doi: 10.1128/JVI.00496-06

72. Yu C, Zhang S, Wang Y, Zhang S, Luo L, Thorlacius H. Platelet-Derived CCL5 Regulates CXC Chemokine Formation and Neutrophil Recruitment in Acute Experimental Colitis. *J Cell Physiol* (2016) 231(2):370–6. doi: 10.1002/jcp.25081
73. Propst SM, Denson R, Rothstein E, Estell K, Schwiebert LM. Proinflammatory and Th2-Derived Cytokines Modulate CD40-Mediated Expression of Inflammatory Mediators in Airway Epithelia: Implications for the Role of Epithelial CD40 in Airway Inflammation. *J Immunol* (2000) 165 (4):2214–21. doi: 10.4049/jimmunol.165.4.2214
74. Teran LM, Mochizuki M, Bartels J, Valencia EL, Nakajima T, Hirai K, et al. Th1- and Th2-Type Cytokines Regulate the Expression and Production of Eotaxin and RANTES by Human Lung Fibroblasts. *Am J Respir Cell Mol Biol* (1999) 20(4):777–86. doi: 10.1165/ajrcmb.20.4.3508
75. Rodland EK, Ueland T, Pedersen TM, Halvorsen B, Muller F, Aukrust P, et al. Activation of Platelets by Aspergillus Fumigatus and Potential Role of Platelets in the Immunopathogenesis of Aspergillosis. *Infect Immun* (2010) 78(3):1269–75. doi: 10.1128/IAI.01091-09
76. Bennouna S, Bliss SK, Curiel TJ, Denkers EY. Cross-Talk in the Innate Immune System: Neutrophils Instruct Recruitment and Activation of Dendritic Cells During Microbial Infection. *J Immunol* (2003) 171 (11):6052–8. doi: 10.4049/jimmunol.171.11.6052
77. Yadav A, Saini V, Arora S. MCP-1: Chemoattractant With a Role Beyond Immunity: A Review. *Clin Chim Acta* (2010) 411(21-22):1570–9. doi: 10.1016/j.cca.2010.07.006
78. Herold S, von Wulffen W, Steinmueller M, Pleschka S, Kuziel WA, Mack M, et al. Alveolar Epithelial Cells Direct Monocyte Transepithelial Migration Upon Influenza Virus Infection: Impact of Chemokines and Adhesion Molecules. *J Immunol* (2006) 177(3):1817–24. doi: 10.4049/jimmunol.177.3.1817
79. Lai C, Wang K, Zhao Z, Zhang L, Gu H, Yang P, et al. C-C Motif Chemokine Ligand 2 (CCL2) Mediates Acute Lung Injury Induced by Lethal Influenza H7N9 Virus. *Front Microbiol* (2017) 8:587. doi: 10.3389/fmicb.2017.00587
80. Mercer PF, Johns RH, Scotton CJ, Krupiczojc MA, Konigshoff M, Howell DC, et al. Pulmonary Epithelium Is a Prominent Source of Proteinase-Activated Receptor-1-Inducible CCL2 in Pulmonary Fibrosis. *Am J Respir Crit Care Med* (2009) 179(5):414–25. doi: 10.1164/rccm.200712-1827OC
81. Cushing SD, Berliner JA, Valente AJ, Territo MC, Navab M, Parhami F, et al. Minimally Modified Low Density Lipoprotein Induces Monocyte Chemotactic Protein 1 in Human Endothelial Cells and Smooth Muscle Cells. *Proc Natl Acad Sci USA* (1990) 87(13):5134–8. doi: 10.1073/pnas.87.13.5134
82. Gschwandtner M, Derler R, Midwood KS. More Than Just Attractive: How CCL2 Influences Myeloid Cell Behavior Beyond Chemotaxis. *Front Immunol* (2019) 10(2759):2759. doi: 10.3389/fimmu.2019.02759
83. Yoshimura T, Takahashi M. IFN-Gamma-Mediated Survival Enables Human Neutrophils to Produce MCP-1/CCL2 in Response to Activation by TLR Ligands. *J Immunol* (2007) 179(3):1942–9. doi: 10.4049/jimmunol.179.3.1942
84. Maus UA, Waelsch K, Kuziel WA, Delbeck T, Mack M, Blackwell TS, et al. Monocytes Are Potent Facilitators of Alveolar Neutrophil Emigration During Lung Inflammation: Role of the CCL2-CCR2 Axis. *J Immunol* (2003) 170(6):3273–8. doi: 10.4049/jimmunol.170.6.3273
85. Matsushima K, Larsen CG, DuBois GC, Oppenheim JJ. Purification and Characterization of a Novel Monocyte Chemotactic and Activating Factor Produced by a Human Myelomonocytic Cell Line. *J Exp Med* (1989) 169 (4):1485–90. doi: 10.1084/jem.169.4.1485
86. Reichel CA, Rehberg M, Lerchenberger M, Berberich N, Bihari P, Khandoga AG, et al. Ccl2 and Ccl3 Mediate Neutrophil Recruitment *via* Induction of Protein Synthesis and Generation of Lipid Mediators. *Arterioscler Thromb Vasc Biol* (2009) 29(11):1787–93. doi: 10.1161/ATVBAHA.109.193268
87. Jiang Y, Beller DI, Frendl G, Graves DT. Monocyte Chemoattractant Protein-1 Regulates Adhesion Molecule Expression and Cytokine Production in Human Monocytes. *J Immunol* (1992) 148(8):2423–8.
88. Roca H, Varsos ZS, Sud S, Craig MJ, Ying C, Pienta KJ. CCL2 and Interleukin-6 Promote Survival of Human CD11b+ Peripheral Blood Mononuclear Cells and Induce M2-Type Macrophage Polarization. *J Biol Chem* (2009) 284(49):34342–54. doi: 10.1074/jbc.M109.042671
89. Rollins BJ, Walz A, Baggiolini M. Recombinant Human MCP-1/JE Induces Chemotaxis, Calcium Flux, and the Respiratory Burst in Human Monocytes. *Blood* (1991) 78(4):1112–6. doi: 10.1182/blood.V78.4.1112.1112
90. Winter C, Taut K, Srivastava M, Langer F, Mack M, Briles DE, et al. Lung-Specific Overexpression of CC Chemokine Ligand (CCL) 2 Enhances the Host Defense to Streptococcus Pneumoniae Infection in Mice: Role of the CCL2-CCR2 Axis. *J Immunol* (2007) 178(9):5828–38. doi: 10.4049/jimmunol.178.9.5828
91. Zhang B, Hirahashi J, Cullere X, Mayadas TN. Elucidation of Molecular Events Leading to Neutrophil Apoptosis Following Phagocytosis: Cross-Talk Between Caspase 8, Reactive Oxygen Species, and MAPK/ERK Activation. *J Biol Chem* (2003) 278(31):28443–54. doi: 10.1074/jbc.M210727200
92. Walzog B, Jeblonski F, Zakrzewicz A, Gaehtgens P. Beta2 Integrins (CD11/CD18) Promote Apoptosis of Human Neutrophils. *FASEB J* (1997) 11 (13):1177–86. doi: 10.1096/fasebj.11.13.9367353
93. Yan SR, Sapru K, Issekutz AC. The CD11/CD18 (Beta2) Integrins Modulate Neutrophil Caspase Activation and Survival Following TNF-Alpha or Endotoxin Induced Transendothelial Migration. *Immunol Cell Biol* (2004) 82(4):435–46. doi: 10.1111/j.0818-9641.2004.01268.x
94. Park SJ, Burdick MD, Mehrad B. Neutrophils Mediate Maturation and Efflux of Lung Dendritic Cells in Response to Aspergillus Fumigatus Germ Tubes. *Infect Immun* (2012) 80(5):1759–65. doi: 10.1128/IAI.00097-12
95. Guerra ES, Lee CK, Specht CA, Yadav B, Huang H, Akalin A, et al. Central Role of IL-23 and IL-17 Producing Eosinophils as Immunomodulatory Effector Cells in Acute Pulmonary Aspergillosis and Allergic Asthma. *PloS Pathog* (2017) 13(1):e1006175. doi: 10.1371/journal.ppat.1006175
96. Lilly LM, Scopel M, Nelson MP, Burg AR, Dunaway CW, Steele C. Eosinophil Deficiency Compromises Lung Defense Against Aspergillus Fumigatus. *Infect Immun* (2014) 82(3):1315–25. doi: 10.1128/IAI.01172-13
97. Serrano-Gomez D, Dominguez-Soto A, Ancochea J, Jimenez-Heffernan JA, Leal JA, Corbi AL. Dendritic Cell-Specific Intercellular Adhesion Molecule 3-Grabbing Nonintegrin Mediates Binding and Internalization of Aspergillus Fumigatus Conidia by Dendritic Cells and Macrophages. *J Immunol* (2004) 173(9):5635–43. doi: 10.4049/jimmunol.173.9.5635
98. van Gisbergen KP, Sanchez-Hernandez M, Geijtenbeek TB, van Kooyk Y. Neutrophils Mediate Immune Modulation of Dendritic Cells Through Glycosylation-Dependent Interactions Between Mac-1 and DC-SIGN. *J Exp Med* (2005) 201(8):1281–92. doi: 10.1084/jem.20041276
99. Gafa V, Lande R, Gagliardi MC, Severa M, Giacomini E, Remoli ME, et al. Human Dendritic Cells Following Aspergillus Fumigatus Infection Express the CCR7 Receptor and a Differential Pattern of Interleukin-12 (IL-12), IL-23, and IL-27 Cytokines, Which Lead to a Th1 Response. *Infect Immun* (2006) 74(3):1480–9. doi: 10.1128/IAI.74.3.1480-1489.2006
100. Taylor PR, Roy S, Leal SM Jr, Sun Y, Howell SJ, Cobb BA, et al. Activation of Neutrophils by Autocrine IL-17a-IL-17RC Interactions During Fungal Infection is Regulated by IL-6, IL-23, RORgammat and Dectin-2. *Nat Immunol* (2014) 15(2):143–51. doi: 10.1038/ni.2797
101. Van Ziffle JA, Lowell CA. Neutrophil-Specific Deletion of Syk Kinase Results in Reduced Host Defense to Bacterial Infection. *Blood* (2009) 114(23):4871–82. doi: 10.1182/blood-2009-05-220806

Conflict of Interest: The authors declare that the research was conducted in the absence of any commercial or financial relationships that could be construed as a potential conflict of interest.

Advantages of publishing in Frontiers

OPEN ACCESS
Articles are free to read for greatest visibility and readership

FAST PUBLICATION
Around 90 days from submission to decision

HIGH QUALITY PEER-REVIEW
Rigorous, collaborative, and constructive peer-review

TRANSPARENT PEER-REVIEW
Editors and reviewers acknowledged by name on published articles

Frontiers
Avenue du Tribunal-Fédéral 34
1005 Lausanne | Switzerland

Visit us: www.frontiersin.org
Contact us: frontiersin.org/about/contact

REPRODUCIBILITY OF RESEARCH
Support open data and methods to enhance research reproducibility

DIGITAL PUBLISHING
Articles designed for optimal readership across devices

FOLLOW US
@frontiersin

IMPACT METRICS
Advanced article metrics track visibility across digital media

EXTENSIVE PROMOTION
Marketing and promotion of impactful research

LOOP RESEARCH NETWORK
Our network increases your article's readership